HUNGARIAN UNIVERSITY OF AGRICULTURE AND LIFE SCIENCES

Performance enhancement of flat plate solar collector using nanofluids

DOI: 10.54598/004250

PhD Dissertation

by

Ahmed Mohsin Ajeena

Gödöllő
2023

Doctoral school

Denomination: Doctoral School of Mechanical Engineering

Science: Mechanical Engineering

Leader: Prof. Dr. Gábor Kalácska, DSc
Institute of Technology
Hungarian University of Agriculture and Life Sciences, Szent István Campus, Gödöllő, Hungary

Supervisor: Prof. Dr. István Farkas, DSc
Institute of Technology
Hungarian University of Agriculture and Life Sciences, Szent István Campus, Gödöllő, Hungary

Co-Supervisor: Dr. Piroska Víg, PhD
Institute of Mathematics and Basic Science
Hungarian University of Agriculture and Life Sciences, Szent István Campus, Gödöllő, Hungary

……...…… ….....……

Affirmation of supervisor Affirmation of head of school

CONTENTS

NOMENCLATURE AND ABBREVIATIONS

A_a	Area of solar collector (m^2)
APS	Actual particle size (nm)
C_p	Heat capacity ($Jkg^{-1}\ K^{-1}$)
$C_{p,\ bf}$	Heat capacity of base fluid ($Jkg^{-1}\ K^{-1}$)
$C_{p,\ nf}$	Heat capacity of nanofluid ($Jkg^{-1}\ K^{-1}$)
$C_{p,\ np}$	Heat capacity of nanoparticles ($Jkg^{-1}\ K^{-1}$)
$\dot{E}\mathbf{x_{dest}}$	Rate of irreversibility (W)
$\dot{E}\mathbf{x_{heat}}$	Exergy rate received from solar radiation (W)
$\dot{E}\mathbf{x_{in}}$	Exergy rate at inlet (W)
$\dot{E}\mathbf{x_{mass,in}}$	Exergy rate associated with mass at inlet (W)
$\dot{E}\mathbf{x_{mass,out}}$	Exergy rate associated with mass at outlet (W)
$\dot{E}\mathbf{x_{out}}$	Exergy rate at outlet (W)
$\dot{E}\mathbf{x_{work}}$	Exergy output rate from the system (W)
$\dot{\mathbf{E}}\mathbf{x}$	Exergy (W)
F_R	Heat removal factor
G_t	Global solar radiation (Wm^{-2})
h	Specific enthalpy (Jkg^{-1})
h_{in}	Specific enthalpy at inlet (Jkg^{-1})
h_{out}	Specific enthalpy at outlet (Jkg^{-1})
k	Thermal conductivity ($Wm^{-1}\cdot K^{-1}$)
m	Mass (kg)
$\dot{\mathbf{m}}$	Mass flow rate (kgs^{-1})
p_{in}	Fluid pressure at inlet (Pa)
p_{out}	Fluid pressure at outlet (Pa)
$Q_{\ sun;\ in}$	Energy gain rate (W)
Q_s	Energy rate engrossed (W)
Q_u	Useful energy gained (W)
R	Ideal gas constant ($JK^{-1}\ mol^{-1}$)
S_{in}	Entropy generation at inlet (Jkg^{-1})
S_{out}	Entropy generation at outlet (Jkg^{-1})
SSA	Specific surface area ($m^2\ g^{-1}$)
$\dot{\mathbf{S}}_{\mathbf{gen}}$	Entropy generation rate (WK^{-1})
t	Time (s)
T_a	Ambient temperature (K)
T_b	Bulk temperature (K)
T_i	Inlet fluid temperature of collector (K)
T_o	Outlet fluid temperature of collector (K)
T_s	Surface temperature (K)
U_{ba}	Bottom loss coefficient ($Wm^{-2}\ K^{-1}$)
U_L	Overall heat transfer loss coefficient ($Wm^{-2}\ K^{-1}$)
U_t	Top loss coefficient ($Wm^{-2}\ K^{-1}$)

Greek symbols

$\tau\alpha$	Absorption-transmittance product
$\boldsymbol{\eta}$	Efficiency

$\boldsymbol{\rho}_{nf}$	Density of nanofluid (kgm^{-3})
$\boldsymbol{\rho}_{np}$	Density of nanoparticles (kgm^{-3})
$\boldsymbol{\rho}_{bf}$	Density of the base fluid (kgm^{-3})
φ	Volume fraction of nanoparticles (%)
μ	Dynamic viscosity (Pas)
$\boldsymbol{\rho}$	Density (kg/m^3)
γ	Shear rate (s^{-1})
τ	Shear stress (Pa)
τ	Transmittance of a glass cover
α	Absorptance of the absorber plate

Subscripts

a	Ambient, air
bf	Base fluid
c	Collector
g	Glass
i	Inlet/initial
nf	Nanofluid
np	Nanoparticle
o	Outlet, overall
p	Absorber plate, apple
u	Useful
vol	Volume
w	Water

Abbreviations

ASHRAE	American Society of Heating and Air Conditioning Engine
CFD	Computational Fluid Dynamics
DW	Distilled water
EG	Ethylene glycol
Exp	Experimental data
FESEM	Field Emission Scanning Electron Microscope
FPSC	Flat Plate Solar Collector
F_R	Heat removal factor
F_R ($\tau\alpha$)	Absorbed Energy parameter
F_RU_L	Energy loss parameter
MOD	Margin of Deviation
NFs	Nnanofluids
NPs	Nanoparticles
Nu	Nusselt number
Pr	Prandtl number
Pred	Predicted value
RDV	Relative dynamic viscosity
TCR	Thermal conductivity ratio
THW	Transient hot wire
XRD	X-ray diffraction

1. INTRODUCTION, OBJECTIVES

In this chapter, the background and the importance of the current research are presented as well as the objectives of this research.

1.1. Introduction

Energy has consistently been a critical and highly valuable global commodity. As the pollution of the environment deteriorates as a result of the unlimited usage of fossil fuels, there has been increased focus on renewable energies as a substitute for fossil fuels. Renewable energies come in various forms including solar energy, which is beneficial because of it being environmentally friendly and limitless. A keyway in which solar energy is used is by acquiring solar radiation through the use of solar collectors (Mussard, 2017). Various types of solar collector are available, including compound parabolic concentrators, direct absorption, evacuated tube, and flat plate. Furthermore, they can be classed as being low, medium, or high temperature according to the temperature at which they are operated. Due to the fact that solar collectors are frequently employed for supplying hot water and heating to buildings, they have the potential to lower the amount of energy generated by fossil fuels that such buildings consume (Hussein, 2016; Imran et al., 2016).

The flat plate solar collector (FPSC) generates heat energy by absorbing solar energy from the sun utilising the high absorbing black plate which help to maximize energy absorption. This plate heats the working fluid by passing the absorbed energy to the fluid. The heat energy generates by FPSCs that can be used in various productive works. Many factors affect the performance and energy generation ability of FPSCs (Ajeena et al., 2023a; Gorjian et al., 2020a; Hamzat et al., 2022). The traditional working fluids' low thermal conductivity is the most important of these factors, as it has a significant impact on the solar collector's performance. Therefore, experts are concerned about enhancing the collector efficiency for greater retention of solar energy (Ahmed M Ajeena et al., 2024; Elcioglu et al., 2020).

There is now significant interest in solar thermal systems in the engineering field. Although flat plate solar collectors (FPSC) were the first such systems to be developed and have high applicability, the amount of heat lost is comparatively high, thus making them less thermally efficient. Today, the efficiency of such solar systems can be improved via optimisation techniques along with state-of-the-art technologies and materials. Improving the thermal performance of FPSCs can reduce their dimensions and result in an increased outlet temperature of the fluid in terms of heating water in commercial and residential buildings (Elsheikh et al., 2018). Nonetheless, the installation of FPSCs can be costly, and they offer reduced energy-conversion efficiency; therefore, researchers have focused on how the costs of installation can be reduced while also making them more efficient (Faizal et al., 2013; Farhana et al., 2019).

FPSCs' thermal performance is significantly affected by the working fluid, a parameter that has considerable importance. The importance of the working fluid (often water) is characterized by its heat transfer performance and thermal conductivity. Recently, scientists have laid great emphasis on the significance of nanoparticles. The nanoparticles when added to fluids resulted in an improvement in fluid properties (Verma and Tiwari, 2015; Wahab et al., 2019). The nanofluid is said to be mono nanofluid when it is produced by adding a single nanoparticle to the base fluid

whereas the nanofluid is said to be hybrid nanofluid when it is produced by adding numerous nanoparticles to the base fluid. Consequently, the thermal solar collector devices offered better efficiency and performance by using nanofluids as a working fluid. It is also noticed a higher heat transfer rate could be noticed between the collector and the fluid when the nanofluid with higher thermal conductivity is used inside the collector (Said et al., 2021). Nanofluids have gained a lot of popularity because of their extraordinary properties with several studies being performed globally to identify the contribution rendered by nanofluids in enhancing the FPSC performance (Sheikholeslami et al., 2021; Verma et al., 2020).

Literature is enriched with experimental and computational research works on the potential of nano-additives to be used for enhancing the efficiency of FPSC devices. In this context, Said et al. (2015) investigated the exergy and energy efficiency of a FPSC filled with SWCNT/water. They revealed that the solar collector showed the highest rise of 95.12% in energy efficiency and the highest rise of 26.25% in exergy efficiency while the same collector depicted energy and exergy efficiency by 42.01% and 8.77% when using water base fluid. Chaji et al. (2013) also attempted to use TiO_2/water nanofluids in the FPSC to find out the effects of this nanofluid on the performance of the collector which revealed higher efficiency of the collector with the introduction of 0.3 wt% of TiO_2 nanoparticles. Ranga Babu et al. (2018) has examined the hybrid nanofluid influence on a FPSC thermal efficiency. They discovered a 2.59% rise in thermal efficiency when using a hybrid nanofluid. They also noticed a 3.31% decline in entropy production in the case of hybrid nanofluids, a 1.35% decline in Cu/H_2O nanofluids and a 2.96% decline in CuO/H_2O nanofluids. Eltaweel and Abdel-Rehim (2019) investigated the ability of MWCNTs nanoparticles with base fluid distilled water on FPSCs. The maximum energetic and second law efficiencies of 34.13% and 23.35% were accomplished with a 0.1 wt% of MWCNTs on a thermosiphon FPSWH. Okonkwo et al. (2020) determined that the thermal properties of a low temperature collector were increased by nanofluid. When nanoparticles of Alumina were added to water to create the nanofluid, the efficiency of the collector rose by 2.16%. However, in comparison to water, a 6.9% increase in exergy efficiency was detected.

1.2. Objectives

Recent developments in the study of solar collectors indicate the growing interest of experts in the use of nanotechnology in solar devices to obtain greater efficiency. However, the fact that research in the domain of nanofluid application in heat transfer for solar collectors is only limited to some selected nanofluids. Moreover, all the studies adopted different procedures and yielded different outcomes. The studies were also attributed with diverse outcomes and were based on the use of different methods and techniques. The studies also used the first law of thermodynamics and also attributed insight into qualitative performance. Besides this, none of the studies presented comprehensive analysis that could determine the exergy analysis and entropy generation while exergy destruction in FPSC filled with nanofluid rarely studies. The silicon carbide, zirconium oxide and hybrid nanofluids in FPSC have not been reported to be considered in any study performed till now. Considering these points, the current study can be deemed significant since it is the first one to consider the overlooked details mentioned above and provide valuable information in this domain. This study intended to overcome these gaps and consider different types of nanofluids. Therefore, the researcher emphasizes the importance of this study as being the pioneer in exploring the use of SiC/DW, ZrO_2/DW and ZrO_2-SiC (50–50%)/DW nanofluids and

its effects on the performance and efficiency of the FPSC. It is true to state that this is the first-ever study to determine changes in FPSC performance when replacing distilled water with these nanofluids. It is also recommended to study the properties of different nanofluids like the solid volume fraction of nanoparticles in fluid, dynamic viscosity, thermal conductivity, rheological behaviour, and flow rates. This will allow the researchers to determine and compare the properties and effects of different nanofluids to identify the best among them that can enhance thermal conductivity and performance of solar collectors. This study renders main objectives listed below:

- To quantify the rheological behaviour of mono and hybrid nanofluids based on nanoparticle concentration in the nanofluid and temperature.
- To experimentally evaluate the dynamic viscosity of SiC/DW, ZrO_2/DW, and ZrO_2-SiC (50–50%)/DW nanofluids based various temperatures and solid volume fraction.
- To experimentally determine the thermal conductivity of SiC/DW, ZrO_2/DW, and ZrO_2-SiC (50–50%)/DW nanofluids at different concentrations and temperatures.
- To study the effect of various concentrations and flow rate of nanofluids on the thermal performance of the FPSC system.
- To explore the new correlations for estimate the Nusselt number of mono and hybrid nanofluids.
- To assessment the effect of nanofluids as working fluids on the exergy destruction, entropy generation, and exergy efficiency of the FPSC system.
- To validate the ANSYS simulation models with experimental results that estimation of the performance of the FPSC with mono and hybrid nanofluid.

2. LITERATURE REVIEW

In this chapter, many major topics related to FPSC are covered, including an overview of flat plate solar collector, structure of FPSC, heat transfer element, and applications of FPSCs. Also, this chapter seeks to provide a thorough overview of NFs, their main thermophysical properties, preparation, and possible applications in different thermal devises. Besides, the main analysis of the key facts in the field NFs with their application in FPSC and influential aspects are also presented and discussed. This part will provide various recent numerical, theoretical, and experimental studies about the usage of the common kinds of NF as solar fluid in FPSC. Hence, this study intended to overcome obstacles and gaps in the existing literature, which is considered the reason for initiating this research.

2.1. General overview of flat plate solar collector system

Solar energy collectors are thermal circulation devices that convert sunray into direct energy inside solar fluids. It is the main part of every solar system. The solar collectors are divided into two main categories, namely, nonconcentrated (stationary) and concentrated. In general, a nonconcentrated collector has the same solar radiation collection and interception area (Wang et al., 2015). In contrast, a concentrated collector for sun tracking usually has concave surfaces for reflecting and focusing sunbeam radiation on smaller area, with flux increasing. The FPSC is a stationary collector and an exchanger system that transforms sunray to thermal energy in solar systems. When solar radiation penetrates the glazing and reaches the absorber plate, the energy is absorbed and transformed into the transferred heat to the fluid that passes through the absorber flow tubes to increase temperature. FPSCs may be classified as unglazed and flat glass plates (Chauhan et al., 2018; Choudhary et al., 2020). The advantages and disadvantages of FPSCs are summarised as follow: (a) FPSC is inexpensive to manufacture, (b) FPSC is permanently fixed in place, thus is no need to track the sun, (c) Various kinds of FPSC have been built, ranging from glass plates to plastic plates. Many different materials, such as aluminium, copper, steel, iron, and various working fluids such as water, NF and air. Fig. 2.1 shows different types of FPSC, (d) Solar collectors that use flat plates are easy to install and require little maintenance, (f) However, in cold weather uses, these systems have significant disadvantages, which impact their technical feasibility and economy. With low insolation and ambient temperatures in northern Europe during the winter season, FPSCs have low thermal efficiency. Moreover, heat losses, heat transfer circulation loop and inadequate thermal insulation are the disadvantages of the FPSC.

2.1.1. Structure of flat plate solar collector

The main parts of a typical FPSC are the following:

a. Cover: One or more glass sheets or other material that transmits radiation can be utilised in FPSC. The cover is a transparent blanket over the adsorbent surface used to minimise convection and radiation heating losses.
b. Riser tubes and fins: A working fluid is heated by a groove system (riser tubes) attached to fins to increase the heat dissipation between an absorbing surface and the unit's riser tubes.
c. Absorber plate: The absorber plate is a corrugated, flat, or grooved plate surface of a conductive material (aluminium, copper, etc.) used to collect solar energy and provide heat energy to the fluid flowing in the riser tubes. The plate usually has high absorption and low emittance on its surface by coating.

d. Manifold/header: Pipes are used to admitting and allowing discharge fluid before and after heating.
e. Insulation: It is necessary to conduct insulation on the bottom and sides of the collector to decrease heat loss.
f. Casing or container: The parts that make up the FPSC are installed in a casing or cover to protect from water, dust, and other material. Fig. 2.2 shows the major components of FPSC.

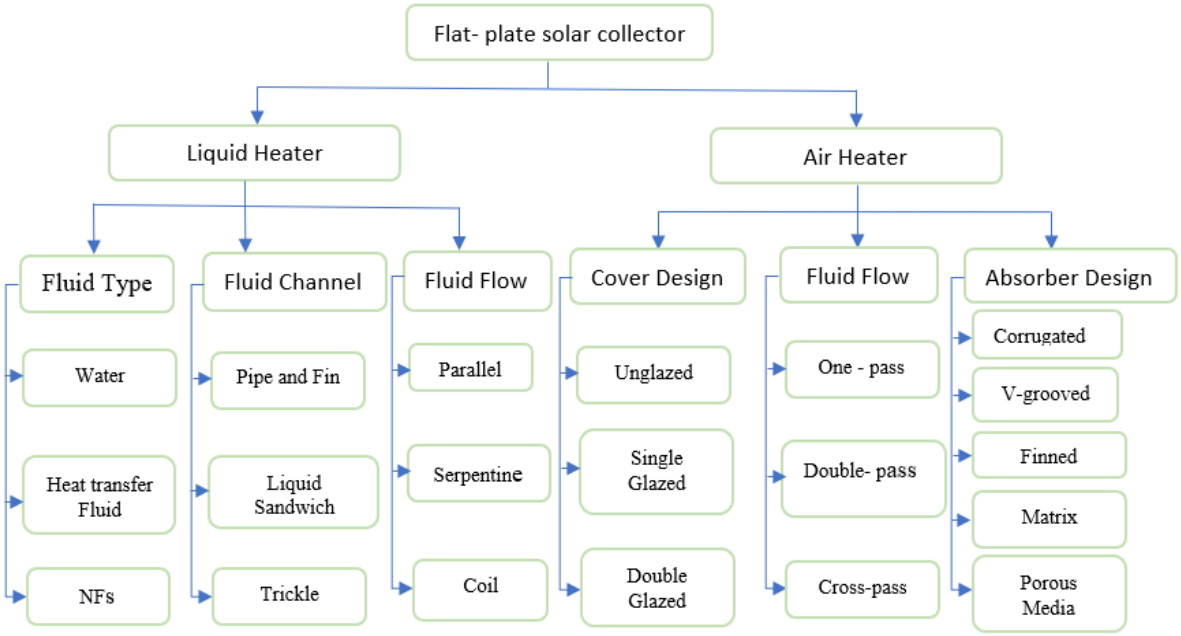

Fig. 2.1. Classification of FPSC (Gorjian et al., 2020a)

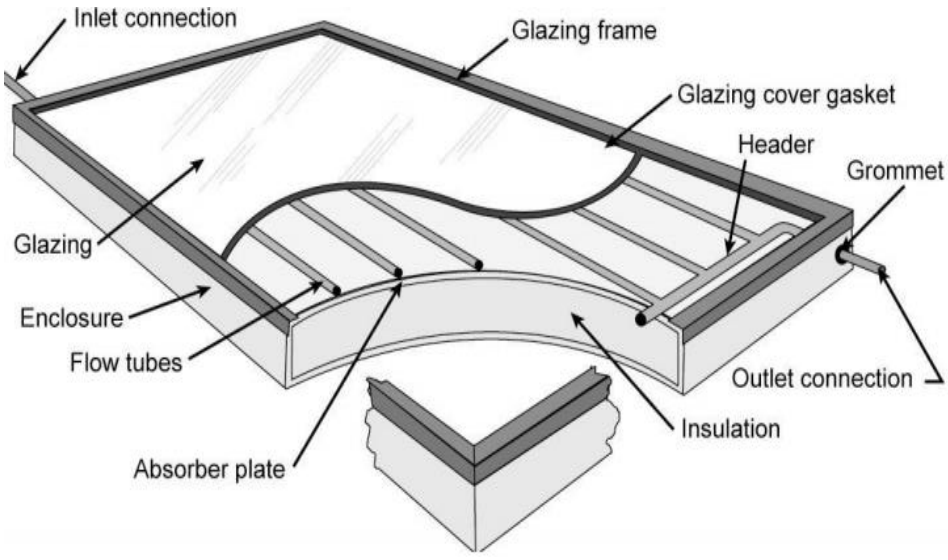

Fig. 2.2. Structure of FPSC

2.1.2. Solar water heating systems

At present, solar water-heating systems (SWHS) are widely known in FPSC applications. The solar heating system utilises thermal technology to convert solar radiation from the sun into heat and transmit it to a transfer media such as air or water. This system can often replace traditional water heating systems, such as traditional fossil fuels and heating water. Small systems are used for residential water and space heating applications, while larger systems are used for industrial processes (Hossain et al., 2011; Jamar et al., 2016).

The major components of SWHS such as the solar collector, storage tank, working fluid, pump (required in the active system only), piping units, heat exchange and auxiliary heating unit. The basic concept behind SWHS is that water heating involves contacting a fluid with a dark surface that causes the fluid temperature to rise while the heat is absorbed. This fluid can be induced by direct heating of water called a direct system or by heat transmission via heat exchanger called an indirect system. Fig. 2.3 shows the classification of the SWHS. In contrast, the passive system utilises the thermosyphon system and the integral collector storage system. The active systems include fluid heater collectors, which system works using electrical pumps, controllers, and valves to move working fluids through the collectors. Forced circulation (FC) is the name given to this system, which can be used in either an open-loop mode or a closed-loop (indirect) model (Kumar et al., 2019). When defining the passive system, the passive solar thermal heating system must be built on two bases: Firstly, collector and storage are primarily responsible, thus combined to its structure. For illustration, rooms and windows can work as collectors properly, whereas storage can deliver moderate heat to the building structure and its content as the temperature changes. Secondly, this system does not provide moving (mechanical) fluid, but radiation absorption temperature gradients move fluid and energy. The passive system utilises the natural convection heat transfer method to flow solar liquids between the collector and the tank without mechanical devices (Ajeena et al., 2022; Shukla et al., 2013).

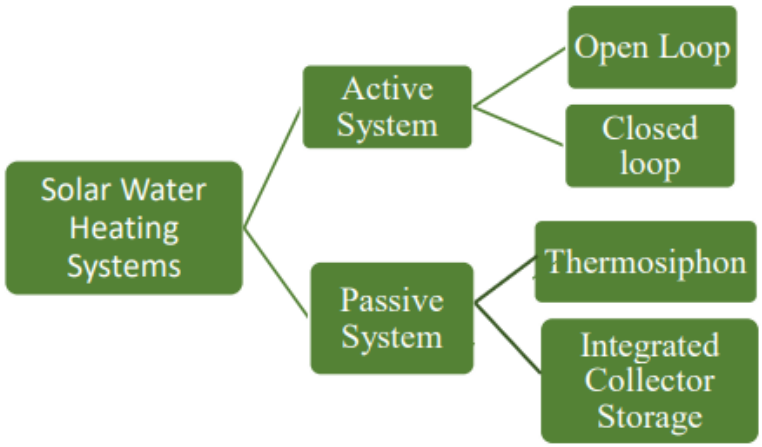

Fig. 2.3. Types of solar water heating systems

2.1.3. Heat transfer processes

The thermal network consists of primary heat transfer mechanisms of convection, conduction, and radiation for FPSC as shown in Fig. 2.4.

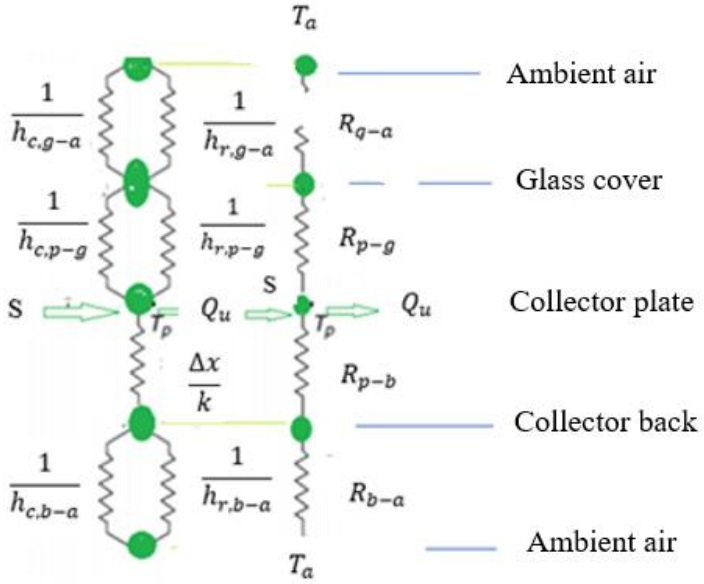

Fig. 2.4. Resistance thermal network for single cover FPSC

(a) Convection

The convection heat loss from the absorber to the glass cover can be calculated using the following equation:

$$Q_{tc,\text{absorber plate to glass cover}} = A_c h_{c,p-g}(T_p - T_a) \quad (2.1)$$

The convective heat transfer coefficient, $(h_{c,p-g})$, can be expressed by (Duffie et al., 1985):

$$Nu = \frac{h_{c,p-g}L}{k} = 1 + 1.446\left[1 - \frac{1708}{Ra \times \cos(\theta)}\right]\left\{1 - \frac{1708[\sin(1.8\theta)]^{1.6}}{Ra \times \cos\theta}\right\}\left\{\left[\frac{Ra \times \cos\theta}{5830}\right]^{0.333} - 1\right\} \quad (2.2)$$

The Rayleigh number, Ra, can be obtained by:

$$Ra = \frac{g\beta' Pr}{V^2}(T_p - T_g)L^3 \quad (2.3)$$

The convective heat transfer coefficient for vertical collectors, $h_{c,p-g}$, can be calculated as (Kalogirou, 2004):

$$Nu = \frac{h_{c,p-g}L}{k} = \left[1 + \left(\frac{0.0665Ra^{0.333}}{1 + \left(\frac{9600}{Ra}\right)^{0.25}}\right)^2\right]^{0.5} \quad (2.4)$$

(b) Conduction

Insulation at the bottom and edges of FPSC allows heat to be conducted, where estimating the heat loss due to conduction from the collector's bottom is possible using the formula below (Kalogirou, 2004):

$$U_{b,conduction} = \frac{K_b}{T_b} \tag{2.5}$$

Estimating the loss of heat conduction from the solar collector's edges should be done as follows:

$$U_{e,conduction} = \frac{K_e}{T_e} \tag{2.6}$$

(c) Radiation

Any contact between two surfaces results in a radiation heat transfer in FPSC and is capable of being transmitted, reflected, and absorbed. Radiation in FPSC consists of two parts. The formula for calculating heat transfer between absorber and glass cover is as follows (Kalogirou, 2004):

$$Q_{r,absorber\ plate\ glass\ cover} = \frac{A_c\sigma\left({T_p}^4 - {T_g}^4\right)}{\left(\frac{1}{\varepsilon_p} + \frac{1}{\varepsilon_g}\right) - 1} \tag{2.7}$$

The formula to calculate the radiation coefficient between the glass cover and the absorber is found here:

$$h_{r,p-g} = \frac{\sigma\left(T_p + T_g\right)\left({T_p}^2 + {T_g}^2\right)}{\left(\frac{1}{\varepsilon_p}\right) + \left(\frac{1}{\varepsilon_g}\right) - 1} \tag{2.8}$$

The formula to calculate the radiation coefficient between the glass cover and the ambient is found here (Duffie et al., 1985):

$$h_{r,g-a} = \varepsilon_g\sigma\left(T_g + T_a\right)\left({T_g}^2 + {T_a}^2\right) \tag{2.9}$$

2.2. Nanofluids

2.2.1. Concept and applications of nanofluids

The use of traditional fluids with lower thermal conductivity is associated with the issue of a lower rate of heat transfer. With the increasing use of heat transfer systems, experts are working on the development of techniques yielding better heat transfer performance. As a result of these efforts, nanofluids were discovered which were found to enhance the heat transfer performance of heat systems. Keeping this situation in mind, the use of nanofluids is deemed an effective means to prevent such issues. The introduction of nanofluids by Choi (1995) has proven to be a historic contribution to the field of heat transfer. Nanofluids are colloids or mixtures composed of base-fluid containing dispersed nano-sized particles. Two types of nanofluids include the mono nanofluids and hybrid-based types. Conventional nanofluids, also referred to as mono nanofluids, contain only a single nanomaterial. Nanofluids that contain more than one nanomaterial are referred to as hybrid nanofluids and are developed to enhance the nanofluid's efficiency. The nanofluids are more preferably used in heat transfer applications in comparison to additives having sizes in millimetres and micrometres. Also, it was found that nanofluids deliver better heat transfer performance than the traditional base fluids. Commonly used base fluids include water, ethylene

glycol, and engine oil. The main properties of nanofluids that make them preferable for use in heat transfer applications include higher stability and higher thermal conductivity. Such novel fluids have recently been the subject of increased focus among scientists due to their capability to facilitate perceptible transfer of heat compared with standard fluids. There is widespread agreement that nanofluids that has particular significance when applied in engineering and industrial applications such as thermal energy storage (Shin and Banerjee, 2011), solar cells (Otanicar and Golden, 2009), parabolic trough systems (Heyhat et al., 2020), solar stills (Gnanadason et al., 2012), direct absorption systems (Duangthongsuk and Wongwises, 2009), micro-channel heat sinks (Khan et al., 2021), photovoltaic/thermal systems (Tian et al., 2021), circular heat exchanger (Ahmed and Khan, 2021), solar thermoelectric cells (Fan et al., 2011), and solar ponds (Singh et al., 2011), air-conditioning system (Ahmed et al., 2021), solar organic Rankine cycle (ORC) system (Refiei et al., 2020), dish solar collectors (Ouyang et al., 2021). Some researchers have investigated the use of NFs in FPSC for low-thermal applications (Angayarkanni and Philip, 2015). Fig. 2.5 illustrates applications of NFs in different technology areas.

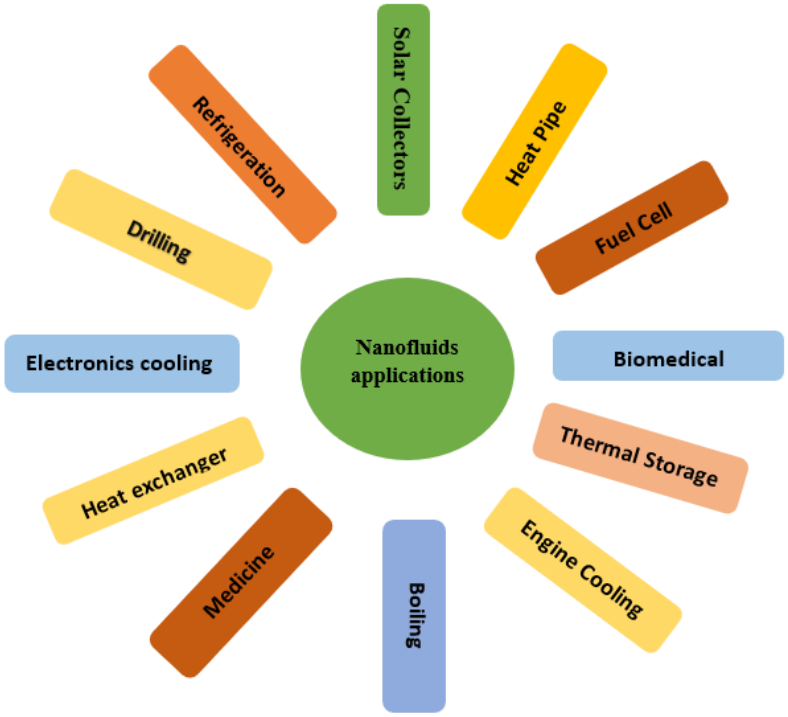

Fig.2.5. NFs applications

2.2.2. Classification of nanofluids

Nanofluids is a term for describing fluids containing nanoscale dispersed particles. NFs is separated into several classes according to the types of NPs (Nagarajan et al., 2014). The classification of NFs is illustrated in Fig. 2.6. The transportation characteristics of NF depend on the distribution in a basic fluid of various types of NPs. Given the physical composition and chemical characteristics, NPs vary in their density and heat capacity as thermal conductivity. The two categories can be divided into mono NFs and hybrid NFs (Uddin et al., 2016). Choi in 1995, first proposed the idea of a single-material NF (mono NF) and it has since become the standard form of NFs for suspension with a single type of NPs (Reddy et al., 2017). Several authors reported

that nanoflows of this category perform superior because their thermophysical properties are much more favourable than their basic fluid. Moreover, hybrid nanoparticle (Hybrid NF) is an advanced nanoparticle that contains more than one type of nanoparticle (NP) and is suspended in the base fluid. In order to increase thermal conductivity, these types of nanofluids were utilised (Jana et al., 2007).

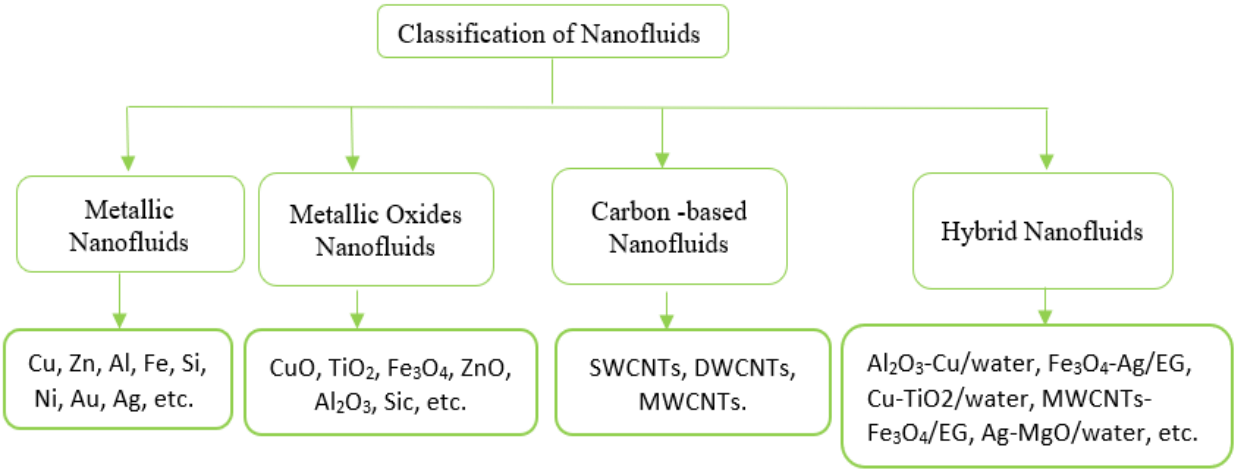

Fig. 2.6. Classification of NF

2.2.3. Preparation of nanofluids

The most pressing concern with conducting fluid NF research is obtaining a uniform distribution of NPs and keeping them uniform in size. The particles' dispersion uniformity is mainly due to the preparation method, affecting the NF's thermophysical properties. The NFs are affected more severely because they must be created using specific conditions within a liquid–solid mixture: homogeneity, physical and chemical stabilities, durability and dispersibility. The uneven distribution of the larger particles causes a very uneven distribution that alters the properties of NPs. The NF's preparation is an essential stage in the use of NP during heat transfer. Two different ways to create NFs are identified, namely, the single-step approach (bottom-up) and the two-step approach (top-down) (Devendiran and Amirtham, 2016).

2.2.3.1. Single-step approach

Firstly, a single-step process is used for NPs that may change composition or aggregate when NPs distributed in the base liquid. A direct evaporation technique for creating NFs generally transforms a vapour depositing solid solution and solidifies NPs within a base fluid. This method eliminates the need for NP processing such as dispersion, drying, transportation and storage. One disadvantage of the method is that concentrated contaminants remain in the NFs, thus challenging to separate impurities from NFs. Using a single-step preparation of NPs in a uniformly distributed condition, the particles are not likely dispersed and using this method is its nonproduction of pure metallic nano powder and the difficulty of contaminant disposal (Eastman et al., 2001; Wagener et al., 1997). Fig. 2.7 shows the single-step preparation for NFs.

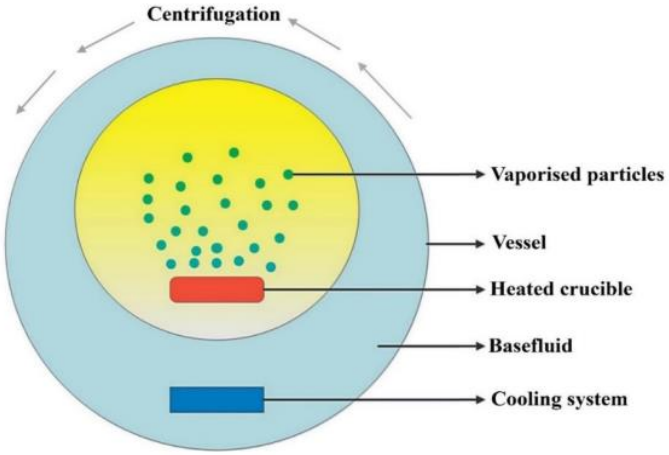

Fig. 2.7. Description of the single-stage approach (Almurtaji et al., 2020)

2.2.3.2. Two-step approach

The two-stage process is a widely used technique to prepare NFs. The dry fine particles of NPs, nanofibers, nanotubes, etc. are produced initially with physical and chemical methods. NPs are distributed to the base fluid using ultrasonic vibration, magnetic disturbing of energy, shear mixing, and homogenising ball milling. The two-stage method is often used because it is cheaper, and the materials are commercially readily available. Researchers say that the two-stage process is usually considered the best choice for preparation of NFs (Babar and Ali, 2019). The major drawback of the two-step method is that NPs can form clusters during preparation, hence avoiding NPs' proper synthesis within the conventional fluid. The most common way to improve the NPs' stability in thermal transmission fluids is by physical treatment methods (Arshad et al., 2019). The two-step preparation approach for NFs is shown in Fig. 2.8.

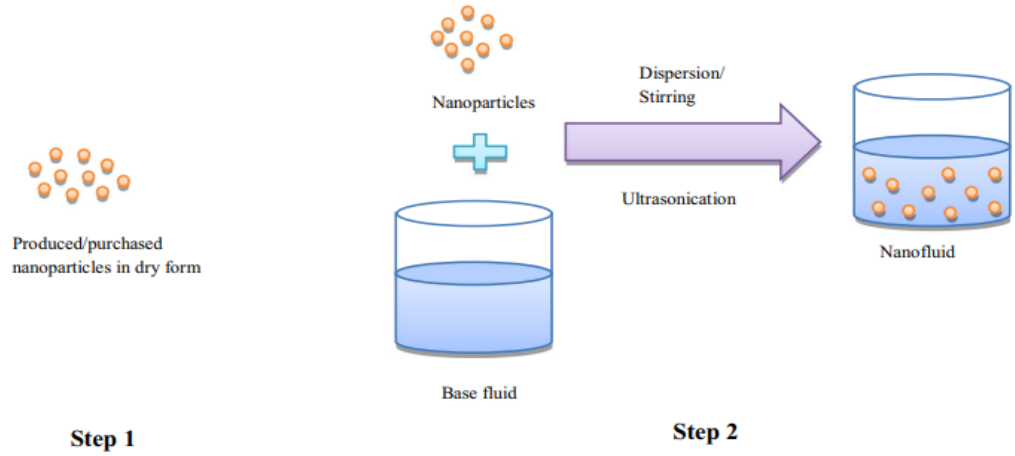

Fig. 2.8. Description of the two-step approach (Arora and Gupta, 2021)

2.2.4. Thermophysical properties of nanofluids

NP's thermal properties are fundamental to the performance for the NFs. The properties of the base fluid, such as viscosity, pressure drop, thermal conductivity, and specific heat, are affected by the addition of NPs. Some of the key factors which change thermophysical properties are the temperature variation, ambient conditions, basic fluid type, NP size, shape and volume concentration are the operating parameters. In consideration of all parameters, selecting the proper NF is necessary to optimise the results (Ajeena et al., 2023b; Eggers and Kabelac, 2016).

2.2.4.1. Thermal conductivity

Thermal conductivity is when a given material can transfer heat. The conductivity rate differs in different materials based on their ability to conductivity. Materials such as metals conduct heat at a faster rate compared to materials that are used in insulation, such as glass wool. The thermal conductivity rate is influenced by other factors such as temperature gradient, the material's chemical phase, length, and the conductor's cross-sectional area (Ajeena et al., 2023c). A nanoparticle is any particle with a diameter measuring one hundred nanometres. The particles do not undergo sedimentation as they undergo the Brownian motion (Amrollahi et al., 2008; Hemmat Esfe et al., 2015; Jafari et al., 2022). Nanofluids are fluids that contain nanoparticles. The heat transfer potential of NF is necessary to be known of the thermal conductivities. One factor that contributes to an improvement in thermal effectiveness is the Brownian movement. Also, Temperature affects the conductivity of nanofluids differently. The thermal conductivity of NFs increases with an increase in temperature, and vice versa is true. Thermal conductivity is widely used in many industries to add or remove energy generated in the system (Moradi et al., 2020; Sarode et al., 2020; Toghraie et al., 2016). Many theoretical and experimental work has been done to study the thermal conductivity of NFs. According to published papers, the properties of nanofluids make them ideal for use in industries. Studies were done by Das et al. (2003) to measure the thermal conductivity of aluminium oxide water and copper oxide/water nanofluids. They used the temperature oscillation method by applying different temperature gradients and concentrations. The studies' results showed that the nanofluids' thermal conductivity was increased by 24.3% by increased temperature and concentration. Chon et al. (2005) did a similar study, but he used the transient hot wire method to measure the thermal conductivity of aluminium oxide nanofluid. The results showed that thermal conductivity decreases with an increase in the size of the nanoparticle used in the nanofluid. The conductivity also increases by approximately 28% at maximum temperature and concentration for a smaller-sized particle. Li and Peterson (2007) did a study using the steady state method to determine if the diameter of a nanoparticle has any effect on the thermal conductivity of aluminium oxide /water nanofluid. Results showed that an increase in diameter from 36 nm to 47 nm while keeping the temperature constant lowers the enhancement to conductivity by 2%. A study was done Aberoumand and Jafarimoghaddam (2018) to test the thermal conductivity and the dielectric strength of a hybrid nanofluid containing Tungsten (III) oxide and silver using transformer oil as the liquid base. The nanoparticles are used in varying weight fractions of 1%, 2%, and 4%. The temperature on the nanofluids ranged between 40 °C and 100 °C, and the thermal conductivity was measured using a KD2 Pro thermal properties analyser. Results from the experiment led to the conclusion that thermal conductivity increases at a higher weight fraction and maximum temperature. On the contrary, electrical conductivity decreases with an increase in the nanoparticle's weight fraction. Sharifpur et al. (2021) conducted an experimental study to determine the thermal conductivity of Zinc oxide/water nanofluid in a square cavity compared to deionized water. They used ZnO nanoparticles that were 20 nm in diameter and added them to deionized water at different volume fractions of 0.1, 0.18, 0.36, 0.5 and 1.0%. The ZnO/water nanofluid and deionized water were passed through a rectangular cavity where the opposite sides had different temperatures. Results from the experiment show that thermal conductivity was enhanced by 9.14% compared to deionized water. Karthikeyan et al. (2008) conducted a study to determine how the concentration of nanoparticles used in a nanofluid affects the thermal conductivity of the nanofluid. Copper oxide nanoparticles of 8 nm were used in the experiment. Results showed that thermal conductivity was enhanced by 31.6% and 54% relative

to water and ethylene glycol base fluids, respectively. The conclusions drawn from the results show that the size of nanoparticles, the particles' dispersion, and the particles' volume fraction significantly influence the thermal conductivity of nanofluids. Yiamsawasd et al. (2012) did an experiment to measure the thermal conductivity of nanofluids containing titanium and aluminium as nanoparticles. To prepare the nanofluids, titanium oxide and aluminium oxide nanoparticles were suspended in two base fluids, water, and ethylene glycol, in a 20/80 ratio. The concentrations prepared ranged from 0 to 8 percent volume fractions, and a temperature range of 15–65 °C was used. The transient-hot wire method was used to measure thermal conductivity. Results showed that, relative to the base fluid, the nanofluids' thermal conductivity increased with concentration and temperature.

2.2.4.2. Dynamic viscosity

The study of nanofluids revealed that viscosity is one of the main features that make nanofluids specifically beneficial for industrial and engineering applications. After this discovery, several research studies were conducted on nanofluids and their dynamic viscosity. The rise in the dynamic viscosity of nanofluids may be attributed to the addition of nanoparticles in the base fluid leading to changes in other properties of velocity field and friction forces. The cumulative effect of all these factors causes a considerable increment in the heat transfer performance of heat transfer systems. Nanofluids and base fluids differ from each other in terms of their thermo-physical properties (Ahmed M. Ajeena et al., 2024; Ajeena et al., 2023d). Nanofluids are characterized by higher viscosity than base fluids due to the presence of the weight of nanoparticles in the nanofluids. Several studies have been conducted recently in the domain of dynamic viscosity of nanofluids. For instance, Afrand et al. (2017) demonstrated that when Fe_3O_4 nanoparticles are dispersed into water, the Newtonian behaviour of the base fluid remained constant. Additionally, they found that decreasing the temperature and increasing the volume fraction resulted in the amplification of the nanofluid viscosity. Pastoriza-Gallego et al. (2011) conducted a study in which the effects of the size of particles, solid weight fraction and temperature on CuO/water nanofluids' viscosity were investigated. Weight fractions with a maximum of 10% and a temperate range between 10 °C and 50 °C were used in the experiments. According to their findings, as the solid weight fraction increased, the nanofluids' viscosity increased in parallel, whereas it decreased as the temperature and nanoparticle size increased. In the study of Asmat et al. (2023), the viscosity of SiO_2/water nanofluid with solid volume fractions varying between 0.5% and 4% as well as a temperature of 30 °C was measured. Their results demonstrated that the increase in viscosity reached 50% with a nanoparticle volume fraction of 4%. In the study of Duangthongsuk and Wongwises (2009), the viscosity and temperature-dependent thermal conductivity TiO_2–water nanofluids was measured. They demonstrated that an increase in the concentration of particles caused both variables to increase to a level that exceeded that of the base fluids. Sadri et al. (2014) demonstrated the ability of carbon nanotubes (CNTs) to enhance the thermal performance of standard working fluids. Their results showed that sonication time is a factor that influences the thermal conductivity and viscosity of such nanofluids. In the research of Li et al. (2014), ZnO nanofluids based on ethylene-glycol were analysed in terms of their viscosity and thermal conductivity. They reached the conclusion that as expected, an increased concentration of ZnO nanoparticles caused the nanofluid's viscosity to increase, whereas it decreased as the temperature rose. Jarahnejad et al. (2015) explored how the dynamic viscosity of nanofluids based on water that contained nanoparticles of titania (TiO_2) and alumina (Al_2O_3) were affected by factors such

as temperature as well as nanoparticle size and concentration. Their findings indicated that in general, the viscosity of the nanofluids that contained nanoparticles of TiO_2 nanoparticles was greater compared to those containing Al_2O_3 when the loading was the same. Abbasi et al. (2016) investigated the effects of temperature and concentration on the flow behaviour and viscosity of nanofluids containing TiO_2 nanoparticles, pristine MWCNTs, oxidised MWCNTs, and decorated MWCNTs were impacted by concentration and temperature in terms of the viscosity and flow characteristics. Their findings revealed that nanofluids' properties are dependent on concentration and temperature, while a decrease in the viscosity of the produced nanofluids was observed as the temperature rose and the concentration decreased.

2.2.4.3. Density and specific heat of nanofluids

Density is another essential thermophysical property to assess the NFs heat transfer performance. NF density is proportional to the system's solid (NPs) and liquid (base fluid) volume proportion. When the solid density is higher than that of fluids, NF density generally increases as NPs are added to the fluid. Teng and Hung (2014) determined alumina density (Al_2O_3)/water NF. The outcomes show that the density variation with the equation of density is between 0.015%–0.06% and 0.25%–2.53%. The calculated density results were further differentiated as the NF particle load increased.

The specific heat plays a predominant role in influencing the rate at which NFs are transferred. It is the amount of heat required to raise the temperature of 1 kg of NF by 1 °C. The specific heat of materials is a significant property to determine their thermal performance. The specific heat remains constant at constant pressure and with a wide variety of temperatures for conventional materials. The specified NF heat can vary depending on the nanomaterial type, temperature, base fluids and NP concentration in basis fluids. Saeedinia et al. (2012) examined the specific heat capacity of 0.2%–2% CuO-base oil NFs at different temperatures with particle weight fractions. In this experiment, NFs have shown a less specific heat capacity than base fluid and decreased with an increased NPs concentration. The result further showed that the specific heat of 2 wt% NFs was approximately 23% lower than that of the base fluid at 40 °C. Zhou and Ni (2008) studied the CuO NF specific heat capacity decrement by 1.16%–5% with base fluid EG for volume fraction 0.1%–0.6%, with a 25 nm–500 nm particle size. Some NFs have an abnormal volume-concentration behaviour. Starace et al. (2011) stated that SiO_2 NPs special heat capacity in EG base fluid decreased and increased. Shahrul et al. (2014) conducted a comparative study on NF-specific heat for energy applications. They found that the specific heat decreases as the volume fraction of most nanomaterials in base liquids increases.

2.2.5. Stability of nanofluids

NF stability plays the most important role in improving the performance of every system. NPs have tremendously small sizes and high kinetic energies because of Brownian motion. Despite their extremely large sizes and stability, they do not remain suspended. NPs settle from the solution with time under the gravity influence. NFs have poor stability due to the interaction of the particles and between them and the surrounding liquid, which influences the NFs commercialisation (Sezer et al., 2019). This sort of behaviour can be linked to two opposing forces: (a) the well-known Van der Waals attraction on the part surface, which attracts particles to each other and then forms clusters or agglomerations and settles at the bottom by gravity and (b) the repulsive electric double layer, which tends to reverse the force of gravity, steric and electrostatic mechanisms of repulsion.

The repulsive force of the electric double layer should exceed the attractive forces of the Van der Waals to achieve a stable NF. From a practical point of view, clustering, and sedimentation cause two difficulties. Firstly, the photothermal and thermal properties of the NF are lost. Secondly, the sediment accumulation in solar collectors, causing clogging. Sediments cause abrasion of the wall tube, and sediments accumulate to reduce flow. Therefore, the stability and performance of the NFs are essential to maintain dispersed NPs. Stability is an essential aspect of NF marketing as it extends the product's shelf life while maintaining its thermophysical qualities. For applications, the long-term stability of NFs is crucial. To improve stability and reduce the concentrations and sedimentation of NPs, researchers used various techniques. NFs' long-term stability and thermal properties were supported by chemical treatment such as addition of the surfactants and physical treatment such as ultrasonic and homogenisation.

2.2.5.1. Chemical treatment for enhance nanofluid stability

The NPs and base fluid nature determine NF stability. Surfactants are surface-active substances that link the NPs and the base fluids to avoid the particles aggregation. Also, Surfactants addition is an effective method to increase stability, which prevents NF agglomeration of NPs and a simple and cost-effective chemical method that reduces base fluid surfaces and improves NP immersion (Byrne et al., 2012). Oil-soluble and water-soluble surfactants can be classified. The surfactants are composed of a hydrophobic tail (e.g., hydrocarbons with long-chain) and the hydrophilic polar heads, which tend to increase their hydrophilic behaviour between the base fluid and the NPs. The surface charges of NPs and the type of used base fluid primarily determine which surfactant is chosen. Based on the head composition, the dispersant can be grouped into four classes: (a) the negative charge head group of ionic surfactants (e.g., long-chain fatty acids, alkyl sulphates, sulfonates and sulfosuccinate), (b) the neutral head group non-ionic surfactants (e.g., polyethylene oxide, alcohols and other polar groupings), (c) the positive charge head group of cationic surfactants (e.g., long-chain quaternary ammonium compounds and long-chain amines), and (d) amphoteric surfactants of zwitterionic headgroups (charge is a pH-dependent) (Tawfik, 2017). Several surfactants are commonly used in the NFs research such as polyvinylpyrrolidone (PVP), sodium dodecyl sulphate (SDS), oleic acid (OA), hexadecyl trimethyl ammonium bromide (HCTAB), Poly (acrylic acid sodium salt), Sodium dodecyl benzene sulfonate (SDBS) and dodecyl trimethylammonium bromide (DTAB) (Tiara et al., 2017). The disadvantage of the NF stabiliser dispersant is its sensitivity to hot temperatures because the increased temperature causes damage to the bonds between the NPs and the surfactant and can chemically respond in the production of foams in certain cases (Chen et al., 2008). In addition, excessive surfactants affect the thermophysical properties of the NF, increasing the NF's viscosity and reducing its thermal conductivity.

2.2.5.2. Physical treatment for enhance nanofluid stability

This treatment used high energy to break the cluster of NPs and create a well-dispersed colloidal suspension by ultrasonication. Ultrasonic baths/probes are usually used to disperse clusters of NPs physically. Fig. 2.9 shows both types. Probe sonication of the physical treatment methods is used most often for NFs stabilisation. A programmed period is used to disperse NPs into base fluids and break up NPs clusters (Ganesan et al., 2016). Sound energies at the ultrasonic level are at 20 kHz and above. For various intervals, researchers used ultrasound at various levels of power and frequency. Optimum sonication conditions can differ with different parameters such as particulate concentration, particle size, type of particle, type of fluid base, etc. Many scientists have employed

ultrasonic in the preparation and stabilisation of NFs. Mahbubul et al. (2016) studied ultrasonic time influence on water based Al_2O_3 NF stability. Better colloidal dispersion and lower viscosity were detected by increasing the sonication time.

Fig 2.9. Ultrasonics types. (a) Probe (b) Bath

2.2.5.3. Nanofluid stability evaluation method

The stability of NF is essential during the long period, but solid phase NPs are in constant Brownian motion and can interact earlier (or later) with others. During these interactions, strong attractiveness forces create the aggregation of particles. The agglomerations gradually increase and start to become unstable under gravity. NFs become unstable. The sedimentation process also reduces the thermal performance of NFs in addition to blocking flow channels in the collectors. Therefore, assessing the long-term stability when a NF is produced is important (Verma et al., 2018; Zayed et al., 2019a). No current standard method for measuring the stability of NFs exists. Visual inspections (sedimentation) and zeta potential are the most extensively used techniques for analysing suspension stability. Some studies showed the results of zeta potential analysis, while others have only reported stability through visual inspection (Timofeeva et al., 2007; Tiznobaik and Shin, 2013).

NF stability can be determined by measuring the electrical potential between the dispersed medium and the fixed fluid layer attached to the particle. Zeta potential (ζ -potential) is a key indicator of colloidal dispersion stability. Zeta is the possible difference between the NPs' surface and the stationary fluid layer attached to NPs. Zeta potential magnitude designates the electrostatic repulsion extent between nearby and equally charged particles in a dispersion. High zeta potential NFs are electrically stabilised (negative or positive), while low zeta potential NFs are unstable (Chen et al., 2008). The method more used for evaluating suspension stability is the Zeta potential test.

2.2.6. Advantages of using nanofluid in the solar collectors

Nanofluids have many advantages in comparison to traditional fluids, allowing them highly effective in the field of solar collectors. The benefits offered by nanofluids in this field have been listed as follows (Akram et al., 2020; Alawi et al., 2021; Gorjian et al., 2020b):

- The nanofluids are characterized by high thermal conductivity. Hence, they enhance the heat transfer properties of the suspension leading to greater thermal conductivity.

Moreover, the nanoparticles are associated with Brownian motion which also has a positive effect on the heat transfer performances.

- The minimum size of the nanoparticles allows easy mixing with fluids and these particles can easily pass through solids with tiny pores. When added to base fluid, the nanoparticles readily mix in the fluid facilitating swift movement and flow even within the solid.
- The use of micrometre or millimetre-sized particles in solar collectors led to quick settling of the particles affecting the fluid flow. This issue has been resolved with the use of nanoparticles.
- Using nanofluid allows changing particle concentration to make appropriate changes in the fluid's thermal conductivity, viscosity, density, and specific heat as per the requirements of particular applications.
- The nanofluids are characterized with high stability and Brownian motion which allow the fluid to maintain its liquid state for longer periods.
- As the surface area between the fluid and nanoparticles increases, they get more surface for heat transfer leading to greater transfer of heat.
- Replacing the base fluid in a solar collector with nanofluid leads to a rise in the efficiency of the collector because of a rise in output temperature. In a regular solar collector, high output temperatures can only be attained by increasing the surface area for facilitating more heat absorption leading to a rise in cost and bulky-sized collectors.
- Nanofluids offer the advantage of greater heat transfer without increasing the surface area of heat absorption. Hence, they improve the collector efficiency without involving costly processes and without the need to manufacture space-consuming plates for heat absorption.

2.3. Use of nanofluids in flat plate solar collector system

In recent years, an increase in consideration of renewable energy resources in all countries because of the shortage of energy resources is observed. One renewable energy source that has come into prominence is the solar thermal energy systems for homes and industrials applications. Flat-plate collectors have been operating for over 30 years with little change in the designs or operating principles. FPSC has some advantages: being reliable, durable, and inexpensive, but have some disadvantages such as low sensitivity and low efficiency at low irradiance and ambient temperature (Akram et al., 2019; Hussein, 2016; Raj and Subudhi, 2018). The FPSC is effectively used for industrial and domestic applications and absorbs sunlight and converts it into thermal, passing through a clear working fluid such as oil, water and EG (Zayed et al., 2019b). The disadvantages of FPSCs are the low convective heat transfer coefficients and low thermal efficiencies between working fluid and absorber. Therefore, enhancing the efficiency of solar collectors has become one of the current development areas. Working fluid is a critical feature that affects the thermal performance of flat plate collectors. One of the methods of increasing the efficiency of solar collectors to use NPs in solar collectors (Ramezanizadeh et al., 2018; Sarsam et al., 2015; Tagliafico et al., 2014). With the advancement in material technology, the possibility of high-performance NF has been realised. Moreover, key parameters such as size and kind of NP, mass flow rate, particle concentration and collector area can influence the thermal efficiencies of FPSC. This part will provide various recent studies associated to the potential enhancing the efficiency for the utilisation of nanofluids within FPSC (Huang and Marefati, 2020; Liu et al., 2020).

Sint et al. (2017) conducted theoretical analysis of how the use of a CuO/water nanofluid impacted the performance of an FPSC under a laminar flow regime. Their analysis was dependent on calculating the thermal efficiency as a function of the nanoparticles' volume concentration and size. The findings showed that an improvement in energy efficiency occurred when the concentration was increased up to 2.0%, while the thermal efficiency was not significantly changed by the size of the nanoparticles. They reached the conclusion that an improvement of as much as 5% in FPSC efficiency could be achieved when using 2 wt% CuO/water nanofluid with a mass rate of 1.2 kg/min.

Amini and Kianifar (2016) conducted analysis on the effects of dispersing nanoparticles of Fe_3O_4 and MgO in the base fluid of the FPSC. Their investigation involved concentrations of between 1% and 4%. Their findings showed that when the nanofluid used comprised Fe_3O_4/water, it was possible to obtain increased values for nanofluid outlet temperature, energy and exergy efficiencies compared to when a MgO/water was used, with a concentration of (4% wt.) and mass flow rate of 0.75 kg/min. The experimental study of Noghrehabadi et al. (2016) examined a square FPSC with a nanofluid of SiO_2/water nanofluid and a weight concentration of 1% under turbulent flow and laminar regimes. The researchers found that in tests involving mass flow rates of 0.5 kg/min and 2.8 kg/min, improvements of 1% and 2.5% were respectively recorded when 1 wt% SiO_2/water nanofluid was employed. In the study of Anin Vincely and Natarajan (2016), the FPSC was investigated employing nanoparticles of GO in an absorbing liquid comprised of deionized water (DI). Analysis was conducted on the impacts of various nanofluid concentrations (0.005%, 0.025% and 0.05%). Additionally, measurements of the characteristics of the GO-nanofluid including the viscosity, thermal conductivity, and specific heat as well their impacts with regard to temperature were examined. The conclusion was reached that when 0.02 wt% GO nanofluid was used, increases of 7.3% and 11.5% in thermal efficiency and heat transfer were respectively observed in comparison to water at a mass flow rate of 1.002 kg/min.

Hajabdollahi and Premnath (2017) reported that the thermal efficiency of a nanofluid of CuO/water nanofluid was maximised when the volume concentration was lower compared with different nanofluids like SiO_2/ water and Al_2O_3/water as a result of the increased thermal conductivity level. According to the thermo-economic analysis, a reduction of 27.88% was achieved in the yearly costs when a nanofluid of CuO/water was used at a constant effectiveness 0.564. The nanofluid of Al_2O_3/water was regarded as being a superior to HTF as its weight is lower and less maintenance is required.

Choudhary et al. (2020) performed an experiment whereby MgO nanofluids were examined to find out if these nanofluids were stable enough to be introduced in a FPSC. For this experiment, they added different nanoparticle concentrations, ranging from 0.08 to 0.4% to the base fluid to determine changes in nanofluid stability. The results depicted that the nanofluid's stability was higher in the case of 0.04% concentration. In addition, the nanofluids showed maximum thermal efficiency of about 69.1% inside the FPSC, at 0.2% concentration and 1.5 lit/min volumetric flow rate. Hence, the addition of nanoparticles led to 16.36% higher thermal efficiency than the EG/ water base fluid.

Salavati Meibodi et al. (2015) attempted to discover performance and thermal efficiency of nanofluid when employed in the FPSC experimentally whereby they introduced nanofluid prepared with SiO_2 particles in a mixture of Ethylene glycol (EG) and water. They considered a 1.59 m^2 collector plate area, volume concentration of 0.5%, 0.75%, 1% and mass flow rate of

0.018, 0.032, and 0.045 kg/s in this experiment. The thermal efficiency changed from 4% and 8% as the nanoparticle concentration in the working fluid was changed from 0.5% to 1% provided the heat loss parameters are kept zero. However, in the presence of heat loss parameters, the nanofluid with lower nanoparticle concentration offers greater stability and proves more economical. The mass flow rate was observed to exert positive effects on efficiency. Hence, they revealed that FPSCs are expected to deliver higher efficiency when SiO_2 nanofluid is used.

Kiliç et al. (2018) found out that FPSC yielded an increment in the thermal efficiency from 36.20% (for the pure water) to 48.67% (for TiO_2/water nanofluid). TiO_2 addition has increased the thermal efficiency since TiO_2/water nanofluid is characterized by high specific heat capacity when the volume concentration is 0.2% and the mass flow rate is 0.033 kg/s. The theoretical investigation made by Tiwari et al. (2013) deliberated the Al_2O_3/water usage inside the FPSC. The nanofluid acted as an absorbing medium for collecting solar energy to be used for heating the water. The theory considered various volume concentrations of nanoparticles between 0.5% and 2%. They studied how the FPSC efficiency changed under the particle volume fraction and mass flow rate changes. They found a nearly 31.64% increment in the FPSC thermal efficiency at optimum particle volume fraction 1.5% as compared to the FPSC efficiency-based water.

Zamzamian et al. (2014) used a nanofluid prepared by dispensing Cu-synthesized nanoparticles in ethylene glycol base inside an FPSC to identify the effects of this nanofluid on collector efficiency. The nanoparticles considered in this experiment were estimated to have about 10 nm average diameter and 0.2% and 0.3% of nanofluid weight fractions. The volume flow rates fluctuated between 0.016 and 0.050 kg/s throughout the experiment. The results showed higher collector efficiency as the concentration of nanoparticles increased in the working fluid.

Syam Sundar et al. (2021) considered the FPSC containing ND-CO_3O_4/water hybrid nanofluid. The FPSC depicted a considerable rise in thermo-physical properties and rate of heat transfer of ND-CO_3O_4/water hybrid nanofluid. Consequently, the absorber showed better energy efficiency than the efficiency obtained while it was filled with water. The FPSC showed a maximum rise in thermal conductivity around 15.71% and a nearly 45.83% rise in dynamic viscosity when the temperature is set at 60 ℃ and a concentration of 0.15 by weight. At this concentration of 0.15% by weight of nanoparticles, the Nusselt number (Nu) showed about a 21.23% rise while the maximum friction penalty showed 1.13 times increase in comparison to that obtained with base fluid, H_2O. The absorber showed 59% efficiency when filled with 0.15 wt% of nanofluid whereas it showed 48% efficiency when filled with water.

Concerns and limitations can be pointed in use of nanofluids in FPSC technology as follows: (a) Continuous and long-term usage of NFs in the solar collectors causes erosion and corrosion of walls of thermal equipment, (b) Higher cost for operating and production of NFs is a major threat in the use of NFs in solar collectors,(c) Another drawback is the inclination of nanoparticles to sedimentation in base fluids at long-term utilizing of nanofluids in solar collectors, (d) The addition of NPs in the base fluid results raise in viscosity of NFs. Therefore, due to which there is increased pressure drop and thus higher pumping power is required.

2.4. Computational fluid dynamics

The technology of Computational Fluid Dynamics (CFD) is employed for modelling various phenomena occurring inside solar collectors like fluid flow, chemical reactions, and heat transfer. The study on solar collectors took a new turn with the revolution brought about by computers in

computational capabilities. Various researchers investigated solar collectors by employing commercial simulation tools for the application of numerical CFD simulations. Numerous studies have used numerical simulations and modelling for investigating flat plate solar collectors filled with nanofluids.

Moghadam et al.(2017) studied the 3D Al_2O_3/water NF in flat plate solar collector by ANSYS Fluent at 30 inclination angles. The NF was Al_2O_3/water with different concentrations of 0%-4% and particulate matter diameter 25–100 nm. With the Reynolds number increase, the coefficient of heat transfer from convection to conduction increased, the Richardson number increased, and the increase in the Richardson number and the particle volume fraction decreased. Results show that when NF is introduced, the heat transfer coefficient increased from 45% to 58%. The simulation also showed that entropy is generated quickly as the number of Reynolds increases and as the number of Richardson and the concentration of increased NF decrease. When a particle size of 25 nm increased the Richardson number, the pressure drop was significant. Although the Richardson number was considered constant, the pressure decrease value was reduced. The efficiency of FPSC in this study improved by 2% compared with the previous literature.

Genc et al. (2018), conducted a transient numerical study on FPSWH using a nanofluid of alumina-water with proportions of 1%, 2%, 3% and mass flow rates of 0.004 kg/s and 0.06 kg/s. At a mass flow rate of 0.06 kg/s, the thermal efficiency of FPSWH peaked at 83.9%, while when the mass flow rate was reduced, an increase in 7.2% in the outlet temperature was observed with a fraction of 3%.

Hawwash et al. (2018) used water and alumina fluids in the concentrations of 0.1%-3% for FPSC. A computer simulation was performed with a single-phase with temperature-dependent properties in an ANSYS/FLUENT study. The thermal efficiency of FPSC was most optimal when a concentration of 0.5% exists. Adding NPs with volumes above 0.5% does not enhance the solar collector's efficiency due to NPs' agglomeration.

Moravej et al. (2020) examined the results of a study using the asymmetric square absorbers of TiO_2/H_2O NF instead of H_2O as circulating fluids. Increases in solar irradiance or flow rates are influenced thermal performance. The highest increase in efficiency was about 78% with 1 wt% TiO_2/H_2O, representing the highest and average efficiency gains of 9.80% and 6.64% compared with H_2O. In addition, efficiency rates of 1 wt%, 3 wt% and by 5 wt% were improved by 17. 41%, 27.09% and 33.54%, respectively.

Bazdidi-Tehrani et al. (2018) developed a 3D numerical model of a ribbed absorber using TiO_2 - H_2O and CuO-H_2O NFs. An increase in the volume percentage of NPs moderately improved the solar collector's efficiency. The ribbed absorber in comparison with the plain duct shows a rise of around 10%. The CuO/H_2O sample provided more energy efficiency than the TiO_2/ H_2O sample compared with the NFs tested. Therefore, the performance achieved the highest value by 2.04 Vol % of CuO/H_2O NF at 89%.

Farajzadeh et al. (2018) investigated the thermal performance of FPSC (1.85 m^2) with the same concentration ratio of the Al_2O_3 -water (20 nm at 0.1%) and TiO_2-water (15 nm at 0.1%). The NFs were prepared using CTAB as a surfactant by a two-step method. The experimental and numerical investigation software was used for ASHRAE standard 93 and open-source computational fluid dynamics (CFD). Different flow volume rates at 1.5 l min^{-1}, 2.0 l min^{-1} and 2.5 l min^{-1} were considered. Based on the experimental results, a 0.1 mass% increase of Al_2O_3-water, TiO_2- water

and 0.1 mass% of its mixture were observed in the thermal efficiency compared with 21% and 26% (water). The thermal efficiency was further enhanced with the mixture concentration from 0.1% to 0.2% mass. As NPs from TiO_2 are more expensive than Al_2O_3, their mixtures are more economical and efficient. Table 2.1 presents a summary of other earlier studies deal with the FPSC energy and exergy efficiencies enhancement adopting different nanofluids.

Table 2.1. A summary of recent studies on FPSC using nanofluids

References	Type of study	Base fluid	NPs	Remarks
Tong et al. (2020)	Exp	W	WO_3, CeO_2, and Al_2O_3	• The use of Al_2O_3 nanofluids led to a maximum efficiency of 87%. • The WO_3 nanofluid depicted the least amount of heat loss coefficient. • The CeO_2 nanofluid showed high sensitivity performance.
Michael et al. (2020)	Exp	W	CeO_2	• At a concentration of 0.05% and flow rate of 2 l/h, the collector with nanofluid depicted a 28% rise in maximum efficiency along with a 5.8% rise in maximum exergy. The collector area showed a 24.52% maximum reduction.
Hussein et al. (2020)	Exp	W	CF-MWCNT	• At a 4 l/h flow rate, the collector showed a 21.9% rise in efficiency at the concentration of 0.1 while an 11.8% rise for 0.05% concentration.
Sundar et al. (2020)	Exp	W	Cu	• The collector without twisted tapes indicated 58% efficiency while that with twisted tapes depicted 65% efficiency at a volume fraction of 0.3 %. • The maximum reduction in collector area was found to be 11.53%.
Sarsam et al. (2020)	Exp	W	GNPs	• The use of 0.1% GNPs in solar collectors resulted in a maximum efficiency enhancement of 10.53%. • The results showed consistency between the theoretical values and values obtained during the experiment.
Akram et al. (2019)	Exp	W	GNP	• In comparison to base fluid, the use of a 0.1% concentration of nanoparticles in the fluid yielded an 18.2% maximum rise in collector efficiency.
Verma et al. (2016)	Exp	W	MgO	• The collector depicted a maximum rise of 9.34% in thermal efficiency while its exergy efficiency showed a maximum rise of 32.23% for a volume concentration of 0.75 % and flow rate of 1.5 l/min.
Yousefi et al. (2012)	Exp	W	MWCNT	• The collector yielded maximum efficiency at a flow rate of 0.05 kg/s for 0.4 wt% concentration.
He et al. (2014)	Exp	W	Cu	• A maximum rise of 23.83% was observed in collector efficiency.
Michael and Iniyan (2015)	Exp	W	CuO	• Maximum rise of 6.3% was observed in the collector's efficiency.
Ahmadi et al. (2016)	Exp	W	Graphene	• In the beginning, as the mass flow rate was increased, a rise in collector efficiency was observed. However, a further increase in mass flow rate resulted in a decline in efficiency. At 0.015 kg/s flow rate, the collector showed maximum efficiency.

Kumar et al. (2021)	Exp	W	GNPs	• A maximum rise of 24.09% in efficiency was noted at a concentration of 0.1 wt% and a flow rate of 1.5 l/min. • At 0.1 wt%, the exergy efficiency increased by 5.3%.
Kim et al. (2017)	Exp	W	Al_2O_3	• The solar collector filled with Al_2O_3 nanofluid in 1 vol% concentration of particles with 20 nm size depicted a maximum rise of 24.1% in efficiency at 0.047 kg/s mass flow rate.
Devarajan and Munuswamy (2016)	Exp	W	Al_2O_3 and CuO	• The efficiency of the collector for different working fluids was noted as follows; water (38%), Al_2O_3 (55%) and CuO (51.3%).
Munuswamy et al. (2015)	Exp	W	Al_2O_3 and CuO	• The enhancement efficiency of the FPSC for different working fluids was noted as follows; Al_2O_3 (12%) and CuO (7%).
Jamal-Abad et al. (2013)	Exp	W	Cu	• The collector filled with 0.05 wt% of nanofluid showed 24% higher efficiency than the collector filled with pure-base fluid.
Goudarzi et al. (2014)	Exp	W	CuO	• The collector showed a maximum rise of 25.6% at 0.1 wt% nanofluid and a mass flow rate of 0.0083 kg/s.
Alawi et al. (2019)	Exp	W	GNP	• In comparison to water, solar collectors filled with 0.1% GNP showed a 13.3% maximum rise in efficiency.

2.5. Summary of literature review

The increasing energy demand and continuous confrontation of energy generation costs are preceded by a terrible depletion of fossil fuel power reserves and increased environmental pollution. Thus, the present era belongs to renewable energy as it is eco-friendly and allows more energy generation. Flat plate solar collectors (FPSC) are well-known and widely used, thus utilised in low and medium thermal different domestic applications. However, FPSCs are less efficient due to their limited ability of solar energy to be converted into thermal energy due to the inefficient heat transfer in solar fluids on the collector's flow tubes. Recently, scientists have laid great emphasis on the significance of nanoparticles. Replacing traditional base fluids in FPSC with nanofluids offers various benefits enhancing the collector efficiency. According to the literature review, the subsequent points will present a detailed discussion of the all-research gaps and the key contributions of this study to bridge gaps are as follows:

- The above-mentioned review indicated studies revealed no detailed investigation of on the properties of zirconium oxide (ZrO_2) and silicon carbide SiC nanoparticles specifically when used in FPSC. Another reason behind this study selected the zirconium oxide (ZrO_2) and silicon carbide (SiC) due to have various properties of these nanoparticles. Some of these properties have been listed as follows: (a) The easy availability, accessibility, and preparation of SiC and ZrO_2 nanoparticles make them preferable for use in various applications, (b) The easy availability of ZrO_2 and SiC nanoparticles makes them financially affordable, thus supporting sustainability, (c) The particles are also found to be eco-friendly due to their non-combustible and nontoxic nature, and (d) ZrO_2 and SiC nanoparticles are more stable in water than other nanoparticles.

- The literature review shows that numerous previous studies have discussed the methods used to prepare nanofluids. However, the author of this study does not know any study that sheds light on the preparation of SiC/DW, ZrO_2/DW, and ZrO_2-SiC (50–50%)/DW hybrid nanofluid.
- The literature review also suggested a lack of studies focusing on SiC/DW, ZrO_2/DW, and ZrO_2-SiC (50–50%)/DW hybrid nanofluid and its contribution to enhancing the efficiency of flat plate solar collectors. Hence, the gap in the literature will be bridged by this study that aims to explore how the efficiency of FPSC changes when filled with a hybrid nanofluid instead of the base fluid. The study will also explore how the thermodynamic properties of the FPSC change when filled with nanofluids. In this regard, the study will evaluate the factors of entropy generation, exergy analysis, Nusselt number, and exergy destruction. The researcher emphasizes the importance of this study as being the pioneer in exploring the use of these nanofluids and its effects on the performance and efficiency of the FPSC. This research may serve as a guide for future researchers to identify the potential of nanofluids to be used in renewable energy applications.
- This study is the first study that evaluates the solid volume fraction as well as the temperature of SiC/DW, ZrO_2/DW, and ZrO_2-SiC (50–50%)/DW hybrid nanofluids to determine the thermal conductivity, rheological behaviour, and dynamic viscosity of the given nanofluids. The devices used in this evaluation included the Brookfield rotational viscometer and KD2-Pro thermal properties analser. I examined the numerical results for the temperature between 20 and 60 °C generally recommended in the literature, and for nanofluids with 0 - 0.1 wt% concentration. The ranges can of course be changed according to the requirements of the application area. The temperature range I examined is just right for summer use as a solar liquid in a flat plate collector, but e.g. in the case of yearly operation, the analyzation of the properties should be extended to a wider temperature range.
- Various techniques were employed in this work for studying nanofluid properties like particle size and shape, fluid stability, and distribution as follows: (a) The nanoparticles have an ultrafine structure and hence their structure is studied with the help of a scanning electron microscope (FESEM), (b) The nanofluid stability is estimated based on their dispersion value by using the Zeta potential, and (c) The crystal structure is examined through images obtained from X-ray diffraction (XRD).

Lastly, to the best of the authors' knowledge, the current study is a pioneering attempt and offers an insight into the prospects to investigate the efficiency of a flat plate solar collector utilizing nanofluids of SiC/DW, ZrO_2/DW, and ZrO_2-SiC/DW. Hence this study intended to overcome all research gaps highlighted above and consider different types of nanofluids. The study also indicated that given nanofluids have good thermal properties that can facilitate heat transfer in solar collectors. Additionally, the study also explains that incorporating multiple types of nanoparticles in the fluid forms the hybrid nanofluids which outperform the nanofluids and may yield incredible outcomes when applied in the domain of solar collector. Moreover, this research can be used in future works to explore the potential of applying the given nanofluids in renewable energy applications.

3. MATERIALS AND METHODS

This chapter presents the experimental methodology, materials, instrumentation, procedures, and processes used in the research, including the scientific methods involved in the experimental measurements and the description of the test systems to obtain the set research objectives.

3.1. Experimental methodology

This paper comprised three sections, in which the first one presents various techniques like XRD and FESEM are engaged for the nanoparticle's characterization, particle shape and evaluating of nanofluids. In the same section, nanofluid preparation will be discussed and zeta potential measurement will be applied to determine the stability of mono nanofluids (SiC/DW and ZrO_2/DW) and hybrid nanofluid (ZrO_2-SiC (50:50%)/DW). Moreover, the given nanofluids thermo-physical properties are studied including their dynamic viscosity, rheological behaviour, and thermal conductivity. In the second section, the experimental setup used for the analysis of the flat plate solar collector are described, along with information on the approach used for testing, and a discussion on the different equations needed to calculate the range of efficiencies and parameters. Also, the uncertainty analysis will be presented to determine the uncertainty in the evaluated parameters. In the third section, this part sheds light on the numerical modelling of the fluid flow inside the pipes of FPSC, computational fluid dynamics (CFD) is used to analyse the thermal and exergy efficiencies of collector.

3.2. Preparation and thermophysical properties of nanofluids

3.2.1. Material

In the present study, nanofluids for ZrO_2/DW, SiC/DW, and ZrO_2-SiC (50:50%)/DW samples at volume fractions of 0.025, 0.05, 0.075, and 0.1 % were created by dispersing nanoparticles of ZrO_2 and SiC into the distilled water. The ZrO_2 and SiC nanoparticles were purchased from US Research Nanomaterials, Inc. The specifications of zirconium oxide and silicon carbide were given in Table 3.1. The images of zirconium oxide and silicon carbide nanoparticles are shown in Fig. 3.1.

Table 3.1. Physical and chemical properties of zirconium oxide and silicon carbide nanoparticles

Properties	**Zirconium Oxide**	**Silicon Carbide**
Chemical formula	ZrO_2	SiC
Purity (%)	99.95	99
Colour	white	grayish white
Morphology	near spherical	cubic
Specific Surface Area (SSA) (m^2/g)	30-60	40-80
Actual particle size (APS) (nm)	20	45-65
Stock code	US3659	US2028
CAS No.	1314-23-4	409-21-2
Density (ρ) (g/cm^3)	5.89	3.216
Specific heat (J/kgK)	455	680
Thermal conductivity (W/mK)	2.7	370

Fig. 3.1. Images of zirconium oxide and silicon carbide nanoparticles

3.2.2. Instrumentations

In this study, ZrO_2 and SiC nanoparticles and samples of nanofluids were characterized by various techniques. The X-ray diffraction (XRD) (GNR company, model: Explorer, Italy), was recorded using the radiation (X-rays) with wavelength (Cu-Ka = 1.541874 Å) at 20℃ room temperature with a resolution of 0.010 (step size). The shapes and compositions of the ZrO_2 and SiC nanoparticles were studied by field emission scanning electron microscope (FESEM) (Model: TESCAN MIRA3, Czech). Moreover, the stability of nanofluids examined by Zeta potential analysis with Zeta compact (Zeta meter, CAD Instruments, France). For synthesis of nanofluids with various solid volume fraction of nanoparticles a special amount of zirconium oxide and silicon carbide nanoparticles were weighted by advanced analytical balance (A&D Weighing, GE-320, USA). Afterward, the ultrasonic processor (PS 30A 6L, Germany) and magnetic stirrers (HS-12, HU) were used for prevention of nanoparticles agglomeration. The thermal conductivity of nanofluids was measured by KD2 Pro thermal property analyser (Decagon devices, USA). A hot-water bath (Thermal /Haake C10 K20 Digital Control, Artisan Technology Group, USA) was used to maintain and control the temperature while measuring thermal conductivity. The dynamic viscosity was measured by Brookfield rotational viscometer (Model: DV2TRVTBG, USA). All images of the devices used for given nanofluids in this study are shown in Fig. 3.2.

Fig. 3.2. Laboratory devices: (a) XRD, (b) FESEM, (c) Zeta potential analyser (d) Magnetic-stirrers, (e) Digital scale, (f) Ultrasonic, (g and h) KD2-Pro plus temperature control, and (k) Rotational viscometer

3.2.3. Characterization of nanoparticles

The crystal structure of the nanoparticles was examined using the XRD technique. In this method, an X-ray beam is passed over the nanoparticle sample that gets spread because of the various atoms, which are used to examine the crystalline size. The ZrO_2 and SiC nanoparticles were subjected to X-ray diffraction analysis. When using an XRD instrument, the positions of X-ray beams (both incident and reflected beams) and samples are changed to achieve an appropriate distance required for better focus. The angle of incidence and the angle of reflection are equal to θ (theta), making the angle between the reflected and incident X-rays equal to 2θ. The sample's crystallinity is reflected graphically from the peak intensity. The researcher used a GNR Explorer,

Italy, X-ray diffraction analysis for XRD tests. The test involved the application of (Wavelength, Cu -Kα = 1.541874 Å) radiation at an angle of 2θ (20° to 80°). Fig. 3.3 presents the position of peaks and their intensities in the XRD analysis of ZrO_2 and SiC nanoparticles. There's a strong peak at an angle of 28.29 degrees (2θ) for ZrO_2 nanoparticles. Also, the SiC nanoparticles showed typically sharp peaks at 2θ=35.78°, and some smaller peaks can be seen on the graph too.

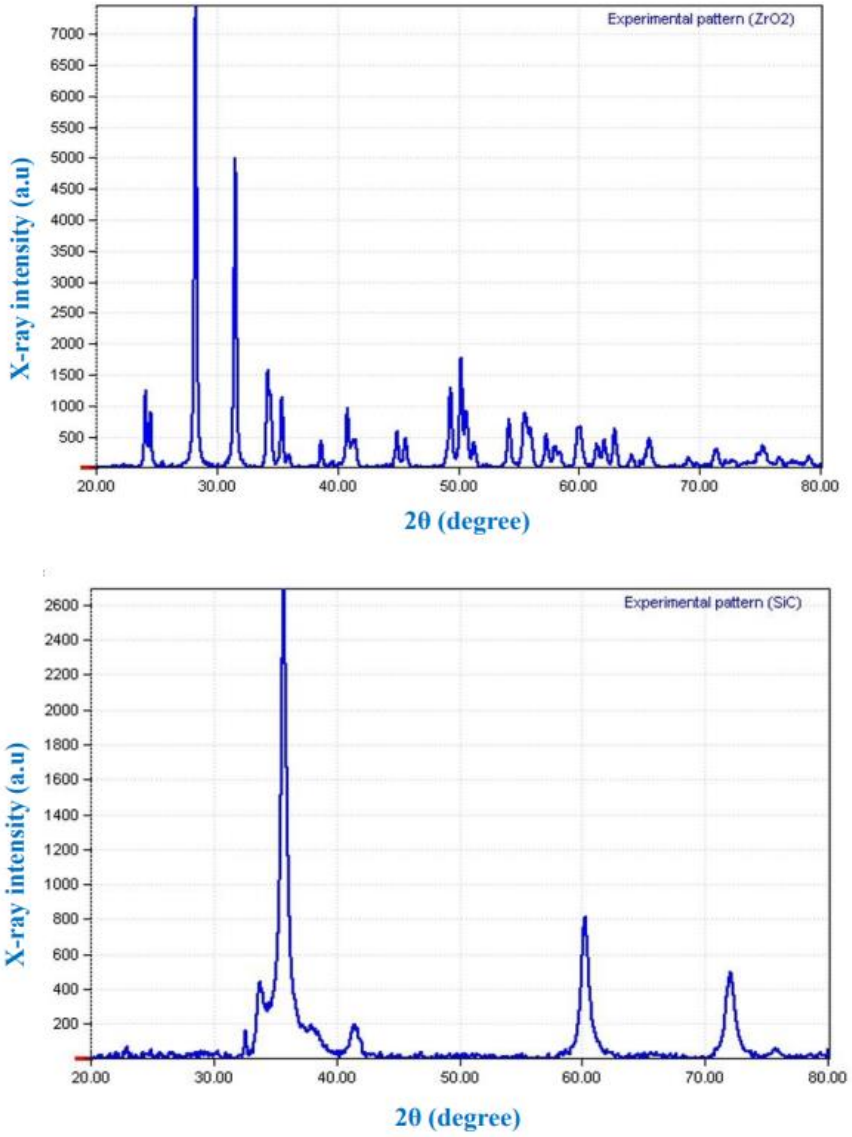

Fig. 3.3. X-ray diffraction pattern with analysis for ZrO_2 and SiC nanoparticles

The morphology of the synthesized silicon carbide and zirconium oxide nanoparticles was examined using field emission scanning electron microscopy (FESEM). The FESEM images with the magnification scales of 200 nm, 500 nm and 1 μm of the silicon carbide and zirconium oxide nanoparticles are shown in Fig. 3.4. Weakly agglomerated and roughly near spherical morphology for ZrO_2 particles and cubic shape for SiC particles with smaller sizes can be seen. A vital part was played by the capping agent in avoiding the tendency of agglomeration and merging of nanoparticles. As a result of their interconnected structure and planar surface, nanoparticles of silicon carbide and zirconium oxide are capable of creating conduction paths via the formation of networks.

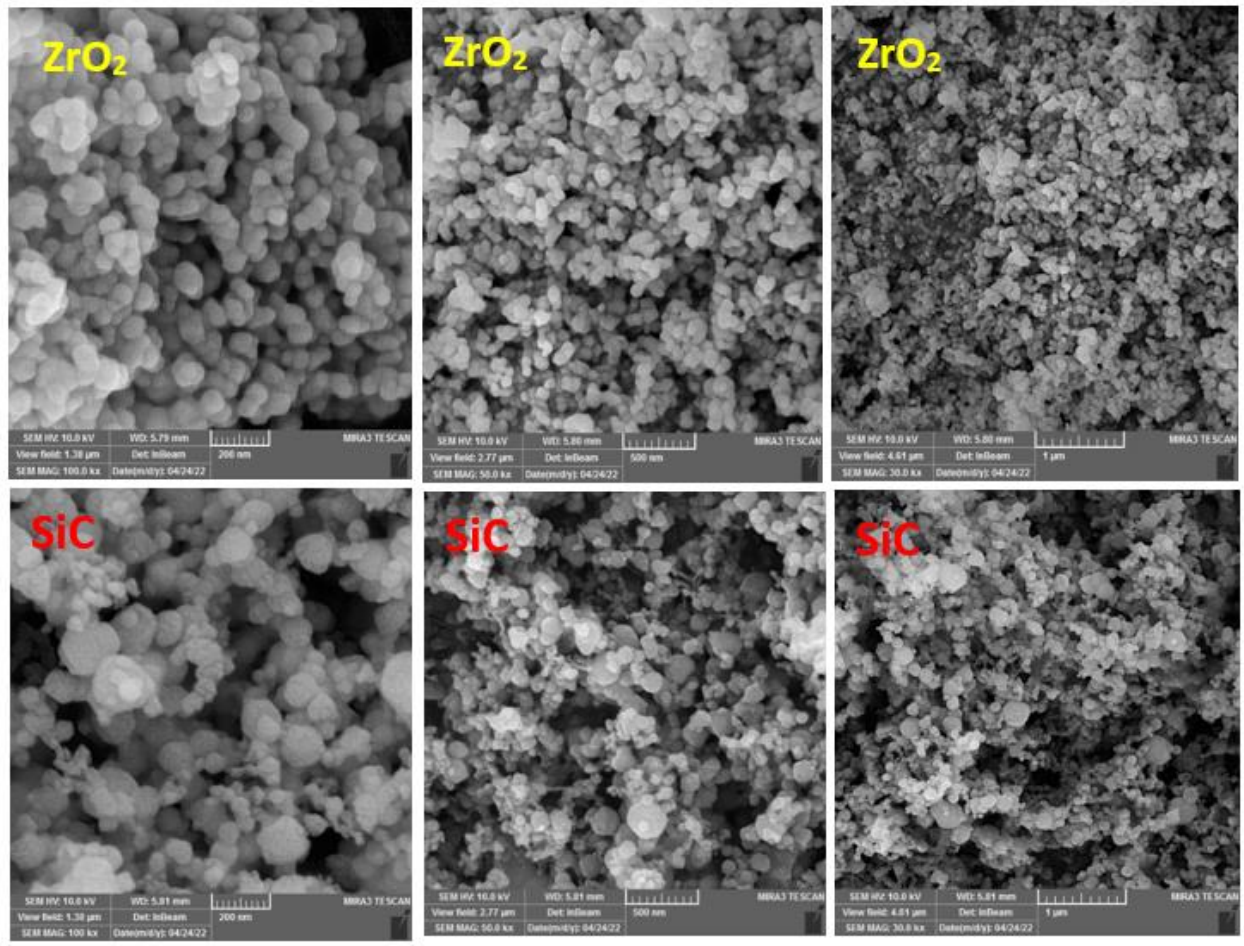

Fig. 3.4. FESEM images with different magnifications on ZrO_2 and SiC nanoparticles

3.2.4. Preparation of nanofluids

A two-step approach was used to obtain samples of ZrO_2/DW, SiC/DW, and ZrO_2-SiC (50:50%)/DW nanofluids. Subsequent to weighting, nanoparticles of ZrO_2 and SiC at the intended solid volume fraction (0.025, 0.05, 0.075, and 0.1%) were added to purified water. It was necessary to firstly calculate the necessary mass amounts before the various nanofluid fractions could be prepared. For the purpose of calculating the nanoparticle and base fluid values and the respective amounts needed to prepare various volume fractions, Eq. (3.1) was employed:

$$\varphi = \left[\frac{\left(\frac{m}{\rho}\right)_{nanoparticles}}{\left(\frac{m}{\rho}\right)_{nanoparticles} + \left(\frac{m}{\rho}\right)_{DW}} \right] \times 100 \qquad (3.1)$$

A digital scale with high sensitivity was used for measuring the materials' weight. When the experiment started, computation of the mass amounts was performed in terms of the nanoparticles' density. Subsequent to the addition of nanoparticles to the water, the mixture was stirred using a magnetic stirrer for approximately 1.5 h. Afterward, suspensions were entered into an ultrasonic processor for the process of breaking down the agglomeration among the particles as well as preventing sedimentation, ensuring the particles were uniformly dispersed and the suspension was stable; this process lasted approximately 3–4 h. Fig. 3.5 shows preparation process of the given

nanofluids. Finally, a zeta potential test is performed to check the stability of the prepared samples of nanofluids. The photographs of the prepared nanofluids are depicted in Fig. 3.6.

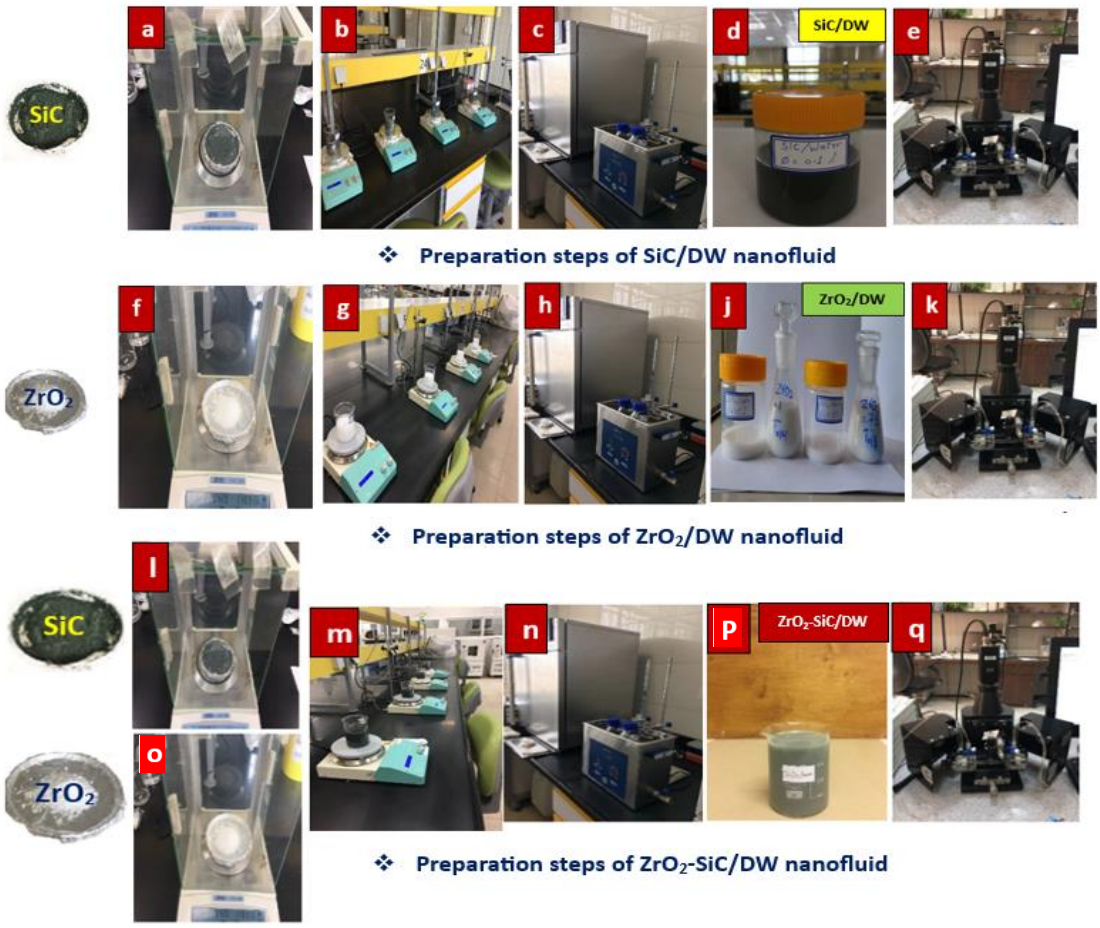

Fig. 3.5. Preparation process of ZrO_2/DW and SiC/DW, and ZrO_2-SiC/DW nanofluids: (a, f, l, o) Digital scale, (b, g, m) Magnetic stirrers, (c, h, n) Ultrasonic, (d) Silicon Carbide nanofluid, (j) Zirconium Oxide nanofluid, (p) ZrO_2-SiC/DW hybrid nanofluid, and (e, k, q) Zeta potential analyser

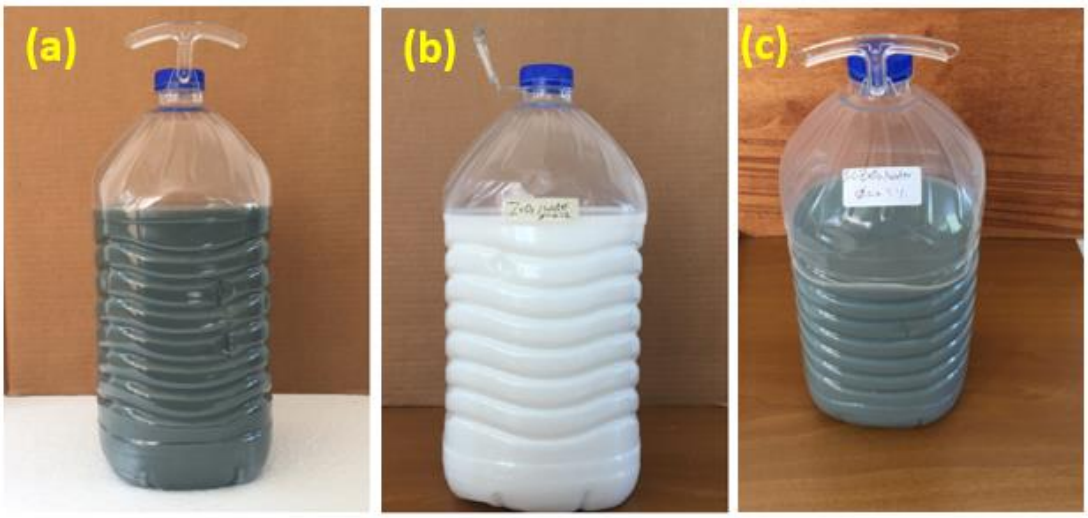

Fig. 3.6. Nanofluids (a) SiC/DW, (b) ZrO_2/DW and (c) ZrO_2-SiC/DW

3.2.5. Measurement of thermal conductivity

Several methods can be used to measure thermal conductivity. They include the guarded hot plate method, the heat-flow meter, the hot wire, and laser flash diffusivity methods. The transient hot-wire method is used to measure thermal conductivity in this research. A KD2-Pro device from Decagon devices Inc was used for measuring the thermal conductivity of the three nanofluids; ZrO_2/DW, SiC/DW, and ZrO_2-SiC/DW in this study at volume concentrations of 0.025%, 0.05%, 0.075%, and 0.1% for 20 °C to 60 °C temperatures. A hot-water bath was used to maintain and control the temperature while measuring thermal conductivity. A horizontal stand was placed next to the temperature bath to align the KS-1 probe vertically in the centre of the sample vial and prevent it from moving. The sensors, KD2 Pro KS-1, 60 mm long with a diameter of 1.27 mm, were inserted in the nanofluids' vials. A sensor is put in the sample fluid, and the temperature response time is recorded. The thermal properties of a material, such as thermal conductivity, determine the temperature response time. The only measurable property is heating conduction. Liquids can transfer heat through convection, which may lower heat transfer by conduction. Therefore, heat transfer by convection needs to be insignificant when determining the amount of heat transferred through liquids. Heat transfer by convection occurs when the fluid moves, which means it can be kept to a minimum by preventing the sample fluid and the sensor from moving. Thermal conductivity was recorded after every 60 s. The heat was changed every 30 s, and the temperature was allowed to equilibrate for 30 s before heating was done again. The experiment was repeated three times in all the volume fractions and temperatures with an interval of 5 min for the accuracy of the results.

3.2.6. Measurement of dynamic viscosity

In the current study, a Brookfield DV2TRVTBG rotational viscometer was used for measuring the ZrO_2/DW, SiC/DW, and ZrO_2-SiC/DW nanofluids' viscosity as well as for identifying their rheological characterization when influenced by varying parameters. Such viscometers function by taking measurements of fluid's resistance caused by the torque from the spindle placed into the fluid. Additionally, to ensure the temperature remained stable as well as to determine how nanofluids' viscosity is impacted by temperature, a temperature bath with significant accuracy was linked with the viscometer. Hence, this facilitated the process of conducting analysis of the nanofluids' rheological properties and viscosity according to the effects of shear rate and temperature at varying concentrations. Therefore, via the connection between the viscometer and temperature bath, the parameters of the experiment were fixed such that the temperature ranged between 20 and 60 °C to measure the nanofluids' dynamic viscosity at different solid volume fractions. All measurements were performed using a ULA spindle that was a small for sampling adapter system. Furthermore, calibration of the viscometer was performed prior to taking measurements using water as the base fluid at an ambient temperature.

3.3. Application of nanofluids in flat plate solar collector system

3.3.1. Study location

The experiment for examining the FPSC was carried out at the forecourt of the solar energy laboratory belongs to MATE-Szent Istvan Campus, Gödöllő, Hungary shown in Fig. 3.7. The location of solar collectors plays vital role to provide efficient solar energy collection, as seen in Fig. 3.7. The collector is placed out of the shadow effect. The solar collector's azimuth and tilt

angles define its orientation. The optimum tilt angle and direction of tested FPSCs also essential in improving the solar energy collection of FPSCs. The solar collector orientation is such that it always receives the highest sun radiation throughout the day and is in a perpendicular direction to the noon solar rays. The ideal orientation in the northern hemisphere is towards the south and the north in the southern hemisphere. This is why the FPSCs are placed facing the south in this study and tilted at an angle of 45° with respect to the horizontal. Besides, the longitude and latitude of the FPSCs are 19.36° E and 47.59° N, respectively (shown in Fig.3.8). It is worth mentioning that the tilt angle has a significant impact on the energy amount captured by the system for non-tracking solar collectors. Literature studies revealed that the optimal tilt angle for solar collectors is equal to the latitude. In this experiment, a tilt angle of 45° is used, which is the ideal to receive the greatest average radiation.

Fig. 3.7. Solar energy laboratory at MATE, Gödöllő, Hungary: (a) side view, (b) front view

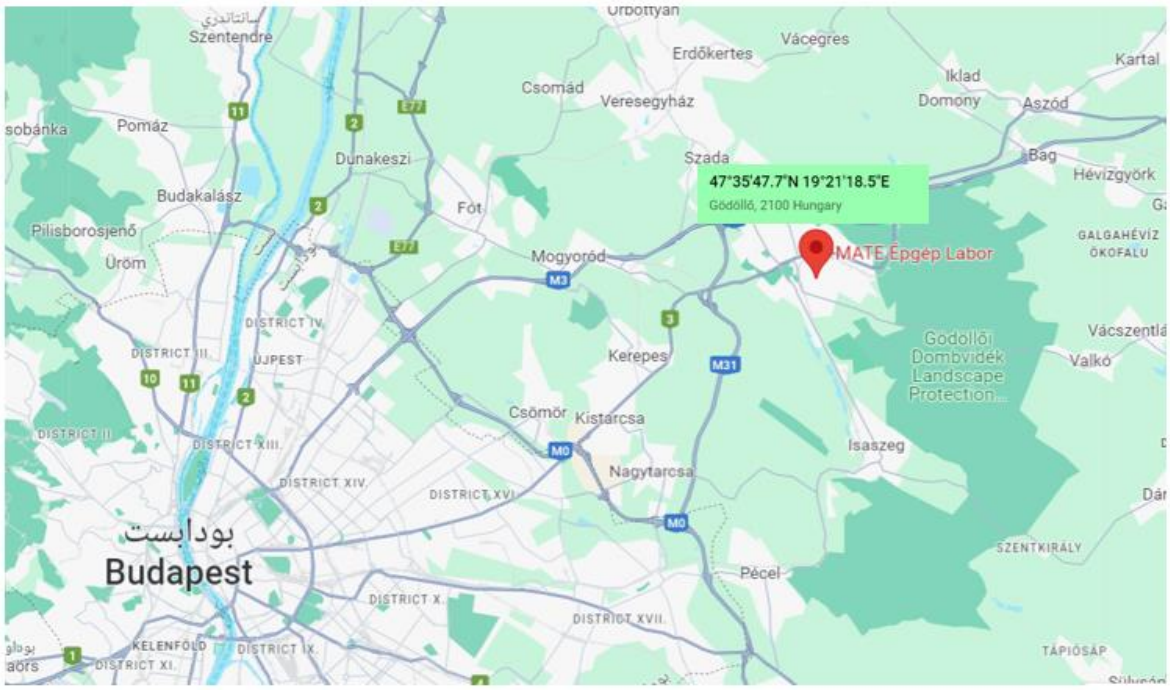

Fig. 3.8. Latitude and longitude of study location

3.3.2. Experimental setup description

The tests were performed on the FPSC in the laboratory of solar energy under the Hungarian weather conditions. Table 3.2 shows the collector specifications in which SKV-3 collector type is used that has been provided by Fiorentini Hungary Kft., a solar systems supplier in Hungary. A photograph of the FPSC and a schematic of the experimental arrangement is demonstrated in Figs. 3.9 and 3.10, respectively. The FPSC is the supreme important part of the tested system. The FPSC is kept at an angle of 45 degrees. There are two loops in the FPSC, in which the first loop comprised the working nanofluid. The nanofluid extract heat from the FPSC while circulating by a pump. This nanofluid is circulated using a pump and subsequently heating of the nanofluid is performed by the solar collector. After being heated by the collector, the nanofluid exits via the collector and passes to the heat exchanger to transmit heat to the water that passed in second loop. The hot fluid is kept continuously in the tank in the second loop. The tank has a capacity of around 50 liters. In the first loop, the nanofluids is storage in the tank around 5 liter .Various devices are used to obtain the measurements, such as calibrated thermocouples (type: K-type, TP-01, UK; accuracy: ±0.4 °C; range: -75–250 °C) to determine the inlet/outlet flow temperature, and a flow sensor to identify the fluid flow rate, which is regulated with a simple valve. A KIPP-CM11 pyranometer (model: Kipp and Zonen CM11, Delft, the Netherlands; directional error: <10 W/m^2; range: 1– 4000 W/m^2) is used to quantity the solar radiation. In addition, a thermocouple was used to measure the ambient air temperature. This study used weight concentrations of 0.025%, 0.05%, 0.075% and 0.1%. Before the electric pump (type: circulation pump for solar collector heating systems, model: Avansa 25/40/130), a flow sensor was attached to the water pipe. A simple valve was attached to the water pipe after the electric pump to regulate the mass flow rate of working fluid within the solar system. The fluid temperatures in the inlet and outlet of the FPSC were measured using four K-type thermocouples. In addition, the air temperature was measured using one thermocouple. The sensors were linked to a 12-channel digital temperature recorder with a data logger (Lutron BTM-4208SD). In addition, Wind Transmitter, First Class, Advanced Anemometer type was used

to carry out scrolling of wind speed with the uncertainty of ±0.2% (stated by the manufacturer). Interfaces can be used to connect each measuring instrument (A KIPP-CM11 pyranometer and temperature data logger) to the computer. The measuring instruments were calibrated before conducting the experiment.

Table 3.2. Specifications of the FPSC

Specification	Dimension/specification
Collector size	2030 *1100*78 mm
Absorption area	1.85 m^2
Header pipes	D=22 mm
Weight	47 kg
Riser pipes	D= 10 mm
Glass thickness	4 mm
Riser Pipe inner diameter	D=9 mm
Tilt angle	45°
Insulation layer thickness	40 mm
Martial of absorber plate	Copper
Martials of pipes	Copper
Longitude of location	19°
Latitude of location	47°
No. of riser Pipes	7
Martial of Insulation Layer	Glass wool
Fluid capacity	1.5 l
Frame	Aluminum alloy

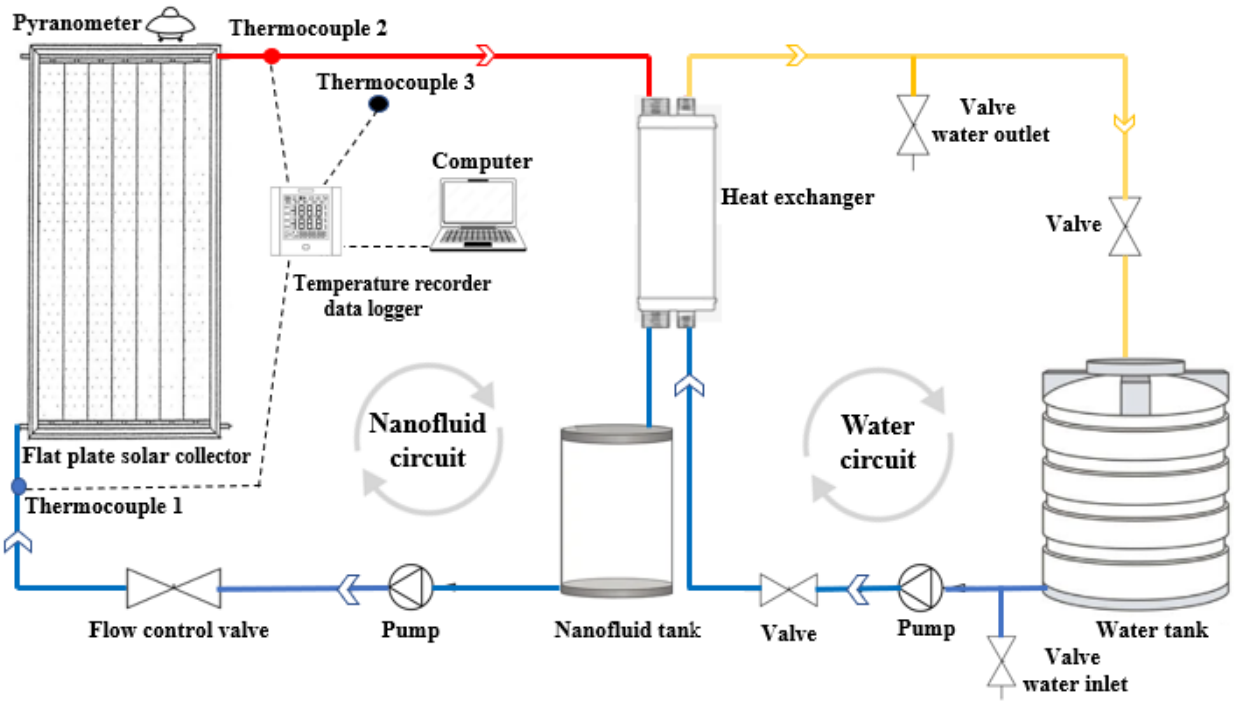

Fig. 3.9. Schematic view of the experimental system

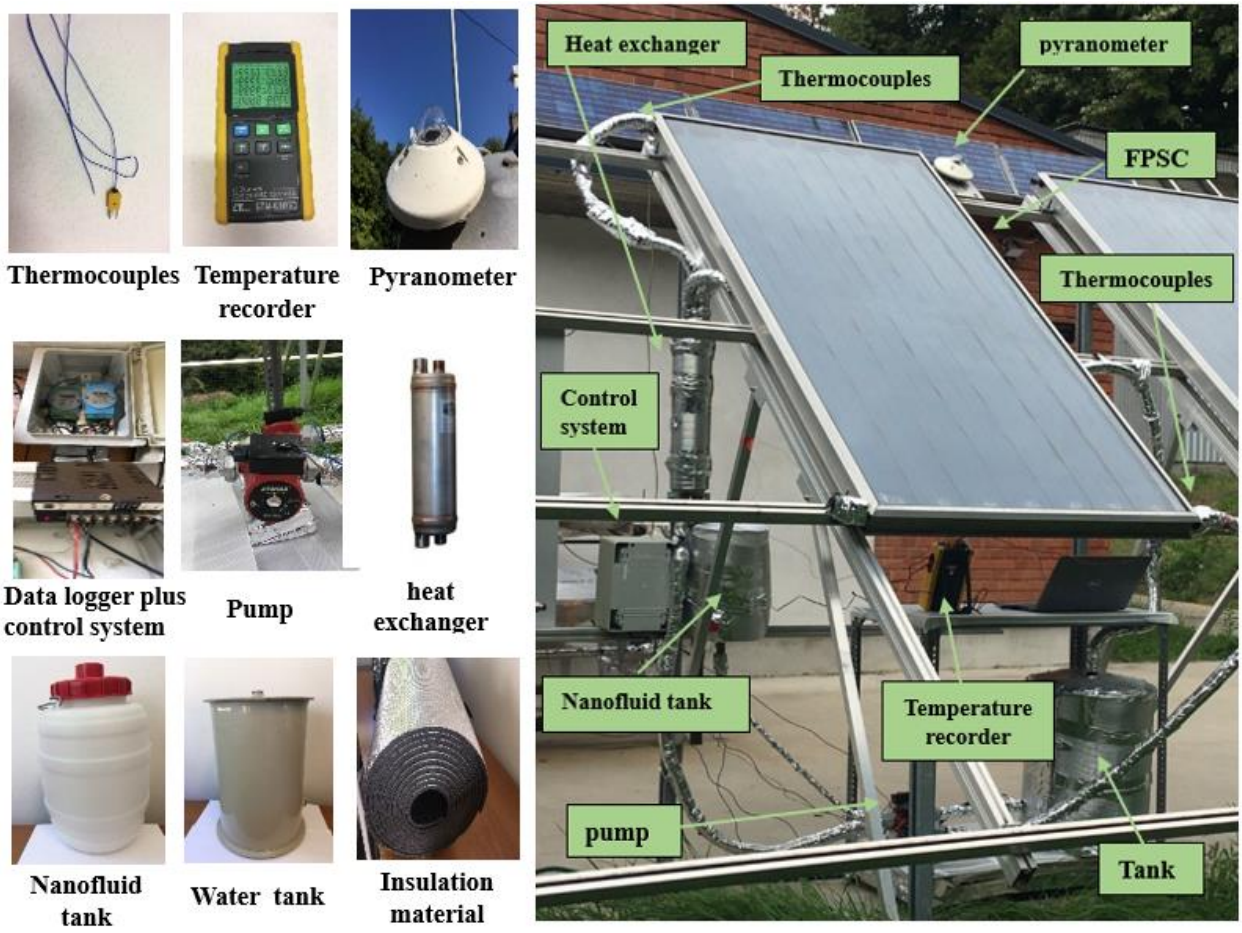

Fig. 3.10. Major components of solar system for the experimental setup

3.3.3. Experimental method

The thermal performance of the FPSC was examined using the ASHRAE Standard 93–2003. This standard has the objective of presenting test methods that could be applied to determine the thermal performance of solar collectors. Instantaneous efficiency for distinct combinations of ambient temperature, incident radiation, and inlet fluid temperature is determined to calculate the FPSC thermal performance. Data analysis and computations for the FPSC were carried out employing the first law of thermodynamics. For this, experimental measurements are required for the incident solar radiation rate, and the rate of energy added to the working fluid when it circulates into the collector, under steady-state or quasi-steady-state conditions. According to ASHRAE Standard, the tests should be accomplished in different inlet temperatures. In addition, they should be carried out symmetric to the solar noon and should fulfil certain conditions, such as the least solar radiation of 790 W/m^2. As it is mandatory to meet the steady state conditions, the mass flow rate should be kept within ± 1%, the outdoor ambient air temperature should not change by over ± 1.5 °C, irradiation should remain constant within ± 32 W/m^2, and the inlet temperature should remain within ± 1 °C for the whole test duration. Maintaining the steady-state conditions is not only important during the data period, but also during a given time period before the data curation, which is referred to as the pre-data period. Both the data and the pre-data periods are included in a test period. The pre-data period for outdoor tests that use a fixed test period of 15 min, while the data period is suggested to be a maximum of 5 min. The mass flow rates of 0.025, 0.033, 0.041 kg/s are used in our experiments. The experiments were carried out from 10 a.m. to 3 p.m. (local

time) on sunny days. There were five-time intervals in this period, with each time period (or test run) extending for 60 min. Each test run was further divided into various test intervals of 15 min to develop a quasi-steady state condition that is required according to ASHRAE Standard. Graphs were formulated to present the experimental results, which demonstrated the FPSC efficiency for a decreased temperature parameter [(Ti-Ta)/GT]. The tested runs were obtained across a span of many days and the best findings were selected. It was determined that the highest variations in ambient and inlet temperatures in each test period were ± 0.9 °C and ± 0.7 °C, respectively, whereas the highest variation in global radiation was ± 28 W/m^2. This confirms that the tests were carried out in quasi-steady state conditions and conform to the ASHRAE Standard 93–2003. The FPSC efficiency was determined at different mass flow rates of 0.025, 0.033 and 0.041 kg/s. This study involved various assumptions listed below that were taken during the experiments of the solar collector.

- The thermocouples were used to measure fluid temperature. These devices were checked and adjusted using a platinum resistance thermometer. Calibration was performed at different temperature settings to ensure that the thermocouples were accurately reading the temperatures.
- Three thermocouples were strategically placed in the pipes of FPSC. They were positioned at the fluid inlet and outlet. The readings were obtained from each of the three thermocouples and the average fluid temperature was evaluated which was found to be close to the reading obtained from the middle thermocouple.
- The area 3 m above ground level and 2 m away from the system and reservoir was considered as the ambient air. The temperature of this area was taken as the ambient temperature.
- The parts have been designed to have total isolation, allowing for the transfer of heat only to the working fluids.
- The steady or quasi-steady state is maintained while taking the readings.
- It is essential to ensure that testing is done under conditions of at least 790 W/m^2 average solar radiation when the sky is clear of clouds. The average solar radiation must not depict more than ± 32 W/m^2 deviation for two-time constants.
- All data sets must be obtained at ambient temperatures of ± 1.5 °C.
- The stability of the given nanofluid was ensured at various concentrations and flow rates.
- It must also be ensured that the average wind velocity is in the range of 2 to 5 m/s for two-time constants.
- The experiment involved multiple readings followed by an evaluation of the average reading to ensure the accuracy of the results.

In addition, the following methods were taken into consideration to achieve tested conditions throughout the outdoor experiment.

- The experimenter must ensure that the collector is exposed to sunlight without fluid flow until the fluid inside reaches a temperature equal to or slightly higher than the inlet fluid temperature. This step is essential for obtaining reliable outcomes about the efficiency of solar collectors under steady-state conditions. Then, the working fluid must be inserted and allowed to flow through the pipes exposed to the sun for at least 30 minutes. After this period, the data is collected to evaluate the thermal efficiency. Throughout the experiment,

the fluid flow rate must be consistent with only ±1% deviation. It must also be ensured that the solar radiation falls on the collector with the same intensity.

- While flowing through the pipes in the collector, the working fluid must depict a constant flow rate for each data point. This must be ensured for every reading.
- Test data should be collected both before and after solar noon. The reason behind this condition is to ensure symmetry around solar noon and to prevent bias in the collected data because of "transient effects.
- The experimenter must ensure that the exposed envelope of the pyranometer and the collector plate are free from moisture. The part particularly the pyranometer must be wiped and dried before the experiment. The main reason behind this step is to prevent dust particles and other environmental factors from affecting the thermal transfer of the envelope.
- The pre-data and data periods collectively form the test period when performing Outdoor tests. The pre-data period lasts 15 minutes, while the data period must be at most 5 minutes for steady-state conditions.
- The experimenter needs to ensure appropriate insulation of module parts due to the working fluids should receive the total transferred heat.
- The testing days must be selected keeping in view the weather conditions to ensure that Tests must be done on days with average radiation falling on the collector over 15 minutes meets the determined criteria.
- The collector must be placed where nearby buildings or surfaces won't reflect or emit significant energy onto it during the test. Also, it should be positioned to avoid any shadows falling on it during the test period.

3.3.4. Energy and exergy efficiencies of flat plate solar collector

Hybrid nanofluid characteristics are initially determined by volume fraction. Nanoparticles can be measured by their volume fraction, which is the percentage of nanoparticle volume to total hybrid nanofluid volume. The equation used to estimate the hybrid nanofluid density is as follows (Takabi and Salehi, 2014; Zhou and Ni, 2008):

$$\rho_{nf} = \rho_{np1}(\varphi_1) + \rho_{np2}(\varphi_2) + \rho_{bf}(1 - \varphi_1 - \varphi_2) \tag{3.2}$$

The hybrid nanofluid heat capacity can be determined using the formula below:

$$\left(\rho C_p\right)_{nf} = \left(\rho C_p\right)_{np1}(\varphi_1) + \left(\rho C_p\right)_{np2}(\varphi_2) + (\rho C_{bf})_{bf}(1 - \varphi_1 - \varphi_2) \tag{3.3}$$

The Eqs. (3.4) and (3.5) are used to calculate the characteristics of the mono nanofluid, specifically the density and the specific heat, respectively:

$$\rho_{nf} = \rho_{np}(\varphi) + \rho_{bf}(1 - \varphi) \tag{3.4}$$

$$\left(\rho C_p\right)_{nf} = \left(\rho C_p\right)_{np}(\varphi) + (\rho C_{bf})_{bf}(1 - \varphi) \tag{3.5}$$

The instantaneous efficiency is the quantity of useful heat energy to the amount of solar energy that the FPSC absorber plate catches. Eq. (3.6) was used in its calculation:

$$\eta = \frac{Q_u}{A_c G_t} \tag{3.6}$$

Using formula (3.7), the useful rate of heat energy, usually known as Q_u, could be determined as follows (ASHRAE Standard 93-2003; Duffie et al., 2013):

$$Q_u = \dot{m}C_p(T_{fo} - T_{fi}) \tag{3.7}$$

Useful heat energy rate could also be determined as the difference between the energy absorbed by the absorber plate and the energy lost by the absorber, as follows:

$$Q_u = A_c F_R[G_t(\tau\alpha) - U_L(T_{fi} - T_a)] \tag{3.8}$$

The heat absorbed by the fluid is calculated from the below Eqs. (3.9) and (3.10):

$$Q_u = \dot{m}C_p(T_{fo} - T_{fi}) = U_o A_o (T_s - T_b) \tag{3.9}$$

$$\frac{1}{U_o A_o} = \frac{1}{h_i A_i} + \frac{\ln(\frac{D_o}{D_i})}{2\pi kL} \tag{3.10}$$

It follows that the instantaneous efficiency Eq. (3.11) can be reformulated in one of the following forms of Eqs. (3.11) – (3.13):

$$\eta = \frac{\dot{m}C_p(T_{fo} - T_{fi})}{G_t A_c} \tag{3.11}$$

$$\eta = F_R\left[\tau\alpha - \frac{U_L(T_{fi} - T_a)}{G_t}\right] \tag{3.12}$$

$$\eta = F_R(\tau\alpha) - F_R U_L \frac{(T_{fi} - T_a)}{G_t} \tag{3.13}$$

Collector efficiency is represented as a straight line in Eq. (3.11). The point where this line meets the efficiency axis (vertical) is F_R (τα). When the inlet temperature to the FPSC is at the same level as the ambient temperature, the collector's efficiency is at its highest. The parameter F_R (τα) is often referred by the terms "absorbed energy parameter" or the "optical thermal efficiency".F_R U_L, also known as the "removed energy parameter," is the slope of a straight line that expresses the amount of energy lost from a solar collector. The instantaneous efficiency is defined by Eq. (3.11), widely known as the Hottel-Whillier equation. The collector heat removal factor, denoted by F_R, is determined by the formula (3.12):

$$F_R = \frac{\dot{m}c_p\,[T_{fo} - T_{fi}]}{A_c\,[G_t(\tau\alpha) - U_L\,(T_{fi} - T_a)]} \tag{3.12}$$

Eqs. (3.13) -(3.15) are used to calculate the Reynolds number, Prandtl number and Nusselt number of fluids:

$$Re = \frac{4\dot{m}}{\pi D_i \mu} \tag{3.13}$$

$$Pr = \frac{\mu c_p}{k} \tag{3.14}$$

$$Nu = \frac{h_i D_i}{k} \tag{3.15}$$

One of the essential factors that play an important role in evaluating the performance of thermal systems is energy efficiency (first law of thermodynamics). This parameter allows evaluation of

the thermal performance of flat plate solar collectors although it is not possible to completely identify the quantitative and qualitative performance of thermal systems based on the first law of thermodynamics. Therefore, the researcher evaluated the FPSC system by applying the first (energy) and second (exergy) laws of thermodynamics. These laws were applied for thermodynamic analysis (including qualitative and quantitative analyses) for the evaluation of energy and exergy of the FPSC. The energy analysis determined the thermal efficiency of the system . Exergy analysis indicated the exergy required for the optimum performance of the system. The second thermodynamic laws could be used to perform an exergy analysis, which can be thought of as the maximum amount of work created by a system or a mass or energy flow as it achieves equilibrium with a reference environment. Exergy analysis, in comparison to energy analysis, allows to gain a greater knowledge of the fundamental physics of a process. Irreversibility increases the system's entropy while causing a decrease in the system's exergy. The exergy equilibrium can be conveyed by the general equation provided in Eq. (3.16) (Adapa and Schoenau, 2005; Chamoli, 2013):

$$\dot{E}x_{heat} - \dot{E}x_{work} - \dot{E}x_{mass,in} - \dot{E}x_{mass,out} = \dot{E}x_{dest} \tag{3.16}$$

Eqs. (3.17) – (3.19) can be used to calculate the heat and flow exergy at the collector's input and exit, as follows:

$$\dot{E}x_{heat} = \left(1 - \frac{T_a}{T_{sur}}\right)\dot{Q}_s \tag{3.17}$$

$$\dot{E}x_{mass,in} = \dot{m}(h_{in} - h_a) - T_a(S_{in} - S_a) \tag{3.18}$$

$$\dot{E}x_{mass,out} = \dot{m}(h_{out} - h_a) - T_a(S_{out} - S_a) \tag{3.19}$$

Eq. (3.20) is the outcome of substituting these Eqs. (3.17) - (3.19) into Eq. (3.16):

$$\left(1 - \frac{T_a}{T_{sur}}\right)\dot{Q}_s - \dot{m}(h_{out} - h_{in}) - T_a(S_{out} - S_{in}) = \dot{E}x_{dest} \tag{3.20}$$

where Q_s is the total energy rate collected from solar radiation by the FPSC absorber plate, given by Eq. (3.21) (Esen, 2008; Ucar and Inalli, 2006):

$$Q_s = G_t A_c(\tau\alpha) \tag{3.21}$$

Eqs. (3.22) and (3.23) presents the change in entropy and enthalpy of the nanofluid in the solar collector (Jafarkazemi and Ahmadifard, 2013):

$$\Delta h = h_{out} - h_{in} = C_p(T_{fo} - T_{fi}) \tag{3.22}$$

$$\Delta s = s_{out} - s_{in} = C_p \ln\frac{T_{fo}}{T_{fi}} - R \ln\frac{P_{out}}{P_{in}} \tag{3.23}$$

Replacing Eqs. (3.22) and (3.23) in Eq. (3.20), then the exergy loss expression is presented by Eq. (3.24):

$$\left(1 - \frac{T_a}{T_{sur}}\right)G_t A_c(\tau\alpha) - \dot{m}C_p(T_{fo} - T_{fi}) + \dot{m}C_p T_a \ln\frac{T_{fo}}{T_{fi}} - \dot{m}RT_a \ln\frac{P_{out}}{P_{in}} = \dot{E}x_{dest} \tag{3.24}$$

where $\dot{E}x_{dest}$ is the exergy destruction rate (or irreversibility) that could be calculated by Eq. (3.25) in terms of ambient temperature and entropy generation:

$$\dot{E}x_{dest} = T_a \dot{S}_{gen} \tag{3.25}$$

The efficiency according to the second law (or exergy) is represented by Eq. (3.26):

$$\eta_{ex} = 1 - \frac{T_a \dot{S}_{gen}}{\left(1 - \frac{T_a}{T_{sur}}\right) \dot{Q}_s} \tag{3.26}$$

3.4. Experimental uncertainty analysis

3.4.1. Uncertainty in thermal conductivity

The experiment began with the calibration of the KD2 Pro device with the help of a standard fluid. This step is essential to ensure the accuracy of readings. As in the case of any measurement, the evaluation of nanofluid properties is also characterized by errors. The accuracy of the measurement tools plays a critical role in calculating the uncertainties or errors in data measurement. The experimenter performed the uncertainty analysis for each test by individually evaluating the errors encountered in the measurement of temperature, thermal conductivity, and nanoparticle concentration. Firstly, the researcher evaluated the errors in the measurement of thermal conductivity; the KD2 Pro was used with (±5%) accuracy (indicated in the manufacturer's manual), the thermal circulator bath with a temperature of (± 0.01 °C), and a weight balance of (±0.004 g). After that, the collected values were inserted in Eq. (3.27) to calculate the uncertainty in the measurement of thermal conductivity. The outcome showed a maximum error of 6.5% in thermal conductivity measurement.

$$U_k = \sqrt{\left(\frac{\Delta k}{k}\right)^2 + \left(\frac{\Delta m}{m}\right)^2 + \left(\frac{\Delta T}{T}\right)^2} \tag{3.27}$$

3.4.2. Uncertainty in dynamic viscosity

The uncertainty of the experimental results in this study was defined by the measurement errors of the parameters, which included the dynamic viscosity, temperature, and weight. For this objective, the experimental uncertainty in obtaining dynamic viscosity was computed using the accuracy of the viscometer (± 1%), the accuracy of the temperature (± 0.003 °C), and the precision of the electric balance (± 0.004 g). Dynamic viscosity measurement uncertainty was determined by Eq. (3.28). The maximum uncertainties in the viscosity measurements were estimated to be 4.2%.

$$U_\mu = \sqrt{\left(\frac{\Delta \mu}{\mu}\right)^2 + \left(\frac{\Delta m}{m}\right)^2 + \left(\frac{\Delta T}{T}\right)^2} \tag{3.28}$$

3.4.3. Uncertainty in efficiency of flat plate solar collector

In the context of the current study, uncertainty defines the lack of precision in any measurement or outcome. I define experimental uncertainty as "my estimation of potential errors through calibration if feasible". The uncertainty analysis is crucial for assessing uncertainties in experimental measurements and results. It's especially essential to perform uncertainty analysis while planning experiments to enable researchers to identify potential issues, preventing the waste of time, money, and effort. It's also essential for validation processes. There is a strong association between experimental uncertainties and validation. Hence, this study describes validation in the context of experimental uncertainty analysis. There is always a probability of error in data

acquisition because of the lack of absolute measurements. The experimental data is checked for accuracy by conducting the uncertainty analysis. My measurements involve two groups of errors. One group arises from direct measurement parameters like temperature, flow rate, solar radiation flux, and pressure. On the other hand, the second group of errors stems from indirect measurements, including energy and exergy efficiencies. The use of multiple tools and instruments in the current study makes it essential to confirm the precision of measurements and to get absolute measurements. uncertainty in measurement of any instrument for reduction data errors. Therefore, this research utilized experimental data collected from a flat plate solar collector to calculate efficiency uncertainty. Hence, this study makes use of Eq. (3.29) to perform uncertainty analysis to set a range within which the data obtained can be considered accurate. Based on this analysis, the maximum collector efficiency uncertainty was calculated to be 4.23%. Table 3.3 shows the uncertainties evaluated for each instrument and sensors involved in this study.

$$\frac{\delta\eta}{\eta} = \left[\left(\frac{\delta\dot{m}}{\dot{m}}\right)^2 + \left(\frac{\delta G_t}{G_t}\right)^2 + \left(\frac{\delta T_o}{T_o}\right)^2 + \left(\frac{\delta T_i}{T_i}\right)^2 + \left(\frac{\delta C_p}{C_p}\right)^2\right]^{0.5} \tag{3.29}$$

Table 3.3. List of uncertainty for instruments used in FPSC

Instrument and sensor type	Uncertainty (%)
Flow meter	± 0.5
Data logger	± 1
Thermometer	± 0.2
Pyranometer	± 2.5
Thermocouples	± 0.1
Anemometer	± 0.3
Specific heat	± 3.5

3.5. Numerical simulation of flat plate solar collector

3.5.1. Computational Fluid Dynamics flow chart

This study involves using ANSYS-Fluent 2022 for the numerical simulation of FPSC with a nanofluids-based collector. ANSYS (pre-processing, solution, and post-processing) were the primary solution processes used to analyse each model during this investigation. Fig. 3.11 depicts the Computational Fluid Dynamics (CFD) flow chart.

3.5.2. Assumptions

According to the following physical assumptions, the model is simplified:

- ZrO_2 and SiC nanoparticles are stable in water and do not slip under thermal conditions.
- Fluid is both continuous and incompressible.
- Based on the kind of nanoparticle, the characteristics of the base fluid, and the volume fraction of the nanoparticles, the nanofluid flow is simulated as a single phase with various features.
- It adopts steady state model.
- Laminar flow.

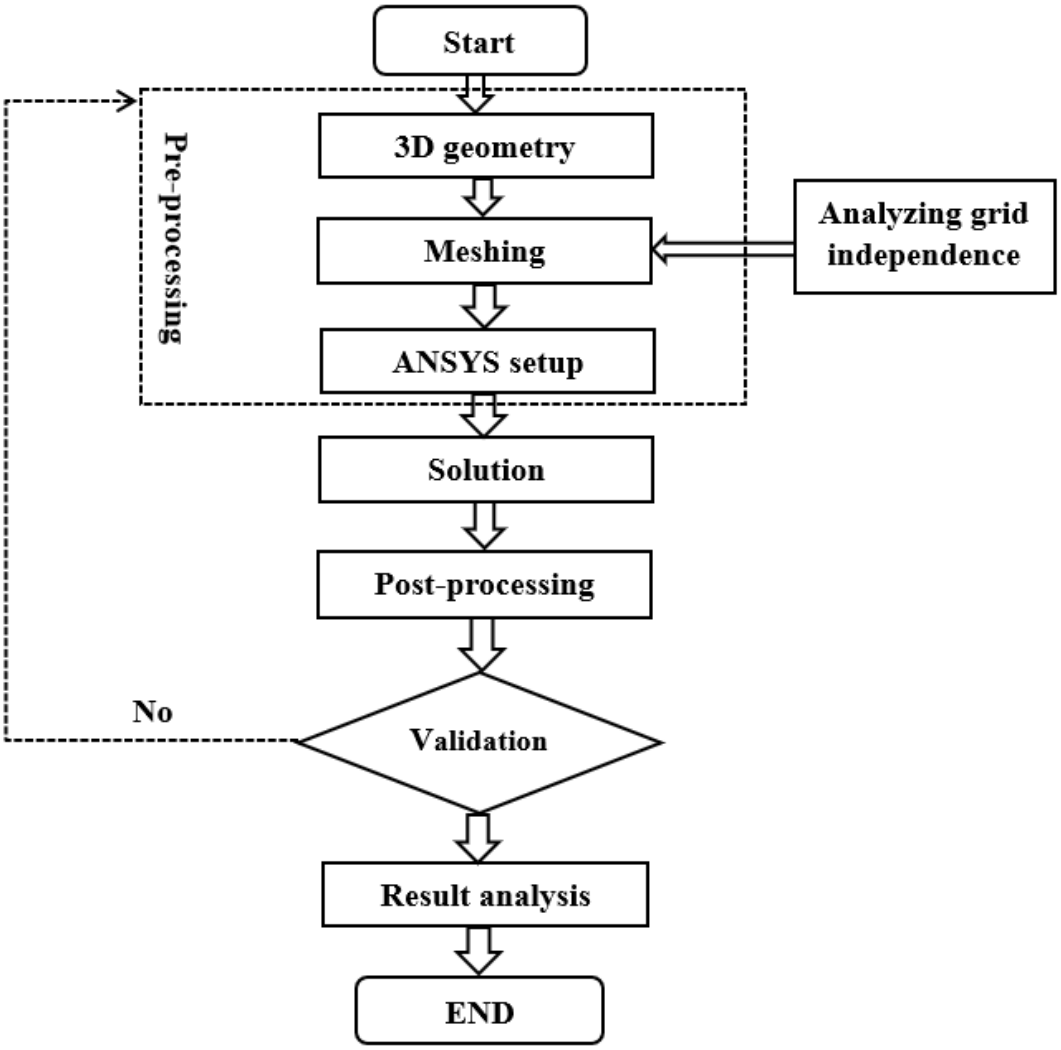

Fig. 3.11. CFD flow chart

3.5.3. Description of the model geometry

A 3D geometry was modelled using Design Modeler of ANSYS 2022R1. A flat plate solar collector attached to a circular pipe that is continuously heated to imitate solar radiation makes up the physical model. The system's geometrical of the computational domain for the FPC is presented in Fig. 3.12. ANSYS FLUENT is used to numerically solve the 3D model, which includes a copper absorber plate, a fluid input, riser tube, and fluid outlet. To minimize the time cost required for the simulation, the computational fluid dynamics (CFD) model is reduced by representing it as a single riser tube connected to the absorber plate. The flowrate in the riser tube is obtained by dividing the total flow rate of the collector by the number of risers.

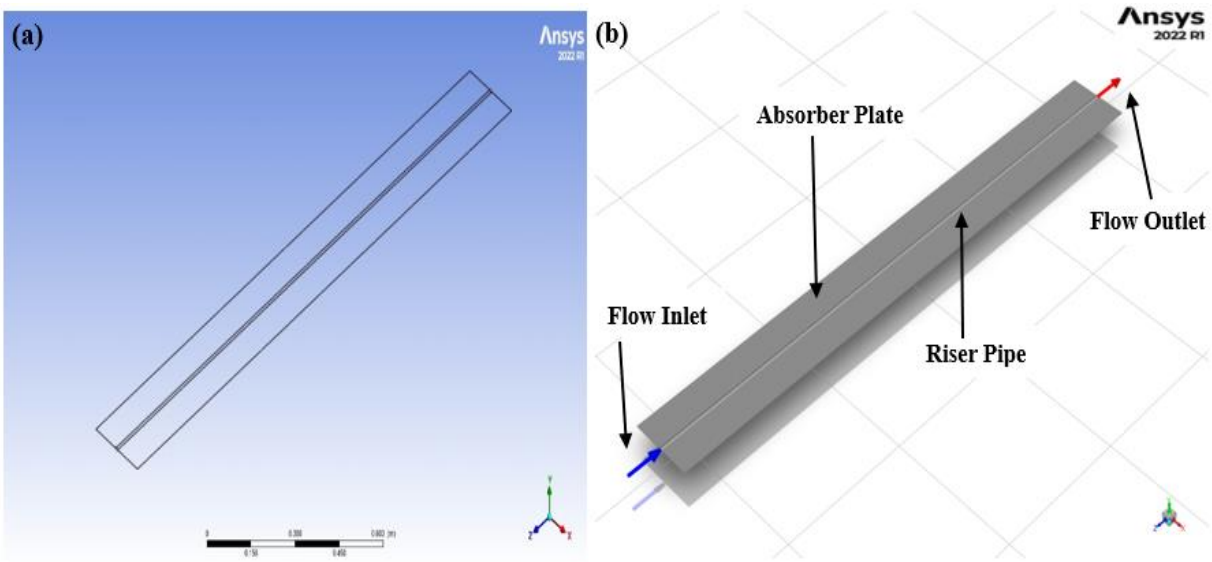

Fig. 3. 12. Model geometry of the computational domain of FPSC (a) Isometric wireframe view and (b) 3D design

3.5.4. Mesh generation and grid independent

The accurate selection of the number and structure of the mesh analysis along with the work's validation are crucial in numerical calculations. Even if we approach closer to the correct conclusion, an incorrectly determined mesh structure or number may cause us to lose time and effort by giving incorrect results. For the model we are looking at, tetrahedrons were chosen as the mesh model and quadratic structure as the element order. In transitional zones, such as the region where the riser pipes, as well as the working fluid input and exit regions, finer meshes are used. The mesh distribution for the riser tube, and absorber is shown in Fig. 3.13.

A key factor in striking a balance between computation speed and accuracy is the grid-independence test. Although accuracy is increased by adding additional elements, calculation times also increase. Four various grids are tested to identify the quality of mesh independence. The quantity of elements is 1370633, 1878472, 2785452, and 2927110. The variation of the water outlet temperature for various grid systems. According to the observations, there is just a slight increase in the outlet temperature value which is not more than 0.2% after 2785452 elements. Despite more improvement in the grid size, the answer is hence found to be unchanged after 2785452 elements, which is suitable to be the optimal mesh quality for this investigation.

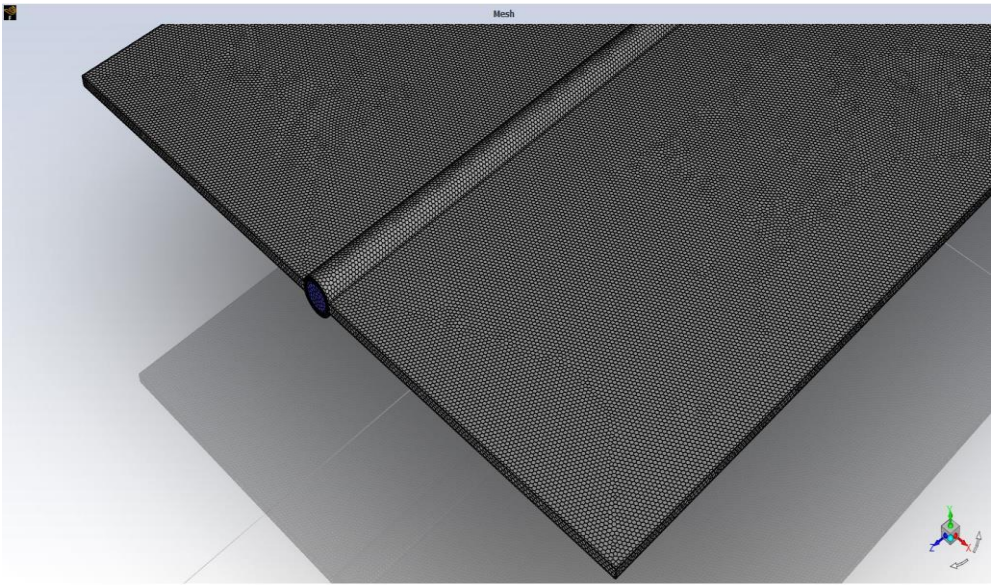

Fig. 3.13. Mesh generated of the computational domain

3.5.5. Boundary conditions

Boundary conditions have been assumed to be a constant mass flow rate at the entrance and a pressure outlet at the exit for fluid moving through the carrier pipe. A similar boundary condition operating under a conjugate laminar heat transfer model was applied to the current geometry, which has the same dimensions as the experimental investigation, to compare the numerical results with the findings. According to the experiment's flow rates and circumstances, a uniform velocity and beginning temperature are applied at the inlet domain. The absorber bottom is applied a heat transfer coefficient while the applied solar radiation at the absorber top. Applying a heat transfer coefficient at the absorber bottom replicated the FPSC's heat loss coefficient. The no-slip condition was applied inside the riser pipe, and the fluid flow was considered constant while ignoring the effects of compressibility and radiation. The normal and flow directions are also affected by gravitational influences.

3.5.6. Numerical method

Using a CFD code (such as Fluent), the flow-governing equations for a single-phase problem have been numerically solved. Using the finite volume method to discretize the fluid domain, which enables the transformation of partial differential equations (PDEs) into streamlined algebraic equations, the whole set of governing equations was solved. Convergence is one of the key issues in numerical simulation, and achieving convergence calls for the right numerical approach. A pressure-based solver and the segregated iterative approach were used to solve the flow-governing equations within the given boundary conditions. For spatial discretization, the least-squares cell-based gradient method was taken into consideration. Through the combined solution of the pressure-velocity coupling of the SIMPLE algorithm, the continuity equation, momentum equations, and energy equation have all been determined. The momentum and energy equations have been set to "Second Order Upwind" and the pressure equation has been set to "Standard". "Green-Gauss Node Based" has been chosen as the Gradient setting for the analyses. Continuous, laminar, and incompressible conditions are used to evaluate the calculations of the flow.

3.5.7. Validation

The most crucial stage of the numerical simulation is validation, where the expected outcomes are contrasted with known facts. In the current study, The Sider-Tate equation (found in Eq. 3.30) and shah equation (found in Eq. 3.31) were used as a preliminary step in the numerical model's validation, with water serving as the working fluid in FPSC. Fig.3.14 presents the comparison's findings in brief. It is noted that the Nu obtained using Eq. (3.30) and Equation (3.31) matches the results predicted by the numerical methods quite well, with 3.88% being the maximum variance. The numerical method was determined to be appropriate for further investigation because the compared results showed a satisfactory match with each other. Hence, the findings of the present investigation align with the given correlations:

$$\mathrm{Nu} = 1.86(\mathrm{Re}\,\mathrm{Pr}\,\mathrm{Di}/\mathrm{L})^{1/3}\mu^{0.14} \tag{3.30}$$

$$\mathrm{Nu} = 4.364 + 0.0722(\mathrm{Re}\,\mathrm{Pr}\,\mathrm{Di}/\mathrm{L}) \tag{3.31}$$

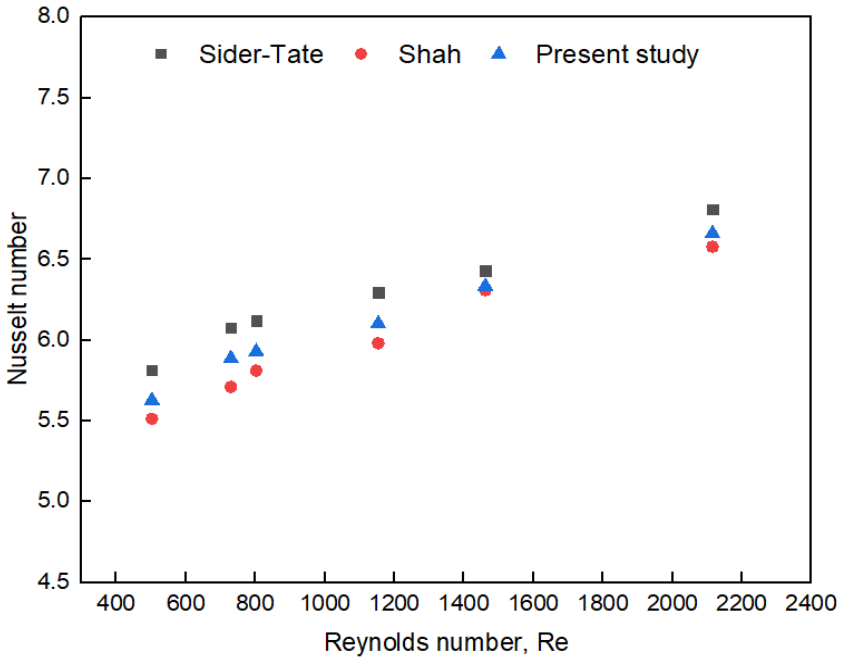

Fig. 3.14. Verification of the Nu numbers of the current model compare with Sider-Tate and shah equations using different correlations at various Re numbers

4. RESULTS

The experiments' results are presented in this chapter, along with discussions, suggestions, and new findings. The chapter includes the experimental studies conducted to specify thermo-physical properties of nanofluids including their viscosity and thermal conductivity, rheological behaviour, and nanoparticles characterization. This chapter sheds light on the performance of FPSC was investigated using theoretical and experimental observations. In the end, new findings drawn from the studies are listed.

4.1. Stability of nanofluids

The stability of the nanofluid is a significant thermophysical property that needs to be examined before it can be used. A significant part is played by the stability in the behaviour of the nanofluid and in improving its role as a heat carrier. Various methods were used by the researchers to examine the stability of nanofluids, e.g., the sedimentation procedure, absorption spectroscopy, and zeta potential analysis. In this research, the stability of nanofluids was determined using zeta potential. This method involves measuring the electric charge between the nanoparticles. The zeta potential test allows evaluation of the disparity in the electrical potential of the slipping layer and that observed at distance from the particle. The density of particles is directly associated with zeta potential. The surface charge on the particles results in colloid stability. The particles experience a repulsion force between them due to similarly charged loads and thus, they remain apart from each other leading to higher stability and weaker agglomeration. Subsequent to conducting various experiments involving the nanofluid of SiC/DW, ZrO_2/DW, and ZrO_2-SiC/DW, it was observed that the stability was reduced when the concentration was increased; therefore, such concentrations were selected ranging from 0.025% to 0.1%. After about 15 days, the given nanofluids samples with different volume concentrations (0.025%− 0.1%) were checked for stability revealing adequate stability. The criteria for nanofluid stability based on zeta potential values is as follows: values higher than 30–50 mV indicate good stability while values higher than 50 mV indicate excellent stability. As per the consensus of researchers and experts, nanofluid stability is questionable in the case of an absolute zeta potential value lower than 30 mV, there is a high likelihood of nanoparticle agglomeration and sedimentation in the fluid, because of which these fluids are considered unstable. But, the nanofluid stability is deemed adequate in case of zeta potential amounting to 30 mV or above. The zeta potential of the SiC, ZrO_2 and ZrO_2-SiC nanofluids used in this study are demonstrated in Fig. 4.1. The results indicated stable nanofluids as evident from the values of zeta potential shown in this figure. It can be seen from the results that there is high and appropriate stability of the nanofluids used in this study, and this confirms that the work steps are reliable and that precise measurements have been obtained.

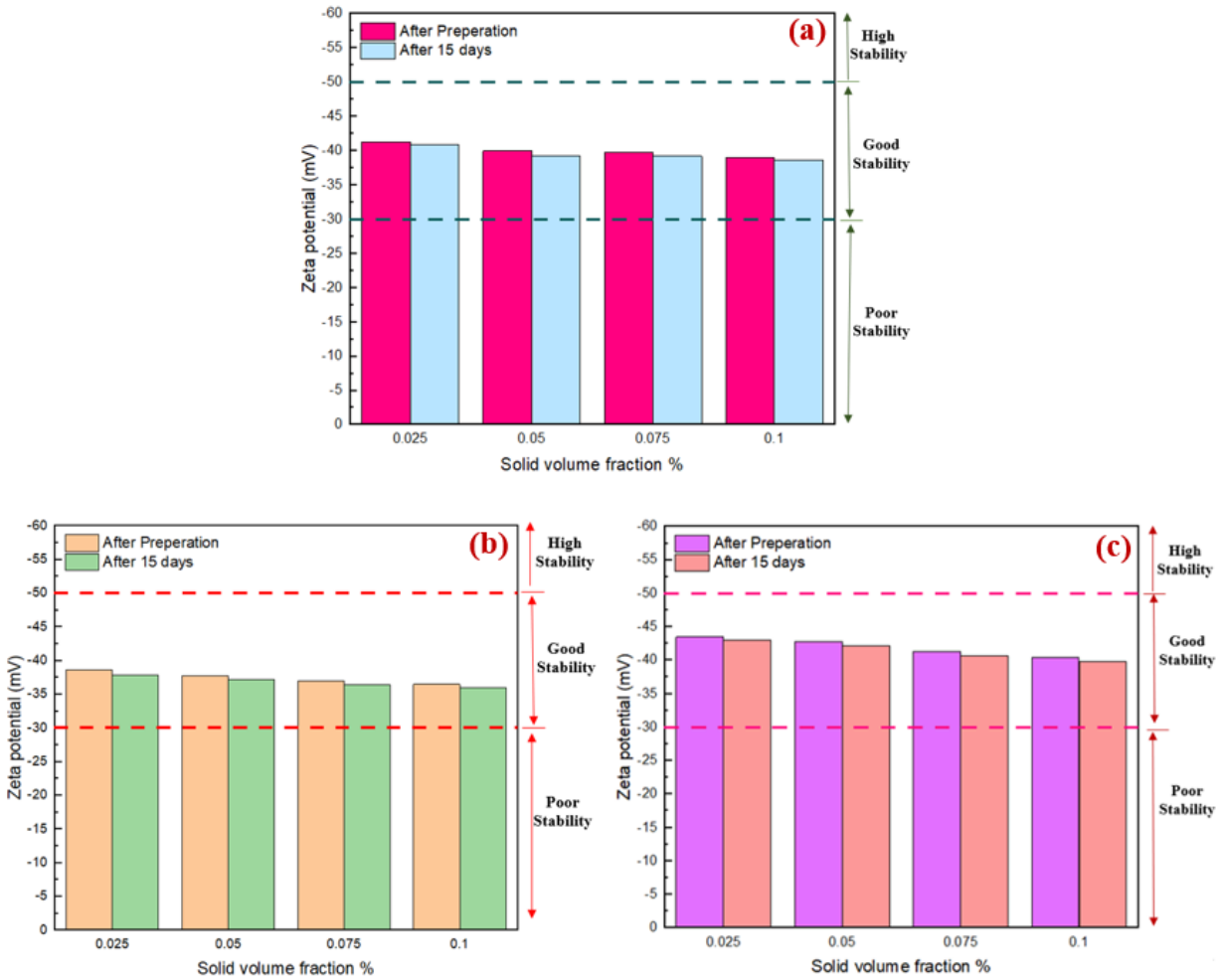

Fig. 4.1. Stability analysis of (a) ZrO_2-SiC/DW, (b) ZrO_2/DW, (c) and SiC/DW nanofluids

4.2. Rheological behaviour and dynamic viscosity of nanofluids

4.2.1. Nanofluids rheological behaviour

It is a critical thermophysical characteristic and has a considerable effect on lubrication and pumping power, which in turn affects convective heat transfer. Hence, for the purpose of evaluating the rheological properties of ZrO_2/DW, SiC/DW and ZrO_2-SiC/DW nanofluids, measurements of the nanofluids' viscosity were taken at varying shear rates to get insight into the rheological behaviour of the given nanofluid. A fluid's rheological behaviour is based on the given Eq. (4.1).

$$\tau = \mu\gamma \tag{4.1}$$

Where τ, μ, and γ symbolize the shear stress (Pa), dynamic viscosity (Pas), and shear rate (1/s), respectively. Based on this equation, a fluid is defined as being Newtonian in cases where the shear stress is a linear function of the shear rate. In Fig. 4.2, the shear stress is shown as a function of shear rate for mono nanofluids of ZrO_2/DW and SiC/DW and hybrid nanofluid of ZrO_2-SiC/DW where the solid volume fraction is 0.1% and the temperatures vary. As the changes in shear stress as result of the shear rate show a linear pattern, it can be deduced that the given nanofluids exhibit Newtonian characteristics, which supports the standard rule proposed by Venerus et al. (2010). Moreover, Fig. 4.3 demonstrates the changes in dynamic viscosity according to the shear rate at

various temperatures and volume fraction of 0.1 % for the given nanofluids. As the dynamic viscosity remains constant with regard to the shear rate, this suggests that the nanofluids of ZrO_2/DW, SiC/DW and ZrO_2-SiC/DW behave in a Newtonian manner.

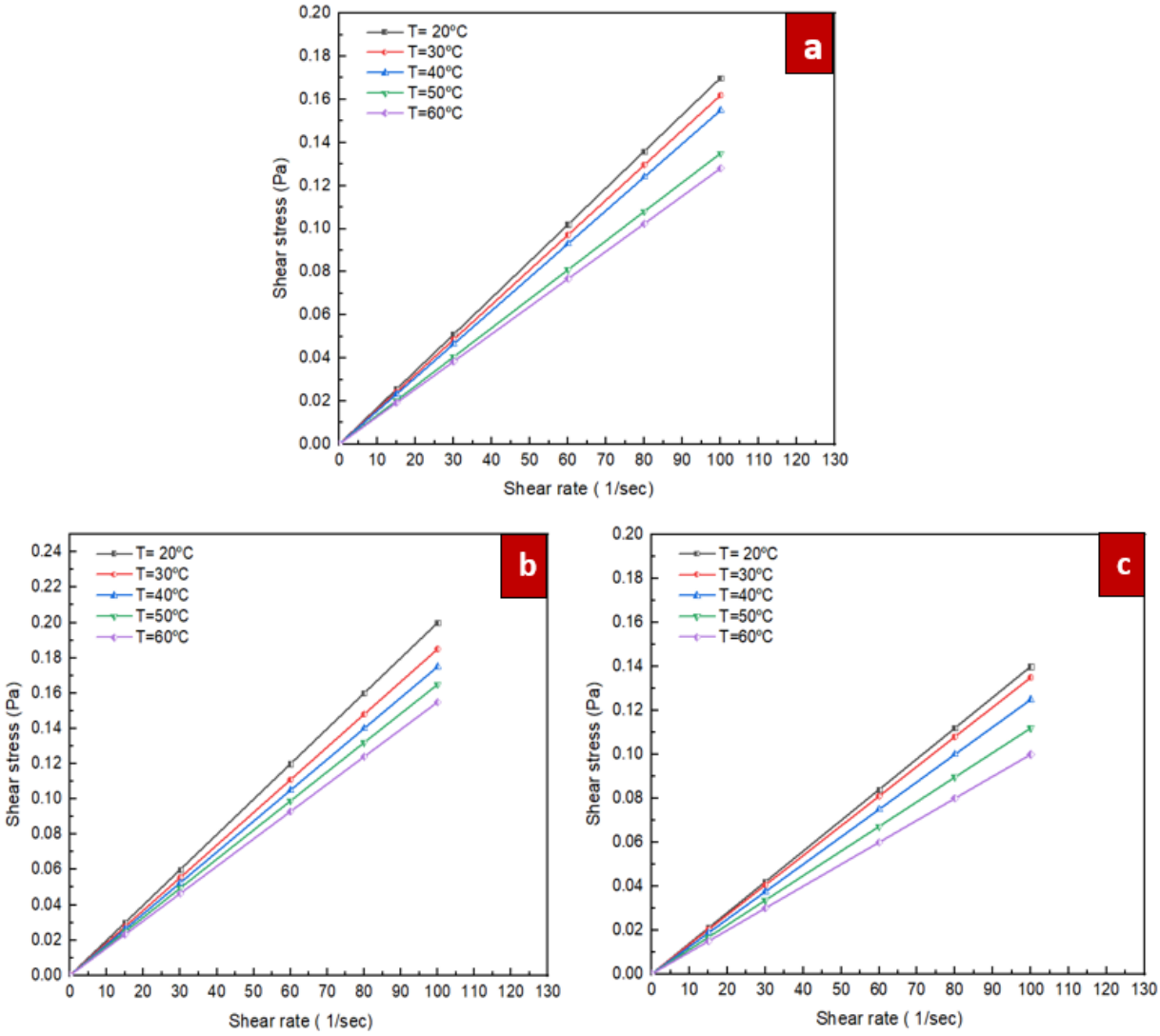

Fig. 4.2. Shear stress vs. shear rate at solid volume fraction of 0.1% for different temperatures, (a) ZrO_2-SiC/DW, (b) ZrO_2/DW and (c) SiC/DW nanofluid

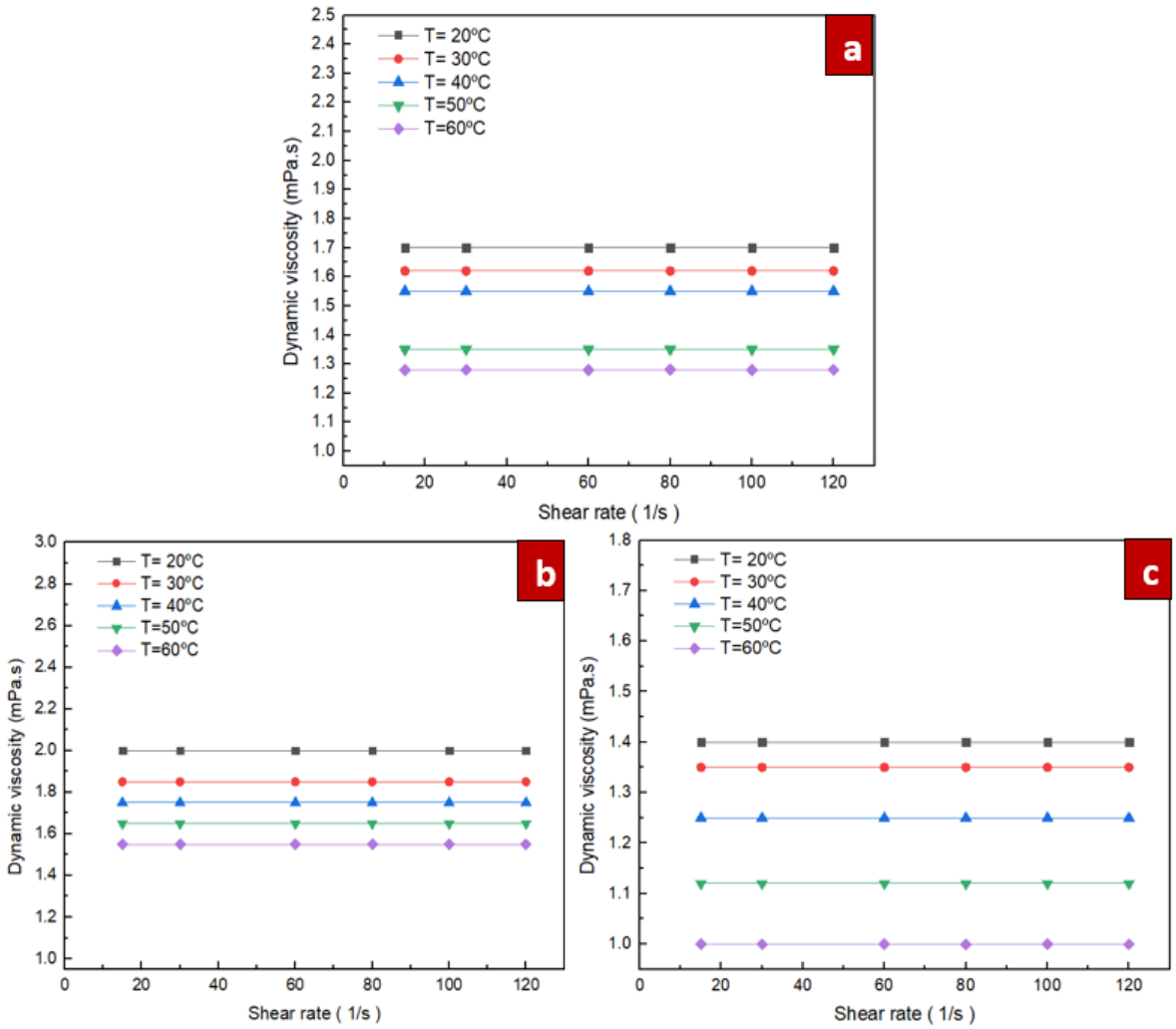

Fig. 4.3. Dynamic viscosity vs. shear rate at solid volume fraction of 0.1 % for different temperatures, (a) ZrO_2-SiC/DW, (b) ZrO_2/DW and (c) SiC/DW nanofluid

4.2.2. Dynamic viscosity in different temperatures and solid volume fraction

The viscosity of a fluid is a thermophysical characteristic and manifests in cases were slipping among the layers of fluid happens. It is the characteristic due to which a fluid offers resistance to relative motion among molecules of the fluid. Viscosity is more evident when the layers of the fluid experience movements. The mechanism underling the creation of viscosity in fluids is Van der Waals forces among molecules. When this occurs, frictional forces are formed according to the value of viscosity. The strength of the friction force rises in line with the viscosity. The addition and dispersion of nanoparticles among the molecules of the base fluid results in tighter slippage of the fluid layers. Hence, the strength of the frictional force formed among the layers of fluid within the nanofluid is enhanced.

The dynamic viscosity of the distilled water-based hybrid nanofluid of ZrO_2-SiC nanoparticles was recorded for different temperature and concentration settings. The obtained dynamic viscosity has been shows in Fig. 4.4. The figure shows that the nanofluid's dynamic viscosity declines as the temperature goes higher regardless of changes in solid volume fractions. However, when the temperature is kept unchanged, the change in solid volume fraction affects the nanofluid's dynamic viscosity differently. The dynamic viscosity increases with greater solid volume fraction.

Additionally, a more significant increase in viscosity was noted at lower temperatures. Fig. 4.5 shows a change in viscosity in response to a change in temperature at various concentrations of nanoparticles. The maximum increase of 169.4% in the nanofluid viscosity was seen at 60 ◦C in the presence of 0.1% nanoparticle concentration while the minimum rise of 29.6% was observed at 20 °C in the presence of 0.025% solid volume fraction. In the same way, the results indicated that the given nanofluid showed low dynamic viscosity increase (lower than 60%) in the presence of 0.025% nanoparticle concentration at T = 20, 30, 40, 50, and 60 °C. This implies that the given nanofluid can yield good performance in terms of pressure drop and required pumping power in industrial and engineering applications.

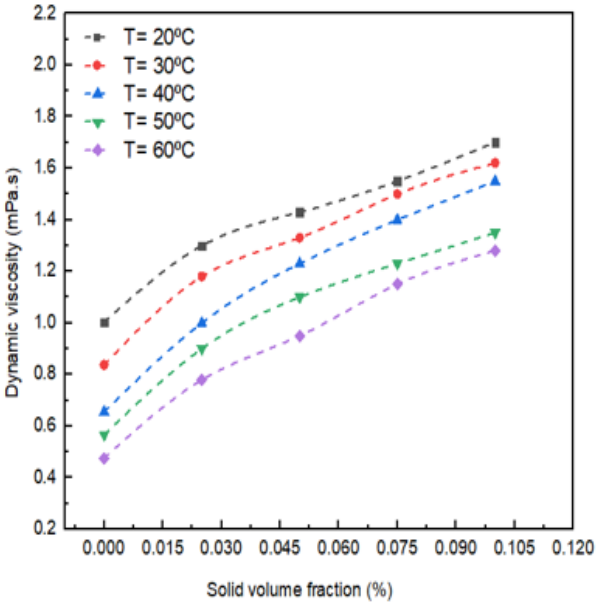

Fig. 4.4 Dynamic viscosity of the hybrid nanofluid with respect to temperatures at different solid volume fraction

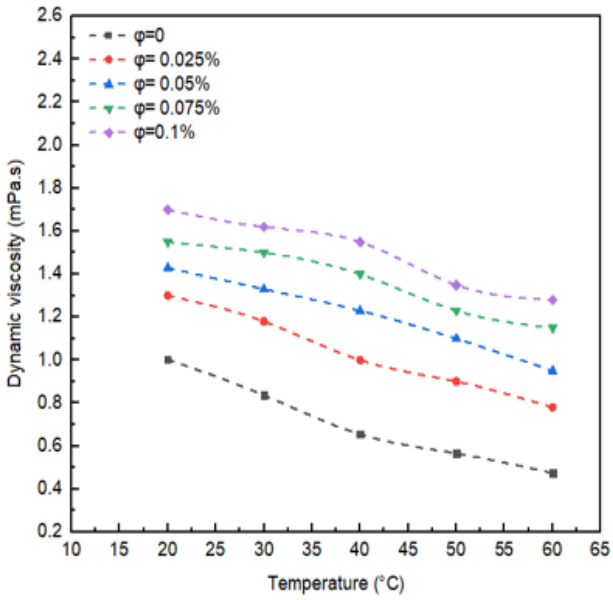

Fig. 4.5 Dynamic viscosity of the of the hybrid nanofluid respect to solid volume fraction at different temperatures

In Fig. 4.6, the changes in dynamic viscosity according to temperature at various volume fractions are shown for the ZrO_2/DW and SiC/DW nanofluids. As illustrated in the figure, as the temperature rises, the viscosity of the liquid is lowered. This is due to the fact that the interactions between molecules and the Van der Waals forces are weakened when the temperature increases. It is an intriguing finding that when the temperature remains the same, when the solid concentration increases, the nanofluid's dynamic viscosity also increases accordingly. The rise is more discernible when temperatures are reduced as opposed to increased. Based on the findings, when the volume fractions are increased, the temperature has a more discernible impact on the viscosity of the nanofluid. Indeed, when the volume fraction is elevated, there is an increased likelihood that agglomeration will occur among solid particles within the base liquid, the bonds connecting articles break more frequently, and the changes in viscosity are more pronounced, in comparison to situations where the temperature is reduced.

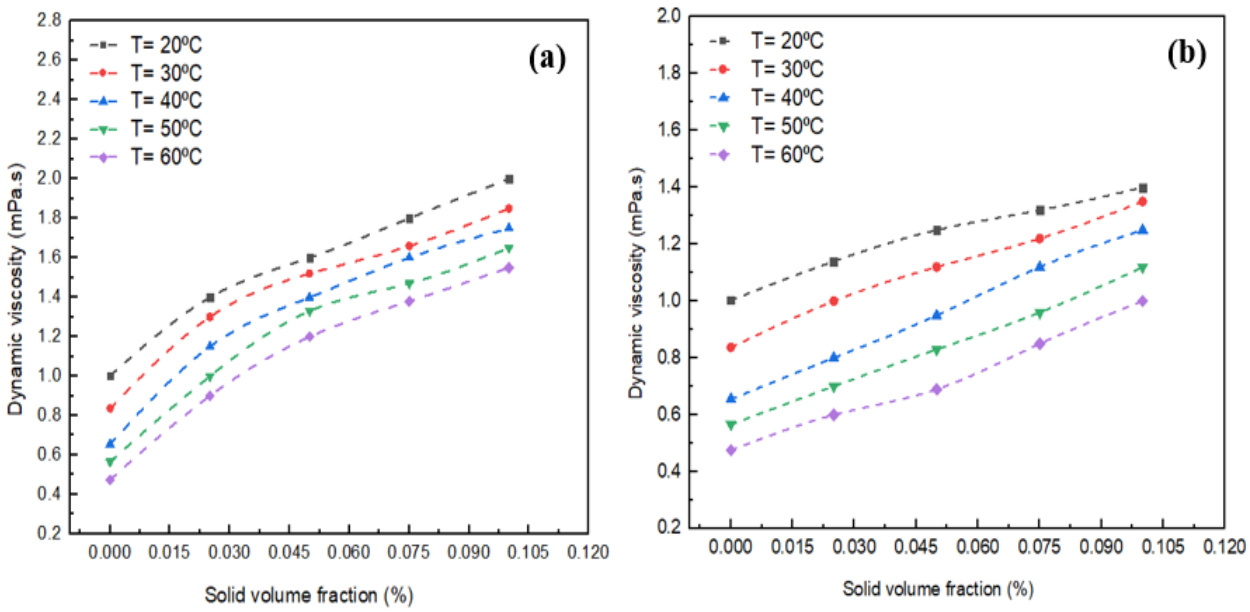

Fig. 4.6. Differences of dynamic viscosity of nanofluids with solid volume fraction at different temperatures for (a) ZrO_2/DW and (b) SiC/ DW nanofluid

In Fig. 4.7, the changes in dynamic viscosity for the mono nanofluids of ZrO_2/DW and SiC/DW according to the volume fraction at various temperatures are shown. As illustrated in the figure, as the volume fraction rises, nanofluids viscosity increases accordingly. This is due to the fact that the addition of nanoparticles to the base fluid causes the molecules of the liquid and the solid particles to interact to a greater extent, thus causing the viscosity to increase. Nanoclusters with greater magnitude are formed when the proportion of solid particles within a particular volume of base liquid is increased because of the greater Van der Waals forces among them. The resultant nanoclusters restrict layers of water from moving easily on each other, which causes the viscosity to rise to a large extent. Additionally, Van der Waals forces improve the viscosity according to the volume when the temperature is reduced. The reason for this is that when the temperature is increased, particles are capable of overcoming Van der Waals forces, which causes the rate at which the viscosity increases to decelerate as the volume fraction rises, in comparison to situations where the temperature is reduced. On the other hand, minimum increases of 39.5% and 13.6% were observed for the ZrO_2/DW and SiC/DW nanofluids, respectively, when the solid concentration was 0.025 % and temperature was 20 °C. Another remarkable finding was that when the solid concentration was 0.025% and the temperature was set at 20, 30, 40, 50, and 60 °C, the dynamic viscosity of the ZrO_2/DW nanofluid was under 89 %, whereas it was approximately 26% for the SiC/DW nanofluid; this shows the potential of these nanofluids for application in industrial and engineering settings due to the increased importance of pumping strength at reduced pressures. It should be noted that in the case of the ZrO_2/DW nanofluid, the dynamic viscosity increase was maximised and minimised at 226.3% and 39.5%, whereas for the SiC/DW nanofluid, its maximum and minimum increase were 110.5% and 13.6%, which manifested at sold concentrations and temperatures of 0.025% and 20 °C for the former, and 0.1% and 60 °C for the latter.

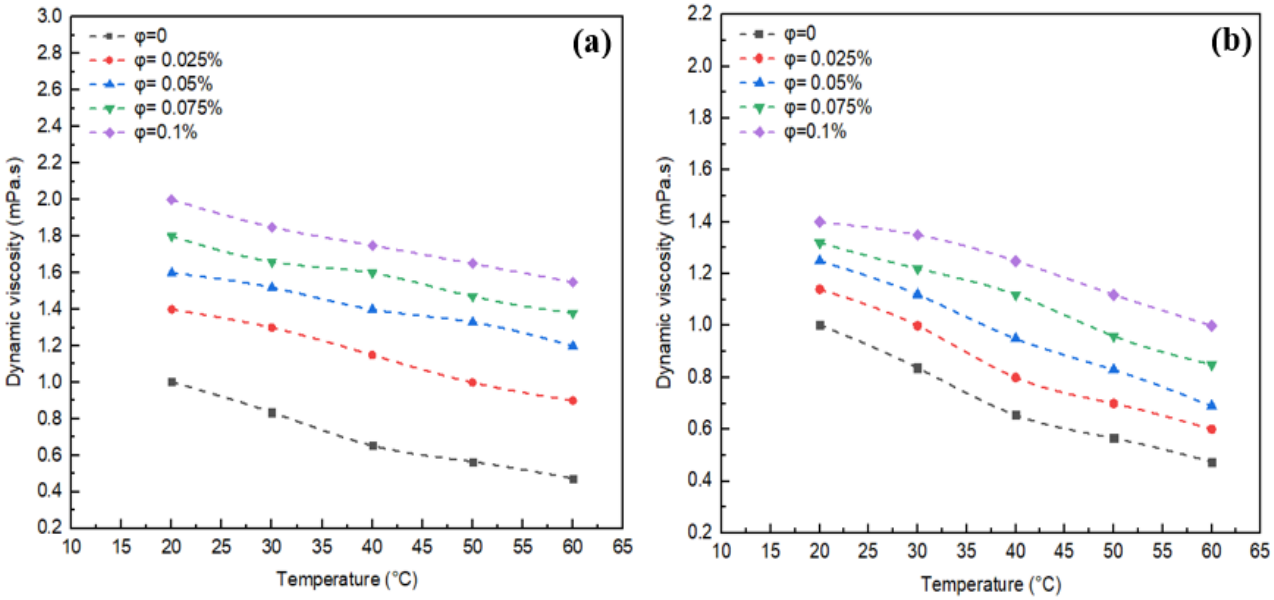

Fig. 4.7. Differences of dynamic viscosity of nanofluids with temperatures at different solid volume fraction for (a) ZrO_2/DW and (b) SiC/ DW nanofluid

According to Figs. (4.5) – (4.7), Higher concentration or volume fraction of nanoparticles in nanofluid led to a rise in the dynamic viscosity. Considering the effect of temperature, a temperature rise resulted in lower dynamic viscosity. This process may be accredited to the following reasons:

- As the nanofluids are dispersed in the base fluid, they undergo continuous collisions with base fluid particles leading to a random movement called the Brownian motion which increases the viscosity of the base fluid.
- With the addition of nanoparticles to base fluid, the van der Waals force is created between the nanoparticles and fluid leading to the formation of large Nano clusters which impedes the contact of the base fluid with the particles and hence causes a rise in viscosity.
- The formation of intermolecular force with increasing nanoparticle concentration leads to a rise in the value of viscosity.

It was evident that a temperature rise resulted in a decline in nanofluid viscosity provided the concentration of nanoparticles is kept constant. This phenomenon may be attributed to the reasons listed below:

- Viscosity refers to the liquid's property of being thick because of internal friction. Temperature changes were found to affect these intermolecular forces of viscosity. A temperature rise leads to a decline in the viscosity of a liquid. As temperature rises, more energy exerts its impact on the molecules of liquids and seizes the intermolecular cohesive forces. Consequently, the smoother motion of energetic molecules is observed. The resistance to flow also declines with the rise in temperature and the consequent weakening of intermolecular forces leading to lower viscosity of the Newtonian nanofluid.
- The temperature rise stimulates Brownian motion in nanoparticles leading to changes in nanofluid viscosity.
- The rise in temperature increases the intermolecular gap between base fluid and nanoparticles. Consequently, the flow resistance drops and so does the viscosity.

4.2.3. Relative dynamic viscosity

According to the measurements, the definition of the "relative viscosity" is based on the ratio between the dynamic viscosity of nanofluids and the viscosity of distilled water, expressed in Eq. (4.2). It can be seen in Fig. 4.8 that relative dynamic viscosity of hybrid nanofluid of ZrO_2- SiC is associated with parameters like solid volume fraction and temperature. As seen in Fig. 4.8a, the solid volume fraction causes a direct rise in the relative viscosity of a nanofluid. Previous research works also showed similar outcomes. Fig. 4.8b shows that a rise in temperature causes a slight rise in the viscosity with the viscosity rising more evidently at higher concentrations of nanoparticles. Hence, it can be inferred that temperature changes do not have a significant effect on relative viscosity specifically at lower solid volume fractions. In short, at low nanoparticle concentrations, relative viscosity is independent of temperature. The relative dynamic viscosity of the ZrO_2-SiC/DW hybrid nanofluids increased to a maximum of 2.69 times that of the base fluid at a temperature of 60 °C and a solid volume fraction of 0.1%. The fluid showed higher relative dynamic viscosity as the volume fraction was increased with a more prominent rise at higher nanoparticle concentration because of the occurrence of chain-like aggregation of nanoparticles. Particle aggregation was found to be positively associated with viscosity leading to sedimentation and clustering of nanoparticles. The relative viscosity was only slightly affected by a rise in temperature at lower nanoparticle concentrations. However, as the concentration increased, the effect became stronger. At higher concentrations, the relative viscosity showed a rise with a temperature rise. In conditions when the system was exposed to maximum temperature and concentration, it depicted the maximum rise in relative viscosity. Hence, it can be said that a higher density of nanoparticles led to higher relative.

$$\text{Relative viscosity} = \frac{\mu_{nf}}{\mu_{bf}} \tag{4.2}$$

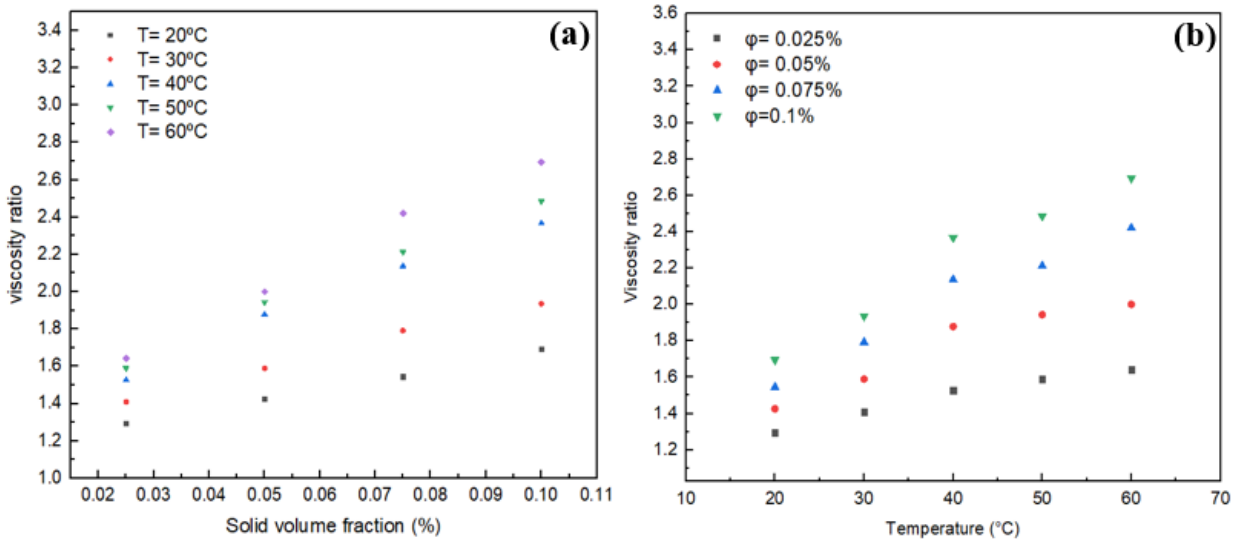

Fig. 4.8.(a) Relative viscosity vs. solid volume fraction for various temperatures and (b) Relative viscosity vs. temperatures for various solid volume fractions

In Figs. 4.9-10, the relative dynamic viscosity in relation to temperature and solid volume fraction for the nanofluids of ZrO_2/DW and SiC/DW is shown. The figures clearly show that as the solid volume fraction is increased, the relative viscosity is increased. This pattern was also supported in past studies. As shown in Figures, the relative viscosities increased marginally as the temperature

rose, and this was more observable when the solid volume fractions also increased. In the solid volume fraction range from 0.025% to 0.05%, and with temperature of 60 °C, the relative viscosity of ZrO_2/DW nanofluid changed the most by 33%, whereas for SiC/DW, it changed by 15%. Furthermore, augmenting the particle ration with a volume fraction of 0.1% to approximately 72% and 67% for the ZrO_2/DW and SiC/DW nanofluids, respectively, caused the relative viscosity to change by the greatest amount. This result implies that volume fraction as opposed to temperature has a greater influence on nanofluids' viscosity.

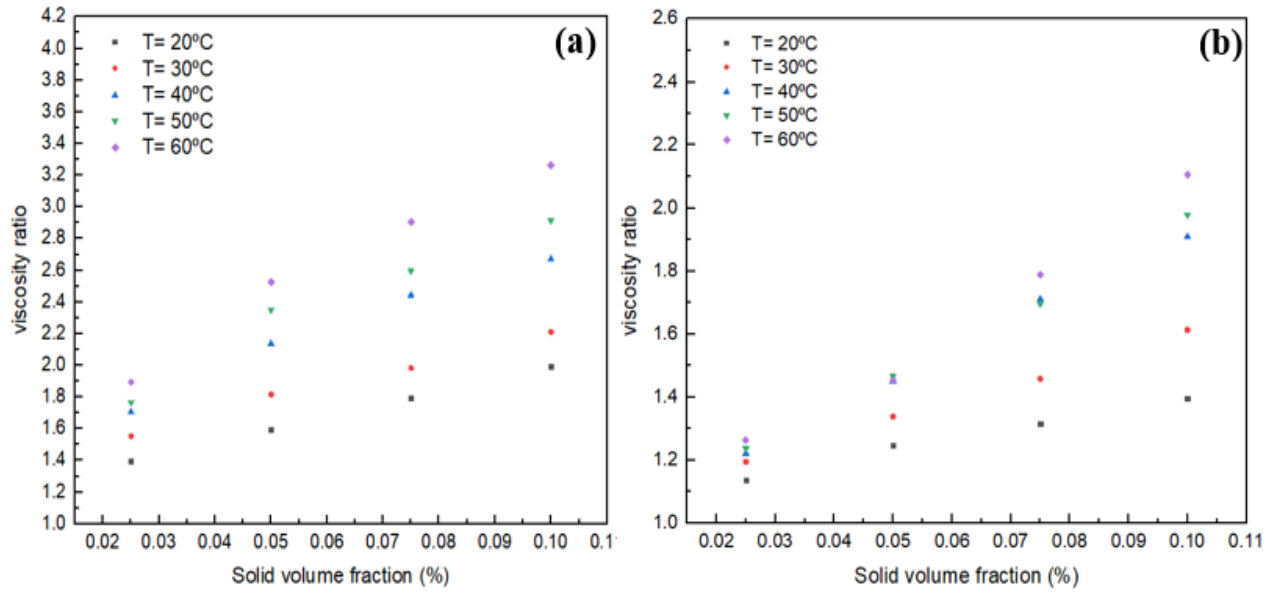

Fig. 4.9. Differences of relative dynamic viscosity with solid volume fraction at different temperatures for (a) ZrO_2/DW and (b) SiC/DW nanofluid

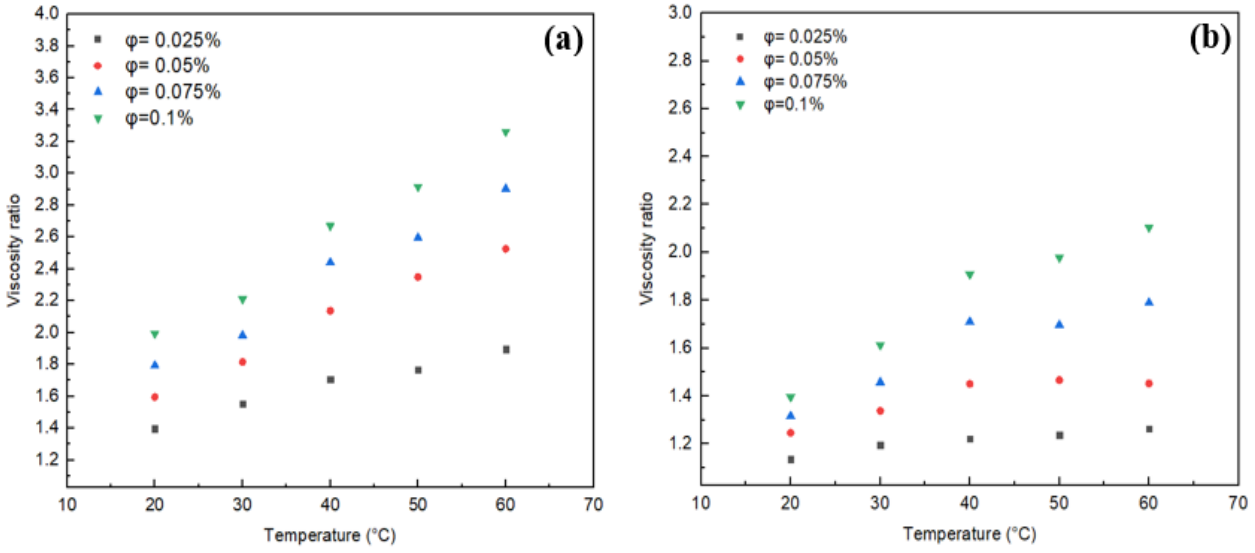

Fig. 4.10. Differences of relative dynamic viscosity with temperature at different solid volume fraction for (a) ZrO_2/DW and (b) SiC/DW nanofluid

When nanofluids applied in engineering applications, it is frequently to demonstrate usually call for mathematically expressing nanofluid's thermo-physical properties in equation form since equations allow experts to accurately predict values of dynamic viscosity of fluids based on the

given values of temperature (T) and solid volume fraction (φ). Fig. 4.11 illustrate the influence of temperatures and solid volume fraction on relative dynamic viscosity of given nanofluid are plotted in 3-dimensional surfaces. In the current research, the fitting method along with Levenberg–Marquardt algorithm by Origin Pro program was applied to the data obtained from the experiments, which facilitated the development of a novel model capable of predicting the dynamic viscosity of the investigated nanofluids with respect to solid concentration and temperature. New correlations for the prediction of the dynamic viscosity of nanofluids as functions of solid concentration (φ) and temperature (T) is developed through Eqs. (4.3) - (4-5), for ZrO_2/DW, SiC/DW, and ZrO_2-SiC /DW respectively, as shown below. The value of the coefficient of determination (R^2) is 98.92% for ZrO_2/DW, by 99.11% for SiC/DW and by 98% for ZrO_2-SiC/DW nanofluids which indicates an acceptable level of accuracy of the proposed model in terms of predicting the data.

ZrO_2-SiC/DW hybrid nanofluid:

$$\frac{\mu_{nf}}{\mu_{bf}} = 0.7096 + 3.84\varphi + 0.022T - 24.284\varphi^2 - 0.0002T^2 + 0.228\varphi T \quad (4.3)$$

ZrO_2/DW mono nanofluid:

$$\frac{\mu_{nf}}{\mu_{bf}} = 0.7986 + 9.72\varphi + 0.013T - 62.174\varphi^2 - 0.00006T^2 + 0.261\varphi T \quad (4.4)$$

SiC/DW mono nanofluid:

$$\frac{\mu_{nf}}{\mu_{bf}} = 0.8814 - 1.6\varphi + 0.013T + 10.465\varphi^2 - 0.0002T^2 + 0.204\varphi T \quad (4.5)$$

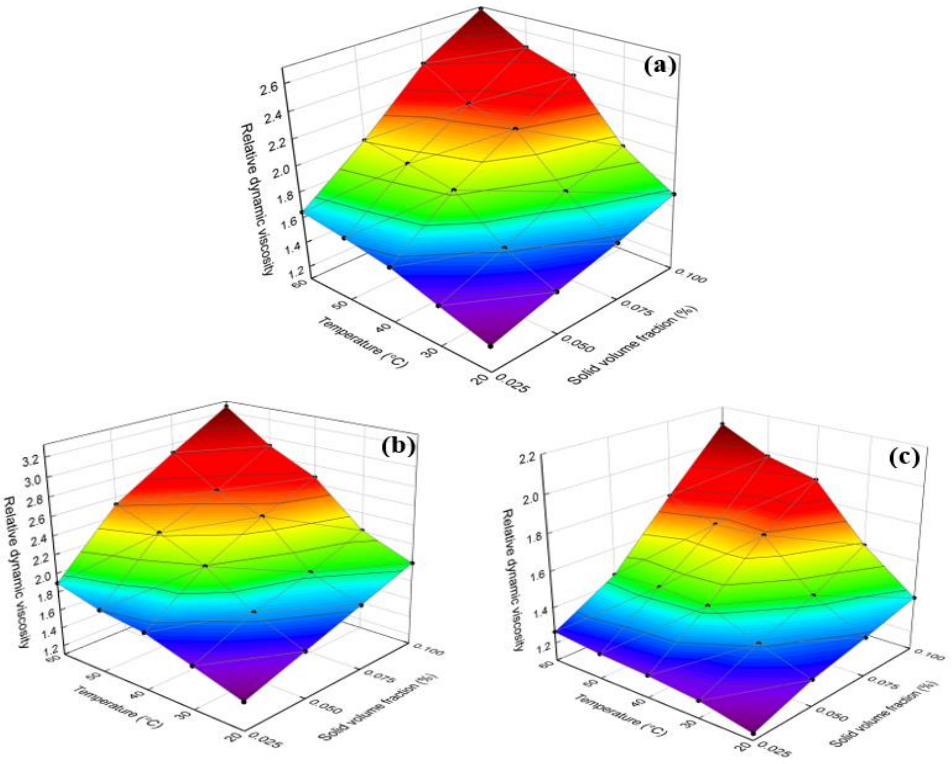

Fig. 4.11. 3D surface of relative dynamic viscosity at various volume concentrations and temperatures for (a) ZrO_2-SiC/DW, (b) ZrO_2/DW, and (c) SiC/DW nanofluids

The validation of the experimental model by using Margin of Deviation (MOD). The MOD method allows for confirming the adequate accuracy, validity, and quality of the experimental model. The method makes a comparison between the predictive data and the experimental data to check for correspondence between both data. Consequently, the MOD values are determined by using Eq. (4.6). The MOD results indicated high accuracy of the experimental model as evident from the overlap or only slight deviations in experimental and predicted values seen in Fig.4.12. This overlap shows agreement between the predicted and experimental values. Hence, it was deduced that the proposed correlation and model have the potential to make accurate predictions since it does not show any impact of dependent and independent variables. Moreover, for the nanofluids of ZrO_2/DW, SiC/DW, and ZrO_2-SiC the margin of deviation peaked at 5.38%, 5.27%, and 3.51%, respectively which indicates acceptable accuracy and validity of the proposed model.

$$\text{MOD}\ (\%) = \left[\frac{\left(\frac{\mu_{nf}}{\mu_{bf}}\right)_{Exp} - \left(\frac{\mu_{nf}}{\mu_{bf}}\right)_{Pred}}{\left(\frac{\mu_{nf}}{\mu_{bf}}\right)_{Exp}}\right] \times 100 \qquad (4.6)$$

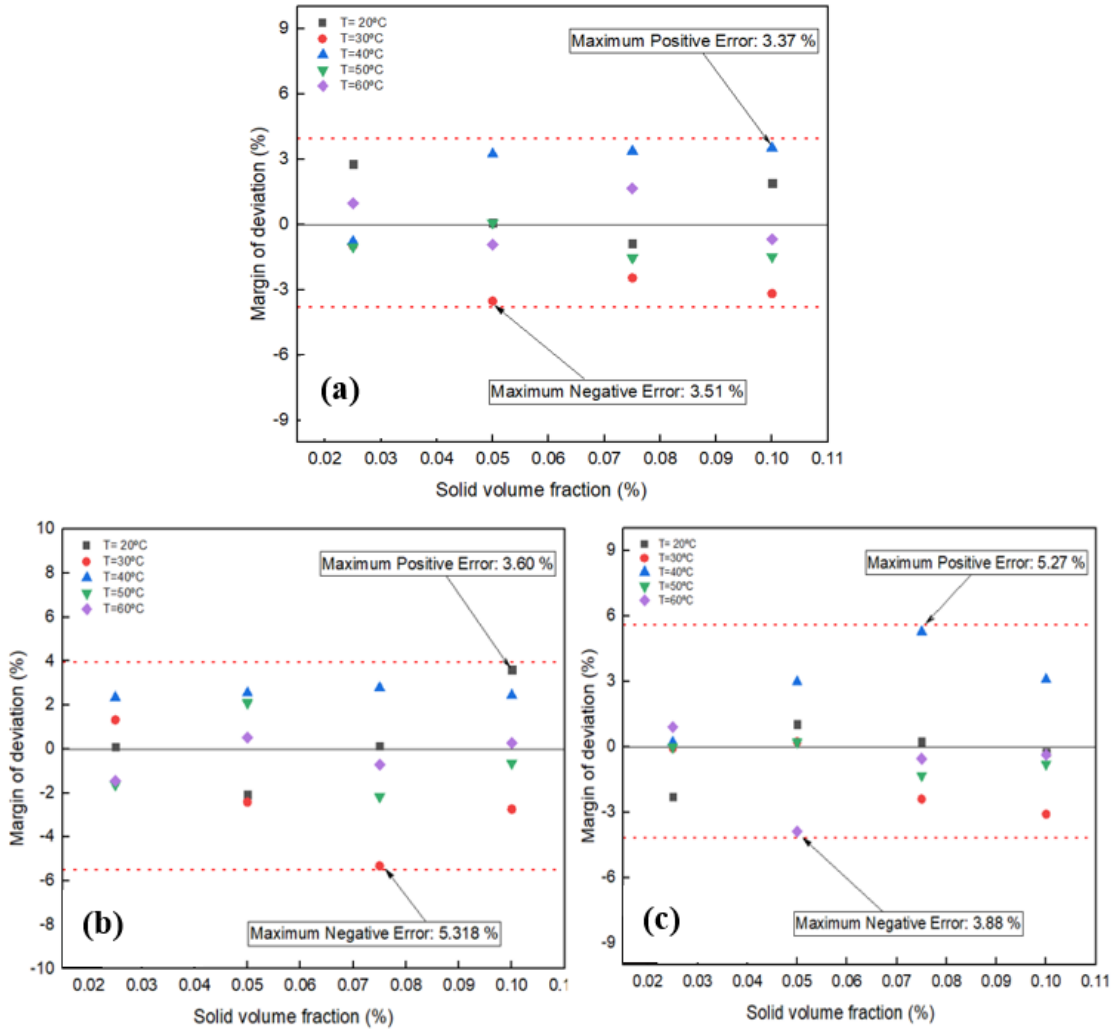

Fig. 4.12. Margin of deviation of dynamic viscosity for (a) ZrO_2-SiC/DW, (b) ZrO_2/DW, and (c) SiC/DW

4.3. Thermal conductivity of nanofluids

4.3.1. The effect of volume fraction on thermal conductivity

Fig. 4.13 is an illustration of the thermal conductivity of ZrO_2-SiC/DW hybrid nanofluid recorded at different solid volume fractions (0.025%, 0.05%, 0.075%, and 0.1%) and temperatures (20–60 °C). The thermal potentials of the fluid increase with a rising temperature due to intermixing of layers. For instance, at the same temperature (T = 20 °C), a difference of 4.36% is seen in the thermal conductivity of the base fluid and the nanofluid prepared by dispersing 0.025% nanoparticles to distilled water. Moreover, at 20 °C, thermal conductivity was enhanced by 9.06% and 16.1% respectively as the nanoparticle volume fraction was increased to 0.05% and 0.075%. Further increment in volume fraction to 0.1 % at the same temperature yields thermal conductivity of 20.8%. With increasing concentrations of nanoparticles, they form clusters which result in more rapid heat transfer in comparison to the fluid state, hence enhancing thermal conductivity.

The heat transfer is seen to be even more rapid when the size of nanoparticles is smaller due to the presence of a strong Van der Waals force of attraction between smaller particles. The results indicate the rise in thermal conductivity from 4.36% to 20.8% at 20 °C with increasing volume fraction from 0.025% to 0.1% which implies that maximum thermal conductivity is associated with the highest volumetric fraction. As the temperature is increased to 30 °C, the DW shows a rise in the thermal conductivity by 6.03% in comparison to the base fluid when the volume fraction is enhanced by 0.025%. Likewise, increasing volume fraction to 0.05% and 0.075% yields a 10.44% and 17.29% rise in thermal conductivity respectively. In this way, the volume fraction was increased to 0.1% which yielded thermal conductivity of 22.8% at T = 30 °C. This rise in thermal conductivity with increasing concentrations of nanoparticles indicates that higher nanoparticle concentration in nanofluid and the consequent clustering helps enhance the thermal conductivity specifically at this temperature. The main phenomenon behind this rise in thermal conductivity is that when the temperature is increased, the kinetic energy of nanofluid molecules increases leading to higher energy levels and ultimately higher thermal conductivity. Temperature rise plays an important role in enhancing the thermal conductivity of nanofluids. If the temperature is maintained at T = 40 °C, the thermal conductivity difference between the nanofluid and base fluid reaches 8.68% when the volumetric fraction is increased to 0.025%. Hence, at a given temperature, thermal conductivity shows a positive association with increasing the volume fraction of nanoparticles. As the volume fraction was increased to 0.025% at T = 40 °C, there was about an 23.22% rise in the thermal conductivity which is the highest rise in the thermal conductivity. As the temperature was increased to 50 °C and the concentration of nanoparticles was increased to 0.025%, there was a 10.07% rise in the thermal conductivity. This trend continues and at the volume fraction of 0.1%, a 25.58% rise in the thermal conductivity is noted which is quite high in comparison to the thermal conductivity of base fluid at 50 °C. The study also indicated a 20.9% rise in the thermal conductivity when the temperature of the base fluid changes from T = 20 °C to T = 50 °C and the volume fraction of nanoparticles is increased by 0.075%. The nanofluid shows a 10.6% rise in thermal conductivity at T = 60 °C when the volume fraction is increased to 0.025%. At a volume fraction of 0.1%, the nanofluid shows 25.75% higher thermal conductivity than base fluid provided the temperature is the same. It is, hence, evident that both temperature and volume fraction have a positive effect on thermal conductivity; however, the effect of volume fraction is significant in comparison to temperature.

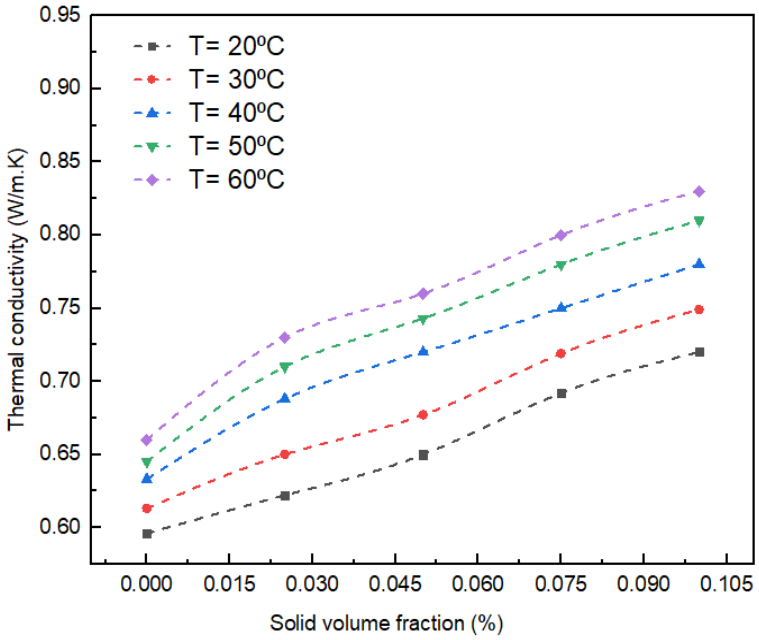

Fig. 4.13. Thermal conductivity of ZrO_2-SiC/DW at various volume fractions at all temperatures

Fig. 4.14 shows the changes in thermal conductivity of nanofluids compared to the volume fraction of ZrO_2 and SiC nanoparticles when different temperatures are applied. The thermal conductivity of ZrO_2/ DW nanofluid increases from 2.34% to 15.77% and SiC/DW from 6.2% to 21.8% when the volume fraction increases from $\varphi = 0.025\%$ to $\varphi = 0.1\%$ at 20 °C as compared to the base fluid at the same temperature. At 30 °C, the thermal conductivity increases from 4.4 to 17.44% for ZrO_2/DW and 7.66 to 24.79% for SiC/DW nanofluid when the volume fraction increases from 0.025% to 0.1% as compared to the base fluid at the same temperature. At a volume fraction of 0.025% and a temperature of 40 °C, the thermal conductivity increases to 6.95% for ZrO_2/DW and 10.58% for SiC/DW compared to the base fluid. The volume fraction of 0.1%, which is the highest, exhibits the most significant percentage increase in thermal conductivity of the nanofluids. Relative to the base fluid, at the volume fraction of 0.1%, thermal conductivity for ZrO_2/DW increases by 18.32% while SiC/DW increases by 25.59% at 40 °C. At 50 °C the thermal conductivity of ZrO_2/ DW nanofluid increases from 8.52 to 19.38% while that of SiC/DW increases from 14.72 to 27.13% relative to the base fluid with an increase in volume fraction from 0.025% to 0.1%. A further increase in temperature to 60 °C, increases the thermal conductivity from 9.09 to 20.45 for ZrO_2/DW and from 15.15 to 30.3% for SiC/DW nanofluids compared to the base fluid. The results from this experiment show that the increase in volume fraction of the nanoparticles used in the nanofluids ZrO_2/DW and SiC/ DW from 0.025% to 0.1% and temperatures of 20 – 60 °C leads to a rise in the thermal conductivity of the nanofluids. The highest increase in thermal conductivity corresponds with the highest volume fraction. The explanation for the results observed from the present study is Brownian motion. When the temperature increases, it sets the nanoparticles contained in the nanofluid into a Brownian motion. When the particles more concentrated or have a higher volume fraction, heat is easily conducted from one particle to another as they are closer than a low concentration. In a higher volume fraction, a lot of the particles are clustered together, and an increase in temperature increases the energy levels in the particles, thereby increasing the interaction between the particles. The interaction between

particles leads to the transfer of energy from a place of high concentration to a place of low concentration, thereby increasing heat conduction. However, the downside of increasing the volume fraction is that there is a limit to which it can be done. Increasing the concentration beyond the limit renders the resulting nanofluid unstable, leading to sedimentation of the particles. The nanofluid's viscosity also increases, requiring higher pumping capacity, and thus more energy is used in heat transfer. Nevertheless, lower nanoparticle volume fraction also has a higher thermal conductivity variation gradient. That is because there is reduced local agglomeration and a lower surface area of the nanoparticles at a lower volume.

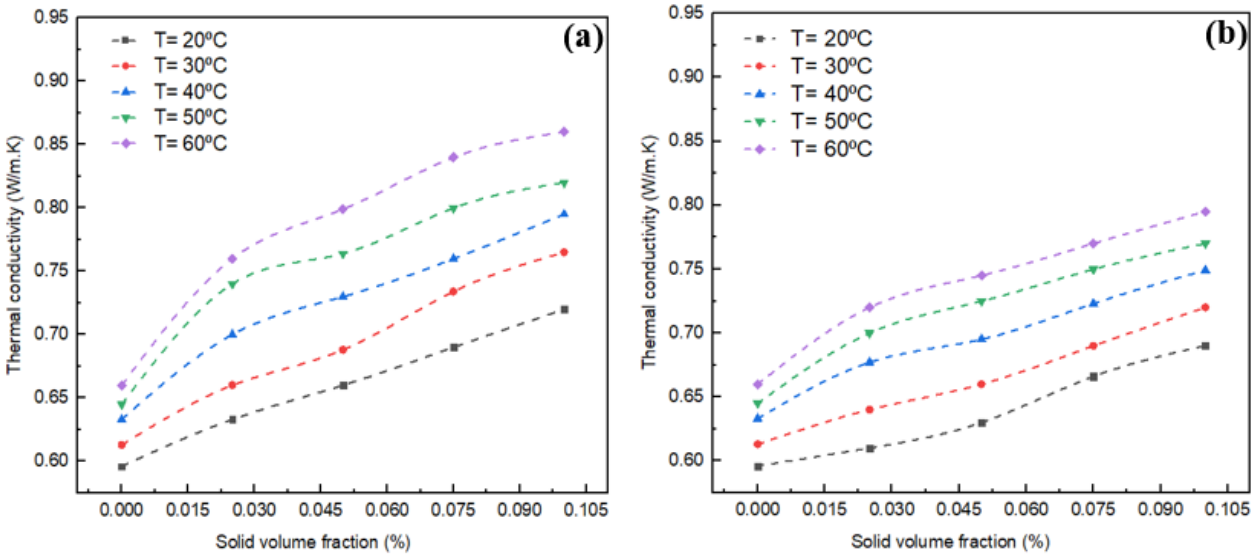

Fig. 4.14. Thermal conductivity at various temperatures at all volume fractions for (a) SiC/DW and (b) ZrO_2/DW nanofluids

4.3.2. The effect of temperature on thermal conductivity

The changes occurring in thermal conductivity with changes in temperature at various nanoparticle concentrations have been indicated in Fig. 4.15. The results in this figure indicate that a rise in temperature leads to a rise in the thermal conductivity of the ZrO_2-SiC/DW hybrid nanofluid specifically when the solid volume fractions are higher. The thermal conductivity increases with a rise in temperature from 20 to 60 °C at a volume fraction of 0.025%; the maximum thermal conductivity was recorded at 60 °C which is 10.6% higher than base fluid. Similarly, the thermal conductivity of the base fluid and nanofluid almost showed similar values at a volume fraction of 0.025%. However, at a volume fraction of 0.05%, the thermal conductivity of nanofluid showed the greatest change in comparison to that of base fluid when the temperature rose to 60 °C. The pattern of change suggests that the thermal conductivity showed a rise from 9.06 to 15.15 % as the concentration of nanoparticles in the base fluid was increased to 0.05%. It is also noted that thermal conductivity depicts the maximum increment of 21.21% at a volume fraction of 0.075% at 60 °C. As the concentration is further increased to 0.1%, a thermal conductivity enhancement of 25.75% is obtained relative to the base fluid (DW) at 50 °C. It is also evident that thermal conductivity increases more proportionately when both temperature and volume fraction is higher. The greater rise in thermal conductivity may be attributed to greater movement of the particles and more clustering at higher temperatures and higher concentrations. Consequently, clusters facilitate heat transfer and thermal conductivity. In short, it can be said that thermal conductivity improves with

increasing concentration of nanoparticles provided the temperature remains the same. The highest value of thermal conductivity was recorded at the volume fraction of 0.1% and a temperature of 60 °C.

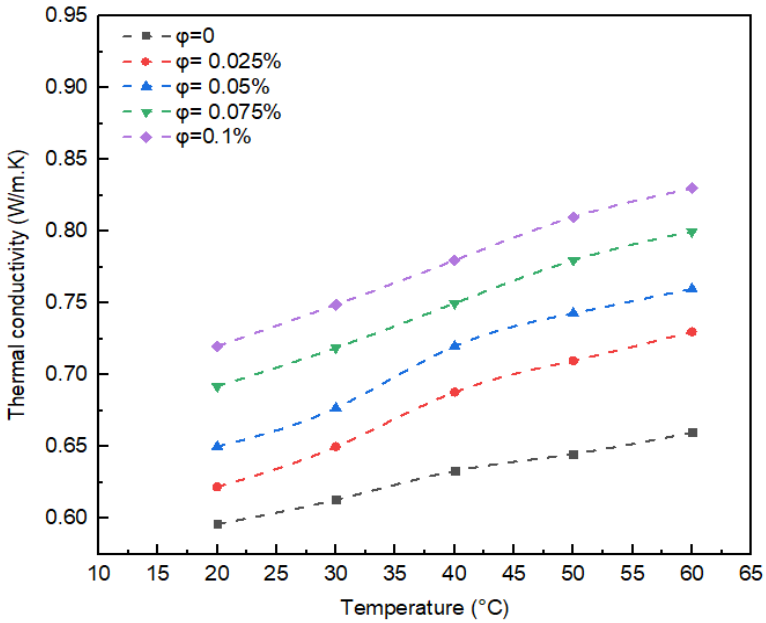

Fig. 4.15. Thermal conductivity of ZrO2-SiC/DW at various temperatures at all volume fractions

Fig. 4.16 show variations in the thermal conductivity of ZrO_2/DW and SiC/DW nanofluids with changes in temperature and volume fractions. At a volume fraction of 0.025%, the thermal conductivity for ZrO_2/DW increases from 2.34% to 9.09% and SiC/DW from 6.2% to 15.1% when the temperature increases from 20 °C to 60 °C. At a volume fraction of 0.05%, the thermal conductivity increases from 5.7% to 12.87% for ZrO_2/DW and 10.73 to 21.06% for SiC/DW with an increase in temperature from 20 °C to 60 °C. Thermal conductivity for ZrO_2/water increases from 11.74% to 16.66% and SiC/DW from 16.77% to 27.27% at a volume fraction of 0.075% when the temperature increases from 20 °C to 60 °C. Lastly, at a volume fraction of 0.1%, the thermal conductivity of ZrO_2/DW increases from 15.27% to 20.45%, and that of SiC/DW increases from 21.8% to 30.3% with a temperature increase from 20 °C to 60 °C. The highest temperature corresponds with the nanofluids' highest thermal conductivity at all volume fractions levels and vice versa. The thermal conductivity of the nanofluids is also compared to that of the base fluid, which is distilled water in this case.

The experimental results show that the nanofluids' thermal conductivity increases when temperature increases. When temperature increases, the particles contained in the nanofluid are set into Brownian motion, thereby making them collide more frequently at an increased rate. As temperature increases further, the kinetic energy of the nanoparticles increases, and heat transfer becomes more rapid, thus increasing the overall thermal conductivity. A lot of similar studies that have been carried out before show the same trend concerning the effect of temperature on the thermal conductivity of nanofluids. Some authors believe that temperature does not significantly enhance thermal conductivity. Also, the authors mention that temperature decreases the viscosity of the nanofluids. Some authors attribute the Brownian motion as the cause of enhanced thermal

conductivity when temperature increases, but others dispute the idea stating that Brownian motion is the mechanism through which thermal conductivity is enhanced even at low temperatures. The main thing that has a more significant effect on thermal conductivity in nanofluids that most researchers agree on is an increase in the volume fraction or the concentration of nanoparticles.

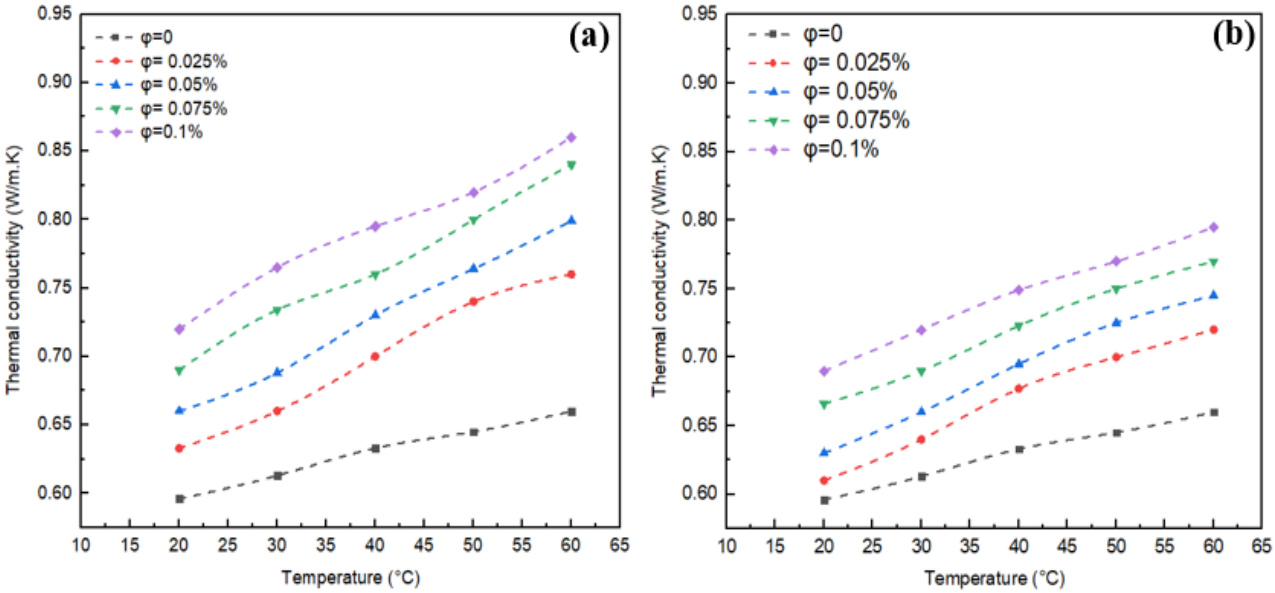

Fig. 4.16. Thermal conductivity at various temperatures at all volume fractions for (a) SiC/DW and (b) ZrO_2/DW nanofluids

4.3.3. Thermal conductivity enhancement

Fig. 4.17 shows the thermal conductivity enhancement (TCE) of ZrO_2-SiC/DW, ZrO_2/DW, and SiC/DW nanofluids recorded at various solid volume fractions and temperatures. Thermal conductivity enhancement, expressed in Eq. (4.7). The maximum thermal conductivity enhancement noticed for hybrid nanofluid is about 25.75%. The maximum TCE observed for ZrO_2/ DW is approximately 20.45%, and that of SiC/DW is 30.3%, was observed at the highest volume fraction of 0.1% and a temperature of 60 °C. When the volume fraction increases, the surface area of the nanoparticles increases. An increase in temperature causes the Brownian motion of the particles, which collide against each other and cause a rapid heat transfer. The key issue in this case is why the addition of nanoparticles results in an increase in thermal conductivity. The first primary reason is Brownian motion or the random motion of nanoparticles in the foundation fluid. This motion produces an extensive number of random collisions between the nanoparticles and the molecules of the base fluid, which increases the amount of heat transmitted throughout the nanofluid. In consequence, enhances the nanofluid's characteristic thermal diffusion. The interfacial layer (or nanolayer) is the second factor. This layer provides an interface for the movement of energy (heat) between the solid nanoparticles and the fluid molecules. Hence, I conclude that the introduction of nanofluids is a landmark in improving the fluids in terms of their

thermal performance. Likewise, this study is an important contribution to the literature relevant to nanofluids since it suggests replacing the conventional fluids with nanofluids.

$$\text{Thermal conductivity enhancement (\%)} = \frac{k_{nf-}k_{bf}}{k_{bf}} \times 100 \tag{4.7}$$

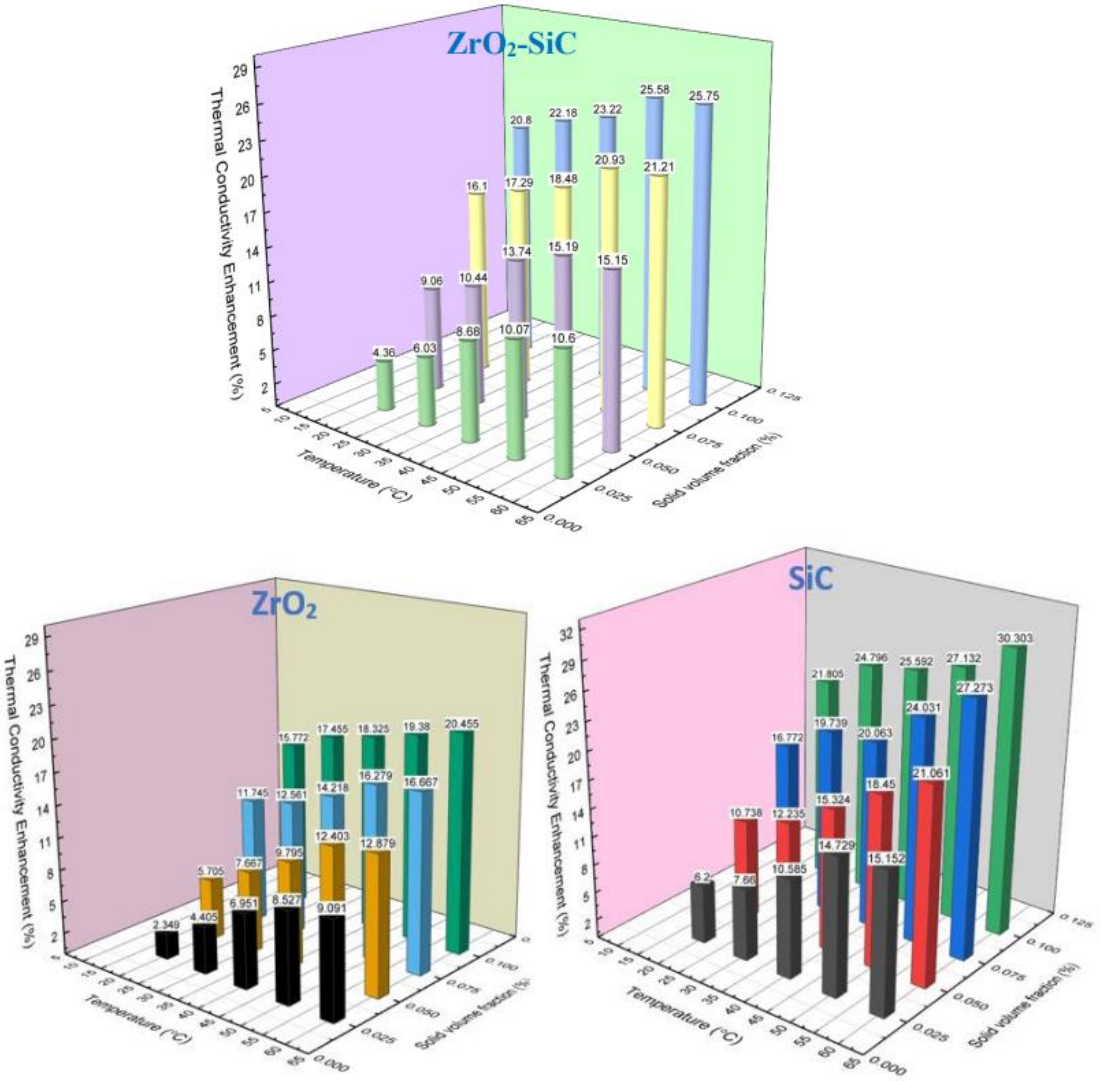

Fig. 4.17. TCE value of ZrO_2-SiC/DW, ZrO_2/DW, and SiC/DW nanofluid at different temperatures and volume fractions

4.3.4. Thermal conductivity ratio

The comprehension of thermal conductivity enhancement needs to understand the meaning of thermal conductivity ratio, expressed in Eq. (4.8), which is the thermal conductivity of a nanofluid divided by the thermal conductivity of the base fluid provided the temperature remains the same. thermal conductivity ratio allows comparison of the rise in thermal conductivity coefficient of the nanofluid and base fluid at various temperatures which enables the experts to gain valuable insight into how increasing volume fraction affects the thermal conductivity. Relative thermal conductivity is also explained with the help of a diagram that shows changes in thermal conductivity because of changes in volumetric fraction. The relative thermal conductivity of ZrO_2-SiC/DW hybrid nanofluid is recorded at different temperatures to plot the graph of relative conductivity shown in Fig. 4.18. It is evident from the figure that relative thermal conductivity

increases with a rise in a volume fraction and temperature. This may be attributed to the clustering of particles at higher concentrations of nanoparticles in the fluid. The clustering is a useful process; however, when volume fractions are extremely high, it results in sedimentation which affects the stability of nanofluid. Besides this, there is also a significant effect on the fluid's viscosity due to the increasing concentration of nanoparticles in the fluid. Consequently, more viscous suspension calls for greater pumping power. Hence, thermal conductivity enhancement must be done using an ideal number of nanoparticles that increases thermal conductivity without making the suspension highly viscous. The thermal conductivity depicts the same behaviour at all temperatures which implies that the thermal conductivity of base fluid rises when nanoparticles are added to it. It is also noted that the surface to-volume ratio also rises with increasing volume fraction which may be attributed to a rise in thermal conductivity. In short, a rise in temperature and volumetric fraction leads to higher thermal conductivity.

$$\text{Thermal conductivity ratio(TCR)} = \frac{k_{nf}}{k_{bf}} \tag{4.8}$$

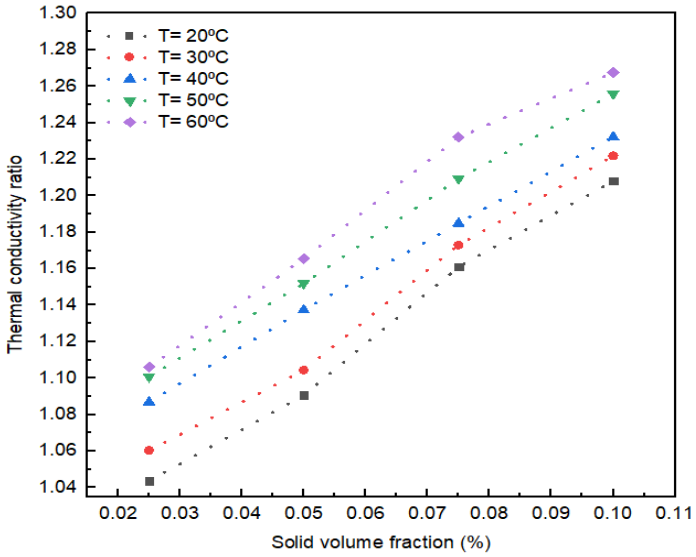

Fig. 4.18. Thermal conductivity ratio of ZrO_2-SiC/DW at various volume fractions at all temperatures

Fig. 4.19 shows the thermal conductivity ratio based on volume fraction at different temperatures. The results show that the highest volume fraction increases thermal conductivity in nanofluids ZrO_2/DW and SiC/ DW. The relative thermal conductivity for ZrO_2/DW increases from 1.09 to 1.204 W/mK and that of SiC/DW from 1.151 to 1.303 W/mK, increasing volume fractions of nanoparticles from 0.025% to 0.1% at 60 °C. Increasing the nanoparticle volume fraction leads to the clustering of particles whereby the particles bind to each other. The clustering of nanoparticles causes a rapid transfer of heat from one particle to another compared to the transfer of heat in a basic fluid such as water. The increasing temperature that is applied to the nanofluid sets the particles into a Brownian motion which has a magnified effect when the particles are clustered, thereby increasing the thermal conductivity ratio of the nanofluid.

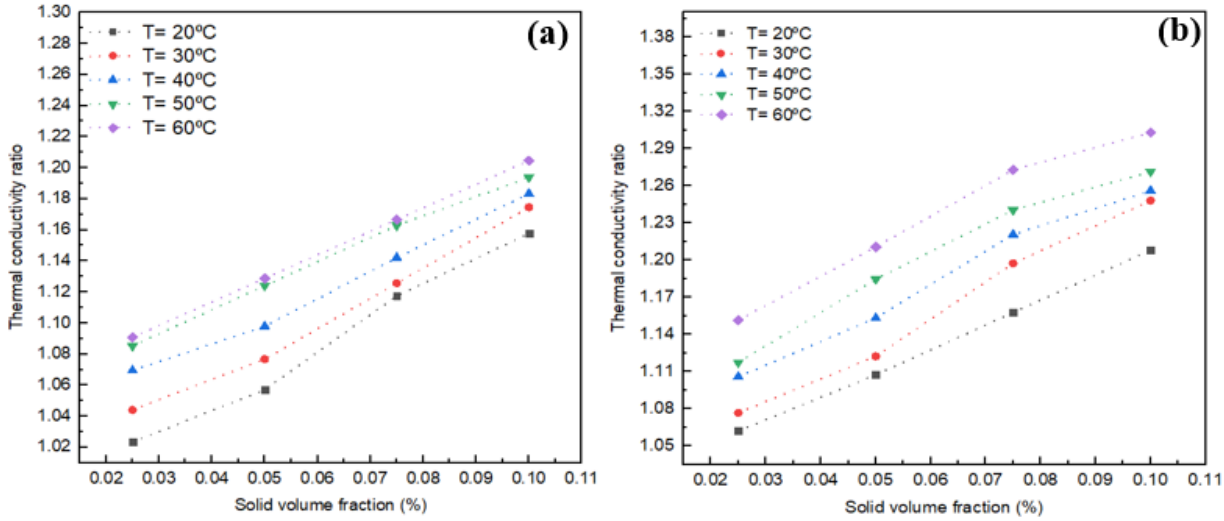

Fig. 4.19. Thermal conductivity ratio of (a) ZrO_2/ DW and (b) SiC/DW nanofluids at various volume fractions at all temperatures

Different values of thermal conductivity of ZrO_2-SiC/DW hybrid nanofluid were observed at different temperatures and different solid volume fractions which have been given in Fig. 4.20. The values indicate that relative thermal conductivity does not show significant change with rising temperature provided the solid volume concentration is low since the Brownian motion is lower at lower concentrations. But, when the volume fraction is higher, the thermal conductivity rises due to the presence of a greater quantity of fluid particles at higher concentrations leading to the clustering of particles. The clustering accelerates heat transfer since heat transfers more quickly from a solid phase in comparison to the fluid phase. Considering temperature changes, as the temperature rises, the nanoparticles move faster leading to higher relative conductivity because of more frequent collisions of surface atoms with fluid molecules. The highest relative thermal conductivity was noted at 60 °C when the solid volume fraction was 0.1%. Different values were obtained for the relative thermal conductivity of the nanofluid at different temperatures between 20 and 60 °C at different volume fractions. By observing the results, the recorded values indicated that rising temperature and increasing volume fraction caused an increment in relative thermal conductivity.

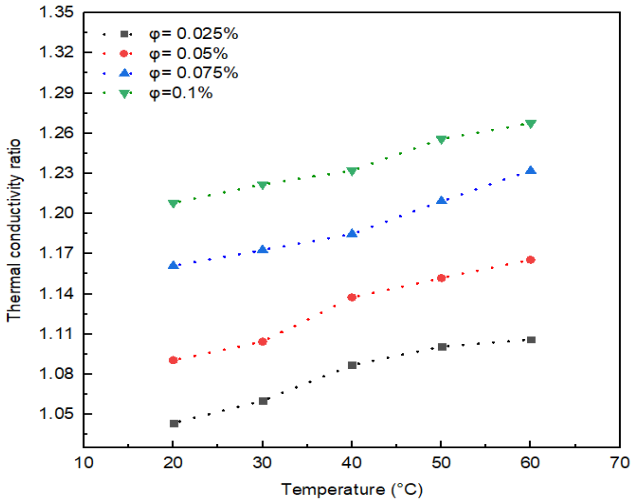

Fig. 4.20. Thermal conductivity ratio of ZrO_2-SiC/DW at various temperatures at all volume fractions

Fig. 4.21 show the thermal conductivity ratio of ZrO_2/DW and SiC/DW nanofluids with a changing temperature from 20 °C to 60 °C. The results show that a lower solid volume fraction has a lower thermal conductivity ratio with an increase in temperature. At a volume fraction of 0.025%, the thermal conductivity ratio of ZrO_2/DW is 1.04%, and that of SiC/DW is 1.07% at 30 °C compared to the base fluid. At a volume fraction of 0.1%, the highest thermal conductivity ratio for ZrO_2/DW and SiC/DW are 1.17% and 1.24%, respectively.

As shown in the results obtained, the thermal conductivity ratio increases with an increase in nanoparticle volume fraction. An increase in temperature has an effect that is less significant than that of volume fraction. The effect of temperature on thermal conductivity has been attributed to a decrease in the particle size and viscosity of the nanofluids. Temperature also causes the Brownian motion effect on the nanoparticles, making them collide and transfer heat faster. However, Brownian motion is also the reason for enhanced thermal conductivity even at lower temperatures. However, the maximum thermal conductivity ratio coincides with the maximum temperature and nanoparticle volume fraction.

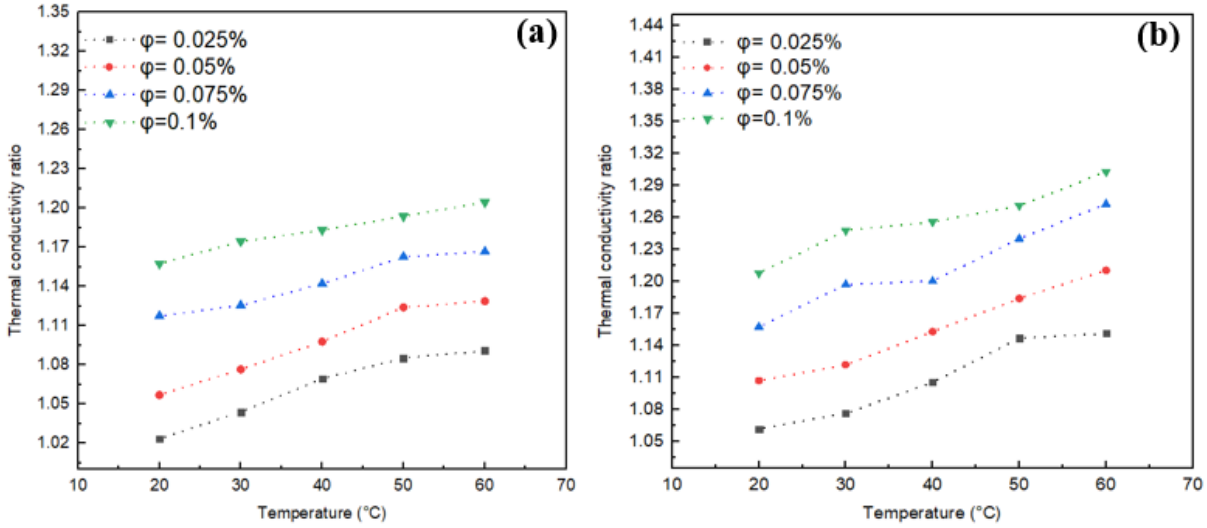

Fig. 4.21. Thermal conductivity ratio of (a) ZrO_2/DW and (b) SiC/DW nanofluids at various temperatures at all volume fractions

Due to the absence of a correlations for effectively predicting the thermal conductivity of ZrO_2/DW, SiC/DW, and ZrO_2-SiC/DW nanofluid, this work will use measurement results to put forward a new mathematical correlation that considers thermal conductivity as a function of temperature and volumetric fraction. Fig. 4.22 illustrate the influence of temperatures and solid volume fraction on thermal conductivity ratio of given nanofluid are plotted in 3-dimensional surfaces. This study uses the Origin Pro program based on the use of the Levenberg–Marquardt algorithm as well as the fitting method to analyse experimental data. As a result, the study came up with new models. The new model enabled the researcher to use the temperature and concentration values of the given nanofluids to estimate their thermal conductivity. In short, the study yields a novel mathematical expression to determine the relative thermal conductivity of the given nanofluids by inserting experimental values in the expression. These correlations, as shown in Eqs. (4.9) - (4.11), applies to engineering implementations due to high accuracy (R^2) is 0.9906 for ZrO_2-SiC/DW, by 0.986 for SiC/DW and by 0.988 for ZrO_2/DW.

ZrO_2-SiC/DW hybrid nanofluid:

$$\frac{k_{nf}}{k_{bf}} = 0.9619 + 2.076\varphi + 0.0015T \quad (4.9)$$

ZrO_2/DW mono nanofluid:

$$\frac{k_{nf}}{k_{bf}} = 0.9606 + 1.609\varphi + 0.0014T \quad (4.10)$$

SiC/DW mono nanofluid:

$$\frac{k_{nf}}{k_{bf}} = 0.9631 + 2.134\varphi + 0.0025T \quad (4.11)$$

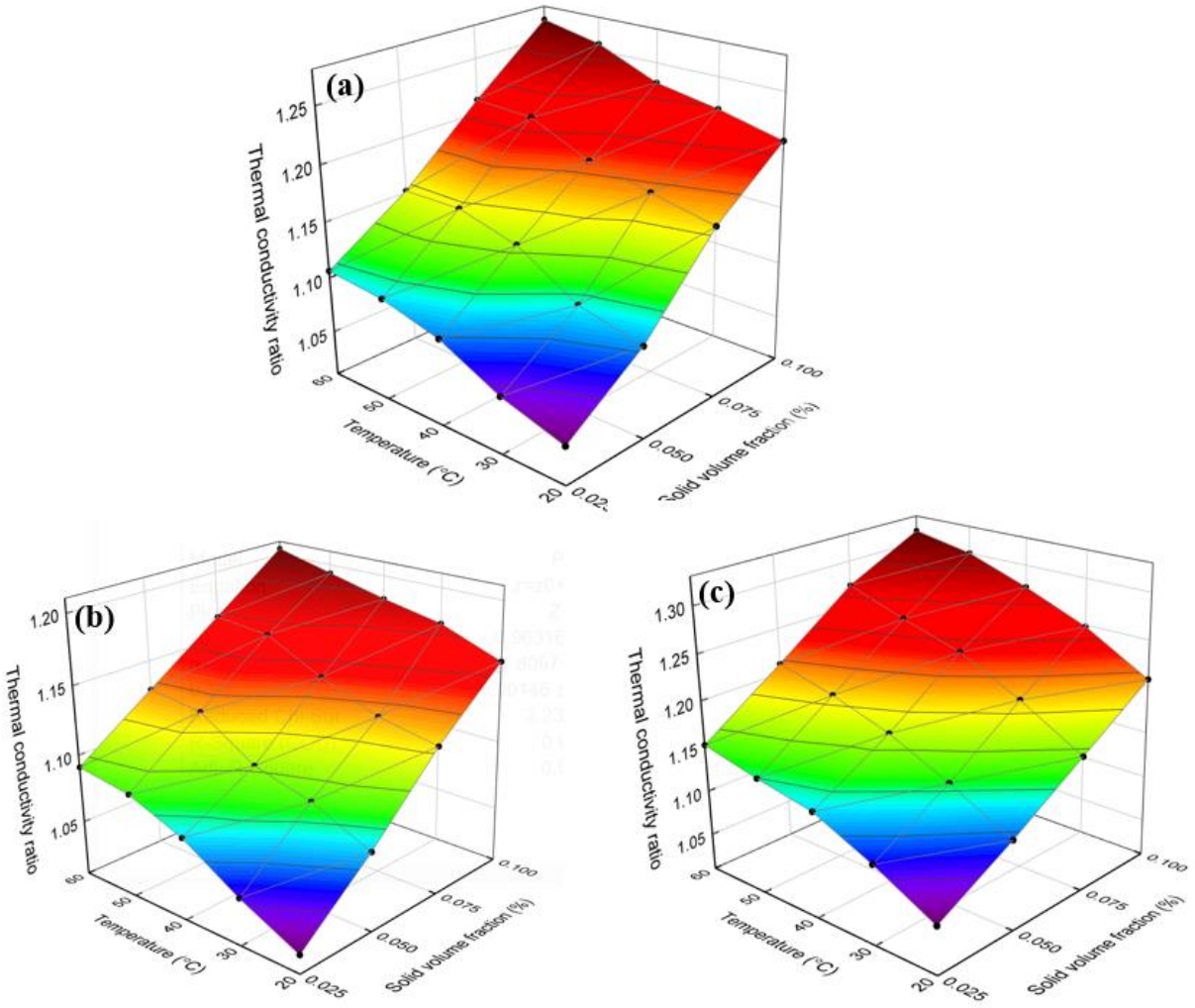

Fig. 4.22. 3D surface of thermal conductivity ratio at various volume concentrations and temperatures for (a) ZrO_2-SiC/DW, (b) ZrO_2/DW, and (c) SiC/DW nanofluids

The accuracy of the proposed correlations is determined using the margin of deviation parameter, expressed in Eq. (4.12). The parameters are used in Eq. (4.12) to show the values obtained from the experiment and the expected values as predicted in the proposed correlations. Fig. 4.23 shows the values of the maximum and minimum margin of deviation between the correlations and results obtained in a laboratory. The maximum value of MOD for hybrid nanofluid is 1.15% while 0.75% was the lowest. The value for the margin of deviation for ZrO_2/DW nanofluid is 1.49%, and that of SiC/DW nanofluid is 1.2%. This MOD value is an acceptable for an experimental correlation.

The conclusion is that since most of the experimental data is close to the correlations output with a small deviation, the proposed correlations have acceptable accuracy.

$$\mathrm{MOD}\ (\%) = \left[\frac{\left(\frac{k_{nf}}{k_{bf}}\right)_{Exp} - \left(\frac{k_{nf}}{k_{bf}}\right)_{Pred}}{\left(\frac{k_{nf}}{k_{bf}}\right)_{Exp}}\right] \times 100 \qquad (4.12)$$

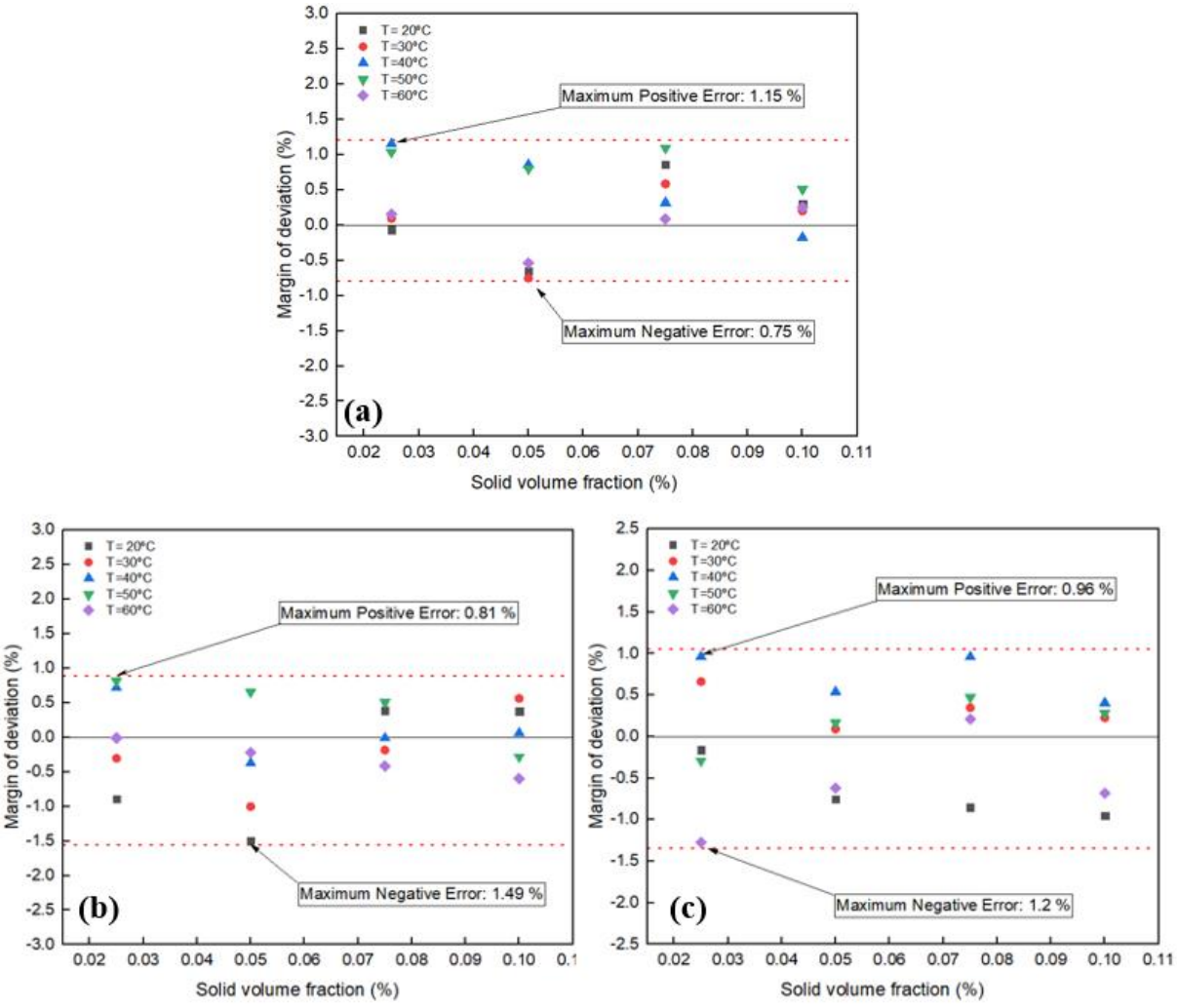

Fig. 4.23. Margin of deviation of thermal conductivity for (a) ZrO_2-SiC/DW, (b) ZrO_2/DW, and (c) SiC/DW

4.4. Thermal performance of flat plate solar collector

The chapter explored the increment of fluids thermal properties when nanoparticles were dispersed. An extensive discussion was carried out to demonstrate the thermal impact on the FPSC thermal system efficiency due to the dispersion of nanoparticles into water. The focus of this part is on determining the impact of adding ZrO_2, SiC and ZrO_2-SiC nanoparticles to distilled water. In this section, the collector's thermal efficiency as a function of the lowered temperature parameter [(Ti-Ta)/GT] is investigated as the independent variable for each of the scenarios researched. As stipulated by the ASHRAE Standard, a linear curve is fitted between thermal efficiency and reduced temperature [(Ti-Ta)/GT]. The line slope is called the removed energy parameter, [F_RU_L)]. The point where it intersects with the y-axis and the reduced temperature

parameter [(Ti-Ta)/GT] equates to zero is called the absorbed energy parameter [F_R (τα)]. The thermal efficiency is maximized when [(Ti-Ta)/GT] equates to zero, and in this situation, the thermal efficiency is defined as the collector's thermo-optical characteristic. In addition, in terms of nanofluids, there is a noteworthy influence of the volume fraction of nanoparticles on the nanofluids thermal properties; thus, the study examines four distinct volume fractions (0.025 %, 0.05 %, 0.075 % and 0.1 %) as well as the impact of three different mass flow rates (0.025, 0.033 and 0.041 kg/s).

4.4.1. Test case 1 distilled water

Graphs and equations are used to present the experimental findings, both of which explain the collector efficiency in terms of the decreased temperature. The FPSC efficiency was tested for different mass flow rates, namely 0.025, 0.033 and 0.041 kg/s. Every test was carried out for days, and the ideal experimental data was ultimately selected. The experimental data was introduced in linear equations to present the characteristics of the FPSC to compare the impact of different volume flow rates. Table 4.1 shows the efficiency parameters, the absorbed energy parameters F_R (τα), and the removed energy parameters F_RU_L at different mass flow rates. It was shown by all mass flow rates that all the experimental data served as the basis for the fitted linear equation. The Root Mean Square Error, i.e., R^2 showed the way data closely emphasizes the linear fitted curve. The differences in FPSC efficiency with the decreased water temperature parameter and distinct mass flow rates are demonstrated in Fig. 4.24. Correlations the developed experimental data to achieve the characteristic parameters of the FPSC and to obtain a better finding regarding how mass flow rate affects thermal efficiency. Accordingly, there is an increase in the FPSC efficiency at a specific value of reduced temperature parameter when the mass flow rate is increased. Besides, the useful heat energy is increased as the mass flow rate increased. In contrast, there is a direct relationship between useful heat energy and efficiency. Accordingly, the FPSC efficiency was increased when the mass flow increased from 0.025 to 0.041 kg/s by a maximum of 4.5%. Further details from Fig. 4.24 are offered in Table 4.1, which also presents the FPSC performance when the water is employed. Also, the Table 4.1 shows that there is an increase in removed energy as well as absorbed energy parameters when the mass flow increases. At a 0.041 kg/s mass flow, F_R (τα) and F_RU_L attained the highest values.

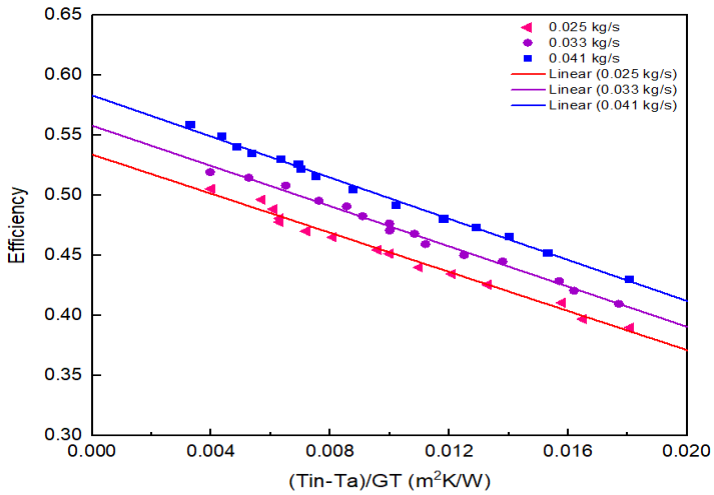

Fig. 4.24. FPSC thermal efficiency for distilled water at different mass flow rates

4.4.2. Test case 2 silicon carbide nanofluid

This study investigates four distinct nanoparticle volume fractions of 0.025%, 0.05%, 0.075, and 0.1% SiC nanofluid. As shown in Fig. 4.25, thermal efficiency is plotted against the reduced temperature parameter [(Ti-Ta)/GT] for water and the respective nanofluids at mass flow rates of 0.025, 0.033 and 0.041 kg/s., respectively. The value of the reduced temperature parameter [(Ti-Ta)/GT] is significant in terms of explaining how this factor alters the solar collector's efficiency. As illustrated in Fig. 4.25, when [(Ti-Ta)/GT] equates to zero, this is called the collector's absorbed energy parameter or thermo-optical efficiency. For mass flow rates of 0.025, 0.033 and 0.041kg/s with distilled water as a working fluid, the solar collector's thermo-optical efficiency is 0.5441, 0.5581 and 0.5713, respectively. As was illustrated in Fig. 16, when the volume fraction is 0.025%, the solar collector's thermo-optical efficiency is 0.654, 0.6751, and 0.6996 for mass flow rates of 0.025, 0.033 and 0.041kg/s, respectively. At a volume fraction of 0.05%, the solar collector has a thermo-optical efficiency of 0.6825 at a mass flow rate of 0.025 kg/s, which increases to 0.7061 when the mass flow rate is changed to 0.033 kg/s. and is maximized at 0.7259 when the mass flow rate reaches 0.041 kg/s. At a volume fraction of 0.075%, the solar collector has a thermo-optical efficiency of 0.6926 at a mass flow rate of 0.025 kg/s, which increases to 0.7259 when the mass flow rate is changed to 0.033 kg/s. and is maximized at 0.7473 when the mass flow rate reaches 0.041 kg/s. Additionally, Fig. 4.25 clearly shows that at a volume fraction of 0.1%, the solar collector's thermo-optical efficiency exhibits an increase, with values of 0.7286, 0.7496 and 0.7743 corresponding to mass flow rates of 0.025, 0.033 and 0.041 kg/s, respectively. According to Fig. 4.25, when nanofluids are used, the solar collector's thermo-optical characteristic is increased in comparison to water, while the addition of an increased volume of nanoparticles also causes it to rise. Additionally, increased mass flow rates cause the collector's thermo-optical characteristic to increase. Resultantly, from all the investigated scenarios, the collector's thermo-optical characteristic was maximized at 0.7743 when the volume fraction and mass flow rate were 0.1% and 0.041 kg/s, respectively. On the other hand, the lowest value was recorded when distilled water was used with a mass flow rate of 0.025 kg/s. The linear fitted curve's slope is called the removed energy parameter. When the mass flow rate was 0.025 kg/s, removed energy parameter of 9.997, 9.823, 9.72, 9.531 and 8.232 were recorded for nanoparticle volume fractions of 0.1%, 0.075%, 0.05%, 0.025% and water, respectively. When the mass flow rate was changed to 0.033 kg/s, the removed energy parameter 10.382, 10.288, 9.915, 9.77 and 8.287 for nanoparticle volume fractions of 0.1%, 0.075%, 0.05%, 0.025% and water, respectively. Lastly, at a mass flow rate of 0.041 kg/s, the removed energy parameter was maximized at 10.521, 10.46, 10.147, 9.853 and 8.353 for nanoparticle volume fractions of 0.1%, 0.075%, 0.05%, 0.025% and water, respectively. Such slope values are clear evidence that the addition of nanoparticles causes the heat loss coefficient to increase, while increasing the mass flow rate also leads to a rise in the coefficient value. Consequently, the collector's absorber is heated to a greater extent and increased heat loss occurs. Therefore, the heat loss coefficient is greater when the volume fraction is 0.1%. The values of the absorbed energy parameter and removed energy are shown in Table. 4.1.

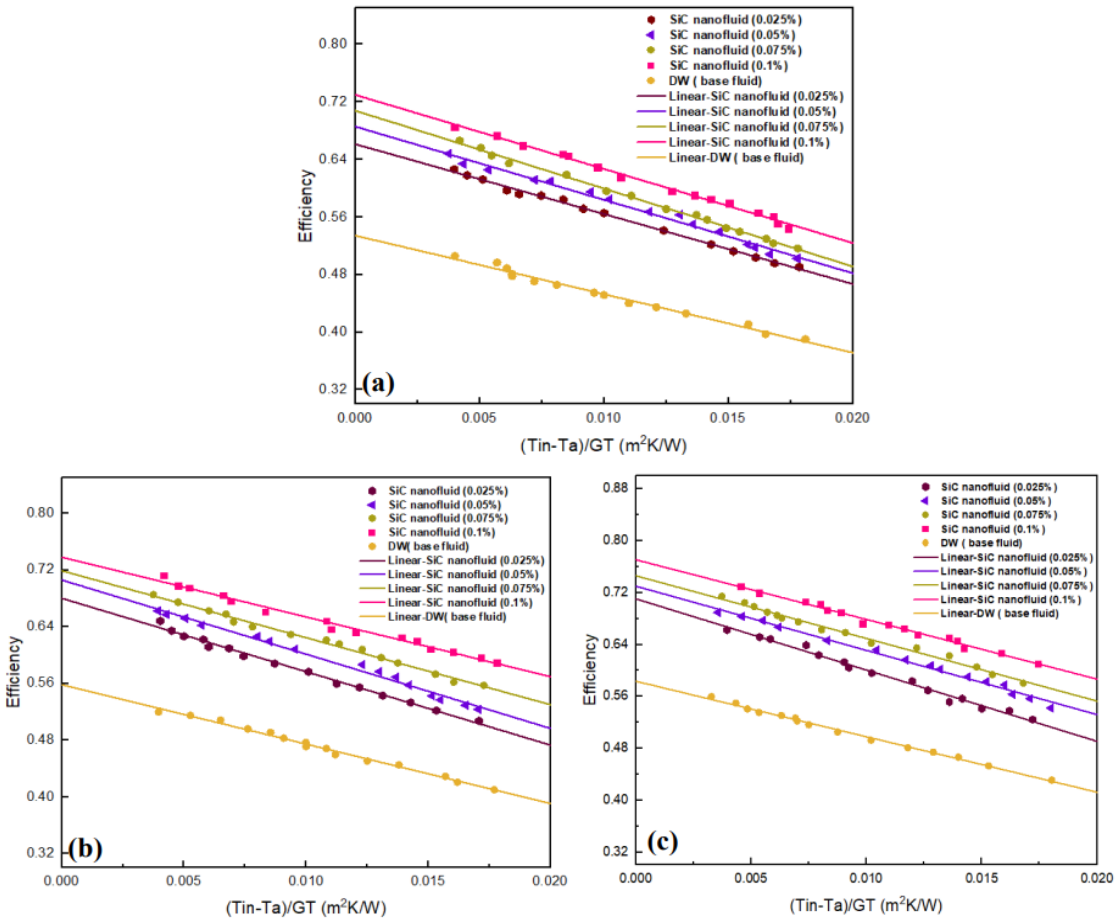

Fig.4.25. The thermal efficiency of FPSC for SiC/DW nanofluid: (a) 0.025kg/s, (b) 0.033 kg/s, and (c) 0.041 kg/s

Table 4.1. Values of F_RU_L and $F_R(\tau\alpha)$for SiC nanofluid and for distilled water with different concentrations and flow rate values

Solid volume fraction φ%	Mass flow rate (kg/s)	$F_R(\tau\alpha)$	F_RU_L	R^2
0.025%	0.025	0.654	9.531	0.9936
	0.033	0.6751	9.77	0.9918
	0.041	0.6996	8.853	0.9842
0.05%	0.025	0.6825	9.72	0.9904
	0.033	0.7061	9.915	0.989
	0.041	0.7259	10.147	0.981
0.075%	0.025	0.6926	9.823	0.9936
	0.033	0.7259	10.288	0.9872
	0.041	0.7473	10.46	0.9976
0.1%	0.025	0.7268	9.997	0.9909
	0.033	0.7496	10.382	0.9919
	0.041	0.7743	10.521	0.9846
Distilled water	0.025	0.5441	8.232	0.9863
	0.033	0.5581	8.2875	0.9914
	0.041	0.5713	8.353	0.9954

Fig. 4.26 shows how the mass flow rate affected the system when the working fluid was the various volume fractions of SiC nanoparticles as a function of the reduced energy parameter [(Ti-Ta)/GT]. In Fig. 4.26a, the effects of nanoparticles with a volume fraction of 0.025% for mass flow rates of 0.025, 0.033 and 0.041 kg/s are shown. Fig. 4.26b reveals how the various mass flow rates of 0.025, 0.033 and 0.041 kg/s affected the outcomes when using a SiC nanoparticle volume fraction of 0.05%. At the range of mass flow values, Fig. 4.26 (c) and (d) illustrate the effects of a SiC nanoparticle volume fraction of 0.075% and 0.1%, respectively. As Figs. 4.25 and 4.26 respectively illustrated the absorbed energy parameter and removed energy for both the nanofluids investigated and water in detail, further explanations are not required. The conclusion can be drawn that the collector's efficiency and heat removed energy parameter are both increased when the mass flow rate rises. This can be explained by the fact an increase in the Reynold's number of the max flow rate causes the heat transfer to be increased as a result of turbulence and the layers of fluid becoming mixed. This is fundamentally a result of Brownian motion, which is regarded as being the primary factor causing nanofluids to have increased thermal conductivity in comparison to water. Such behavior was observed in my research, indicating that in the range I investigated, the efficiency was improved more when the mass flow rate was higher. Therefore, assert that the addition of nanofluids increases the collector's thermal efficiency and aids in obtaining a higher temperature difference, meaning that if an increased outlet temperature is needed, it is necessary to increase the collector's thermal efficiency.

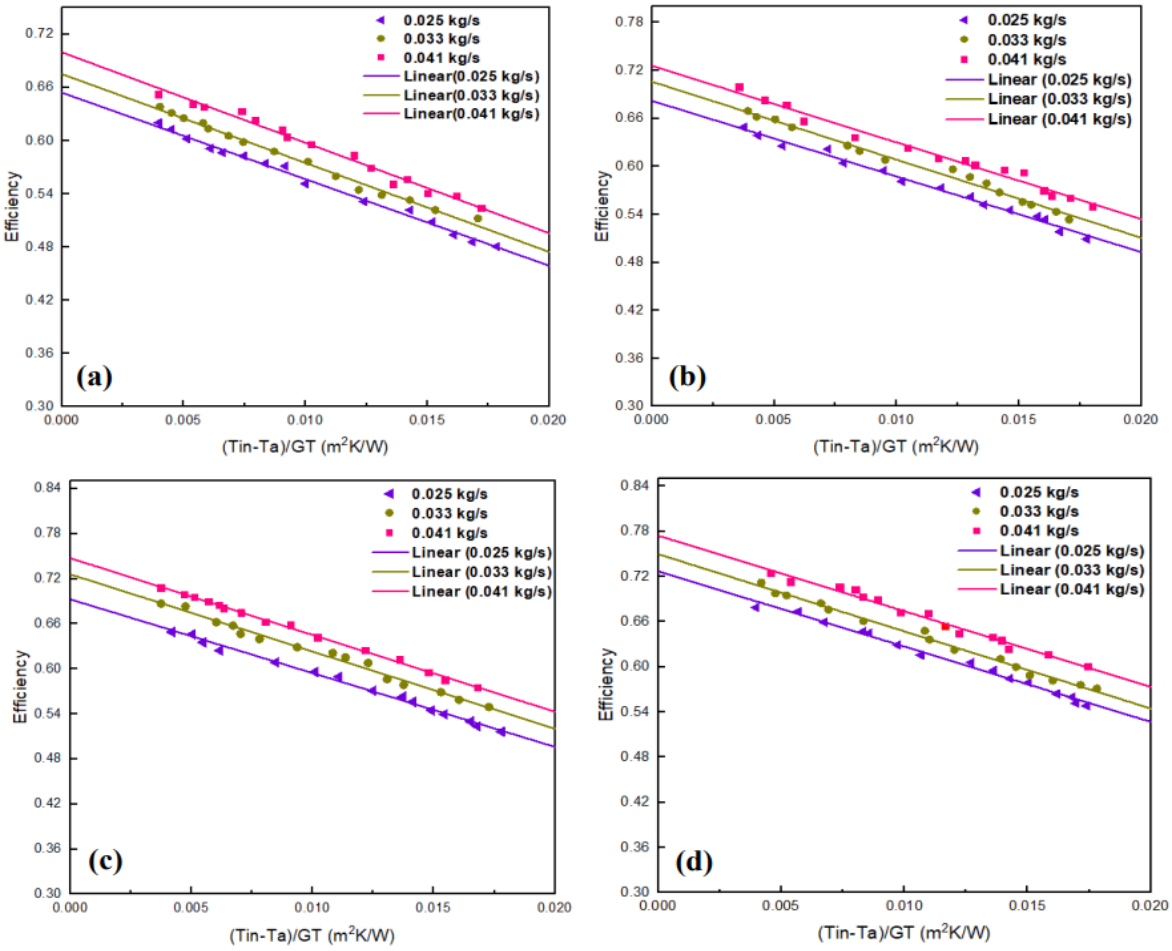

Fig. 4.26. Effect of the mass flow rate of the SiC nanofluid on the FPSC efficiency: (a) 0.025%, (b) 0.05 %, (c) 0.075 %, and (d) 0.1%

In the current research, the fitting method along with Levenberg–Marquardt algorithm by Origin Pro program was applied in 3-dimensional surfaces that the data obtained from the experiments, which facilitated the development of a novel model capable of predicting the thermal efficiency of flat plate solar collector with respect to solid concentration and the reduced temperature factor [(Ti-Ta)/GT]. A new correlation for the prediction of the efficiency of FPSC as functions of solid concentration (φ) and temperature [(Ti-Ta)/GT] is developed through Eq. (4.13) for SiC/DW as a working fluid in solar collector, as shown below:

$$\eta_c = a + b\left(\frac{T_i - T_a}{GT}\right) + c\,\varphi + d\left(\frac{T_i - T_a}{GT}\right)^2 + e\,\varphi^2 \qquad (4.13)$$

The coefficients of the developed thermal efficiency correlation for the FPSC at different mass flow rates:

$\dot{m}$= 0.025 kg/s [a=0.585, b=-9.44, c=2.88, d=-16.92, e=-16.57, R^2 = 0.958]

$\dot{m}$ = 0.033 kg/s [a=0.574, b=-7.35, c=3.51, d=-72.68, e=-19.72, R^2 = 0.954]

$\dot{m}$ = 0.041 kg/s [a=0.585, b=-8.12, c=3.8, d=-47.67, e=-20.31, R^2 = 0.968]

4.4.3. Test case 3 zirconium oxide nanofluid

This part discusses in depth the effect of ZrO_2 nanoparticles concentration fraction on the thermal efficiency performance of the FPSC. Four different volume fractions were analyzed in this experiment, employing distilled water as a working liquid. The chosen volume fraction concentrations which are 0.025%, 0.05%, 0.075%, and 0.1% have great stability and effective thermal performance. Various flow, namely 0.025 kg/s, 0.033 kg/s and 0.041 kg/s were used to conduct this experiment. Fig. 4.27 show the results of these experiments for the respective flow of 0.025 kg/s, 0.033 kg/s, and 0.041 kg/s. The efficiency values versus the reduced temperature parameter, [(Ti-Ta)/GT] are indicated in this figure along with a linear fitted curve to represent the studied case. Abbreviated F_RU_L, the removed energy parameter, is the slope of this line and the heat lost from the FPSC is represented by it. Additionally, F_R (τα), the absorbed energy parameter or the collector's thermal efficiency is the meeting point of this line with the Y-axis. When the inlet fluid temperature equals the ambient temperature, the FPSC efficiency reaches the maximum value since the energy loss stops and hence this value is called (the maximum thermal efficiency, F_R (τα)) of the FPSC. Heat loss increases with the high temperature of the inlet fluid, decreasing the efficiency of the collector which manifests the reason for the negative sign of the removed energy parameter. Table 4.2 shows the values of both the absorbed F_R (τα) and removed energy parameter F_RU_L for every case study. Here, the suitable line curve is displayed as the root which refers to the square error, R^2. In these table and figure, the thermal efficiency increment at the flow of 0.025 kg/s from 0.5441 for DW to 0.6048, 0.6372, 0.6591, and 0.6736 for the concentrations of ZrO_2 of 0.025%, 0.05%, 0.075% and 0.1%, respectively are represented. At the same time, the F_RU_L increased from 8.232 for DW to 9.233, 9.596, 9.719, and 10.137 for the respective solid volume fraction of ZrO_2 of 0.025%, 0.05%, 0.075%, and 0.1%. At the flow of 0.033 kg/s, the efficiency increased to 0.6311, 0.6658, 0.6804, and 0.6966. Simultaneously, the F_RU_L for DW escalated to 9.452, 9.773, 9.955, and 10.347 for the respective solid volume fraction of ZrO_2 of 0.025%, 0.05%, 0.075%, and 0.1%. At the flow rate of 0.041 kg/s, the efficiency and the F_RU_L gained maximum values for DW which are 0.6605, 0.6933, 0.697, 0.721 and 9.623, 9.893, 10.153, and 10.538 for the respective solid fraction of ZrO_2 of 0.025%, 0.05%, 0.075%, and 0.1%. It can

be seen that a higher value is attained for the FPSC thermal efficiency when ZrO_2 was added in contrast to DW, the more the nanoparticles added the increase the thermal efficiency. When 0.1% concentration of ZrO_2 is added at the flow of 0.041 kg/s, the thermal efficiency of the FPSC increased by 25.43% in comparison to DW. However, compared to the values after the ZrO_2 nanoparticles were inserted, the F_RU_L had a lower value for water. Additionally, with higher ZrO_2 nanoparticle volume fraction concentrations, even greater values of the F_RU_L were observed. When the high solid volume fraction of ZrO_2 of 0.1% was added at the flow of 0.041kg/s, the F_RU_L has a maximum value of 10.538. Also, in this figure show that when the [(Ti-Ta)/GT] is equal to zero, the efficiency of the FPSC gains the highest value and the efficiency of the FPSC equals F_R ($\tau\alpha$) and shows no heat loss in the atmosphere. It has been assumed in this study that the nanofluids thermal conductivity is greater than water. The heat absorption is increased as the thermal conductivity increases, increasing the heat removal factor.

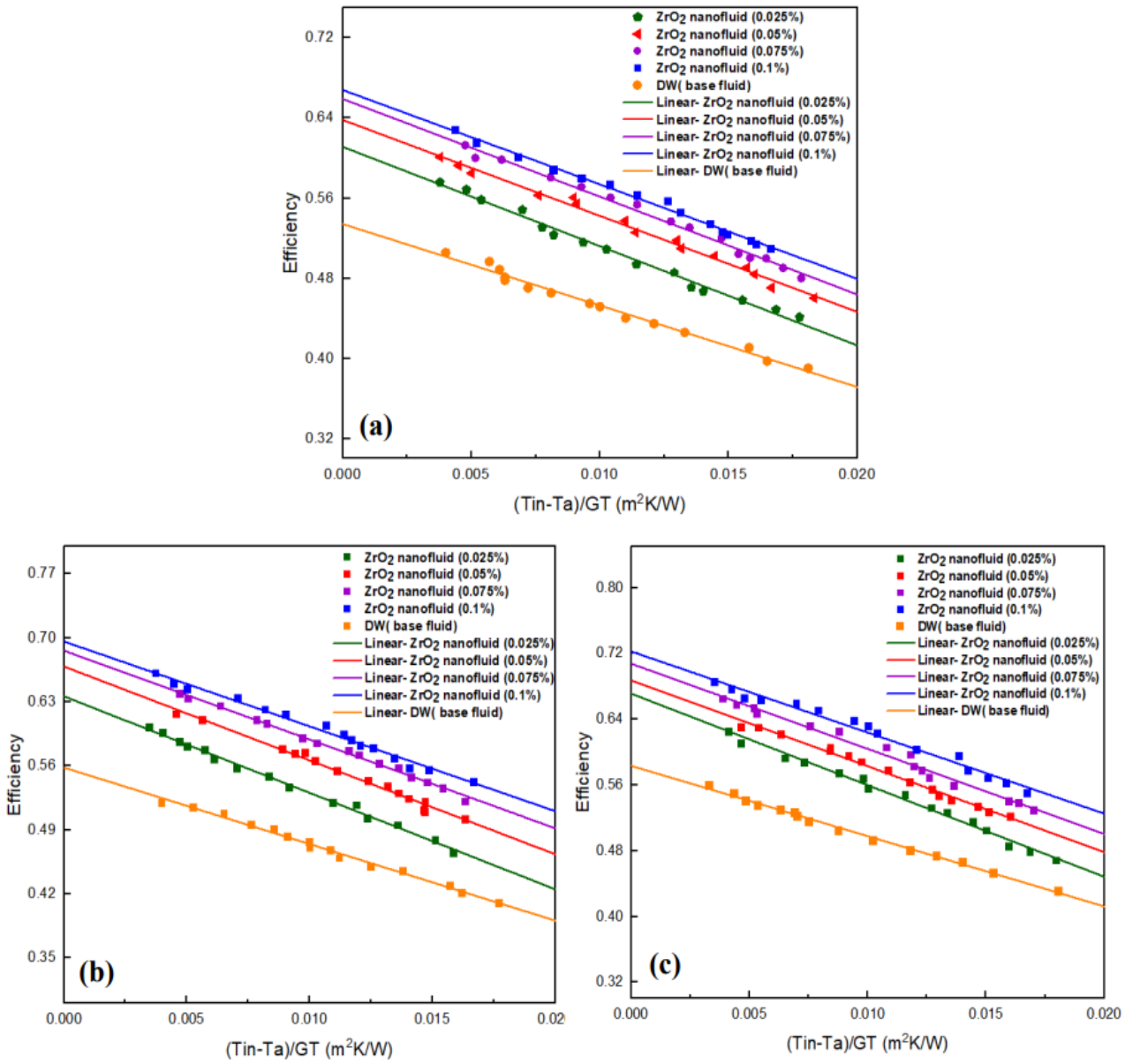

Fig. 4.27. The thermal efficiency of FPSC for ZrO_2/DW nanofluid: (a) 0.025kg/s, (b) 0.033 kg/s, and (c) 0.041 kg/s

In this chapter, thermal efficiency analysed various mass flow rates. Mass flow rates of 0.025, 0.033, and 0.041 kg/s were used by using a variable speed pump. Table 4.2 and Fig. 4.28 show the impact of these distinct mass flow rates. These Figures suggest that as the mass flow rates rise the efficiency of the FPSC increases. At the mass flow rates of 0.041 kg/s, the greatest of the thermal efficiency noted were 0.6605, 0.6933, 0.697, 0.721 for nanofluids and the respective concentration of 0.025%, 0.05%, 0.075%, and 0.1%. Moreover, at the same mass flow rates of 0.041 kg/s, the maximum value of the F_RU_L obtains a maximum. The theory of thermal transfer explains that when the flow rate increases the mixture and turbulence between liquid nanoparticles increase as well as the heat transfer coefficient leading to a rise in the heat transfer rate. Thus, maximum values of efficiency are attained by the flat plate solar collector.

Table 4.2. Values of F_RU_L and F_R ($\tau\alpha$) of FPSC using ZrO_2 nanofluid and distilled water with various concentrations and flow rate values

Solid volume fraction φ%	**Mass flow rate (kg/s)**	**F_R ($\tau\alpha$)**	**F_RU_L**	**R^2**
0.025%	0.025	0.6048	9.233	0.9936
	0.033	0.6311	9.452	0.9918
	0.041	0.6605	9.623	0.9842
0.05%	0.025	0.6372	9.596	0.9904
	0.033	0.6658	9.773	0.989
	0.041	0.6933	9.893	0.981
0.075%	0.025	0.6591	9.719	0.9936
	0.033	0.6804	9.955	0.9872
	0.041	0.697	10.153	0.9976
0.1%	0.025	0.6736	10.137	0.9909
	0.033	0.6966	10.347	0.9919
	0.041	0.721	10.538	0.9846
Distilled water	0.025	0.5441	8.232	0.9863
	0.033	0.5581	8.2875	0.9914
	0.041	0.5713	8.353	0.9954

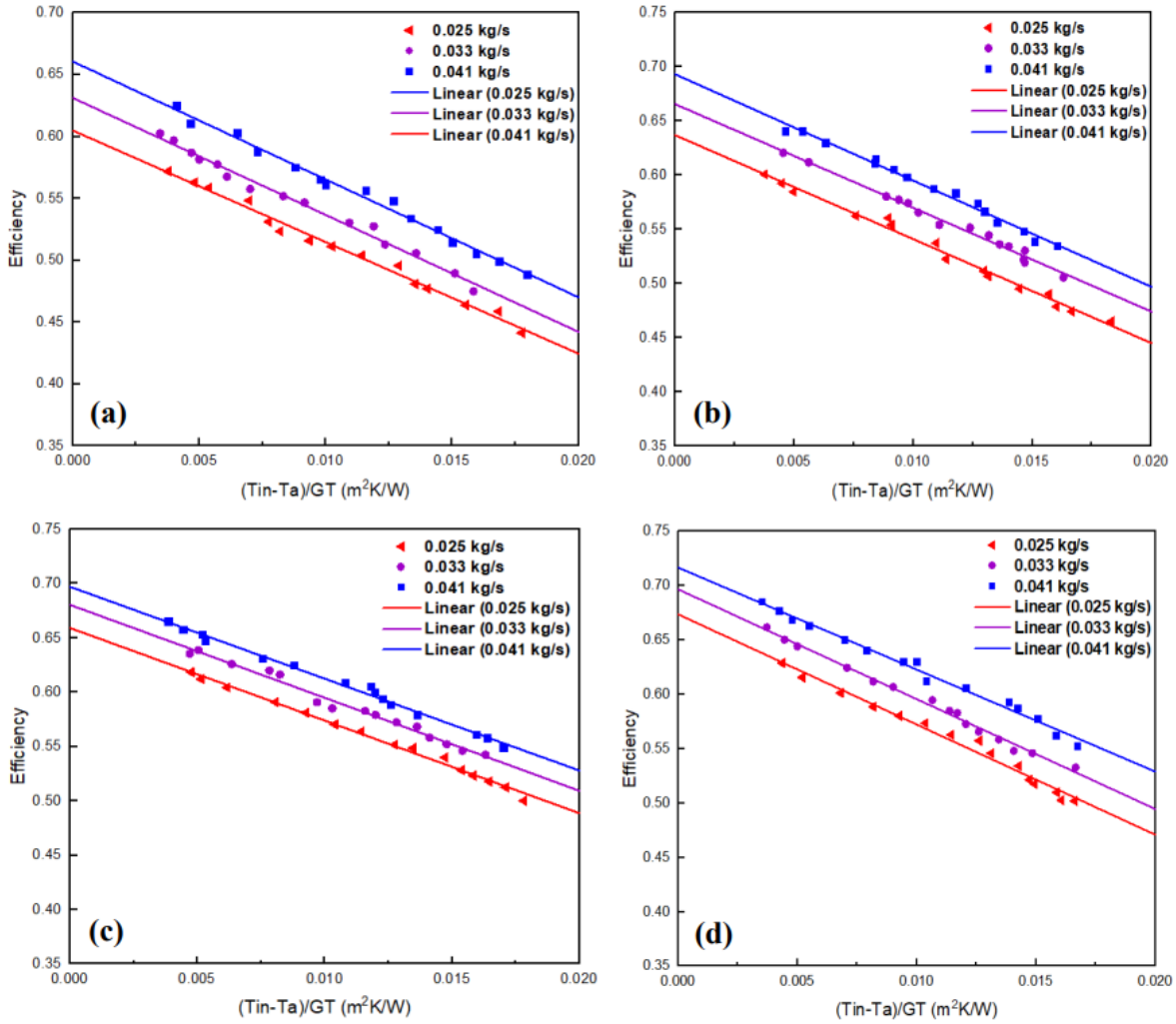

Fig. 4.28. Effect of the mass flow rate of the ZrO_2 nanofluid on the FPSC efficiency: (a) 0.025%, (b) 0.05 %, (c) 0.075 %, and (d) 0.1%

In the current research, the fitting method along with Levenberg–Marquardt algorithm by Origin Pro program was applied in 3-dimensional surfaces that the data obtained from the experiments, which facilitated the development of a novel model capable of predicting the thermal efficiency of flat plate solar collector with respect to solid concentration and the reduced temperature factor [(Ti-Ta)/GT]. A new correlation for the prediction of the efficiency of FPSC as functions of solid concentration (φ) and temperature [(Ti-Ta)/GT] is developed through Eq. (4.14) for ZrO_2/DW as a working fluid in solar collector, as shown below.

$$\eta_c = a + b\left(\frac{T_i - T_a}{GT}\right) + c\,\varphi + d\left(\frac{T_i - T_a}{GT}\right)^2 + e\,\varphi^2 \qquad (4.14)$$

The coefficients of the developed thermal efficiency correlation for the FPSC at different mass flow rates:

$\dot{m}$= 0.025 kg/s [a=0.565, b=-10.95, c=1.98, d=83.45, e=-9.91, R^2 = 0.9823]

$\dot{m}$ = 0.033 kg/s [a=0.571, b=-8.86, c=2.15, d=18.89, e=-9.56, R^2 = 0.96]

$\dot{m}$ = 0.041 kg/s [a=0.592, b=-6.75, c=1.59, d=-108.11, e=-4.34, R^2 = 0.988]

4.4.4. Test case 4 zirconium oxide - silicon carbide hybrid nanofluid

Table 4.3 shows F_R (τα) and F_RU_L reported for FPSCs filled with ZrO_2-SiC/DW hybrid nanofluid. The values are arranged for similar mass flow rates. The reduced temperature parameter, i.e., [(Ti-Ta)/GT] is evaluated for the given hybrid nanofluid to determine the thermal efficiency of the FPSC. Fig. 4.29 and Table 4.3 indicate significant changes in FPSC's efficiency with changes in the volume fraction of ZrO_2-SiC/DW hybrid nanofluid. The experiment revealed that nanofluid depicted higher heat removable factor as compared to water. The value for heat removable factor rises at a higher nanofluid mass flow rate and higher volume fraction. The outcomes also revealed that the nanofluids showed higher convective heat transfer coefficient than the water. The ZrO_2-SiC/DW hybrid nanofluid also showed a rise in the F_R (τα) and F_RU_L. Hence, the ZrO_2-SiC/DW hybrid nanofluid has improved the FPSC efficiency noticeably. The hybrid nanofluid depicted high F_R (τα) in comparison to water irrespective of the volume fractions and mass flow rates. Fig.4.29 (a) and Table 4.3 showed that ZrO_2-SiC/DW hybrid nanofluid showed a rise of 16.32% (for 0.025% volume fraction), a rise of 20.43% (for 0.05% volume fraction), a rise of 24.68% (for 0.075% volume fraction), and a 28.5% rise (for 0.1% volume fraction) in the F_R (τα) at 0.025 kg/s mass flow rate in comparison to water. ZrO_2-SiC/DW hybrid nanofluid showed a rise of 0.89% (for 0.025% volume fraction), a 19.75% rise (for 0.05% volume fraction), a 22.25% rise (for 0.075%volume fraction) and a 24.39% rise (for 0.1%volume fraction) in the F_RU_L. Fig. 4.29 (b) and Table 4.3 show that ZrO_2-SiC/DW hybrid nanofluid depicted 16.86%, 21.59%, 25.3%, and 30.04% higher values of absorbed energy parameter, F_R (τα) at volume fractions of 0.025%, 0.05%, 0.075% and 0.1% at a mass flow rate of 0.033 kg/s in comparison to water. In comparison to water, the use of nanofluid in volume fractions of 0.025%, 0.05%, 0.075%, and 0.1% yielded F_RU_L values of 2.34%, 21.93%, 23.45%, and 27.27%. Fig. 4.29 (c) and Table 4.3 showed 17.6%, 21.93%, 27.44%, and 31.64% rise in F_R (τα) values at 0.025%, 0.05%, 0.075%, and 0.1% volume fractions for 0.041 kg/s mass flow rate. In comparison to water, ZrO_2-SiC/DW hybrid nanofluid showed 3.11%, 22.15%, 23.57%, and 27.46% rise in F_RU_L values at 0.025%, 0.05%, 0.075%, and 0.1% volume fraction. The efficiency of FPSC was found to be associated with the nanoparticle concentration or volume fraction in the nanofluid. The nanoparticle concentration is increased, the rise in the number of nanoparticles leads to a greater heat convection effect between base fluid and nanoparticles resulting in higher values of heat transfer and Nusselt number. Table 4.3 presents the contrast of results obtained at 0.025% to 0.1% volume fraction which indicates maximum absorbed energy and heat loss at 0.1%. The current part also shows that FPSC shows a rise in efficiency with increasing concentration of nanoparticles until the concentration reaches a certain level. The FPSC considered in this study depicted high efficiency at a volume fraction of 0.1%. The amount of heat transfer varied with the volume fraction. It increased at a higher volume fraction more significantly in comparison to a lower volume fraction. Besides the F_R (τα) and F_RU_L values, the solar collector efficiency was affected by other factors like reduced temperature parameters [(Ti–Ta)/GT]. The FPSC yielded higher efficiency at high solar radiation and a lower value of [(Ti–Ta)/GT] provided the concentration of nanoparticles in the nanofluid is 0.1%. The efficiency of the FPSC keeps rising with a lower in [(Ti-Ta)/GT] value when the particle concentrations are 0.075% and 0.05%. The same trend follows and at the minimum value of [(Ti–Ta)/GT] and 0.025% particle concentration, the FPSC showed rise efficiency. The same trend is observed at different mass flow rates of 0.025 kg/s (Fig. 4.29(a)), 0.033 kg/s (Fig. 4.29(b)) and 0.041 kg/s (Fig. 4.29(c)). This is attributed to that when the [(Ti-Ta)/GT] value is small, it indicates a low-temperature difference and high solar radiation. Such a condition calls for higher particle

concentration that facilitates higher heat absorption and lower agglomeration of particles. Heat transfer takes place when particles undergo collision. Therefore, an increase in the volume fraction of nanoparticles (φ) leads to higher efficiency. With a rise in [(Ti-Ta)/GT] values, the temperature and viscosity of the nanofluid also elevate. Consequently, the boundary layer becomes thicker causing a decline in the rate of heat transfer and a consequent decline in efficiency. The nanofluids also show greater thermal conductivity at high temperatures. This results in higher values of the overall heat transfer coefficient as well as the F_RU_L. The study also shows a rise in thermal conductivity with the addition of nanofluid. This may be attributed to the use of a forced circulation pump and the resulting Brownian motion as suggested in this research. The pump stimulated particles to move in random directions. As a result, the solid and liquid particles underwent multiple collisions leading to a higher convective heat transfer coefficient and ultimately higher thermal efficiency.

Table 4.3. F_RU_L, $F_R(\tau\alpha)$, and R^2 of FPSC using ZrO_2-SiC/DW hybrid nanofluid and distilled water with various mass flow rates and concentrations

Solid volume fraction φ%	**Mass flow rate (kg/s)**	**F_R ($\tau\alpha$)**	**F_RU_L**	**R^2**
0.025%	0.025	0.6329	8.306	0.9914
	0.033	0.6522	8.482	0.9932
	0.041	0.6719	8.613	0.992
0.05%	0.025	0.6553	9.858	0.9936
	0.033	0.6786	10.105	0.9868
	0.041	0.6966	10.204	0.9909
0.075%	0.025	0.6784	10.064	0.9937
	0.033	0.6993	10.231	0.9869
	0.041	0.7281	10.322	0.9924
0.1%	0.025	0.6992	10.24	0.9925
	0.033	0.7258	10.548	0.9924
	0.041	0.7521	10.647	0.994
Distilled water	0.025	0.5441	8.232	0.9863
	0.033	0.5581	8.2875	0.9914
	0.041	0.5713	8.353	0.9954

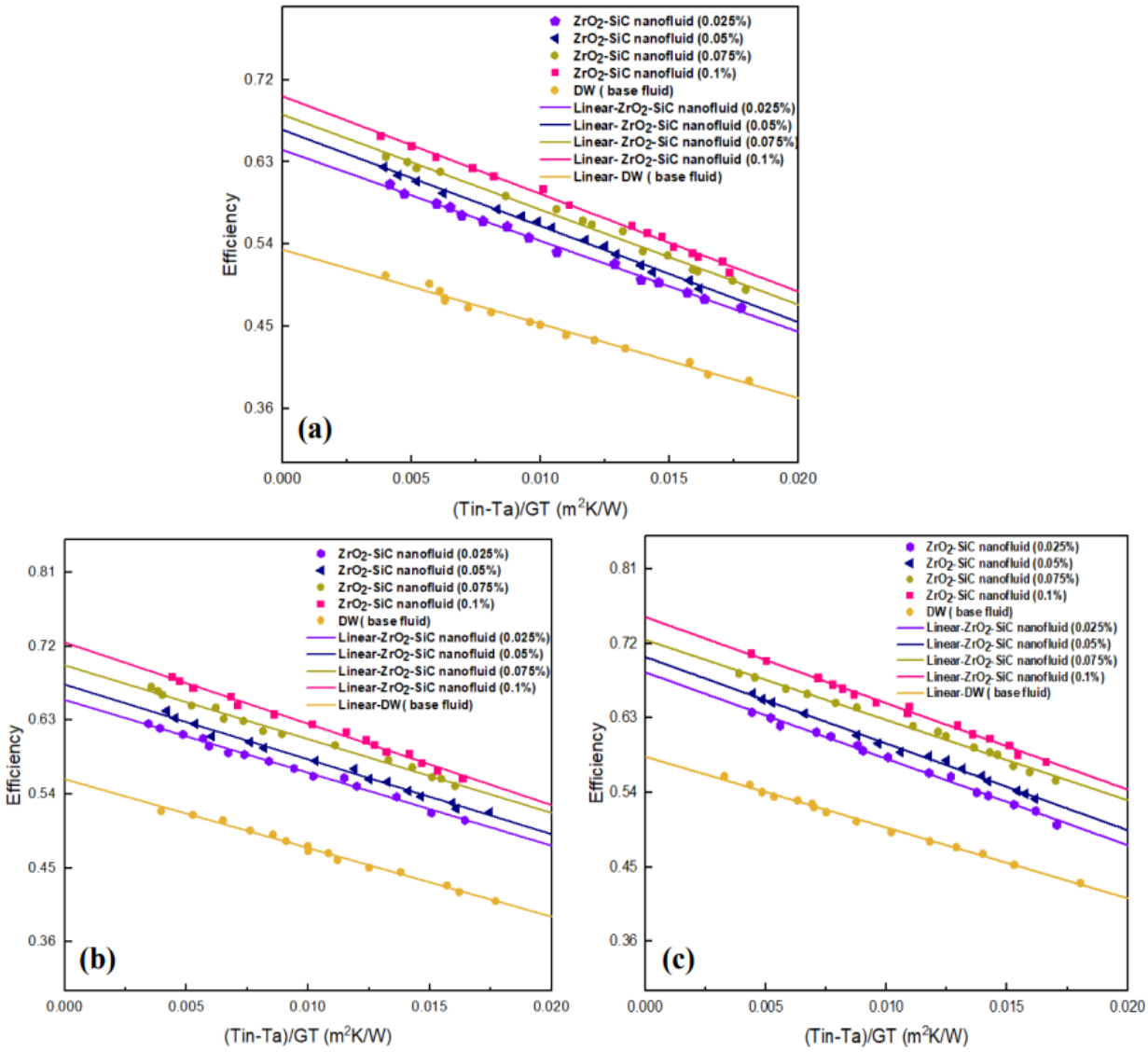

Fig. 4.29. The thermal efficiency of FPSC for ZrO_2-SiC/DW hybrid nanofluid with different Solid **v**olume fraction: (a) 0.025 kg/s, (b) 0.033 kg/s, and (c) 0.041 kg/s

Moreover, the FPSC efficiency was evaluated at different concentrations or volume fractions (φ) of ZrO_2-SiC/DW hybrid nanofluid (0.025%, 0.05%, 0.075%, and 0.1%) and mass flow rates (0.025, 0.05 and 0.1 kg/s). The evaluated efficiencies have been given in Fig. 4.30. Also, Fig. 4.29 and Table 4.3 shows both the F_RU_L and F_R (τα) evaluated for each concentration of hybrid nanofluid. The rise in the value of F_R (τα) energy absorbance is observed with increasing mass flow rate for each volume fraction of hybrid nanofluid. It was noticed that there were no considerable changes in the F_RU_L with changes in volume fractions. However, the value of heat loss factor escalated at a higher mass flux rate since at a higher mass flux rate, there was an increase in particles movement within nanofluid, Brownian motion, the Reynolds and Nusselt numbers.

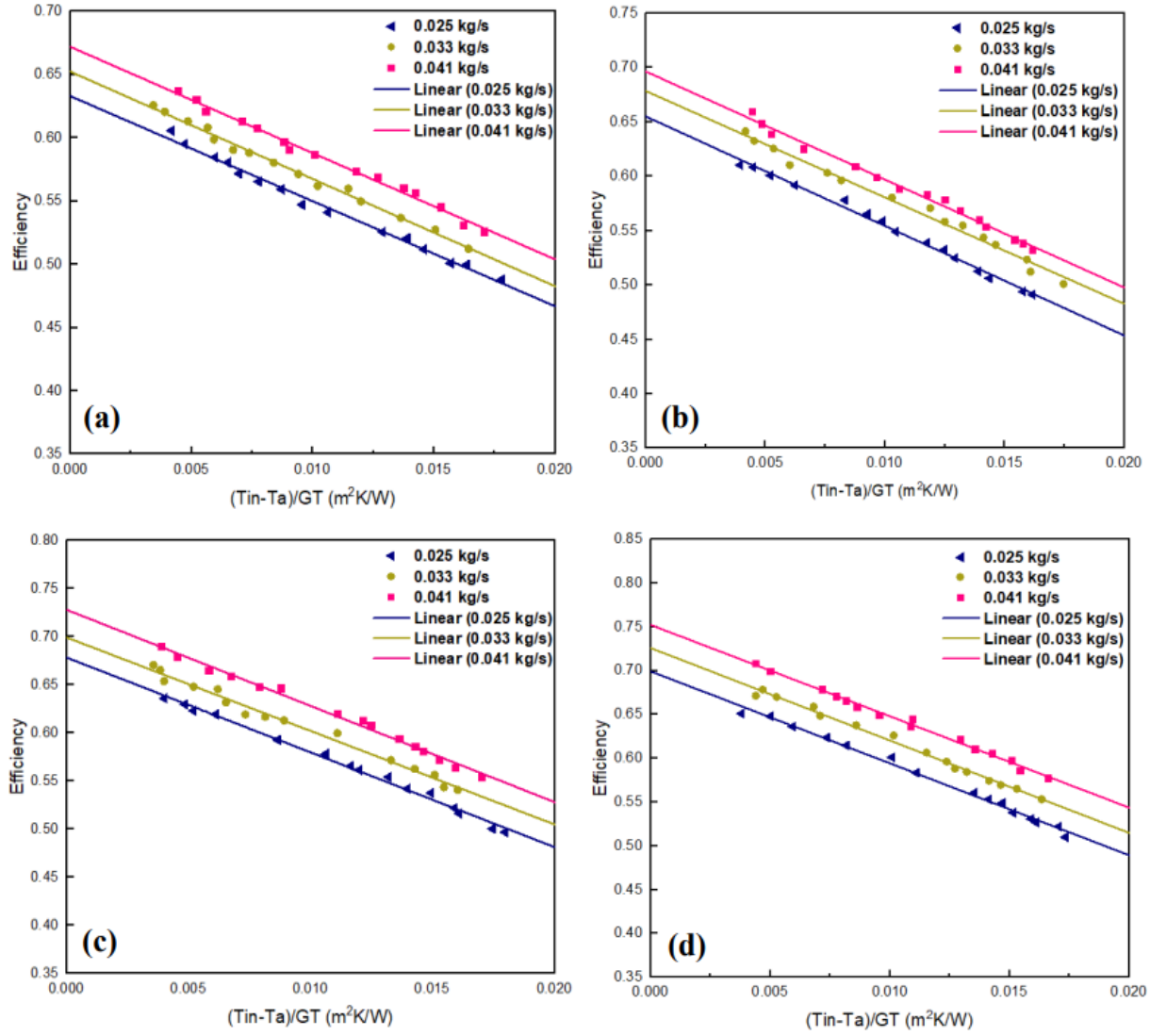

Fig. 4.30. FPSC thermal efficiency for ZrO_2-SiC/DW hybrid nanofluid under different mass flow rates and volume fraction of (a) 0.025%, (b) 0.05 %, (c) 0.075%, and (d) 0.1%

In the current research, the fitting method along with Levenberg–Marquardt algorithm by Origin Pro program was applied in 3-dimensional surfaces that the data obtained from the experiments, which facilitated the development of a novel model capable of predicting the thermal efficiency of flat plate solar collector with respect to solid concentration and the reduced temperature factor [(Ti-Ta)/GT]. A new correlation for the prediction of the efficiency of FPSC as functions of solid concentration (φ) and temperature [(Ti-Ta)/GT] is developed through Eq. (4.15) for ZrO_2-SiC/DW as a working fluid in solar collector, as shown below.

$$\eta_c = a + b\left(\frac{T_i - T_a}{GT}\right) + c\,\varphi + d\left(\frac{T_i - T_a}{GT}\right)^2 + e\,\varphi^2 \qquad (4.15)$$

The coefficients of the developed thermal efficiency correlation for the FPSC at different mass flow rates:

ṁ= 0.025 kg/s [a=0.578, b=-9.3, c=2.43, d=-27.6, e=-13.88, R^2 = 0.963]
ṁ = 0.033 kg/s [a=0.591, b=-7.34, c=2.435, d=-71.77, e=-12.16, R^2 = 0.954]
ṁ = 0.041 kg/s [a=0.6, b=-8.325, c=2.18, d=-18.27, e=-9.28, R^2 = 0.973]

4.4.5. Nusselt number of nanofluids

The Nusselt number is an important parameter discovered by a German engineer, Nusselt Wilhelm (1882–1957). The Nusselt number is applied widely in fluid dynamics and heat transfer. This number quantifies the ratio of convective heat transfer to conductive heat transfer at the surface of a fluid. The volume concentrations and Reynolds number evaluated for the fluid help determine its average Nusselt number. It was observed that nanofluids depicted a higher value of the Nusselt number indicating a higher rate of heat transfer than water. The addition of nanoparticles to the base fluid and increasing the fluid flow rate led to a greater value of Reynolds number. The rise in the Reynolds number and the temperature gradient leads to changes in the Nusselt number since these parameters raise the heat transfer coefficient. The Nusselt number is also associated with heat transfer occurring at the boundary layer of fluid in forced convection. The Nusselt number is the ratio of convective and conductive heat transfer perpendicular to the boundary. Besides, the Reynolds number, the Prandtl number also affects the Nusselt number. It is evident from Fig. 4.31 that using nanofluids instead of base fluid led to a rise in the Nusselt number besides improving the heat transfer properties of the collector. It is noticed that the Nusselt number of nanofluids increases with increase of particle volume concentrations and Reynolds number. Nusselt numbers determined from the experimental tests shows that the nanofluid has a positive impact pertaining to heat transfer where the nanofluids enhances the Nusselt number compared with that of water alone by 24.55%, 25.6%, 27.2%, and 29%, with the corresponding Reynolds number of 2022.04, 1982.39, 1555.4, and 1348.02 for the SiC nanofluid volume ratios of 0.025%, 0.05%, 0.075%, and 0.1%, respectively as Fig. 4.31 show. Besides, the Nusselt number enhancement by 12.3%, 13.18%, 14%, and 20.67% with the corresponding Reynolds number of 1743.13, 1263.7, 1148.88, and 1064.23 for the ZrO_2 nanofluid volume ratios of 0.025%, 0.05%, 0.075% and 0.1%, respectively as Fig. 15 show. In addition, the nanofluids enhances the Nusselt number compared with that of water alone by 16.41%, 17.27%, 18%, and 21.25%, with the corresponding Reynolds number of 1872.25, 1555, 1348, and 1296.18 for the ZrO_2- SiC hybrid nanofluid volume ratios of 0.025%, 0.05%, 0.075%, and 0.1%, respectively as shown in Fig. 4.31.

The following Nusselt number new correlations were developed based on the experimental data of water and different nanofluids.

SiC nanofluid:

$$\mathrm{Nu} = 0.07495\ \mathrm{Re}^{0.5251}\mathrm{Pr}^{0.506}(1+\varphi)^{3.683} \tag{4.16}$$

$$439.57 < \mathrm{Re} < 2115.1;\ 0 < \varphi < 0.1\%;\ 2.67 < \mathrm{Pr} < 6.98$$

ZrO_2 nanofluid:

$$\mathrm{Nu} = 0.10158\ \mathrm{Re}^{0.4742}\mathrm{Pr}^{0.5173}(1+\varphi)^{1.712} \tag{4.17}$$

$$361.07 < \mathrm{Re} < 2115.1;\ 0 < \varphi < 0.1\%;\ 3.06 < \mathrm{Pr} < 6.98$$

ZrO_2-SiC hybrid nanofluid:

$$\mathrm{Nu} = 0.04677\ \mathrm{Re}^{0.5596}\mathrm{Pr}^{0.6468}(1+\varphi)^{2.7573} \tag{4.18}$$

$$421.25 < \mathrm{Re} < 2115.1;\ 0 < \varphi < 0.1\%;\ 3.06 < \mathrm{Pr} < 6.98$$

Fig. 4.32, present the comparison between the proposed Nusselt number new correlations Eqs. (4.16) - (4.18) data and experimental data. The maximum deviation between experimental data and correlations for SiC, ZrO_2, and ZrO_2-SiC nanofluid were 3.04%, 1.81%, and 2.71% respectively.

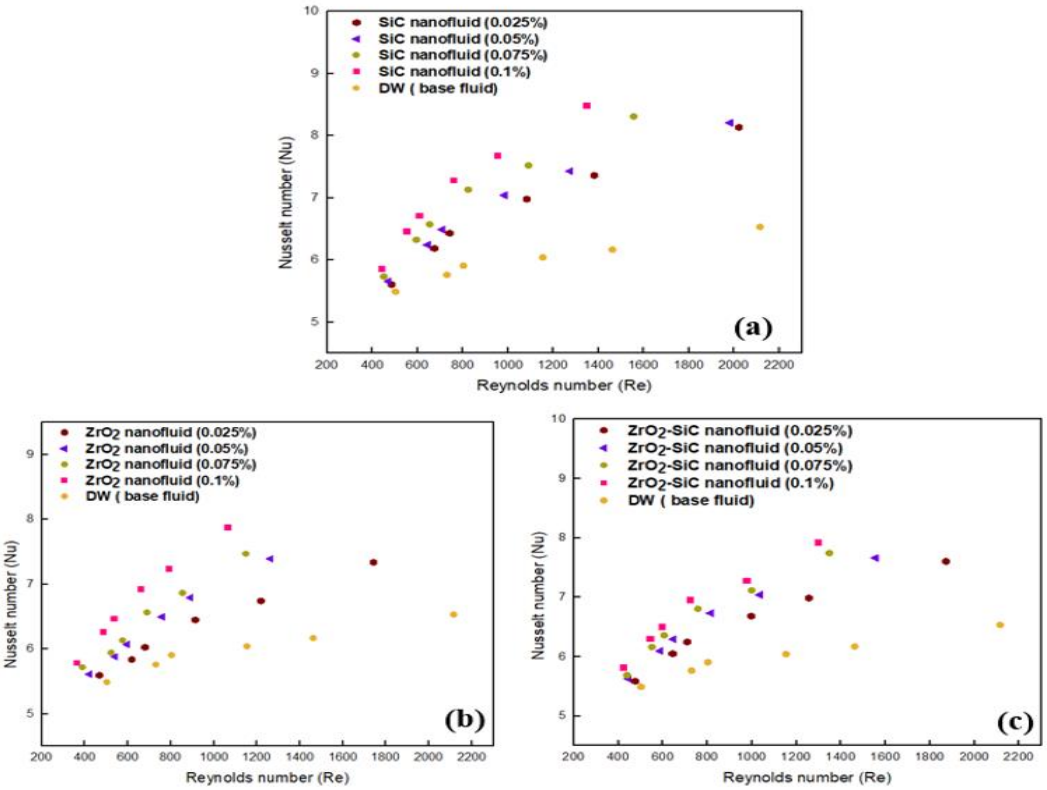

Fig. 4.31. Nusselt number of nanofluids at variation values of solid volume fraction and Reynolds numbers for (a) SiC/DW, (b) ZrO_2/DW, and (c) ZrO_2-SiC/DW nanofluids

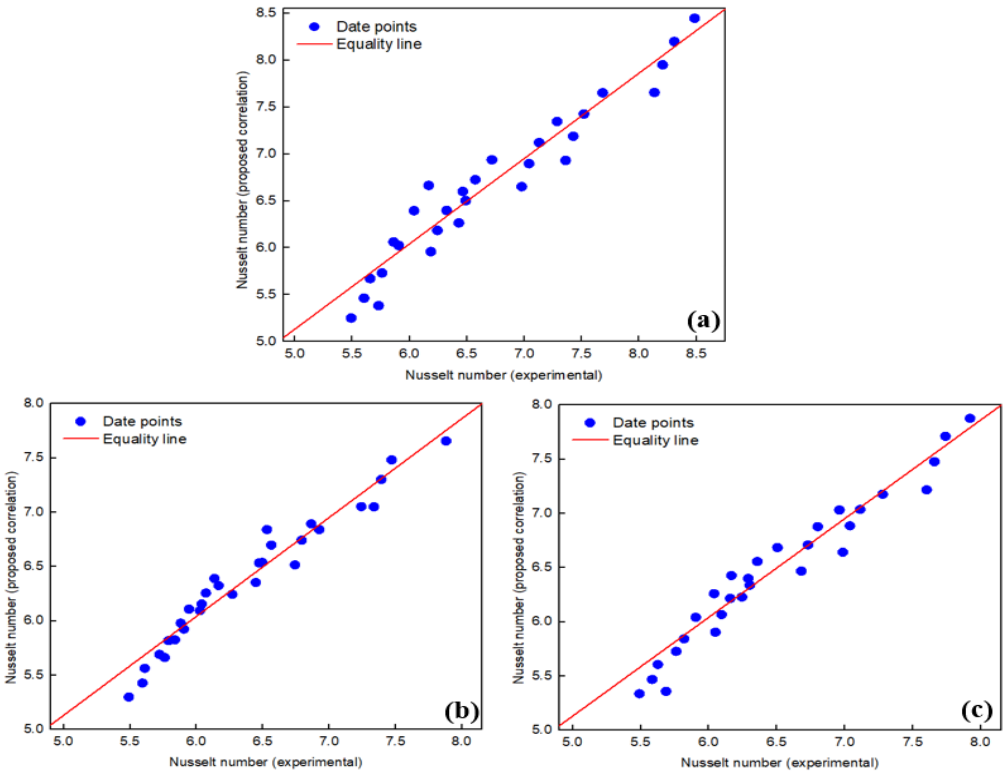

Fig. 4.32. The experimental data compared with the proposed Nusselt number correlation (a) SiC/DW, (b)ZrO_2/DW, and (c) ZrO_2-SiC/DW nanofluids

4.5. Exergy analysis of flat plate solar collector

4.5.1. Entropy generation and exergy destruction

Fig. 4.33 shows the entropy generation and exergy destruction of FPSC evaluated based on different mass flow rate and solid volume fractions of silicon carbide nanofluid. This figure clearly shows that as the volume fraction or SiC nanoparticle concentration increases and mass flow rate of the working fluid is decreased; there is a decline in entropy generation. This may be attributed to higher heat flux on the absorber plate leading to an increase in nanofluids' thermal conductivity and ultimately greater thermal conductivity. The heat transfer occurring in this situation leads to a more significant change in irreversibility than that caused by entropy generation. Conversely, the SiC nanofluids experience a rise in their viscosity as the concentration of nanoparticles in the fluid is increased. Consequently, the fluid friction increases and contributes to entropy generation. The flat plate solar collector was subjected to this analysis since it helps to determine the entropy generation in higher temperature systems to reduce entropy generation since power output can only be enhanced through the minimization of entropy generation in flat plate solar collectors. On the other hand, exergy destruction caused at a different volume fraction of SiC nanofluid and different flow rates has been depicted in this figure. The irreversible losses lead to higher entropy generation and lower thermal proficiency; thus, influencing the thermal system's performance. For performance optimization, it is suggested to evaluate the exergy destruction caused by heat transfer and friction so that the design variables can be adjusted accordingly. This exergy destruction may be attributed to higher heat flux on the absorber plate leading to an increase in nanofluids' thermal conductivity and ultimately greater thermal conductivity. The heat transfer occurring in this situation leads to a more significant change in irreversibility than that caused by entropy generation.

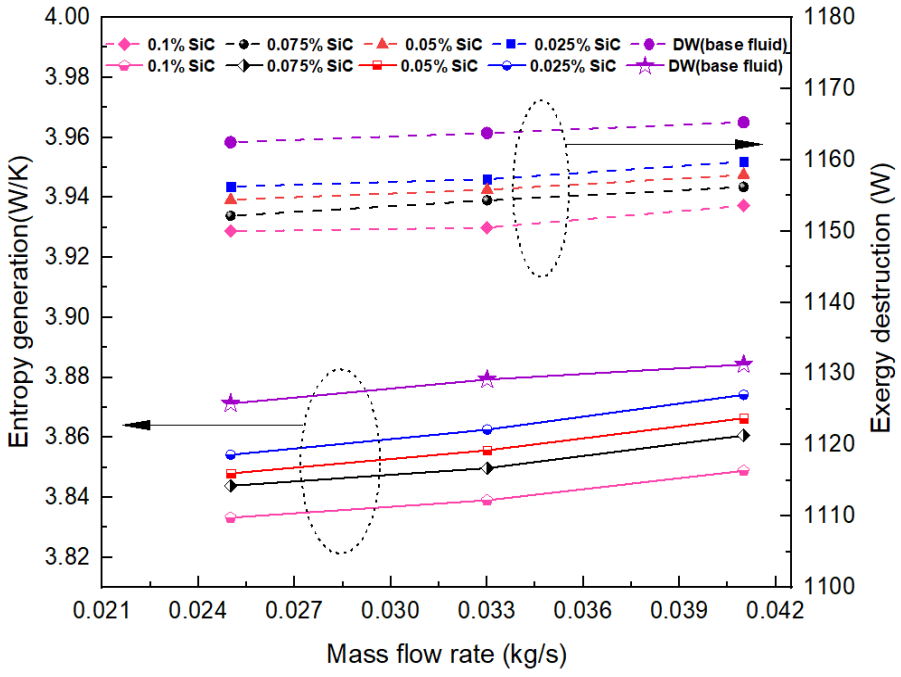

Fig. 4.33. Entropy generation and exergy destruction of FPSC for SiC/DW nanofluid and distilled water at various mass flow rates

The entropy generation and the exergy destruction obtained from flat-plate solar collectors filled with water and the SiC/DW nanofluid under the effect of solar radiation has been depicted in Fig. 4.34. The SiC/DW nanofluid contained different concentrations of particles. The solar collector filled with water and SiC/DW nanofluid showed a rise in entropy generation with increasing solar radiation. At a solar radiation of 900 W/m^2, the solar collector filled with water showed the highest entropy generation while the collector filled with 0.1% SiC/DW nanofluid showed the lowest entropy generation. The solar collector filled with water higher entropy generation than the entropy generated with 0.1% SiC/DW nanofluid. the inverse association between entropy generation and nanofluid concentration, the entropy generation is found to increase with decreasing concentration of nanofluid. Besides this, increasing solar radiation was found to have a direct effect on the exergy destruction of the solar collector. At 900 W/m^2 solar radiation, the solar collector filled with water highest exergy destruction while the collector filled with SiC/DW nanofluid with concentrations of 0.1% showed the lowest exergy destruction. Accordingly, the solar collector filled with water yielded the highest exergy destruction while the collector filled with SiC/DW nanofluid depicted the lowest exergy destruction.

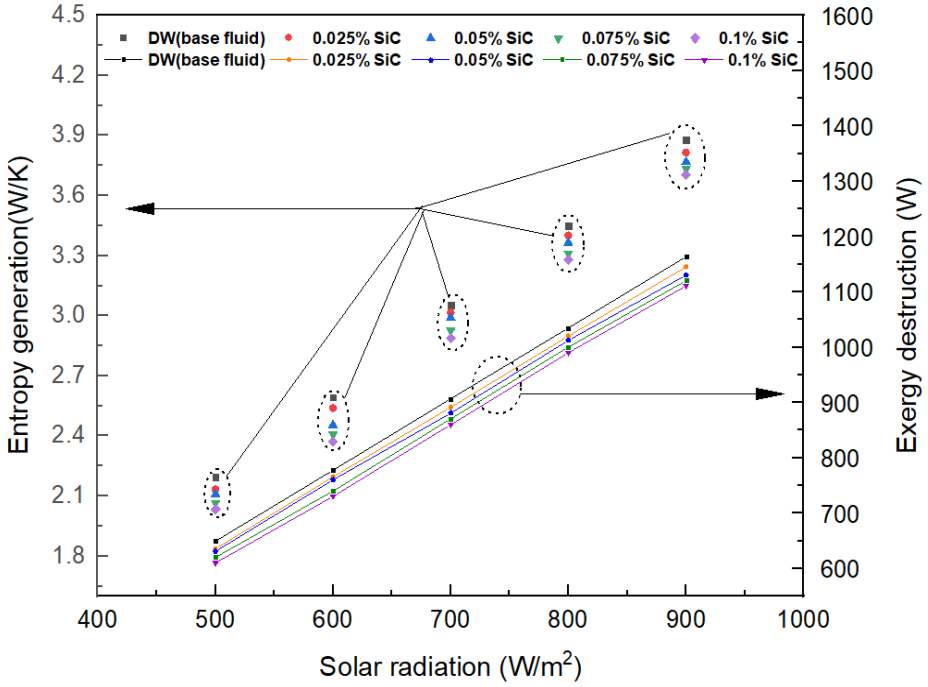

Fig. 4.34. Entropy generation and exergy destruction of FPSC for SiC/DW nanofluid and distilled water at various solar radiation

Fig. 4.35 shows the variations in entropy generation and exergy destruction of FPSC at distinct concentrations of ZrO_2 nanoparticles in the fluid and mass flow rates. There is a heavy dependence on the exergetic efficiency of solar thermal systems on exergy destruction and entropy generation values. It is essential to minimize exergy destruction and entropy generation to improve the efficiency of systems. Therefore, to develop effective and efficient solar thermal systems, it is important to evaluate these factors. It was observed that the entropy generation and exergy destruction were increased as the mass flow rate increased, and the distilled water replaced with ZrO_2/DW nanofluid. According to these results, when the flow increases, the values of exergy destruction and entropy generation also increase, with the weight concentrations remaining constant. The flow rate increment enhances the heat gain, along with a rapid decrease in outlet

fluid temperature in comparison to a decrease in outlet pressure. This results in increased exergy destruction and entropy generation. In contrast, when the flow rate is constant, the exergy destruction and entropy generation decrease due to high heat gain and increased fluid flow outlet temperature, along with increase in ZrO_2 concentration. Additionally, increasing the nanoparticles concentration in the nanofluid enhances thermal conductivity and thermal conductance, resulting in a more substantial decrease in irreversibility due to heat transfer. The results exhibited that the lowest values of entropy generation and exergy destruction were obtained for a 0.025 kg/s flow and 0.1% ZrO_2/DW nanofluid due to their ability to absorb the most heat. Entropy generation is caused by fluid flow and internal irreversibility. It is important to note that high levels of entropy generation should be avoided because they have a negative impact on the system exergy performance. The exergy destruction of the FPSC should be taken into account to enhance the utility of exergy analysis. The first step that includes exergy destruction is the absorbing process. In particular, FPSCs require an energy and exergy analysis to identify and subsequently minimize entropy generation. This is because FPSCs are high-temperature systems and there can be an increase in power output only when entropy generation is reduced.

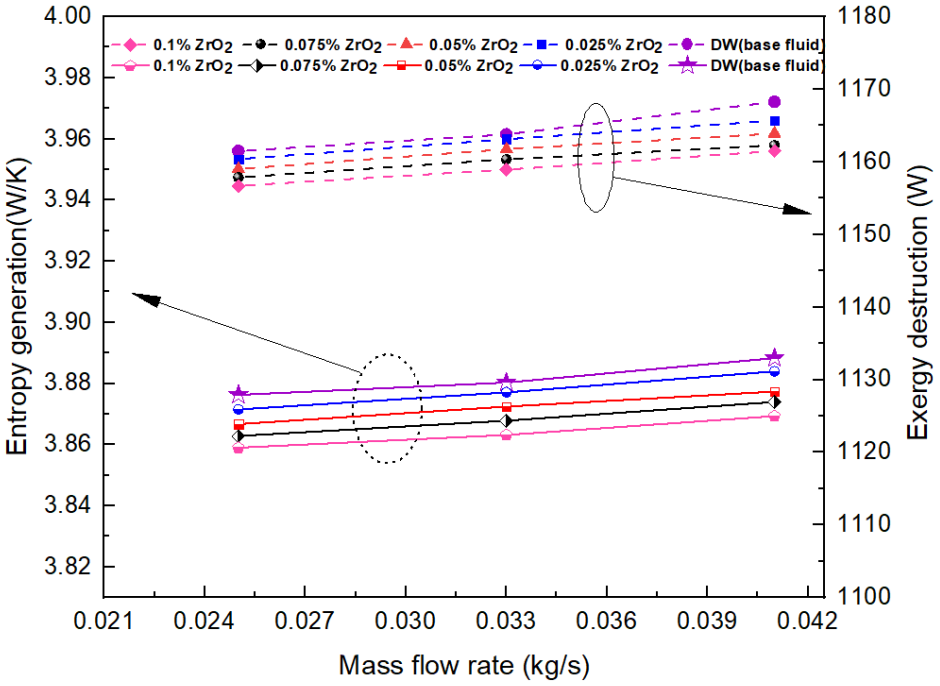

Fig. 4.35. Entropy generation and exergy destruction of FPSC for ZrO_2/DW nanofluid and distilled water at various mass flow rates

Fig. 4.36 displays the entropy generation and exergy destruction processes that occurred within the FPSC filled with ZrO_2/DW nanofluid under the influence of solar radiation. According to the findings, a positive relationship existed between solar radiation and entropy generation within the FPSC, and the working fluid had no impact on this relationship. The FPSC that was filled with water exhibited greater entropy generation compared to the collector filled with ZrO_2 nanofluid. For all cases of 500-900 W/m^2 solar radiation, the highest entropy generation was exhibited by the FPSC filled with water, while the least entropy generation was shown by the FPSC filled with 0.1% nanofluid. In addition, the entropy generation for distinct concentrations of nanoparticles was analysed under the same amount of solar radiation. The fact that entropy offers insight into system irreversibility shows its significance. There was an inverse relationship between entropy

generation and particle concentration in ZrO_2/DW nanofluid, which gives rise to the conclusion that the optimal concentration of ZrO_2 nanoparticles in the working fluid is 0.1%, which results in minimum entropy in FPSCs. In addition, the study findings also disclosed that the amount of exergy destruction in the FPSC was increased as the solar radiation increased. The water filled FPSC exhibited the greatest exergy destruction values from 500-900 W/m^2 solar radiation, while the lowest value was shown by the FPSC filled with 0.1% nanofluid.

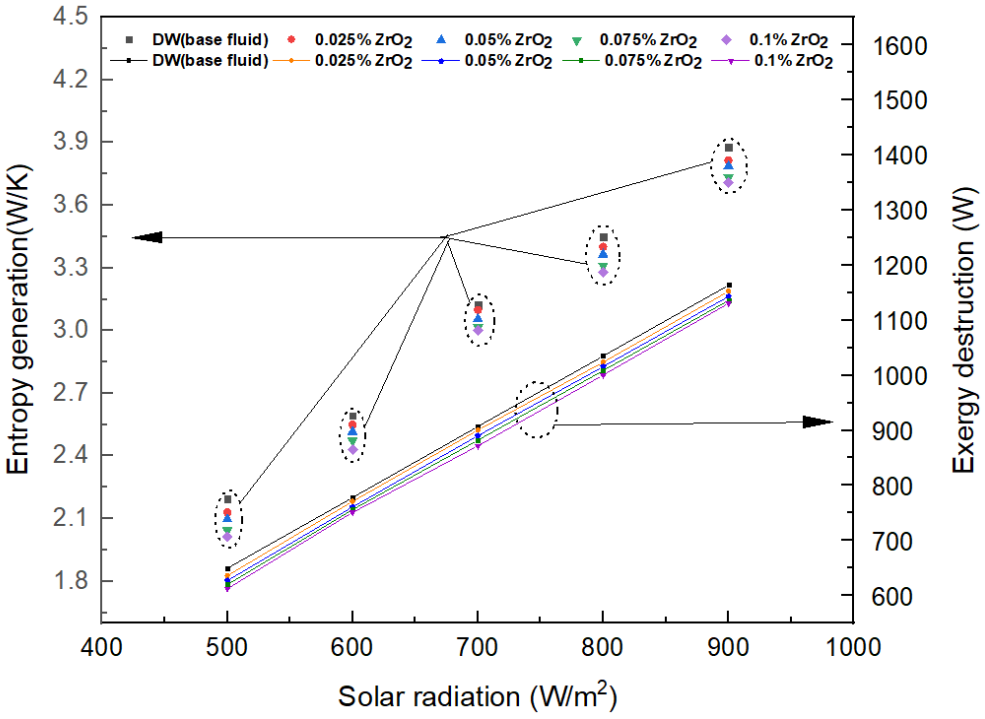

Fig. 4.36. Entropy generation and exergy destruction of FPSC for ZrO_2/DW nanofluid and distilled water at various solar radiation

The value of entropy generation and exergy destruction determine the solar collector's exergetic performance using ZrO_2-SiC/DW hybrid nanofluid as working fluid. The decline in entropy generation and exergy destruction leads to higher exergetic efficiency of thermal systems. Hence, these two parameters need to be carefully considered to ensure higher system efficiency. The values of entropy generation and exergy destruction were obtained at different nanoparticles concentrations in the fluid and mass flow rates have been presented in Fig. 4.37. The increasing mass flow rate caused an escalation of exergy destruction and entropy generation values provided the weight concentration is kept constant. A rise in mass flow rate leads to more absorption of heat and a rapid drop in outlet fluid temperature. As a result, an outlet pressure drop occurs which yields greater entropy generation and exergy destruction. Conversely, when ZrO_2-SiC/DW concentration is increased and the flow rate is kept constant, the fluid depicts a higher outlet temperature accompanied by a rise in friction factor leading to a decline in the values of entropy generation and exergy destruction. This decline may be accredited to high heat absorption as ZrO_2-SiC/DW nanofluid depict a high surface-to-volume ratio as well as a high aspect ratio. The heat absorption capacity of the fluid is highest at maximum concentration 0.1 % of ZrO_2-SiC/DW leading to the least values of exergy destruction and entropy generation. As nanoparticle concentration is increased, the rate of energy loss due to irreversibility (or exergy destruction) goes down. This means that a lesser amount of heat energy is lost during the transfer. Also, the rate of entropy

generation decreases. The decline in Entropy suggests better organization and functioning of the system. As concentration is increased, the number of nanoparticles in the suspension increases, and consequently the thermal conductivity of the suspension increases and heat transfer along the absorber plate becomes more efficient. In the context of solar collectors, it is recommended to keep entropy generation values in control to prevent the depletion of its exergy performance.

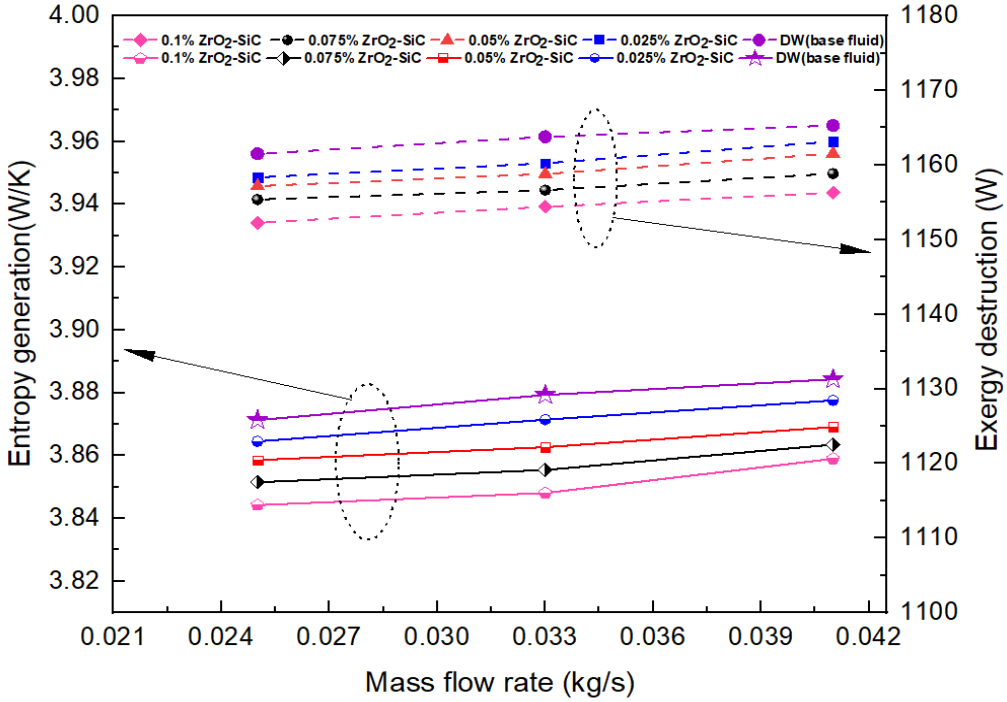

Fig. 4.37. Entropy generation and exergy destruction of FPSC for ZrO_2-SiC/DW nanofluid and distilled water at various mass flow rates

The processes of entropy generation and exergy destruction that took place inside the FPSC filled with ZrO_2-SiC/DW hybrid nanofluid under the solar radiation effects have been depicted in Fig. 4.38. The results showed a positive association between solar radiation and entropy generation within the FPSC irrespective of used working fluid. It must be noted that the FPSC based water showed higher entropy generation than using hybrid nanofluid. Considering the outcome, the water-filled solar collector showed the highest entropy generation in all cases of 500-900 W/ m^2 of solar radiation while the FPSC filled with 0.1% hybrid nanofluid depicted the lowest entropy generation. Moreover, for the same amount of solar radiation, the entropy generation was evaluated for different concentrations of nanoparticles. The significance of entropy is evident from the fact that we can get an idea about system irreversibility by evaluating the entropy. The entropy generation shared an inverse association with particle concentration in ZrO_2-SiC/DW hybrid nanofluid. Hence it can be concluded that 0.1% is the optimal from the examined concentration area of ZrO_2-SiC/DW nanoparticles in the working fluid that yields minimum entropy in the FPSCs. The study outcomes also indicated a higher amount of exergy destruction in the solar collector with increasing solar radiation. From 500-900 W/m^2 solar radiations, the solar collector filled with water showed the highest exergy destruction values while the FPSC filled with 0.1% hybrid nanofluid showed the lowest value.

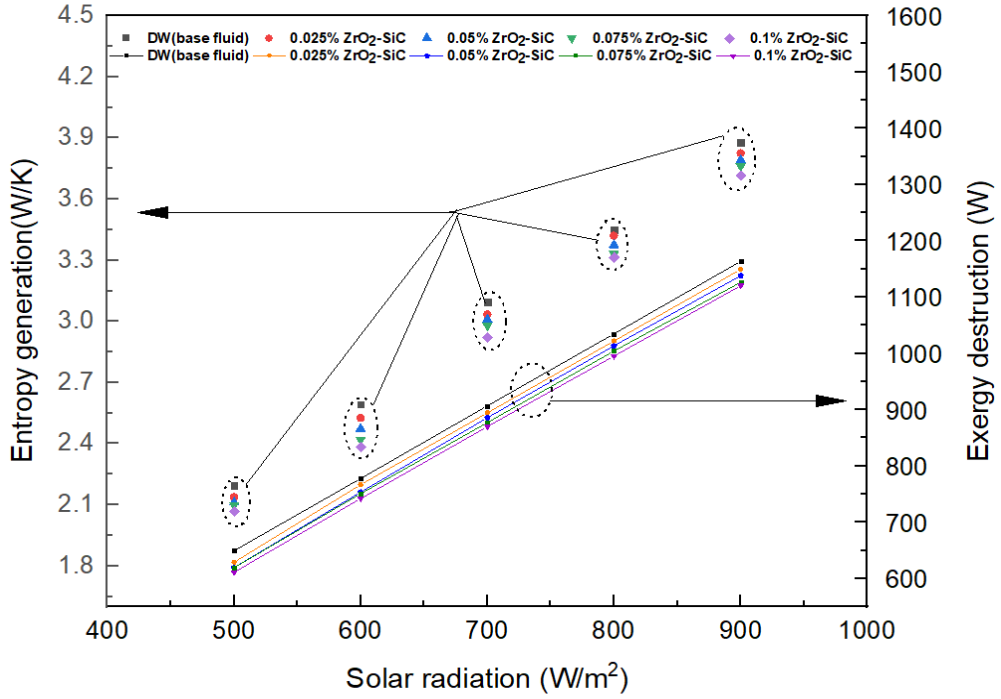

Fig. 4.38. Entropy generation and exergy destruction of FPSC for ZrO_2-SiC/DW nanofluid and distilled water at various solar radiation

4.5.2. Exergy efficiency

Fig. 4.39 shows the changes in exergy efficiency depicted by the solar collector throughout the study for a different mass flow rate and volume fraction of SiC nanofluids. The given nanofluid was found to yield better exergy efficiency. This figure also indicates that when the solar collector is subjected to the highest solar radiation, maximum irreversibility takes place which gradually reduces the declining strength of solar radiation. Considering the exergy efficiency evaluated based on the second law of thermodynamics, the highest value of nearly 37.42% was obtained for 0.1% volume fraction of SiC particles dispersed in water with 0.025 kg/s mass flow rate while 0.025% of SiC particles suspended in water yielded 20.01% exergy efficiency. Hence, the results imply that the performance of the flat plate solar collectors is heavily dependent on solid volume fraction. However, SiC/DW nanofluid offer various benefits like high stability, greater thermal conductivity, higher energy efficiency and higher exergy efficiency. In addition, the flat-plate solar collectors were also found to depict better thermal performance in the presence of 0.1% SiC/DW nanofluid.

In Fig. 4.39, the variations in the FPSC exergy efficiency for ZrO_2 nanofluid with distinct mass flow rates and volume fractions are presented. The tested nanofluid exhibited higher exergy efficiency compared to others. It can be seen that there is a decrease in exergy efficiency when the flow increases for a specific concentration. This essentially happens because of higher entropy generation values. It is also noted that when the weight concentration increases, there is an instantaneous FPSC exergy efficiency increase at constant flow rate. When the concentration of ZrO_2 increased, their exergy efficiency was higher than that of distilled water. The exergy efficiency increase value of 16.05% was attained for a volume fraction of 0.1% ZrO_2 particles dispersed in water with 0.025 kg/s mass flow rate, in comparison to distilled water. On the other hand, a volume fraction of 0.025% ZrO_2 particles suspended in water resulted in an exergy

efficiency of 4.66%. Hence, according to the findings, the solid volume fraction significantly influences the efficiency of FPSC.

In Fig. 4.39 shows how the exergy efficiency is associated with the nanoparticles concentration and mass flow rate. The changes in the exergy efficiency attributed to the change in nanoparticle concentration and the mass flow rate have also been shown in this figure. The experiments revealed that the concentration of nanoparticles has a direct effect on the exergy efficiency which increase as bigger nanoparticles are used in a nanofluid. The exergy efficiency is inversely related to the mass flow rate. The use of ZrO_2-SiC/DW hybrid nanofluid comprised of particles with 0.1 % concentration yields higher exergy efficiency than the water base fluid. Moreover, the high exergy efficiency of hybrid nanofluids compared to water makes it a better absorbing medium. It was also discovered that there is a 28.31% rise in exergy efficiency when a nanoparticles concentration of 0.1% are introduced into the working fluid at mass flow rate of 0.025 kg/s.

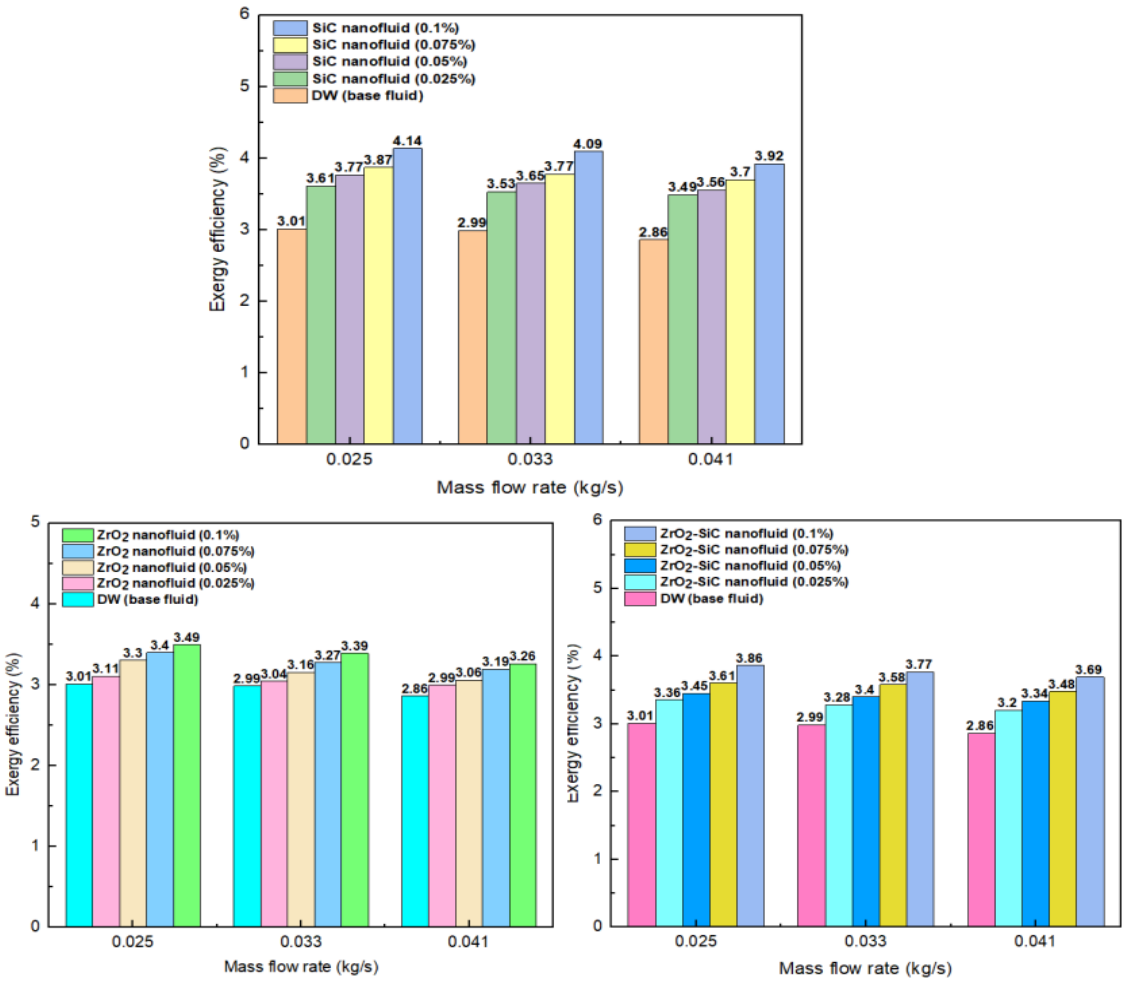

Fig. 4.39. FPSC exergy efficiency for SiC/DW, ZrO_2/DW, and ZrO_2-SiC/DW nanofluids with different mass flow rates

The changes depicted by the flat-plate solar collector in its exergy efficiency because of the effects of solar radiation and the concentration of the SiC/DW nanofluid have been presented in Fig. 4.40. At 900 W/m^2 solar radiation, the solar collector depicted a 20.01%, 25.13%, 28.59%, and 37.42% rise in the maximum exergy efficiency relative to water when using SiC/DW nanofluids in the concentrations of 0.025%, 0.05%, 0.075 and 0.1 %. The solar collector filled with 0.025% SiC/DW nanofluid showed lower exergy efficiency than that depicted in the case of 0.1% SiC/DW

nanofluid. A comparison of this study is made with earlier studies relevant to the domain of water based FPSC and nanofluid.

In Fig. 4.40 shows the effect of FPSC exergy efficiency considering the variations in solar radiation and ZrO2/DW nanofluid concentration. It was determined that there was a positive relationship between exergy efficiency and the two factors. Specifically, the FPSC exergy efficiency using ZrO_2 nanofluid at 0.025%, 0.05%, 0.075%, and 0.1% exhibited an increment by 4.66%, 9.6%, 12.82%, and 16.05%, respectively, compared to distilled water when exposed to 900 W/m^2 solar radiation. It was also determined that the FPSC-filled water demonstrated the lowest exergy efficiency, whereas the collector filled with 0.1% ZrO_2/DW nanofluid exhibited the greatest exergy efficiency.

The effects of changes in solar radiation and ZrO_2-SiC/DW concentration on the exergy efficiency of the FPSC are given in Fig. 4.40. The exergy efficiency showed a positive association with both these factors. The solar collectors filled with hybrid nanofluid on the concentrations of 0.025, 0.05, 0.075, and 0.1% showed 11.46%, 16.82%, 21.7%, and 28.31% rise in the maximum exergy efficiency relative to water when subjected to 900 W/m^2 solar radiation. The solar collector containing water showed the lowest exergy efficiency while that filled with 0.1% ZrO_2-SiC/DW hybrid nanofluid showed the utmost exergy efficiency.

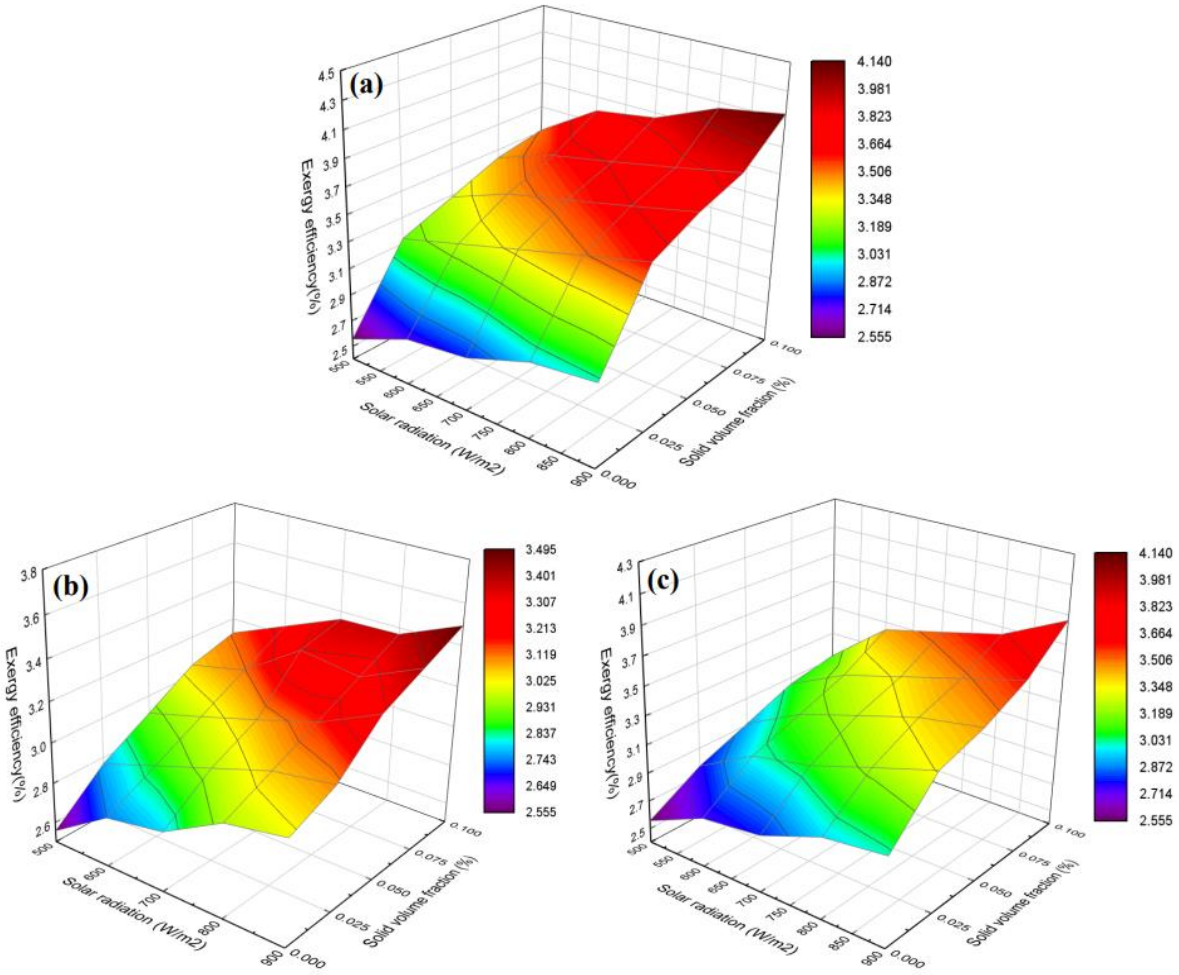

Fig. 4.40. FFPSC exergy efficiency at different solar radiation rats for (a) SiC/DW, (b) ZrO_2/DW and (c) ZrO_2-SiC/DW nanofluid

4.6. Numerical analysis of flat plate solar collector

4.6.1. Temperature distribution on the absorber plate and pipe outlet

The effect of type of the nanoparticles on the absorber plate was studied which revealed a decline in the temperature of the absorber plate with increasing heat transfer of fluids as evident from Fig. 4.41. The observed when using nanoparticles. The capability of the fluid to transfer heat via convection increases with the incorporation of nanoparticles leading to more transfer of heat from the pipe and the fluid inside it. As a result, a decline in the absorber temperature is noted. In short, the absorber temperature exhibits continuous rise as the fluid flows towards the exit. The absorber plate demonstrates the highest temperature in the presence of DW as a working fluid. This may be because the heat transfer coefficient of DW is lower as compared to other fluids. Next comes the ZrO_2/DW whereby the absorber plate depicts second highest temperature while the third-highest plate temperature is seen in ZrO_2-SiC/DW. It is interesting to note that the lowest plate temperature is obtained for SiC/DW which is characterized with the highest heat transfer coefficient. This implies that the efficiency of solar collectors can be improved, and low absorber plate temperatures can be obtained in the presence of SiC which is attributed to the high coefficient of heat transfer.

The temperature distribution of various types of nanofluids via solar collector outlets has been shown in Fig. 4.42. The zones in red colour indicate high-temperature zones while the blue colour indicates zones with lower temperatures. The temperature distribution diagram depicts red zones or high temperatures in parts connected to the outer parts of the heat flux pipe. The temperature decreases towards the middle of the pipe. The diagram illustrates two types of blue zones: one with deep blue colour and the other with light blue colour. The deep blue colour is seen at the centre of the pipe which indicates lower temperature due to lower nanoparticle concentration and the presence of water as a working fluid that reduces the temperature. The lighter blue colour is seen in areas with greater nanoparticle concentration. This blue area is overtaken by red and green zones with the incorporation of more nanoparticles and expansion of heat transfer capability. This outcome is attributed to the association between nanofluids and their increased thermal diffusivity resulting from their lower specific heat capacity and higher thermal conductivity compared to water. As the viscosity decreases, the velocity increases towards the centre of the flow. This accounts for the decrease in temperature as one moves closer to the centre of the flow. Additionally, a result of the higher temperature at the top of the output surface is that the pipe makes contact with the absorber from that point.

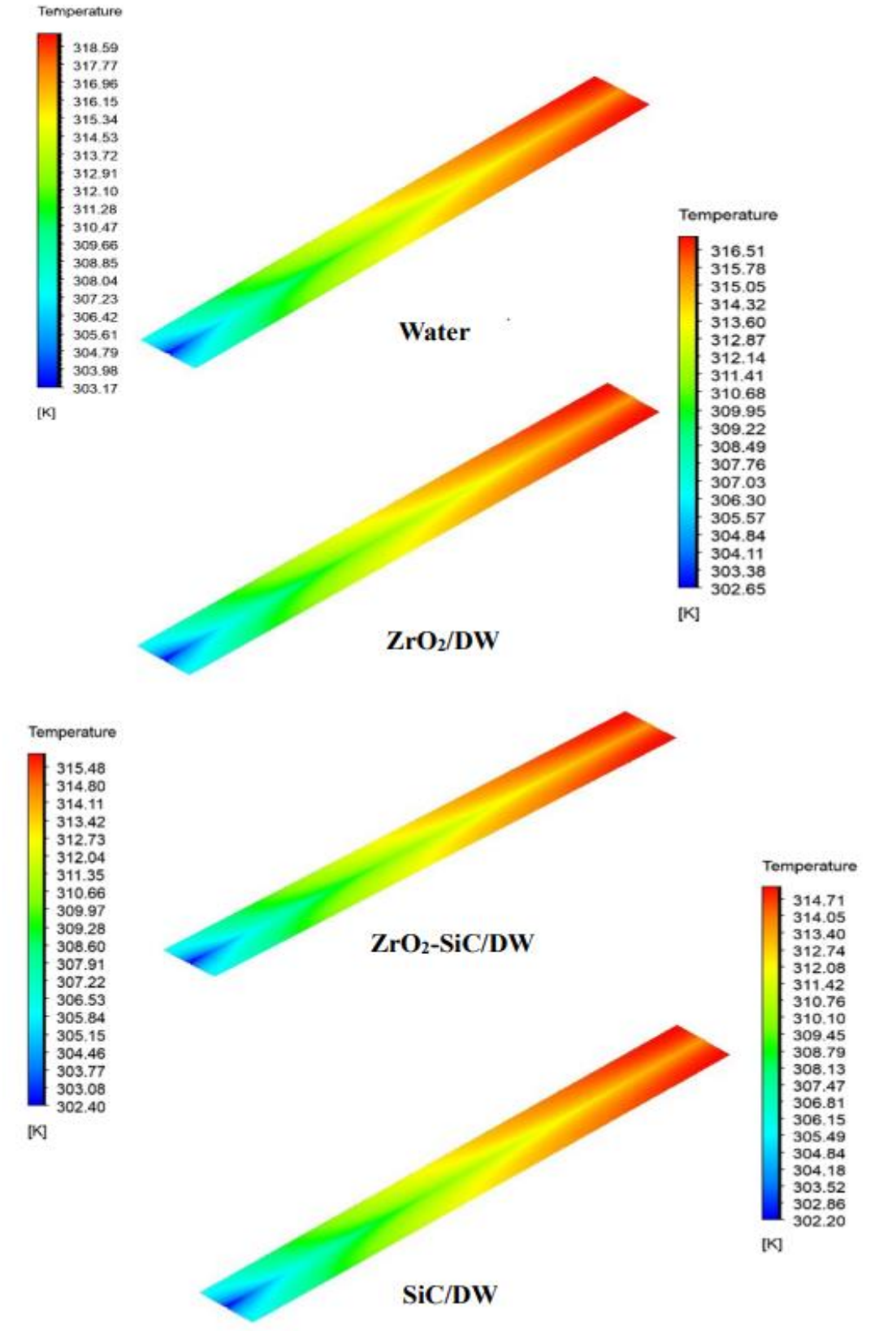

Fig. 4.41. Temperature contour of absorber plate for different nanofluids

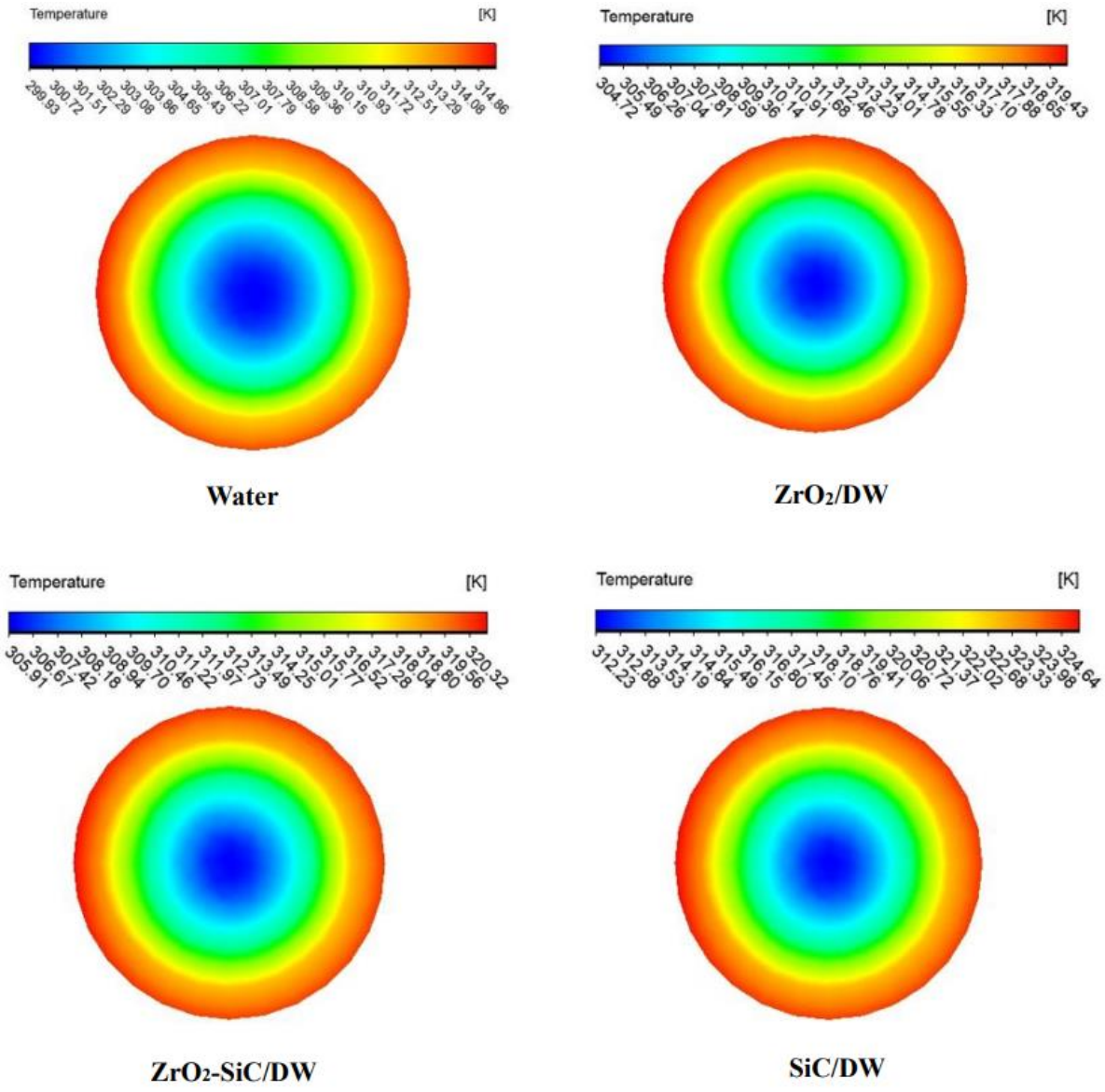

Fig. 4.42. Temperature distribution at pipe outlet for different nanofluids

4.6.2. Energy and exergy efficiencies

This study makes use of the CFD software Ansys Fluent for conducting numerical analysis through simulation of overall 3D heat transfer flow occurring in a flat plate solar collector. The study individually evaluates the efficiency of FPSC filled with three different nanofluids (SiC/DW, ZrO_2/DW and ZrO_2-SiC/DW). The intersection of the line with the vertical axes F_R ($\tau\alpha$) and the slope of the line (F_RU_L) are both variables defining the efficiency line of the FPSC. When fluid inflow temperature to the collector corresponding to the ambient temperature, F_R ($\tau\alpha$) denotes the maximum collector efficiency. The stagnant instance typically appears at zero flow rate and is where the efficiency line intersects the horizontal axis, which is where the efficiency of the collector zeroes out. The line's slope (F_RU_L) indicates the collector's power disposal variable. As demonstrated in the current work and documented in earlier quantitative and empirical research, the application of nanofluids to increase the FPSC system's efficiency is effective regardless of moderate nanoparticle ratios. The differences in the empirical and simulation thermal efficiency numbers against reduced temperature parameter for the 0.041 kg/s mass flow rate at 0.1% volume concentration of the given nanofluid are shown in Fig. 4.43, which the efficiencies were close to

each other. The thermodynamic efficiency of mono and hybrid-nanofluids is superior to that of water as illustrated in this figure. The results obtained from the numerical and experimental investigations showed a high level of agreement, thereby allowing their use for the purpose of validating the numerical analysis. The variation between simulation results of the thermal efficiency of using SiC, ZrO_2 and ZrO_2-SiC nanofluid and experimental results were 3.38%, 2.43% and 2.91% respectively.

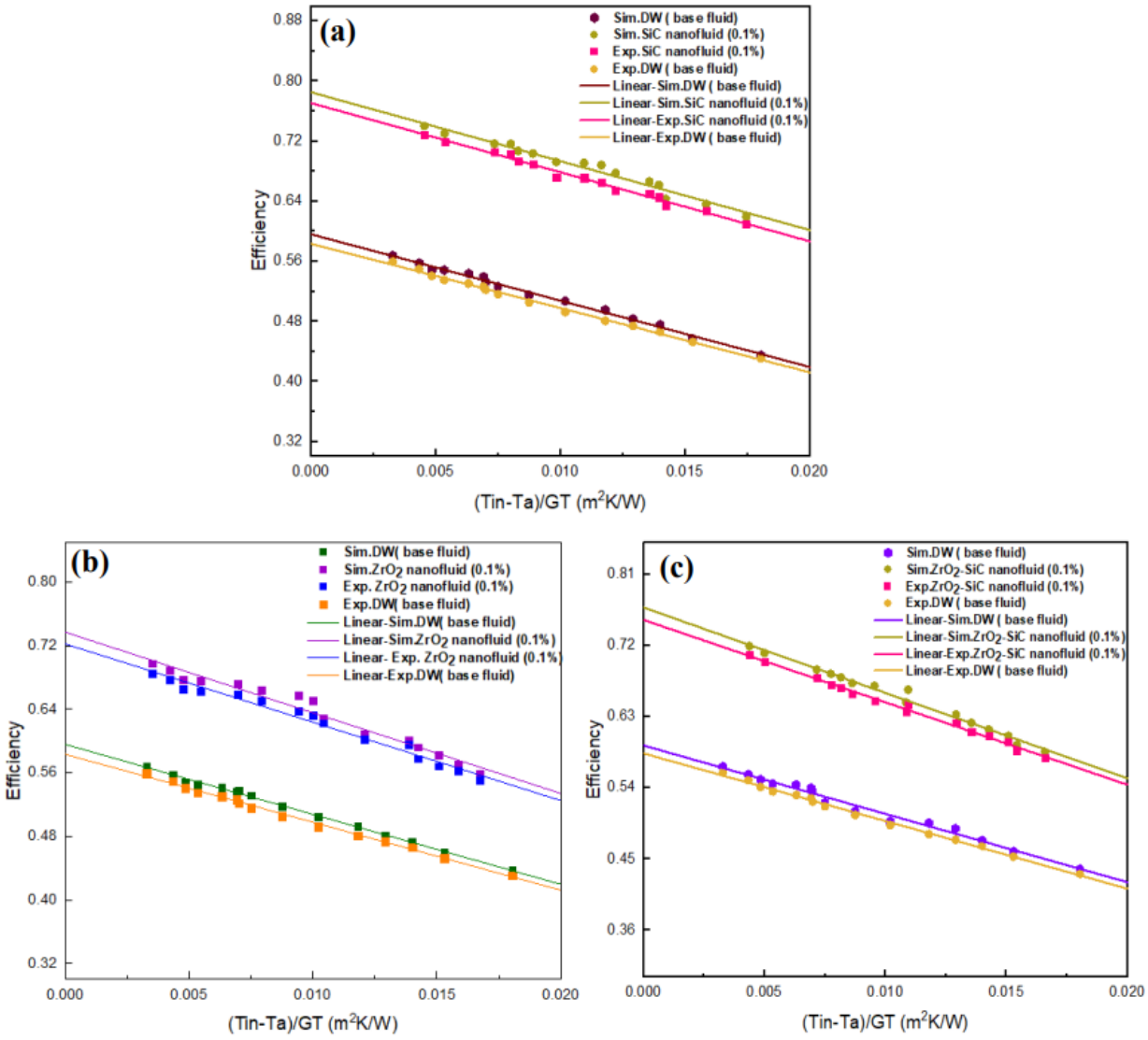

Fig.4.43. The numerical and experimental results of thermal efficiency of FPSC by (a) SiC/DW, (b) ZrO_2/DW and (c) ZrO_2-SiC/DW nanofluids

Considering 0.025 kg/s mass flow rate, the differences in empirical and simulated exergy efficiency against volume fractions of the SiC, ZrO_2, and ZrO_2-SiC nanofluids are shown in Fig. 4.44. It is depicted in the figure that at all flow rates, the simulated readings of exergy efficiency closed proximity or slightly above the numbers obtained from experiments. This was the case because the observed exergy efficiency was derived from the empirical outflow water temperature, while the exergy efficiency was calculated using the CFD anticipated outflow water temperature, which exceeded the empirical results. The results obtained from the numerical and experimental investigations showed a high level of agreement, thereby allowing their use for the purpose of validating the numerical analysis. The variation between simulation results, exergy efficiency of

using SiC, ZrO_2 and ZrO_2-SiC nanofluid and experimental results were 3.4%, 3% and 2.8% respectively.

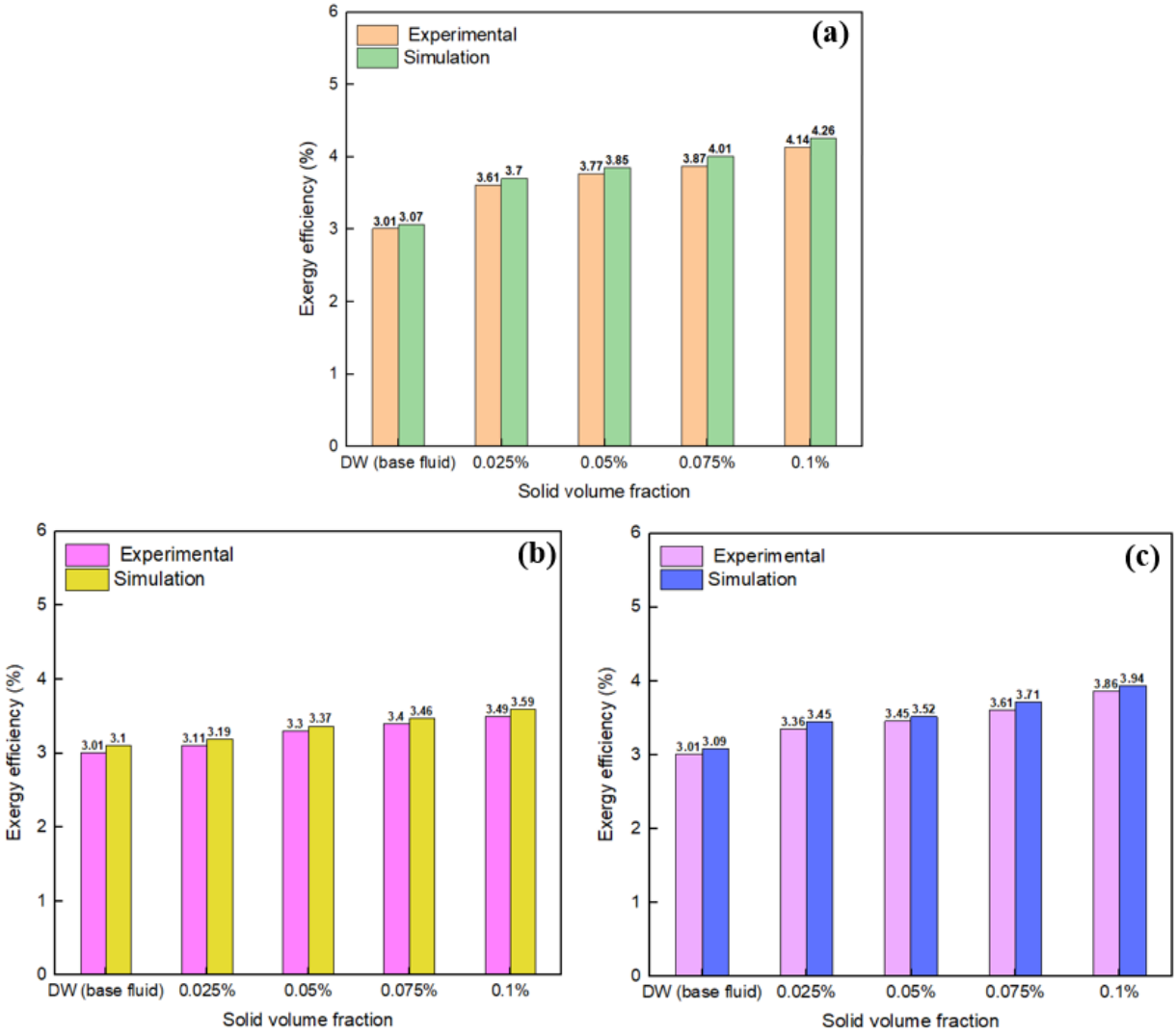

Fig. 4.44. The numerical and experimental results of exergy efficiency of FPSC by (a) SiC/DW, (b)ZrO_2/DW and (c) ZrO_2-SiC/DW nanofluids.

4.7. New scientific results

This section presents the new scientific findings from this research work as follows:

1. Rheological behavior of mono and hybrid nanofluid

I have examined and evaluated the rheological properties of three types new nanofluids (zirconium oxide, silicon carbide and their hybrid (50:50%) by solid volume fraction) based distilled water. In order for nanofluids' rheological behaviour to be researched, it is firstly necessary to determine their viscous behaviour from Newtonian and non-Newtonian perspectives. Besides, for the purpose of evaluating the rheological properties of ZrO_2/DW, SiC/DW and ZrO_2-SiC/DW nanofluids, measurements of the nanofluids' viscosity and shear stress were taken at varying shear rates across the range of temperatures to get insight into the rheological behaviour of the given nanofluid.

Based on the experimental results, I found that the changes in shear stress as result of the shear rate show a linear pattern, it can be deduced that the given nanofluids exhibit Newtonian behavior characteristics. I have also observed that the changes in dynamic viscosity of the given nanofluids according to the shear rate at various temperatures remains constant, this indicated that the nanofluids of ZrO_2/DW, SiC/DW and ZrO_2-SiC/DW behave in a Newtonian manner.

2. Experimental correlation between the relative dynamic viscosity and volume fraction, and temperature nanofluid

According to results obtained from the experiments, I have put forward a novel correlation capable of predicting the investigated nanofluids' viscosity in relation to solid volume fraction and temperature. This correlation is valid for volume fraction (φ) ranging from 0.025% to 0.1% and temperatures (T) ranging from 20 °C to 60 °C.

For ZrO_2/DW nanofluid:

$$\frac{\mu_{nf}}{\mu_{bf}} = 0.7986 + 9.72\ \varphi + 0.013\ T - 62.174\ \varphi^2 - 0.00006\ T^2 + 0.261\ \varphi\ T$$

For SiC/DW nanofluid:

$$\frac{\mu_{nf}}{\mu_{bf}} = 0.8814 - 1.6\ \varphi + 0.013\ T + 10.465\ \varphi^2 - 0.0002\ T^2 + 0.204\ \varphi\ T$$

For ZrO_2-SiC/DW hybrid nanofluid:

$$\frac{\mu_{nf}}{\mu_{bf}} = 0.7096 + 3.84\ \varphi + 0.022\ T - 24.284\ \varphi^2 - 0.0002\ T^2 + 0.228\ \varphi\ T$$

I have observed that the comparison of the laboratory data with the outcomes from the proposed correlation showed a 5.31% margin of deviation and R^2 value of 98.52% for ZrO_2/DW, by 5.27% and 99.11% for SiC/DW, and by 3.51% and 98.92% for ZrO_2-SiC/DW nanofluids, respectively.

3. Effect of volume fraction and temperature on thermal conductivity of nanofluid

I have pointed out that the volume fraction of nanoparticles and temperature strongly influences thermal conductivity of zirconium oxide, silicon carbide, and hybrid nanofluid. I noticed that a positive association of the thermal conductivity of nanofluid with parameters like temperature and solid volume fraction. Besides, I proved experimentally that the thermal conductivity of the given nanofluid increased with rising temperature and higher solid volume fraction. I have also discovered that the effect of higher volume fraction on thermal conductivity of the given nanofluids outshines the effects of temperature.

Through the experimental findings, I have observed that the thermal conductivity enhancement for ZrO_2/DW was 20.45%, 30.3% for SiC/DW and that of ZrO_2-SiC/DW was 25.75% at maximum solid volume fraction and temperature.

Based on experimental results, I have explored a novel proposed correlation for ZrO_2/DW, SiC/DW and ZrO_2-SiC/DW nanofluids thermal conductivity enhancement ratios as a function of volume fraction and temperature. It is accurate and valid for temperatures (T) between 20 and 60 °C and fraction volumes (φ) of 0.025% to 0.1%.

For ZrO_2/DW nanofluid:

$$\frac{k_{nf}}{k_{bf}} = 0.9606 + 1.609\ \varphi + 0.0014\ T, R^2 = 0.9889$$

For SiC/DW nanofluid:

$$\frac{k_{nf}}{k_{bf}} = 0.9631 + 2.134\ \varphi + 0.0025\ T, R^2 = 0.9906$$

For ZrO_2-SiC/DW hybrid nanofluid:

$$\frac{k_{nf}}{k_{bf}} = 0.9619 + 2.076\ \varphi + 0.0015\ T, R^2 = 0.986$$

I found that the comparison between experimental results and correlations outputs showed a good agreement which signifies that the results were accurate. Moreover, I noticed that the proposed correlations gave an acceptable value of the maximum margin of deviation equal to 1.49% for ZrO_2/DW nanofluid, by 1.2% for SiC/DW nanofluid and by 1.15% for ZrO_2-SiC/DW hybrid nanofluid.

4. Effect of nanofluids on the thermal efficiency of FPSC

I have unfolded and improved the experimental thermal efficiency of FPSC by using new nanofluids as a working fluid in solar collector. I experimentally investigated the four solid volume fractions (0.025%, 0.05%, 0.075% and 0.1%) of ZrO_2/DW, SiC/DW, ZrO_2-SiC/DW nanofluids as well as the impact of three different mass flow rates (0.025, 0.033 and 0.041 kg/s). I found that increasing thermal efficiency of FPSC and greater heat transfer in solar system when replace the base fluid (water) inside the solar collectors with the given nanofluids. Besides, I proved experimentally that a rise in mass flow rate with the increase in nanofluid concentration led to a rise in thermal efficiency of FPSC.

Based on experimental results, I have identified that in the case of 0.041 kg/s flow rate, 0.1% volume fraction of SiC/DW, ZrO_2/DW and ZrO_2-SiC/DW nanofluids showed a 35.53%, 26.2% and 31.46%, respectively, in the maximum enhancement of thermal efficiency of FPSC in comparison to water.

According to results obtained from the experiments, I have developed novel correlation for FPSC thermal efficiency as a function of the reduced temperature factor [(Ti- Ta)/GT] and solid volume fraction (φ). Besides, I have estimated all the coefficients of the developed thermal efficiency correlation for the FPSC based nanofluids:

$$\eta_c = a + b\left(\frac{T_i - T_a}{GT}\right) + c\ \varphi + d\left(\frac{T_i - T_a}{GT}\right)^2 + e\ \varphi^2$$

5. Empirical correlation of the Nusselt number for nanofluid in solar collector

Based on experimental results, I have established a new empirical correlation for estimating the Nusselt number for nanofluids in solar collector as a function of volume concentration, Reynold's number, and Prandtl's number.

For ZrO_2/DW nanofluid:

$$Nu = 0.10158\ Re^{0.4742} Pr^{0.5173} (1 + \varphi)^{1.712}$$

For SiC/DW nanofluid:

$$\mathrm{Nu} = 0.07495\ \mathrm{Re}^{0.5251}\mathrm{Pr}^{0.506}(1+\varphi)^{3.683}$$

For ZrO_2-SiC/DW nanofluid:

$$\mathrm{Nu} = 0.04677\ \mathrm{Re}^{0.5596}\mathrm{Pr}^{0.6468}(1+\varphi)^{2.7573}$$

The above correlations are valid for volume concentrations ranging from 0% to 0.1% and Reynolds numbers between 361.07 and 2115.1 while Prandtl's number between 2.57 and 6.98.

6. Impact of nanofluids on the entropy generation and exergy destruction, and exergy efficiency of FPSC

I have evaluated and justified the effect of entropy generation and exergy destruction that took place inside the FPSC filled with new ZrO_2/DW, SiC/DW and ZrO_2-SiC/DW nanofluids on the solar collector's exergetic performance. Hence, these two parameters need to be carefully considered to ensure higher system efficiency. Besides, I experimentally investigated the entropy generation and exergy destruction based on different solid volume fractions of nanofluids and its impact on FPSC performance.

According to experimental results, I have observed that the decline in entropy generation and exergy destruction leads to higher exergetic efficiency of FPSC. I have discovered that using nanofluids as working fluids yields lower values of entropy generation and exergy destruction. This is because a more concentrated nanofluid is characterized by higher thermal conductivity.

Based on the experimental results, I observed that the nanoparticles are good conductors of heat and hence enhance the fluid's thermal conductivity when combined with the fluid. Consequently, the exergy efficiency experiences a rise. I have also discovered that there are 37.42%, 16.05% and 28.31% rise in exergy efficiency when a nanoparticles concentration of 0.1% of SiC/DW, ZrO_2/DW, ZrO_2-SiC/DW nanofluids, respectively.

7. Numerical analysis of FPSC performance

I have developed a new CFD model for flat plate solar collector filled by new nanofluids of silicon carbide, zirconium oxide, and their hybrid nanofluids. This model is like the experiment model in dimensions in order to investigate the performance of FPSC using mono and hybrid nanofluids. To achieve that purpose, I have observed that using ANSYS Fluent software through the adoption of the finite volume method for calculating the output temperature, absorber plate temperature and efficiency of FPSC. I have validated calculated results by comparing experimental data and theoretical results that accounted for Nusselt correlations. Besides, I have found that the results of the experimental and simulation work with DW and both the SiC/DW, ZrO_2/DW, and ZrO_2-SiC/DW nanofluids in FPSC had efficiencies that were close to each other.

5. CONCLUSION AND SUGGESTIONS

The efficiency of FPSC filled with ZrO_2/DW, SiC/DW and ZrO_2-SiC/DW nanofluids was examined in this work. There are limited studies in the literature on the effects of these given nanofluid considering the FPSC thermal and exergy efficiencies. The use of the new nanofluids as a state-of-the-art heat transfer liquid remains in solar collectors and definitely merits further scientific investigation. For this study, nanofluids were prepared with different concentrations, namely 0.025%, 0.05%, 0.075% and 0.1%. Each of the nanofluids was filled inside the solar collector to see the changes it caused in the collector's efficiency. Moreover, following the ASHRAE standard, the study considered different mass flow rates of 0.025, 0.033 and 0.041 kg/s to study the impact of mass flow rates on solar collector efficiency. Based on the findings of the current study, it is possible to make the following inferences:

- The stability of ZrO_2/DW, SiC/DW, ZrO_2-SiC/DW nanofluids, which was tested by zeta potential analysis, was good stability.
- The Newtonian behaviour of the given nanofluids was observed at each temperature setting.
- The results indicate that dynamic viscosity increased to the maximum level at a solid concentration of 0.1% and temperature of 60 °C, where the increase was around 226.3% for the nanofluid of ZrO_2/DW, 110.5% for the nanofluid of SiC/DW, and 169.47% for the hybrid nanofluid of ZrO_2-SiC/DW.
- The thermal conductivity of the examined nanofluid increased with rising temperature and higher solid volume fraction.
- The thermal conductivity enhancement for ZrO_2/DW was 20.45%, 30.3% for SiC/DW, and 25.75% for ZrO_2-SiC hybrid nanofluid at maximum solid volume fraction and temperature.
- The FPSC thermal efficiency was increased as 33.57%, 26.2% and 31.46% for 0.1% SiC /DW, ZrO_2/DW and ZrO_2-SiC/DW nanofluids at flow rate of 0.041 kg/s, respectively, in comparison to water.
- It was revealed during the experiment that the exergy efficiency of the solar collector increases when the distilled water is replaced with nanofluids. The FPSC exergy efficiency increased by 37.42% ,16.05% and 28.31% when SiC/DW, ZrO_2/DW, ZrO_2-SiC/DW nanofluids, respectively, were used.
- The results obtained from the numerical and experimental work were in good agreement, so the outcomes of the experiments served to validate the numerical model.

Further studies can be conducted to navigate ways to improve stability and reduce the sedimentation of NPs in fluid by addition of the surfactants and using homogenization by ball milling. The authors proposed that research needs to focus on more factors that affect nanofluid properties. The factors recommended for future studies include nanoparticle aggregation, shape, size, sonication time and base fluid. The study also emphasizes more research in future on nanoparticles can also be used in solar selective absorber nano coatings to find out they increase efficiency of FPSC. Studies on using nanoparticles in anti-reflective nanocoating on glass cover and their effects on thermal efficiency of FPSC are recommended. Finally, the cost of nanoparticles and nanofluids are high and its making is difficult. Therefore, future research must there is a dire need for efforts in the development of economic, environmental aspects, and effective nanofluids to foretell the technology feasibility.

6. SUMMARY

PERFORMANCE ENHANCEMENT OF FLAT PLATE SOLAR COLLECTOR USING NANOFLUIDS

In this work, comprehensive experimental and numerical investigations were carried out to evaluate the flat plate solar collector's thermal and exergy enhancement using nanofluid were undertaken. To achieve the aims of this research, zirconium oxide ZrO_2 and silicon carbide SiC nanoparticles were obtained, in which the first one present various technique like X-ray diffraction and field emission scanning electron microscopy are engaged for the nanoparticle's characterization and particle shape. The nanofluids were prepared using a two-steps method by dispersing the given nanoparticles in distilled water (DW) by the ultrasonic processor and a magnetic stirrer. Solid volume fractions (φ) of the given nanofluids of 0.025%, 0.05%, 0.075% and 0.1% were used. Stability of nanofluids were examined by zeta potential test. After that, thermal conductivity and viscosity were measured using the using a KD2-Pro thermal analyzer and a Brookfield viscometer, respectively, at temperatures ranging from 20 to 60 °C. In the next step, the nanofluids are employed into a flat plate solar collector (FPSC) to identify the performance change of the collector. Besides, thermal and exergy efficiencies tests were conducted on the solar collector. The investigation of the solar collector's performance was based on ASHRAE Standard 93-2003. This standard is aimed at introducing testing techniques for the detection of solar collector performance. The experiments were conducted on days with sunshine between 10 a.m. and 3p.m. (local time). All experimental investigations on the flat plate solar collector were conducted at the Hungarian University of Agriculture and Life Sciences (MATE) in Gödöllő (Latitude: 47.59° N & Longitude: 19.36° E), Hungary. Ultimately, a CFD model was created to assess the thermal performance of the given nanofluids at FPSC in the experiment indicated above.

The outcomes of the experiment and numerical revealed that the solar collector system showed greater energy and exergy efficiencies in the presence of a nanofluid as compared to the exergy and energy efficiencies shown by the system-based distilled water. The results showed that the thermal conductivity of the nanofluid was enhanced with increased volume fractions and temperature. The thermal conductivity enhancement for ZrO_2/DW at the volume fraction of 0.1% was 20.45%, that of ZrO_2-SiC/DW was 25.75%, and that of SiC/DW was 30.3%. Additionally, according to the results of the experiments, new correlations capable of predicting for both the investigated nanofluids' viscosity and thermal conductivity in relation to solid concentration and temperature have been suggested.

The collector's thermal efficiency was enhanced by 35.53%, 26.2% and 31.64% for a volume fraction of 0.1% of SiC/DW, ZrO_2/DW and ZrO_2-SiC/DW nanofluids, respectively, when the value of [(Ti – Ta)/GT] was zero and mass flow rate of 0.041 kg/s. Additionally, an increase of 37.4%, 16.05% and 28.31% were recorded for the exergy efficiency at volume fraction of 0.1% SiC/DW, ZrO_2/DW and ZrO_2-SiC/DW nanofluids than its value in distilled water. The experiments also discovered new correlations for determining the Nusselt number of the given nanofluids and thermal efficiency of FPSC. After obtaining all readings, the conclusion suggested that FPSC delivered the highest thermal and exergy efficiencies when the given nanofluids are used as operating fluid. Moreover, this study is significant as it presents a new nanofluids that can be used in renewable energy applications.

7. ÖSSZEFOGLALÁS (SUMMARY IN HUNGARIAN)

SÍKKOLLEKTOR TELJESÍTMÉNYÉNEK NÖVELÉSE NANOFOLYADÉKOKKAL

Disszertációmban átfogó kísérleti és numerikus vizsgálatokat végeztem síkkollektorok nanofolyadékok segítségével történő hő- és exergianövelésének értékelésére. A kutatásom során cirkónium-oxid (ZrO_2) és szilícium-karbid (SiC) nanorészecskéket használtam. A kutatási céljaim elérése érdekében elsőként röntgendiffrakciót és téremissziós pásztázó elektronmikroszkópiát alkalmazva vizsgálatokat végeztem a nanorészecskék jellemzésére. A nanorészecskékből a nanofolyadékokat kétlépéses módszerrel állítottam elő: a nanorészecskéket desztillált vízben (DW) diszpergáltattam ultrahangos berendezéssel, majd mágneses keverést alkalmaztam. A kísérleteimben az előállított nanofolyadékok 0,025, 0,05, 0,075 és 0,1 térfogatszázalékos koncentrációját alkalmaztam. A nanofluidok stabilitását zéta potenciál teszttel vizsgáltam. Ezt követően a hővezető képességet és a viszkozitást KD2-Pro termikus analizátorral, illetve Brookfield viszkoziméterrel mértem 20 és 60 °C közötti hőmérséklet tartományban. A következő lépésben egy síkkollektorban szolárfolyadékként alkalmaztam ezeket a nanofolyadékokat, hogy meghatározhassam a kollektor teljesítményváltozását. Emellett, a napkollektornál hő- és exergiahatékonysági vizsgálatokat végeztem. A napkollektor teljesítményének vizsgálata az ASHRAE 93-2003 szabványon alapult, a méréseket napsütéses napokon, helyi idő szerint 10 és 15 óra között végeztem. A napkollektorral kapcsolatos valamennyi kísérleti vizsgálatot a Magyar Agrár- és Élettudományi Egyetemen (MATE) végeztem Gödöllőn (Ész: 47,59º, Kh: 19,36°), Magyarországon. Végül egy CFD-modellt dolgoztam ki az adott nanofolyadékok hőteljesítményének értékelésére a mérések során használt síkkollektorra vonatkozóan.

A mérési és a numerikus eredmények azt mutatták, hogy a napkollektoros rendszer nagyobb energia- és exergiahatékonyságot mutatott a nano szolárfolyadék alkalmazása esetén, mint a referenciaként használt desztillált víznél tapasztalt exergia- és energiahatékonyság.

A mérési eredmények alapján megfogalmazható, hogy a nanofolyadékok hővezető-képessége javult a térfogatarányok és a hőmérséklet növekedésével. A ZrO_2/DW hővezetőképesség-növekedése 0,1 térfogatszázalékos alkalmazásánál 20,45%, a ZrO_2-SiC/DW 25,75%, a SiC/DW nanofolyadéké pedig 30,3%. Ezen túlmenően a kísérletek eredményei alapján olyan új összefüggéseket javasoltam, amelyek mind a vizsgált nanofluidok viszkozitását, mind hővezető képességét előre jelezni tudják a szilárdanyag-koncentráció és a hőmérséklet vonatkozásában a megadott koncentráció- és hőmérséklet tartományban.

A kollektor maximális hatásfoka 35,53%-kal, 26,2%-kal, illetve 31,64%-kal nőtt a SiC/DW, ZrO_2/DW és ZrO_2-SiC/DW nanofluidok 0,1%-os térfogatszázalékos alkalmazása esetén, amikor a tömegáram 0,041 kg/s értékű volt. Emellett 37,4%, 16,05% illetve 28,31% növekedés volt meghatározható az exergia hatékonyságra 0,1 térfogatszázalékos SiC/DW, ZrO_2/DW illetve a ZrO_2-SiC/DW nanofolyadékok alkalmazásánál, a desztillált víz szolárfolyadék esetéhez viszonyítva. A kísérletek új összefüggéseket is feltártak az adott nanofolyadékok Nusselt számának és a síkkollektor termikus hatásfokának meghatározásához.

Az eredmények alapján az a következtetés vonható le, hogy a vizsgált nanofolyadékok hatékonyan alkalmazhatók síkkollektoros rendszer szolárfolyadékaként. Ezen túlmenően a bemutatott vizsgálatok és eredményeik azért is jelentősek, mert új nanofolyadékokat mutatnak be, amelyek megújuló energiaforrásoknál is hatékonyan használhatók.

8. APPENDICES

A1: Bibliography

1. Abbasi, S., Zebarjad, S.M., Baghban, S.H.N., Youssefi, A. and Ekrami-Kakhki, M.S. (2016): Experimental investigation of the rheological behavior and viscosity of decorated multi-walled carbon nanotubes with TiO_2 nanoparticles/water nanofluids, Journal of Thermal Analysis and Calorimetry, 123(1), pp. 81–89. doi:10.1007/s10973-015-4878-4
2. Aberoumand, S. and Jafarimoghaddam, A. (2018): Tungsten (III) oxide (WO_3) – Silver/transformer oil hybrid nanofluid: Preparation, stability, thermal conductivity and dielectric strength, Alexandria Engineering Journal, 57(1), pp. 169–174. doi:10.1016/j.aej.2016.11.003
3. Adapa, P.K. and Schoenau, G.J. (2005): Re-circulating heat pump assisted continuous bed drying and energy analysis, International Journal of Energy Research, 29(11), pp. 961–972. doi:10.1002/er.1103
4. Afrand, M., Abedini, E. and Teimouri, H. (2017) How the dispersion of magnesium oxide nanoparticles effects on the viscosity of water-ethylene glycol mixture: Experimental evaluation and correlation development, Physica E: Low-Dimensional Systems and Nanostructures, 87 (October 2016), pp. 273–280. doi:10.1016/j.physe.2016.10.027
5. Ahmadi, A., Ganji, D.D. and Jafarkazemi, F. (2016): Analysis of utilizing Graphene nanoplatelets to enhance thermal performance of flat plate solar collectors, Energy Conversion and Management 126,pp. 1–11. doi:10.1016/j.enconman.2016.07.061
6. Ahmed, F. and Khan, W.A. (2021): Efficiency enhancement of an air-conditioner utilizing nanofluids: An experimental study, Energy Reports, 7,pp.575–583. doi:10.1016/j.egyr.2021.01.023
7. Ahmed, W. et al. (2021): Experimental investigation of convective heat transfer growth on ZnO and TiO_2/DW binary composites/hybrid nanofluids in a circular heat exchanger, Journal of Thermal Analysis and Calorimetry, 143(2), pp. 879–898. doi:10.1007/s10973-020-09363-x
8. Ajeena, A.M., Farkas, I. and Víg, P. (2023)a: A comparative experimental investigation of dynamic viscosity of ZrO_2/DW and SiC/DW nanofluids: Characterization, rheological behavior, and development of new correlation, Heliyon, 9(10) p. e21113. doi:10.1016/j.heliyon.2023.e21113
9. Ajeena, A.M., Farkas, I. and Víg, P. (2023)b: A comparative experimental study on thermal conductivity of distilled water-based mono nanofluids with zirconium oxide and silicon carbide for thermal industrial applications: Proposing a new correlation, International Journal of Thermofluids, 20(July), p. 100424. doi:10.1016/j.ijft.2023.100424
10. Ajeena, A.M., Farkas, I. and Víg, P. (2023)c: A comprehensive experimental study on thermal conductivity of ZrO_2-SiC/DW hybrid nanofluid for practical applications: Characterization, preparation, stability and developing a new correlation, Arabian Journal of Chemistry, 16(12), p. 105346. doi:10.1016/j.arabjc.2023.105346
11. Ajeena, A.M., Farkas, I. and Víg, P. (2023)d: Performance enhancement of flat plate solar collector using ZrO_2-SiC/DW hybrid nanofluid: A comprehensive experimental study, Energy Conversion and Management: X, 20 (September), p. 100458. doi:10.1016/j.ecmx.2023.100458.

12. Ajeena, Ahmed M., Farkas, I. and Víg, P. (2024): Characterization, rheological behaviour, and dynamic viscosity of ZrO_2-SiC(50–50)/DW hybrid nanofluid under different temperatures and solid volume fractions: An experimental study and proposing a new correlation, Powder Technology, 431(October 2023), p. 119069. doi:10.1016/j.powtec.2023.119069

13. Ajeena, Ahmed M, Farkas, I. and Víg, P. (2024): Energy and exergy assessment of a flat plate solar thermal collector by examine silicon carbide nanofluid: An experimental study for sustainable energy, Applied Thermal Engineering, 236(PD), p. 121844. doi:10.1016/j.applthermaleng.2023.121844

14. Ajeena, A.M., Víg, P. and Farkas, I. (2022): A comprehensive analysis of nanofluids and their practical applications for flat plate solar collectors: Fundamentals, thermophysical properties, stability, and difficulties, Energy Reports, 8, pp. 4461–4490. doi:10.1016/j.egyr.2022.03.088

15. Akram, N. et al. (2019): An experimental investigation on the performance of a flat-plate solar collector using eco-friendly treated graphene nanoplatelets–water nanofluids, Journal of Thermal Analysis and Calorimetry, 138(1), pp. 609–621. doi:10.1007/s10973-019-08153-4

16. Akram, N. et al. (2020): A comprehensive review on nanofluid operated solar flat plate collectors, Journal of Thermal Analysis and Calorimetry. Springer International Publishing. doi:10.1007/s10973-019-08514-z

17. Alawi, O.A. et al. (2021): Nanofluids for flat plate solar collectors: Fundamentals and applications, Journal of Cleaner Production, 291. doi:10.1016/j.jclepro.2020.125725

18. Alawi, O.A., Mohamed Kamar, H., Mallah, A.R., Kazi, S.N. and Sidik, N.A.C. (2019): Thermal efficiency of a flat-plate solar collector filled with Pentaethylene Glycol-Treated Graphene Nanoplatelets: An experimental analysis, Solar Energy, 191(April), pp. 360–370. doi:10.1016/j.solener.2019.09.011

19. Almurtaji, S., Ali, N., Teixeira, J.A. and Addali, A. (2020): On the role of nanofluids in thermal-hydraulic performance of heat exchangers-a review, Nanomaterials, 10(4). doi:10.3390/nano10040734

20. Amini, M. and Kianifar, A. (2016): An analytical study on energy and exergy of a minichannel-based solar collector using Fe_3O_4 and MgO / water nanofluids, International Conference on Researches in Science and Engineering [Preprint], (July 2016)

21. Amrollahi, A., Hamidi, A.A. and Rashidi, A.M. (2008): The effects of temperature, volume fraction and vibration time on the thermo-physical properties of a carbon nanotube suspension (carbon nanofluid), Nanotechnology, 19(31). doi:10.1088/0957-4484/19/31/315701

22. Angayarkanni, S.A. and Philip, J. (2015): Review on thermal properties of nanofluids: Recent developments, Advances in Colloid and Interface Science, 225, pp. 146–176. doi:10.1016/j.cis.2015.08.014

23. Anin Vincely, D. and Natarajan, E. (2016): Experimental investigation of the solar FPC performance using graphene oxide nanofluid under forced circulation, Energy Conversion and Management, 117, pp. 1–11. doi:10.1016/j.enconman.2016.03.015

24. Arora, N. and Gupta, M. (2021): Thermo-hydraulic performance of nanofluids in enhanced tubes - a review, Heat and Mass Transfer/Waerme- und Stoffuebertragung, 57(3), pp. 377–404. doi:10.1007/s00231-020-02958-y

25. Arshad, A., Jabbal, M., Yan, Y. and Reay, D. (2019): *A review on graphene based nanofluids: Preparation, characterization and applications*, Journal of Molecular Liquids.

Elsevier B.V. doi:10.1016/j.molliq.2019.01.153

26. ASHRAE Standard and 93-2003 (2003): Methods of Testing to Determine the Thermal Performance of Solar Collectors, Atlanta, GA, USA, Preprint
27. Asmat, F., Khan, W.A., Usman, Shamshuddin, M.D., Salawu, S.O. and Bouye, M. (2023): Thermal analysis in an electrically conducting fluid with multiple slips and radiation along a plate: A case study of Stokes' second problem, Case Studies in Thermal Engineering, 44 (October 2022), p. 102831. doi:10.1016/j.csite.2023.102831
28. Babar, H. and Ali, H.M. (2019): Towards hybrid nanofluids: Preparation, thermophysical properties, applications, and challenges, Journal of Molecular Liquids, 281, pp. 598–633. doi:10.1016/j.molliq.2019.02.102
29. Bazdidi-Tehrani, F., Khabazipur, A. and Vasefi, S.I. (2018): Flow and heat transfer analysis of TiO_2/water nanofluid in a ribbed flat-plate solar collector, Renewable Energy, 122, pp. 406–418. doi:10.1016/j.renene.2018.01.056
30. Byrne, M.D., Hart, R.A. and Silva, A.K. (2012): International Journal of Heat and Mass Transfer Experimental thermal – hydraulic evaluation of CuO nanofluids in microchannels at various concentrations with and without suspension enhancers, International Journal of Heat and Mass Transfer, 55(9–10), p. 2684–2691. doi:10.1016/j.ijheatmasstransfer.2011.12.018
31. Chaji, H., Ajabshirchi, Y., Esmaeilzadeh, E., Heris, S.Z., Hedayatizadeh, M. and Kahani, M. (2013): Experimental study on thermal efficiency of flat plate solar collector using tio2/water nanofluid, Modern Applied Science, 7(10), pp. 60–69. doi:10.5539/mas.v7n10p60
32. Chamoli, S. (2013): Exergy analysis of a flat plate solar collector, Journal of Energy in Southern Africa, 24(3), pp. 8–13. doi:10.17159/2413-3051/2013/v24i3a3137
33. Chauhan, R., Singh, T., Thakur, N.S., Kumar, N., Kumar, R. and Kumar, A. (2018): Heat transfer augmentation in solar thermal collectors using impinging air jets: A comprehensive review, Renewable and Sustainable Energy Reviews, 82(October 2017), pp. 3179–3190. doi:10.1016/j.rser.2017.10.025
34. Chen, L., Xie, H., Li, Y. and Yu, W. (2008): Nanofluids containing carbon nanotubes treated by mechanochemical reaction, Thermochimica Acta, 477(1–2), pp. 21–24. doi:10.1016/j.tca.2008.08.001
35. Choi, S.U.S. (1995): Enhancing thermal conductivity of fluids with nanoparticles, American Society of Mechanical Engineers, Fluids Engineering Division (Publication) FED, 231(March), pp. 99–105
36. Chon, C.H., Kihm, K.D., Lee, S.P. and Choi, S.U.S. (2005): Empirical correlation finding the role of temperature and particle size for nanofluid (Al_2O_3) thermal conductivity enhancement, Applied Physics Letters, 87(15), pp. 1–3. doi:10.1063/1.2093936
37. Choudhary, S., Sachdeva, A. and Kumar, P. (2020): Investigation of the stability of MgO nanofluid and its effect on the thermal performance of flat plate solar collector, Renewable Energy, 147, pp. 1801–1814. doi:10.1016/j.renene.2019.09.126
38. Das, S.K., Putra, N., Thiesen, P. and Roetzel, W. (2003): Temperature dependence of thermal conductivity enhancement for nanofluids, Journal of Heat Transfer, 125(4), pp. 567–574. doi:10.1115/1.1571080
39. Devarajan, Y. and Munuswamy, D.B. (2016): Analysis on the Influence of Nanoparticles of Alumina, Copper Oxide, and Zirconium Oxide on the Performance of a Flat-Plate Solar Water Heater, Energy and Fuels, 30(11), pp. 9908–9913.

doi:10.1021/acs.energyfuels.6b02264

40. Devendiran, D.K. and Amirtham, V.A. (2016): A review on preparation, characterization, properties and applications of nanofluids, Renewable and Sustainable Energy Reviews, 60, pp. 21–40. doi:10.1016/j.rser.2016.01.055
41. Duangthongsuk, W. and Wongwises, S. (2009): Measurement of temperature-dependent thermal conductivity and viscosity of TiO2-water nanofluids, Experimental Thermal and Fluid Science, 33(4), pp. 706–714. doi:10.1016/j.expthermflusci.2009.01.005
42. Duffie, J.A., Beckman, W.A., McGowan, J. (2013): Solar Engineering of Thermal Processes. Available at: https://aapt.scitation.org/doi/10.1119/1.14178
43. Duffie, J.A., Beckman, W.A. and McGowan, J. (1985): Solar Engineering of Thermal Processes, American Journal of Physics. doi:10.1119/1.14178
44. Eastman, J.A., Choi, S.U.S., Li, S., Yu, W. and Thompson, L.J. (2001): Anomalously increased effective thermal conductivities of ethylene glycol-based nanofluids containing copper nanoparticles, Applied Physics Letters, 78(6), pp. 718–720. doi:10.1063/1.1341218
45. Eggers, J.R. and Kabelac, S. (2016): Nanofluids revisited, Applied Thermal Engineering, 106, pp. 1114–1126. doi:10.1016/j.applthermaleng.2016.06.100
46. Elcioglu, E.B., Genc, A.M., Karadeniz, Z.H., Ezan, M.A. and Turgut, A. (2020): Nanofluid figure-of-merits to assess thermal efficiency of a flat plate solar collector, Energy Conversion and Management, 204(August2019), p. 112292. doi:10.1016/j.enconman.2019.112292
47. Elsheikh, A.H., Sharshir, S.W., Mostafa, M.E., Essa, F.A. and Ahmed Ali, M.K. (2018): Applications of nanofluids in solar energy: A review of recent advances, Renewable and Sustainable Energy Reviews, 82 (November 2017), pp. 3483–3502. doi:10.1016/j.rser.2017.10.108
48. Eltaweel, M. and Abdel-Rehim, A.A. (2019): Energy and exergy analysis of a thermosiphon and forced-circulation flat-plate solar collector using MWCNT/Water nanofluid, Case Studies in Thermal Engineering, 14(February), p. 100416. doi:10.1016/j.csite.2019.100416
49. Esen, H. (2008): Experimental energy and exergy analysis of a double-flow solar air heater having different obstacles on absorber plates, Building and Environment, 43(6), pp. 1046–1054. doi:10.1016/j.buildenv.2007.02.016
50. Faizal, M., Saidur, R., Mekhilef, S. and Alim, M.A. (2013): Energy, economic and environmental analysis of metal oxides nanofluid for flat-plate solar collector, Energy Conversion and Management, 76, pp. 162–168. doi:10.1016/j.enconman.2013.07.038
51. Fan, H., Singh, R. and Akbarzadeh, A. (2011): Electric power generation from thermoelectric cells using a solar dish concentrator, Journal of Electronic Materials, 40(5), pp. 1311–1320. doi:10.1007/s11664-011-1625-x
52. Farajzadeh, E., Movahed, S. and Hosseini, R. (2018): Experimental and numerical investigations on the effect of Al_2O_3/TiO_2[sbnd]H_2O nanofluids on thermal efficiency of the flat plate solar collector, Renewable Energy, 118, pp. 122–130. doi:10.1016/j.renene.2017.10.102
53. Farhana, K. et al. (2019): Improvement in the performance of solar collectors with nanofluids — A state-of-the-art review, Nano-Structures and Nano-Objects, 18. doi:10.1016/j.nanoso.2019.100276

54. Ganesan, P., Vanaki, S.M., Thoo, K.K. and Chin, W.M. (2016): Air-side heat transfer characteristics of hydrophobic and super-hydrophobic fi n surfaces in heat exchangers : A review, International Communications in Heat and Mass Transfer, 74, pp. 27–35. doi:10.1016/j.icheatmasstransfer.2016.02.017

55. Genc, A.M., Ezan, M.A. and Turgut, A. (2018): Thermal performance of a nanofluid-based flat plate solar collector: A transient numerical study, Applied Thermal Engineering, 130, pp. 395–407. doi:10.1016/j.applthermaleng.2017.10.166

56. Gnanadason, M.K., Kumar, P.S., Jemilda, G. and Sherin Jasper, S. (2012): Effect of Nanofluids in a Modified Vacuum Single Basin Solar Still, International Journal of Scientific & Engineering Research, 3(1), pp. 1–7. Available at: http://www.ijser.org

57. Gorjian, S., Ebadi, H., Calise, F., Shukla, A. and Ingrao, C. (2020)a: A review on recent advancements in performance enhancement techniques for low-temperature solar collectors, Energy Conversion and Management, 222 (August), p. 113246. doi:10.1016/j.enconman.2020.113246

58. Gorjian, S., Ebadi, H., Calise, F., Shukla, A. and Ingrao, C. (2020)b: A review on recent advancements in performance enhancement techniques for low-temperature solar collectors, Energy Conversion and Management, 222 (May), p. 113246. doi:10.1016/j.enconman.2020.113246

59. Goudarzi, K., Shojaeizadeh, E. and Nejati, F. (2014): An experimental investigation on the simultaneous effect of CuO-H_2O nanofluid and receiver helical pipe on the thermal efficiency of a cylindrical solar collector, Applied Thermal Engineering, 73(1), pp. 1236–1243. doi:10.1016/j.applthermaleng.2014.07.067

60. Hajabdollahi, F. and Premnath, K. (2017): Numerical study of the effect of nanoparticles on thermoeconomic improvement of a solar flat plate collector, Applied Thermal Engineering, 127, pp. 390–401. doi:10.1016/j.applthermaleng.2017.08.058

61. Hamzat, A.K., Omisanya, M.I., Sahin, A.Z., Ropo Oyetunji, O. and Abolade Olaitan, N. (2022) *Application of nanofluid in solar energy harvesting devices: A comprehensive review*, Energy Conversion and Management. Elsevier Ltd. doi:10.1016/j.enconman.2022.115790

62. Hawwash, A.A., Abdel Rahman, A.K., Nada, S.A. and Ookawara, S. (2018): Numerical Investigation and Experimental Verification of Performance Enhancement of Flat Plate Solar Collector Using Nanofluids, Applied Thermal Engineering, 130, pp. 363–374. doi:10.1016/j.applthermaleng.2017.11.027

63. He, Q., Zeng, S. and Wang, S. (2014): Experimental investigation on the efficiency of flat-plate solar collectors with nanofluids, Applied Thermal Engineering, 88, pp. 165–171. doi:10.1016/j.applthermaleng.2014.09.053

64. Hemmat Esfe, M. et al. (2015): Modeling of thermal conductivity of ZnO-EG using experimental data and ANN methods, International Communications in Heat and Mass Transfer, 63, pp. 35–40. doi:10.1016/j.icheatmasstransfer.2015.01.001

65. Heyhat, M.M., Valizade, M., Abdolahzade, S. and Maerefat, M. (2020): Thermal efficiency enhancement of direct absorption parabolic trough solar collector (DAPTSC) by using nanofluid and metal foam, Energy, 192, p. 116662. doi:10.1016/j.energy.2019.116662

66. Hossain, M.S. et al. (2011): Review on solar water heater collector and thermal energy performance of circulating pipe, Renewable and Sustainable Energy Reviews, 15(8), pp. 3801–3812. doi:10.1016/j.rser.2011.06.008

67. Huang, W. and Marefati, M. (2020): Energy, exergy, environmental and economic comparison of various solar thermal systems using water and Thermia Oil B base fluids, and CuO and Al_2O_3 nanofluids, Energy Reports, 6, pp. 2919–2947. doi:10.1016/j.egyr.2020.10.021

68. Hussein, A.K. (2016): Applications of nanotechnology to improve the performance of solar collectors - Recent advances and overview, Renewable and Sustainable Energy Reviews, 62, pp. 767–792. doi:10.1016/j.rser.2016.04.050

69. Hussein, O.A., Habib, K., Muhsan, A.S., Saidur, R., Alawi, O.A. and Ibrahim, T.K. (2020): Thermal performance enhancement of a flat plate solar collector using hybrid nanofluid, Solar Energy, 204 (December 2019), pp. 208–222. doi:10.1016/j.solener.2020.04.034

70. Imran, M., Rasli, A. and Zaman, K. (2016): Energy crisis , greenhouse gas emissions and sectoral growth reforms : repairing the fabricated mosaic, Journal of Cleaner Production, 112, pp. 3657–3666. doi:10.1016/j.jclepro.2015.08.017

71. Jafari, K., Fatemi, M.H. and Lugo, L. (2022): Influence of MgO concentration and water content on thermal conductivity enhancement of nanofluids based on deep eutectic solvent (choline chloride:glycerol), Journal of Molecular Liquids, 367, p. 120319. doi:10.1016/j.molliq.2022.120319

72. Jafarkazemi, F. and Ahmadifard, E. (2013): Energetic and exergetic evaluation of flat plate solar collectors, Renewable Energy, 56, pp. 55–63. doi:10.1016/j.renene.2012.10.031

73. Jamal-Abad, M.T., Zamzamian, A., Imani, E. and Mansouri, M. (2013): Experimental study of the performance of a flat-plate collector using Cu-water nanofluid, Journal of Thermophysics and Heat Transfer, 27(4), pp. 756–760. doi:10.2514/1.T4074

74. Jamar, A., Majid, Z.A.A., Azmi, W.H., Norhafana, M. and Razak, A.A. (2016): A review of water heating system for solar energy applications, International Communications in Heat and Mass Transfer, 76, pp. 178–187. doi:10.1016/j.icheatmasstransfer.2016.05.028

75. Jana, S., Salehi-Khojin, A. and Zhong, W.H. (2007): Enhancement of fluid thermal conductivity by the addition of single and hybrid nano-additives, Thermochimica Acta, 462(1–2), pp. 45–55. doi:10.1016/j.tca.2007.06.009

76. Jarahnejad, M. et al. (2015): Experimental investigation on viscosity of water-based Al2O3 and TiO2 nanofluids, Rheologica Acta, 54(5), pp. 411–422. doi:10.1007/s00397-015-0838-y

77. Kalogirou, S.A. (2004): *Solar thermal collectors and applications*, Progress in Energy and Combustion Science. doi:10.1016/j.pecs.2004.02.001

78. Karthikeyan, N.R., Philip, J. and Raj, B. (2008): Effect of clustering on the thermal conductivity of nanofluids, Materials Chemistry and Physics, 109(1), pp. 50–55. doi:10.1016/j.matchemphys.2007.10.029

79. Khan, M.Z.U. et al. (2021): Investigation of heat transfer in dimple-protrusion micro-channel heat sinks using copper oxide nano-additives, Case Studies in Thermal Engineering, 28(August). doi:10.1016/j.csite.2021.101374

80. Kiliç, F., Menlik, T. and Sözen, A. (2018): Effect of titanium dioxide/water nanofluid use on thermal performance of the flat plate solar collector, Solar Energy, 164(March), pp. 101–108. doi:10.1016/j.solener.2018.02.002

81. Kim, H., Kim, J. and Cho, H. (2017): Experimental study on performance improvement of U-tube solar collector depending on nanoparticle size and concentration of Al_2O_3 nanofluid, Energy, 118, pp. 1304–1312. doi:10.1016/j.energy.2016.11.009

82. Kumar, L., Hasanuzzaman, M. and Rahim, N.A. (2019): Global advancement of solar thermal energy technologies for industrial process heat and its future prospects: A review, Energy Conversion and Management, 195 (May), pp. 885–908. doi:10.1016/j.enconman.2019.05.081

83. Kumar, L.H., Kazi, S.N., Masjuki, H.H., Zubir, M.N.M., Jahan, A. and Bhinitha, C. (2021): Energy, exergy and economic analysis of liquid flat-plate solar collector using green covalent functionalized graphene nanoplatelets, Applied Thermal Engineering, 192(February), p. 116916. doi:10.1016/j.applthermaleng.2021.116916

84. Li, C.H. and Peterson, G.P. (2007): The effect of particle size on the effective thermal conductivity of Al2O3-water nanofluids, Journal of Applied Physics, 101(4). doi:10.1063/1.2436472

85. Li, H., Wang, L., He, Y., Hu, Y., Zhu, J. and Jiang, B. (2014): Experimental investigation of thermal conductivity and viscosity of ethylene glycol based ZnO nanofluids, Applied Thermal Engineering, 88, pp. 363–368. doi:10.1016/j.applthermaleng.2014.10.071

86. Liu, S., Afan, H.A., Aldlemy, M.S., Al-Ansari, N. and Yaseen, Z.M. (2020): Energy analysis using carbon and metallic oxides-based nanomaterials inside a solar collector, Energy Reports, 6, pp. 1373–1381. doi:10.1016/j.egyr.2020.05.015

87. Mahbubul, I.M., Saidur, R., Amalina, M.A. and Niza, M.E. (2016): In fluence of ultrasonication duration on rheological properties of nano fluid: An experimental study with alumina – water nanofluid, 76, pp. 33–40. doi:10.1016/j.icheatmasstransfer.2016.05.014

88. Michael, J.J. and Iniyan, S. (2015): Performance of copper oxide/water nanofluid in a flat plate solar water heater under natural and forced circulations, Energy Conversion and Management, 95, pp. 160–169. doi:10.1016/j.enconman.2015.02.017

89. Michael Joseph Stalin, P., Arjunan, T. V., Matheswaran, M.M., Dolli, H. and Sadanandam, N. (2020): Energy, economic and environmental investigation of a flat plate solar collector with CeO2/water nanofluid, Journal of Thermal Analysis and Calorimetry, 139(5), pp. 3219–3233. doi:10.1007/s10973-019-08670-2

90. Moghadam, M.C., Edalatpour, M. and Solano, J.P. (2017): Numerical Study on Conjugated Laminar Mixed Convection of Alumina/Water Nanofluid Flow, Heat Transfer, and Entropy Generation Within a Tube-on-Sheet Flat Plate Solar Collector, Journal of Solar Energy Engineering, Transactions of the ASME, 139(4). doi:10.1115/1.4036854

91. Moradi, A., Zareh, M., Afrand, M. and Khayat, M. (2020): Effects of temperature and volume concentration on thermal conductivity of TiO_2-MWCNTs (70-30)/EG-water hybrid nano-fluid, Powder Technology, 362, pp. 578–585. doi:10.1016/j.powtec.2019.10.008

92. Moravej, M. et al. (2020): Enhancing the efficiency of a symmetric flat-plate solar collector via the use of rutile TiO_2-water nanofluids, Sustainable Energy Technologies and Assessments, 40(June). doi:10.1016/j.seta.2020.100783

93. Munuswamy, D.B., Madhavan, V.R. and Mohan, M. (2015): Comparison of the effects of Al2O3 and CuO nanoparticles on the performance of a solar flat-plate collector, Journal of Non-Equilibrium Thermodynamics, 40(4), pp. 265–273. doi:10.1515/jnet-2015-0019

94. Mussard, M. (2017): Solar energy under cold climatic conditions: A review, Renewable and Sustainable Energy Reviews, 74 (December 2016), pp. 733–745. doi:10.1016/j.rser.2017.03.009

95. Nagarajan, P.K., Subramani, J., Suyambazhahan, S. and Sathyamurthy, R. (2014): Nanofluids for solar collector applications: A review, Energy Procedia, 61, pp. 2416–2434. doi:10.1016/j.egypro.2014.12.017

96. Noghrehabadi, A., Hajidavaloo, E. and Moravej, M. (2016): Experimental investigation of efficiency of square flat-plate solar collector using SiO_2/water nanofluid, Case Studies in Thermal Engineering, 8, pp. 378–386. doi:10.1016/j.csite.2016.08.006

97. Okonkwo, E.C., Wole-Osho, I., Kavaz, D., Abid, M. and Al-Ansari, T. (2020): Thermodynamic evaluation and optimization of a flat plate collector operating with alumina and iron mono and hybrid nanofluids, Sustainable Energy Technologies and Assessments, 37(November 2019), p. 100636. doi:10.1016/j.seta.2020.100636

98. Otanicar, T.P. and Golden, J.S. (2009): Comparative environmental and economic analysis of conventional and nanofluid solar hot water technologies, Environmental Science and Technology, 43(15), pp. 6082–6087. doi:10.1021/es900031j

99. Ouyang, P., Xu, Y.P., Qi, L.Y., Xing, S.M. and Fooladi, H. (2021): Comprehensive evaluation of flat plate and parabolic dish solar collectors' performance using different operating fluids and MWCNT nanofluid in different climatic conditions, Energy Reports, 7, pp. 2436–2451. doi:10.1016/j.egyr.2021.04.046

100. Pastoriza-Gallego, M.J., Casanova, C., Legido, J.L. and Piñeiro, M.M. (2011): CuO in water nanofluid: Influence of particle size and polydispersity on volumetric behaviour and viscosity, Fluid Phase Equilibria, 300(1–2), pp. 188–196. doi:10.1016/j.fluid.2010.10.015

101. Raj, P. and Subudhi, S. (2018): A review of studies using nanofluids in flat-plate and direct absorption solar collectors, Renewable and Sustainable Energy Reviews, 84 (September 2016), pp. 54–74. doi:10.1016/j.rser.2017.10.012

102. Ramezanizadeh, M., Alhuyi Nazari, M., Ahmadi, M.H. and Açıkkalp, E. (2018): Application of nanofluids in thermosyphons: A review, Journal of Molecular Liquids, 272, pp. 395–402. doi:10.1016/j.molliq.2018.09.101

103. Ranga Babu, J.A., Kiran Kumar, K. and Srinivasa Rao, S. (2018): Thermodynamic analysis of hybrid nanofluid based solar flat plate collector, World Journal of Engineering, 15(1), pp. 27–39. doi:10.1108/WJE-03-2017-0048

104. Reddy, K.S., Kamnapure, N.R. and Srivastava, S. (2017): Nanofluid and nanocomposite applications in solar energy conversion systems for performance enhancement: A review, International Journal of Low-Carbon Technologies, 12(1), pp. 1–23. doi:10.1093/ijlct/ctw007

105. Refiei, A., Loni, R., Najafi, G., Sahin, A.Z. and Bellos, E. (2020): Effect of use of MWCNT/oil nanofluid on the performance of solar organic Rankine cycle, Energy Reports, 6, pp. 782–794. doi:10.1016/j.egyr.2020.03.035

106. Sadri, R. et al. (2014): An experimental study on thermal conductivity and viscosity of nanofluids containing carbon nanotubes, Nanoscale Research Letters, 9(1), pp. 4–13. doi:10.1186/1556-276X-9-151

107. Saeedinia, M., Akhavan-Behabadi, M.A. and Razi, P. (2012): Thermal and rheological characteristics of CuO-Base oil nanofluid flow inside a circular tube, International Communications in Heat and Mass Transfer, 39(1), pp. 152–159. doi:10.1016/j.icheatmasstransfer.2011.08.001

108. Said, Z., Hachicha, A.A., Aberoumand, S., Yousef, B.A.A., Sayed, E.T. and Bellos, E. (2021): Recent advances on nanofluids for low to medium temperature solar collectors:

energy, exergy, economic analysis and environmental impact, Progress in Energy and Combustion Science, 84. doi:10.1016/j.pecs.2020.100898

109. Said, Z., Saidur, R., Sabiha, M.A., Rahim, N.A. and Anisur, M.R. (2015): Thermophysical properties of Single Wall Carbon Nanotubes and its effect on exergy efficiency of a flat plate solar collector, Solar Energy, 115, pp. 757–769. doi:10.1016/j.solener.2015.02.037

110. Salavati Meibodi, S., Kianifar, A., Niazmand, H., Mahian, O. and Wongwises, S. (2015): Experimental investigation on the thermal efficiency and performance characteristics of a flat plate solar collector using SiO_2/EG-water nanofluids, International Communications in Heat and Mass Transfer, 65,pp.71–75. doi:10.1016/j.icheatmasstransfer.2015.02.011

111. Sarode, H.A., Barai, D.P., Bhanvase, B.A., Ugwekar, R.P. and Saharan, V. (2020): Investigation on preparation of graphene oxide-CuO nanocomposite based nanofluids with the aid of ultrasound assisted method for intensified heat transfer properties, Materials Chemistry and Physics, 251 (August 2019), p. 123102. doi:10.1016/j.matchemphys.2020.123102

112. Sarsam, W.S., Kazi, S.N. and Badarudin, A. (2015): A review of studies on using nanofluids in flat-plate solar collectors, Solar Energy, 122, pp. 1245–1265. doi:10.1016/j.solener.2015.10.032

113. Sarsam, W.S., Kazi, S.N. and Badarudin, A. (2020): Thermal performance of a flat-plate solar collector using aqueous colloidal dispersions of graphene nanoplatelets with different specific surface areas, Applied Thermal Engineering, 172 (October 2019), p. 115142. doi:10.1016/j.applthermaleng.2020.115142

114. Sezer, N., Atieh, M.A. and Koç, M. (2019): A comprehensive review on synthesis, stability, thermophysical properties, and characterization of nanofluids, Powder Technology, 344, pp. 404–431. doi:10.1016/j.powtec.2018.12.016

115. Shahrul, I.M., Mahbubul, I.M., Khaleduzzaman, S.S., Saidur, R. and Sabri, M.F.M. (2014): A comparative review on the specific heat of nanofluids for energy perspective, Renewable and Sustainable Energy Reviews, 38, pp. 88–98. doi:10.1016/j.rser.2014.05.081

116. Sharifpur, M., Giwa, S.O., Lee, K.Y., Ghodsinezhad, H. and Meyer, J.P. (2021): Experimental Investigation into Natural Convection of Zinc Oxide/Water Nanofluids in a Square Cavity, Heat Transfer Engineering, 42(19–20),pp. 1675–1687. doi:10.1080/01457632.2020.1818384

117. Sheikholeslami, M., Farshad, S.A., Ebrahimpour, Z. and Said, Z. (2021): Recent progress on flat plate solar collectors and photovoltaic systems in the presence of nanofluid: A review, Journal of Cleaner Production, 293, p. 126119. doi:10.1016/j.jclepro.2021.126119

118. Shin, D. and Banerjee, D. (2011): Enhancement of specific heat capacity of high-temperature silica-nanofluids synthesized in alkali chloride salt eutectics for solar thermal-energy storage applications, International Journal of Heat and Mass Transfer, 54(5–6), pp. 1064–1070. doi:10.1016/j.ijheatmasstransfer.2010.11.017

119. Shukla, R., Sumathy, K., Erickson, P. and Gong, J. (2013): Recent advances in the solar water heating systems: A review, Renewable and Sustainable Energy Reviews, 19, pp. 173–190. doi:10.1016/j.rser.2012.10.048

120. Singh, R., Tundee, S. and Akbarzadeh, A. (2011): Electric power generation from solar pond using combined thermosyphon and thermoelectric modules, Solar Energy, 85(2), pp. 371–378. doi:10.1016/j.solener.2010.11.012

121. Sint, N.K.C., Choudhury, I.A., Masjuki, H.H. and Aoyama, H. (2017): Theoretical analysis to determine the efficiency of a CuO-water nanofluid based-flat plate solar collector for

domestic solar water heating system in Myanmar, Solar Energy, 155, pp. 608–619. doi:10.1016/j.solener.2017.06.055

122. Starace, A.K., Gomez, J.C., Wang, J., Pradhan, S. and Glatzmaier, G.C. (2011): Nanofluid heat capacities, Journal of Applied Physics, 110(12). doi:10.1063/1.3672685

123. Sundar, L.S., Misganaw, A.H., Singh, M.K., Pereira, A.M.B. and Sousa, A.C.M. (2020): Efficiency, energy and economic analysis of twisted tape inserts in a thermosyphon solar flat plate collector with Cu nanofluids, Renewable Energy Focus, 35(December), pp. 10–31. doi:10.1016/j.ref.2020.06.004

124. Syam Sundar, L., Misganaw, A.H., Singh, M.K., Sousa, A.C.M. and Ali, H.M. (2021): Efficiency analysis of thermosyphon solar flat plate collector with low mass concentrations of ND–CO_3O_4 hybrid nanofluids: an experimental study, Journal of Thermal Analysis and Calorimetry, 143(2), pp. 959–972. doi:10.1007/s10973-020-10176-1

125. Tagliafico, L.A., Scarpa, F. and De Rosa, M. (2014): Dynamic thermal models and CFD analysis for flat-plate thermal solar collectors - A review, Renewable and Sustainable Energy Reviews, 30, pp. 526–537. doi:10.1016/j.rser.2013.10.023

126. Takabi, B. and Salehi, S. (2014): Augmentation of the Heat Transfer Performance of a Sinusoidal Corrugated Enclosure by Employing Hybrid Nanofluid, 2014. doi:10.1155/2014/147059

127. Tawfik, M.M. (2017): Experimental studies of nanofluid thermal conductivity enhancement and applications: A review, Renewable and Sustainable Energy Reviews, 75 (January 2015), pp. 1239–1253. doi:10.1016/j.rser.2016.11.111

128. Teng, T.P. and Hung, Y.H. (2014): Estimation and experimental study of the density and specific heat for alumina nanofluid, Journal of Experimental Nanoscience, 9(7), pp. 707–718. doi:10.1080/17458080.2012.696219

129. Tian, M.W. et al. (2021): Energy, exergy and economics study of a solar/thermal panel cooled by nanofluid, Case Studies in Thermal Engineering, 28, p. 101481. doi:10.1016/j.csite.2021.101481

130. Tiara, A.M., Chakraborty, Samarshi, Sarkar, I., Ashok, A., Pal, S.K. and Chakraborty, Sudipto (2017): Heat transfer enhancement using surfactant based alumina nanofluid jet from a hot steel plate, Experimental Thermal and Fluid Science, 89(August), pp. 295–303. doi:10.1016/j.expthermflusci.2017.08.023

131. Timofeeva, E. V. et al. (2007): Thermal conductivity and particle agglomeration in alumina nanofluids: Experiment and theory, Physical Review E - Statistical, Nonlinear, and Soft Matter Physics, 76(6), pp. 28–39. doi:10.1103/PhysRevE.76.061203

132. Tiwari, A.K., Ghosh, P. and Sarkar, J. (2013): Solar Water Heating Using Nanofluids-a Comprehensive Overview and Environmental Impact Analysis, International Journal of Emerging Technology and Advanced Engineering, 3(January), pp. 221–224. Available at: www.ijetae.com

133. Tiznobaik, H. and Shin, D. (2013): Enhanced specific heat capacity of high-temperature molten salt-based nanofluids, International Journal of Heat and Mass Transfer, 57(2), pp. 542–548. doi:10.1016/j.ijheatmasstransfer.2012.10.062

134. Toghraie, D., Chaharsoghi, V.A. and Afrand, M. (2016): Measurement of thermal conductivity of ZnO–TiO_2/EG hybrid nanofluid: Effects of temperature and nanoparticles concentration, Journal of Thermal Analysis and Calorimetry, 125(1), pp. 527–535. doi:10.1007/s10973-016-5436-4

135. Tong, Y., Chi, X., Kang, W. and Cho, H. (2020): Comparative investigation of efficiency

sensitivity in a flat plate solar collector according to nanofluids, Applied Thermal Engineering, 174(March). doi:10.1016/j.applthermaleng.2020.115346

136. Ucar, A. and Inalli, M. (2006): Thermal and exergy analysis of solar air collectors with passive augmentation techniques, International Communications in Heat and Mass Transfer, 33(10), pp. 1281–1290. doi:10.1016/j.icheatmasstransfer.2006.08.006

137. Uddin, M.J., Rahman, M.M. and Alam, S. (2016) Fundamentals of Nanofluids : Evolution , Applications and New Theory, International Journal of Biomathematics and Systems Biology, 2(1), pp. 1–31

138. Venerus, D.C. et al. (2010): Viscosity measurements on colloidal dispersions (nanofluids) for heat transfer applications, Applied Rheology, 20(4), p. 2. doi:10.3933/ApplRheol-20-44582

139. Verma, S.K., Gupta, N.K. and Rakshit, D. (2020): A comprehensive analysis on advances in application of solar collectors considering design, process and working fluid parameters for solar to thermal conversion, Solar Energy, 208 (September), pp. 1114–1150. doi:10.1016/j.solener.2020.08.042

140. Verma, S.K. and Tiwari, A.K. (2015): Progress of nanofluid application in solar collectors: A review, Energy Conversion and Management, 100, pp. 324–346. doi:10.1016/j.enconman.2015.04.071

141. Verma, S.K., Tiwari, A.K. and Chauhan, D.S. (2016): Performance augmentation in flat plate solar collector using MgO/water nanofluid, Energy Conversion and Management, 124, pp. 607–617. doi:10.1016/j.enconman.2016.07.007

142. Verma, S.K., Tiwari, A.K., Tiwari, S. and Chauhan, D.S. (2018): Performance analysis of hybrid nanofluids in flat plate solar collector as an advanced working fluid, Solar Energy, 167(January), pp. 231–241. doi:10.1016/j.solener.2018.04.017

143. Wagener, M., Murty, B.S. and Guenther, B. (1997): Preparation of metal nanosuspensions by high-pressure dc-sputtering on running liquids, Materials Research Society Symposium - Proceedings, 457, pp. 149–154. doi:10.1557/proc-457-149

144. Wahab, A., Hassan, A., Qasim, M.A., Ali, H.M., Babar, H. and Sajid, M.U. (2019): Solar energy systems – Potential of nanofluids, Journal of Molecular Liquids, 289. doi:10.1016/j.molliq.2019.111049

145. Wang, Z., Yang, W., Qiu, F., Zhang, X. and Zhao, X. (2015): Solar water heating: From theory, application, marketing and research, Renewable and Sustainable Energy Reviews, 41, pp. 68–84. doi:10.1016/j.rser.2014.08.026

146. Yiamsawasd, T., Dalkilic, A.S. and Wongwises, S. (2012): Measurement of the thermal conductivity of titania and alumina nanofluids, Thermochimica Acta, 545, pp. 48–56. doi:10.1016/j.tca.2012.06.026

147. Yousefi, T., Veisy, F., Shojaeizadeh, E. and Zinadini, S. (2012): An experimental investigation on the effect of MWCNT-H_2O nanofluid on the efficiency of flat-plate solar collectors, Experimental Thermal and Fluid Science, 39, pp. 207–212. doi:10.1016/j.expthermflusci.2012.01.025

148. Zamzamian, A., KeyanpourRad, M., KianiNeyestani, M. and Jamal-Abad, M.T. (2014): An experimental study on the effect of Cu-synthesized/EG nanofluid on the efficiency of flat-plate solar collectors, Renewable Energy, 71, pp. 658–664. doi:10.1016/j.renene.2014.06.003

149. Zayed, M.E., Zhao, J., Du, Y., Kabeel, A.E. and Shalaby, S.M. (2019)a: Factors affecting the thermal performance of the flat plate solar collector using nanofluids: A review, Solar Energy, 182 (March), pp. 382–396. doi:10.1016/j.solener.2019.02.054

150. Zayed, M.E., Zhao, J., Du, Y., Kabeel, A.E. and Shalaby, S.M. (2019)b: Factors affecting the thermal performance of the flat plate solar collector using nanofluids: A review, Solar Energy, 182(November 2018), pp. 382–396. doi:10.1016/j.solener.2019.02.054

151. Zhou, S.Q. and Ni, R. (2008): Measurement of the specific heat capacity of water-based Al_2O_3 nanofluid, Applied Physics Letters, 92(9), pp. 1–4. doi:10.1063/1.2890431

A2: Publications related to the dissertation

Refereed papers in foreign languages:

1. **Ajeena, Ahmed M.**, Farkas, I., Víg, P. (2024): Energy and exergy assessment of a flat plate solar thermal collector by examine silicon carbide nanofluid : An experimental study for sustainable energy. Applied Thermal Engineerin, Vol. 236, Paper No 121844. https://doi.org/10.1016/j.applthermaleng.2023.121844 (Scopus: D1, IF: 6.4)
2. **Ajeena, Ahmed M.**, Farkas, I., Víg, P. (2024): Characterization, rheological behaviour, and dynamic viscosity of ZrO_2-SiC (50–50)/DW hybrid nanofluid under different temperatures and solid volume fractions: An experimental study and proposing a new correlation. Powder Technology, Vol. 431, Paper No 119069. https://doi.org/10.1016/j.powtec.2023.119069 (Scopus: Q1, IF: 5.2)
3. **Ajeena, Ahmed M.**, Farkas, I., Víg, P. (2023): Performance enhancement of flat plate solar collector using ZrO_2-SiC/DW hybrid nanofluid: A comprehensive experimental study. Energy Conversion Management X, Vol. 20, Paper No 100458. https://doi.org/10.1016/j.ecmx.2023.100458 (Scopus: Q1, IF: 6.3)
4. **Ajeena, Ahmed M.**, Farkas, I., Víg, P. (2023): A comprehensive experimental study on thermal conductivity of ZrO_2-SiC /DW hybrid nanofluid for practical applications: Characterization, preparation, stability, and developing a new correlation. Arabian Journal of Chemistry, Vol. 16, Paper No 105346. https://doi.org/10.1016/j.arabjc.2023.105346 (Scopus: Q1, IF: 6)
5. **Ajeena, Ahmed M.**, Farkas, I., Víg, P. (2023): A comparative experimental study on thermal conductivity of distilled water-based mono nanofluids with zirconium oxide and silicon carbide for thermal industrial applications: Proposing a new correlation. International Journal of Thermofluids, Vol. 20, Paper No 100424. https://doi.org/10.1016/j.ijft.2023.100424 (Scopus: Q1)
6. **Ajeena, Ahmed M.**, Farkas, I., Víg, P. (2023): A comparative experimental investigation of dynamic viscosity of ZrO_2/DW and SiC/DW nanofluids: Characterization, rheological behavior, and development of new correlation. Heliyon, Vol. 9, Paper No e21113. https://doi.org/10.1016/j.heliyon.2023.e21113 (Scopus: Q1, IF: 4)
7. **Ajeena, Ahmed M.**, Víg, P., Farkas, I. (2022): A comprehensive analysis of nanofluids and their practical applications for flat plate solar collectors: Fundamentals, thermophysical properties, stability, and difficulties. Energy Reports Vol. 8, pp. 4461–4490. https://doi.org/10.1016/j.egyr.2022.03.088 (Scopus: Q1, IF: 5.2)
8. **Ajeena, Ahmed M.**, Farkas, I., Víg, P. (2023): Experimental approach on the effect of ZrO_2/DW nanofluid on flat plate solar collector thermal and exergy efficiencies. Energy Reports, Vol. 10, pp. 4733–4750. https://doi.org/10.1016/j.egyr.2023.11.036 . (Scopus: Q1, IF: 5.2)
9. **Ajeena, Ahmed M.**, Víg P., Farkas I. (2021): TRNSYS simulation of a flat plate solar system for space heating, Mechanical Engineering Letters, Gödöllő, Hungary, 2021, Vol. 20, pp. 89- 95. HU ISSN 2060-3789

10. **Ajeena, Ahmed M.**, Víg P., Farkas I. (2022): Anti-reflection and self-cleaning nanocoating to improve the performance of flat plate solar collector, European Journal of Energy Research, Vol. 2, No. 1, pp. 13-18. ISSN: 2736-5506. https://doi.org/10.24018/ejenergy.2022.2.1.41

Refereed papers in Hungarian:

11. Víg P., **Ajeena Ahmed M.**, Farkas I. (2022): Napkollektorok teljesítményének fokozása szelektív bevonatokkal, Mezőgazdasági Technika, LXII. évf., 2022. március, 2-5. ISSN 0026 -1890.

International conference proceedings:

12. **Ajeena, Ahmed M.**, Víg P., Farkas I. (2021): Modelling and simulation of a solar water heating system, International Conference on Efficiency, Solar and Thermal Energy for the Human Comfort, July 9, 2021, Gödöllő, Hungary, pp. 29-30., ISBN 9789632699585
13. **Ajeena, Ahmed M.**, Víg P., Farkas I. (2023): Effect of SiC/DW nanofluid on the thermal performance of a flat plate solar collector: An experimental study, International Conference of Engineering Sciences (under preparation)

International conference abstracts:

14. **Ajeena, Ahmed M.**, Víg P., Farkas I. (2020): Performance enhancement of flat plate solar collector using nanocoating and nanofluids, Book of Abstracts, 26th Workshop on Energy and Environment, Gödöllő, Hungary, December 10-11, 2020, p. 20., ISBN 978-963-269-928-8.
15. **Ajeena, Ahmed M.**, Víg P., Farkas I. (2021): Fundamentals and application of nanofluids in flat plate solar collectors, Book of abstracts, 20th International Workshop for Young Scientists, BioPhys Spring 2021, Lublin, Poland, May 18-19, 2021, p. 15, ISBN 978-83-89969-68-2.
16. **Ajeena, Ahmed M.**, Víg P., Farkas I. (2021): Nanofluids in solar flat plate collectors: thermophysical properties and limitations, Book of Abstracts, 27th Workshop on Energy and Environment, Gödöllő, Hungary, December 9-10, 2021, p. 9., ISBN 978-963-269-972.
17. **Ajeena, Ahmed M.**, Víg P., Farkas I. (2022): CFD Modelling and preparation of nanofluid filled flat plate solar collector Book of Abstracts, 28th Workshop on Energy and Environment, Gödöllő, Hungary, December 8-9, 2022, p. 11., ISBN 978-963-623-016-6.
18. **Ajeena, Ahmed M.**, Víg P., Farkas I. (2023): Improving the performance of flat plate solar collector by using nanofluid, Book of abstracts, 22nd International Workshop for Young Scientists, BioPhys Spring 2023, Gödöllő, Hungary, June 15-16, 2023, p. 13, ISBN 978-963-623-054-8.

9. ACKNOWLEDGEMENT

This work has been supported financially by the Stipendium Hungaricum Scholarship Program and the Mechanical Engineering Doctoral School at Hungarian University of Agriculture and Life Sciences (MATE), Gödöllő, Hungary.

First of all, I would like to praise the Almighty God who has granted countless blessing and guidance during my studies.

I am grateful to Prof. Farkas for his encouragement and support, which have provided me with an excellent atmosphere for doing research. I would like to thank Dr. Víg for his support, feedback, encouragement, and immense knowledge.

I want to thank everyone in the Institute of Mechanical Engineering workshop for all the help and support they have given me. My thanks also to my colleagues in the Mechanical Engineering Doctoral School, who are not mentioned here but helped me in completing this work.

I am very grateful to my family members and friends for their immeasurable love and sacrifices, which have made this feat possible.

Finally, I wish to acknowledge the Ministry of Higher Education of Iraq and my home university, the University of Kufa- Faculty of Engineering, for nominating and supporting me during this achievement.

Gödöllő, December 2023

Ahmed M. Ajeena